Studies on petrochemicals using thermal analysis coupled to photo ionisation mass spectrometry

Kumulative Dissertation

zur Erlangung des akademischen Grades

doctor rerum naturalium (Dr. rer. nat.)

der Mathematisch-Naturwissenschaftlichen Fakultät

der Universität Rostock

vorgelegt von

Christoph Grimmer

geboren am 2. Mai 1991 in Ludwigslust

Rostock, Januar 2021

The presented work was prepared in the period from March 2016 to September 2020 at the chair of Analytical Chemistry in the working group Analytical and Technical Chemistry of the Institute of Chemistry of the University of Rostock. This dissertation was conducted within the framework of the Joint Mass Spectrometry Centre (JMSC) of the University of Rostock and the HelmholtzZentrum münchen German Research Centre for Environmental Health.

"Any intelligent fool can make things bigger, more complex, and more violent. It takes a touch of genius – and a lot of courage to move in the opposite direction."

- E. F. Schumacher

"Good judgement comes from experience. Experience comes from bad judgement."

- Unknown

"We are not lost. We're locationally challenged."

- John M. Ford

Erklärung gemäß §4 Absatz 1 Buchstaben g und h der Promotionsordnung der Mathematisch-Naturwissenschaftlichen Fakultät der Universität Rostock

Name: Christoph Grimmer   **Matrikelnummer:** 210205681

Anschrift: Margaretenstraße 53

18057 Rostock

Ich habe eine Dissertation zum Thema

Studies on petrochemicals using thermal analysis coupled to photo ionisation mass spectrometry

an der Mathematisch-Naturwissenschaftlichen Fakultät der Universität Rostock angefertigt. Dabei wurde ich von Herrn Prof. Dr. Ralf Zimmermann betreut.

Ich gebe folgende Erklärung ab:

1. Die Gelegenheit zum vorliegenden Promotionsvorhaben ist mir nicht kommerziell vermittelt worden. Insbesondere habe ich keine Organisation eingeschaltet, die gegen Entgelt Betreuerinnen/Betreuer für die Anfertigung von Dissertationen sucht oder die mir obliegenden Pflichten hinsichtlich der Prüfungsleistungen für mich ganz oder teilweise erledigt.

2. Ich versichere hiermit an Eides statt, dass ich die vorliegende Arbeit selbstständig angefertigt und ohne fremde Hilfe verfasst habe. Dazu habe ich keine außer den von mir angegebenen Hilfsmitteln und Quellen verwendet und die den benutzten Werken inhaltlich und wörtlich entnommenen Stellen habe ich als solche kenntlich gemacht.

Rostock, January 2021   _____

Christoph Grimmer

Contribution to scientific publications

The following manuscripts were contributed by Christoph Grimmer as first author or as co-author with significant contribution and published in peer-reviewed journals. The involvement and contribution of Christoph Grimmer to each manuscript is described in detail below.

First-authorships

Title: Description of Steam Cracker Fouling and Coking Residues by Thermal Analysis-Photoionization Mass Spectrometry

Authors: Christoph Grimmer, Christopher P. Rüger, Thorsten Streibel, Fabrice Cuoq, Gerard Kwakkenbos, Miguel Cordova, Rosa Peñalver, and Ralf Zimmermann

Journal: Energy Fuels, *33*, 11, 11592–11602

Year: **2019**

Christoph Grimmer carried out the pretreatment, TA-PI-TOFMS and Pyr-GC-MS analysis of fouling samples from a steam cracker facility, interpreted data, developed a rough quantification method for specific fouling reactions and wrote the manuscript.

Title: Characterization of Polyethylene Branching by Thermal Analysis-Photoionization Mass Spectrometry

Authors: Christoph Grimmer, Lukas Friederici, Thorsten Streibel, Ahmad Naim, Virginie Cirriez, Pierre Giusti, Carlos Afonso, Christopher Rüger, and Ralf Zimmermann

Journal: Journal of the American Society for Mass Spectrometry, *31*, 11, 2362–2369

Year: **2020**

Christoph Grimmer carried out the TA-SPI-TOFMS and Pyr-GC-MS analysis, performed the statistical data analysis and wrote the manuscript.

Co-authorships

Title: Combination of Different Thermal Analysis Methods Coupled to Mass Spectrometry for the Analysis of Asphaltenes and Their Parent Crude Oils: Comprehensive Characterization of the Molecular Pyrolysis Pattern

Authors: Christopher P. Rüger, <u>Christoph Grimmer</u>, Martin Sklorz, Anika Neumann, Thorsten Streibel, and Ralf Zimmermann

Journal: Energy Fuels, *32*, 3, 2699–2711

Year: **2018**

Christoph Grimmer carried out the TA-PI-TOFMS analysis, contributed to the data interpretation and approved the manuscript.

Title: Real time monitoring of slow pyrolysis of polyethylene terephthalate (PET) by different mass spectrometric techniques

Authors: Asma Dhahak, <u>Christoph Grimmer</u>, Anika Neumann, Christopher Rüger, Martin Sklorz, Thorsten Streibel, Ralf Zimmermann, Guillain Mauviel, and Valérie Burkle-Vitzthum

Journal: Waste Management, *106*, 226–239

Year: **2020**

Christoph Grimmer supervised and completed the TA-PI-TOFMS and Pyr-GC-MS analysis, contributed to the data interpretation and approved the manuscript.

Other publications

Title: Structural and electrical properties of $BaZr_{0.7}Ce_{0.2}Y_{0.1}O_{3-\delta}$ proton conducting ceramic fabricated by spark plasma sintering

Authors: Jan Wallis, Laurance Urban, <u>Christoph Grimmer</u>, Wiktor Bodnar, Ralf Zimmermann, Sandrine Ricote, Klaus-Dieter Weltmann, Eberhard Burkel, Angela Kruth

Journal: Solid State Ionics, *345*, 115118

Year: **2020**

Rostock, January 2021

_____

Christoph Grimmer

Acknowledgements

First of all I would like to thank Prof. Ralf Zimmermann for the opportunity to be part of the Analytical Department at the University of Rostock and the good supervision throughout the years. I want to further thank Dr. Thorsten Streibel for being a great co-supervisor, listener, and for every advice he offered.

Thank you to all of my colleagues in Rostock and Munich with whom I shared a lot of good times and who helped me during hardships. I was lucky to supervise Lukas Friederici and Eric Schneider, who are not only eager students but also did a lot of work in the lab. Special thanks are directed to Dr. Christopher Rüger for his educative guidance and friendship.

I am very grateful for the support and love of my family, in particular of my parents Michaela and Thomas Grimmer. Last but not least, I want to thank Johanna for being so patient with me and my sometimes strange working habits.

Table of Contents

List of abbreviations

APCI	Atmospheric pressure chemical ionisation
APPI	Atmospheric pressure photo ionisation
DSC	Differential scanning calorimetry
DTA	Differential thermal analysis
EA	Elemental analysis
EGA	Evolved gas analysis
FID	Flame ionisation detector / Free induction decay
FT	Fourier-transform
FTICR	Fourier-transform ion cyclotron resonance
GC	Gas chromatography
IR	Infrared spectroscopy
LC	Liquid chromatography
MALDI	Matrix-assisted laser desorption/ionisation
MCP	Microchannel plate
MS	Mass spectrometry
NMR	Nuclear magnetic resonance
PDMS	Polydimethylsiloxane
PE	Polyethylene
PET	Polyethylene terephthalate
PI	Photo ionisation
Pyr	Pyrolysis
REMPI	Resonance enhanced multi photon ionisation
SEM	Secondary electron multiplier
SPI	Single photon ionisation
STA	Simultaneous thermal analysis
TA	Thermal analysis
TD	Thermodesorption
TGA	Thermogravimetric analysis
TIC	Total ion current
TOF	Time of flight
XANES	X-ray absorption near edge structure

List of figures

List of tables

Zusammenfassung

Die chemische Analyse von Rohölen und daraus hergestellten Petrochemikalien ist sehr wichtig für die Gewährleistung von Wirtschaftlichkeit und Produktqualität. Nur durch das Identifizieren und Quantifizieren von Bestandteilen können Probleme gelöst und Entwicklungen vorangetrieben werden. Während für leichte Fraktionen leistungsstarke analytische Techniken zur Verfügung stehen, bereiten höher siedende Fraktionen mit ihren herausfordernden physikalischen Eigenschaften oft Probleme. Schwere Fraktionen sind dabei nicht nur weniger flüchtig und löslich, sondern besitzen auch eine gesteigerte Komplexität. Durch die Verschiebung des Marktes von leichten zu schweren Erdölen, gewinnen die schweren Fraktionen zusätzlich an Bedeutung.

Daher ist das Ziel der vorliegenden Arbeit, hochviskose, nicht verdampfbare und komplexe Petrochemikalien mittels thermischer Analyse und gleichzeitiger Emissionsgasanalyse per Photoionisierungsmassenspektrometrie (TA-PI-MS) zu untersuchen. Dabei stehen sowohl der Erkenntnisgewinn über die jeweils untersuchte Probe, als auch die Evaluierung der Technik für zukünftige Anwendungen im Fokus. Durch Ausnutzung von Pyrolyse, weicher universeller und selektiver Ionisierung, sowie einem Massenanalysator mit großem Massenbereich, können sonst schwer zugängliche Daten generiert werden. Anspruchsvolle Proben aus unterschiedlichen Bereichen der erdölverarbeitenden Industrie sollen ein realitätsnahes Szenario simulieren: Asphaltene als wohl problematischste Fraktion im Ausgangsstoff, Ablagerungen aus der Verarbeitung im Steamcracker, verschieden verzweigte Polyethylene als Endprodukte und das Recycling von Polyethylenterephthtalat.

Jede Probe hat ihre spezifischen Eigenschaften, weshalb unterschiedliche analytische Strategien angewandt wurden. Eine detaillierte chemische Beschreibung der Asphaltenprobe konnte durch die multimethodische Untersuchung mit komplementären thermischen Analysetechniken erreicht werden (Publikation 1). Die Hauptstrukturen der Ablagerungen konnten dagegen allein mit TA-PI-MS und Pyr-GC-MS Messungen qualitativ beschrieben werden (Publikation 2). Weiterhin wurden erste Quantifizierungsversuche zum Gehalt des Diels-Alder-Anteils unternommen. Die Differenzierung verschieden verzweigter Polyethylene funktioniert mit TA-PI-MS hervorragend (Publikation 3) und erste Ergebnisse deuten mindestens auf eine semi-quantitative Methode für kurze Verzweigungen. In Publikation 4 wurde die thermische Zersetzung von Polyethylenterephthalat mittels thermischer Analyse gekoppelt an drei weich ionisierende massenspektrometrische Methoden untersucht. Verständnis über Zersetzungsreaktionen und Produkte ermöglicht ggfs. die Anwendung für Recyclingkonzepte wie beispielsweise waste-to-oil.

Abstract

The chemical analysis of crude oils and their respective petrochemical products is very important to guarantee economic efficiency and product quality. Problems can only be solved and innovation enabled by identifying and quantifying components. While powerful analytical techniques are available for light fractions, higher-boiling fractions cause problems, because of their challenging physicochemical properties. Heavy fractions are not only less volatile and soluble but also more complex. Due to the consistent shift in the market towards heavier crude oils, the heavy fractions are also gaining in importance.

Therefore, the aim of this thesis is to investigate highly viscous, non-volatile and complex petrochemicals by means of thermal analysis and subsequent evolved gas analysis based on photo ionisation mass spectrometry (TA-PI-MS). The focus is on retrieving new findings of the examined samples, as well as evaluation of the technique for future applications. By exploitation of pyrolysis, soft universal and selective ionisation, and a versatile mass analyser platform, otherwise difficult to access data can be generated. Demanding samples from different areas of the petroleum industry simulate a realistic scenario: asphaltenes as the most problematic fraction within feed, steam cracker fouling samples occurring during processing, differently branched polyethylene materials as end products and recycling of polyethylene terephthalate waste.

Each sample has its unique characteristics, requiring different analytical strategies for analysis. A detailed chemical description of the asphaltene sample was achieved by a multi-methodological approach of complementary thermal analysis techniques (publication 1). The main structural motifs of fouling samples were qualitatively described by only applying TA-PI-MS and Pyr-GC-MS (publication 2). In addition, first attempts to quantify the Diels-Alder content were conducted. Differently branched polyethylene materials were successfully discriminated by TA-PI-MS (publication 3), and first findings indicate an at least semi-quantitative method for the elucidation of short-chain branching. In publication 4 a study about the thermal decomposition of polyethylene terephthalate was conducted by means of thermal analysis hyphenated to three different soft ionisation mass spectrometry techniques. Understanding of the degradation reactions and product spectrum might enable the application of recycling concepts such as waste to oil.

1   Introduction

Petroleum developed into a key component of economy today. Though, it is known for a long time and was used for several purposes throughout the centuries, its worldwide breakthrough commenced after the beginning of the industrialisation with the discovery of the refining process (~1850). Especially the rising demand for electric power and energy dense (liquid) fuels to power machines more efficiently, lead to a substitution of coal in many fields. Petroleum is a fossil resource, which can be transformed into various fuels, materials and other products. It is often referred to as 'crude oil' in its raw form. Like all other fossil resources, crude oil is transformed biomass, which was subjected to intense heat and pressure over a long period of time (i.e. millions of years). Crude oil and natural gas are formed from large quantities of dead organisms, mostly algae and zooplankton, when buried underneath sedimentary rock, whereas coal and methane are formed from terrestrial plants. The high energetic and anoxic conditions cause the organic matter to alter chemically, leading to the loss of water, carbon dioxide and methane, ultimately increasing the proportion of carbon. In addition, many more reactions, such as cracking or dehydrogenation, take place. The resulting petroleum is a mixture of a large number of many different hydrocarbons, in various shapes and sizes.

During refining, this mixture is fractionated by distillation. Some fractions can be directly used, others need to be further processed. Modern refineries can be quite complex, depending on the requirements of the produced fractions and for environmental and economic reasons. The products are used for transportation, heating, power generation, as building blocks for various materials, as well as for chemical and drug synthesis.

Crude oils from different oil wells can be composed quite differently, which influences their physicochemical properties and thus their behaviour during pumping and refining. Associated problems, such as pipe obstruction, fouling, or simply the monitoring of product quality and yield, call for versatile analytical methods. But the complex nature of petroleum and its fractions is challenging, especially with rising content of heavier constituents.

Different physicochemical approaches were pursued to investigate the composition of crude oil and its products. Each analytical method has its characteristic advantages and disadvantages. Thus, several complementary methods are usually used to get the overall picture. Nevertheless, mass spectrometry has proven to be applicable for diverse fields and provides valuable molecular information. The diversity of mass analyser platforms and ionisation techniques, as well as the ability to hyphenate almost all chromatographic separation techniques, makes it a powerful tool.

Ultra-high resolution mass spectrometry with its remarkable separation power is the state-of-the-art analytical technique for many highly complex, petrochemical problems. Besides mass separation power, the observed complexity can be tackled by additional fractionation, chromatographic separation or selective ionisation. Low-resolution mass spectrometers are less expensive and are widely applied, e.g., combined with soft (selective) ionisation or

chromatographic separation. Soft ionisation means that predominantly molecular ions and fewer fragment ions are generated, which directly reduces the data complexity. Additionally, selective ionisation can be used to filter out or focus on certain substance classes.

Chromatographic separation can be achieved by use of gas or liquid chromatography. In case of non-volatile and insoluble samples, thermal analysis can be used for a similar purpose. In a sense, thermal analysis can be regarded as a very low-resolution thermal separation technique. Volatile and semi-volatile substances evaporate when their vapour pressure reaches the ambient pressure during heating. Non-volatile compounds cannot evaporate and eventually break into smaller fragments, which then often evaporate immediately.

The aim of this PhD thesis is the application and evaluation of thermal analysis coupled to a photo ionisation time-of-flight mass spectrometer towards highly-viscous, non-volatile and complex petrochemical samples. Single photon ionisation and resonance enhanced multi photon ionisation were used to preserve the molecular pattern of samples obtained from different stages of the process chain. New findings about asphaltenes, fouling, polyethylene materials and recycling of polyethylene terephthalate, relatively simple handling of samples (no or little pre-treatment) and high suitability towards non-volatile samples, indicate an interesting and valuable technique.

2   Industrial feedstock

During the agrarian era, wood was used for domestic heating and cooking. In addition to use as a building material, wood remained the chief global fuel for centuries.[1] Then, with the dawn of the industrial era, which began around the second half of the 18th century in Great Britain, coal substituted wood as fuel.[2,3] Especially the invention of steam engines and improved iron smelting procedures favoured coal for its higher energy density and low price.[4,5] In 1847, the chemist James Young obtained a light oil from crude oil distillation, suitable for use as lamp oil, while the thicker oil residue could be used as machine lubricant.[6] But access to crude oil was rare at the time, and Young focused on experiments with coal. Slow distillation of coal resulted in a fluid similar to petroleum, which gave also similar products during further distillation. Soon after, first petrochemical products, such as paraffin (lamp oil), naphtha, lubricant and solid paraffin, derived from coal were commercially available. Enterprises all around the world formed to satisfy the rising demand for these chemicals, including the construction of oil wells.[7] The refining of crude oil is more efficient than distillation of coal, which together with the extensive access to crude oil improved the overall productivity. Crude oil production increased dramatically and is still growing today (**Figure 1**), driven by inventions, increasing standards for living, and progressing globalisation. The internal combustion engine, electric light, electric grid system, and polymers (among others) can be regarded as key inventions.
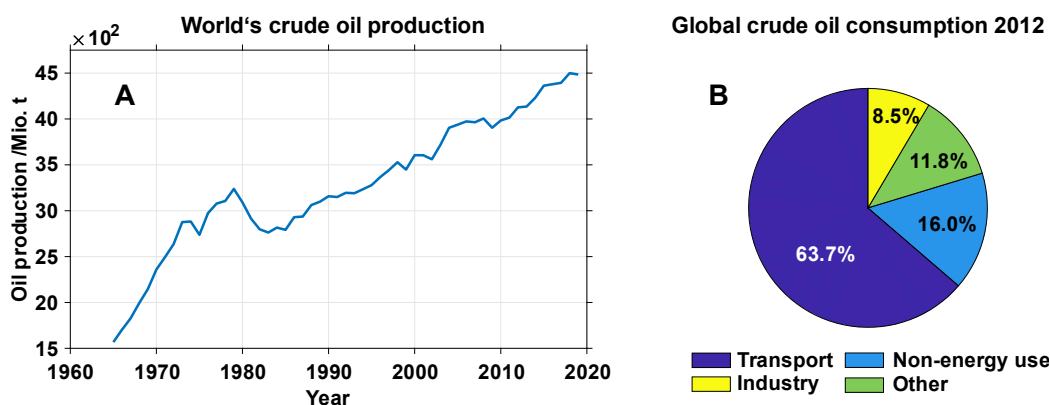
Figure 1. (**A**) world's crude oil production in million tons (1965–2019), (**B**) global crude oil consumption (2012).[8,9]

Though petroleum is in principle generated all the time, its generation rate is so low compared to the rate of consumption, that petroleum is classified as finite resource. Older studies predicted, that the 'peak oil' (maximum of oil producibility) had already happened, but the development of new discovery and production methods lead to an uncertain delay. Nonetheless, oil reservoirs will be depleted sooner or later, when the oil production continues as is or further grows. This, the scientifically proved global warming, caused mainly from burning fossil resources by mankind, and other environmental problems, lead to an increasing interest in renewable feedstock and energy sources.

2.1 Crude oil

Crude oil is a naturally occurring, yellowish-black liquid found in geological formations beneath the Earth's surface.[10,11] It is mainly composed of a mixture of a large number of many different hydrocarbons of varying molecular weight and structure. Besides, water, mineral salts, heteroatoms such as oxygen, nitrogen, sulphur, nickel and vanadium, are abundant. The most prevalent hydrocarbon substance classes are alkanes, naphthenes (cyclic alkanes), aromatics, and heterocyclic compounds. Despite relatively narrow limits of the elemental distribution of crude oils from different origins (**Table 1**), their molecular composition can vary widely (**Table 2**). These variations in chemical composition as well as in the molecular weight distribution (light vs. heavy), result in variable properties.[12]

Table 1. The elemental distribution of regionally different crude oils has quite narrow limits.[13]

Element	Carbon	Hydrogen	Nitrogen	Oxygen	Sulfur	Metals
Percent range /wt%	83–85	10–14	0.1–2	0.05–1.5	0.05–6.0	< 0.1

Table 2. The chemical composition of regionally different crude oils varies widely.[12]

Hydrocarbon	Alkanes	Naphthenes	Aromatics	Asphaltenes
Percent range /wt%	15–60	30–60	3–30	Remainder

A shift towards heavier resources can be recognized in many fields of industrial production or processing in general. This is mainly due to the decline of high quality, light petroleum and increasing exploitation of unconventional sources, such as shale oil, tar oil, and oil sands. These heavy reservoirs contain high amounts of constituents, which cause problems in the up- and downstream process chains.[13–17]

The heaviest and probably most troublesome compounds found in crude oil are asphaltenes. They can be obtained by the so called SARA fractionation, which separates petroleum samples based on solubility. Different procedures were developed for that purpose, but usually an *n*-alkane is used as solvent to precipitate asphaltenes at one point. The remaining petroleum (referred to as maltenes) can be further fractionated into saturates, aromatics, and resins. The polarity of the fractions increases from saturates, aromatics, resins to asphaltenes. Hetero elements are mainly present in the resin and asphaltene fractions.[18–21]

2.2 Refining and fouling

Crude oil can be directly burned for power generation, but high-value products can only be obtained when utilising refining processes. Depending on the used crude oil, location of the refinery, market demands, and regulations, refineries can be composed quite differently (**Figure 2**).[13,17,22,23]

The first step is usually the desalting unit, where mineral salts (calcium, sodium and magnesium chlorides), other inorganic content and water are removed. The desalted crude oil is afterwards distilled under atmospheric pressure into gases, light naphtha, heavy naphtha, kerosene, diesel, atmospheric gasoil, and the atmospheric residue. The composition of these boiling cuts stems from the differences in vapour pressure, which is influenced by molecular weight, aromaticity and polarity. The maximum temperature is limited to 360 °C to avoid thermal decomposition. Subsequently, the distilled fractions are subjected to other fundamental refining processes. Before, it has to be assured, that sulphur and nitrogen containing substances are naturally absent or they have to be removed by hydrotreating to avoid catalyst poisoning. Light naphtha can be send to an isomerisation unit and heavy naphtha to a reformer, both to increase their octane number. Sometimes different options are available: atmospheric gasoil for example can be catalytically cracked either into gasoline blending products or into diesel blending products. Blending of different product streams is used to meet the specifications of fuels.
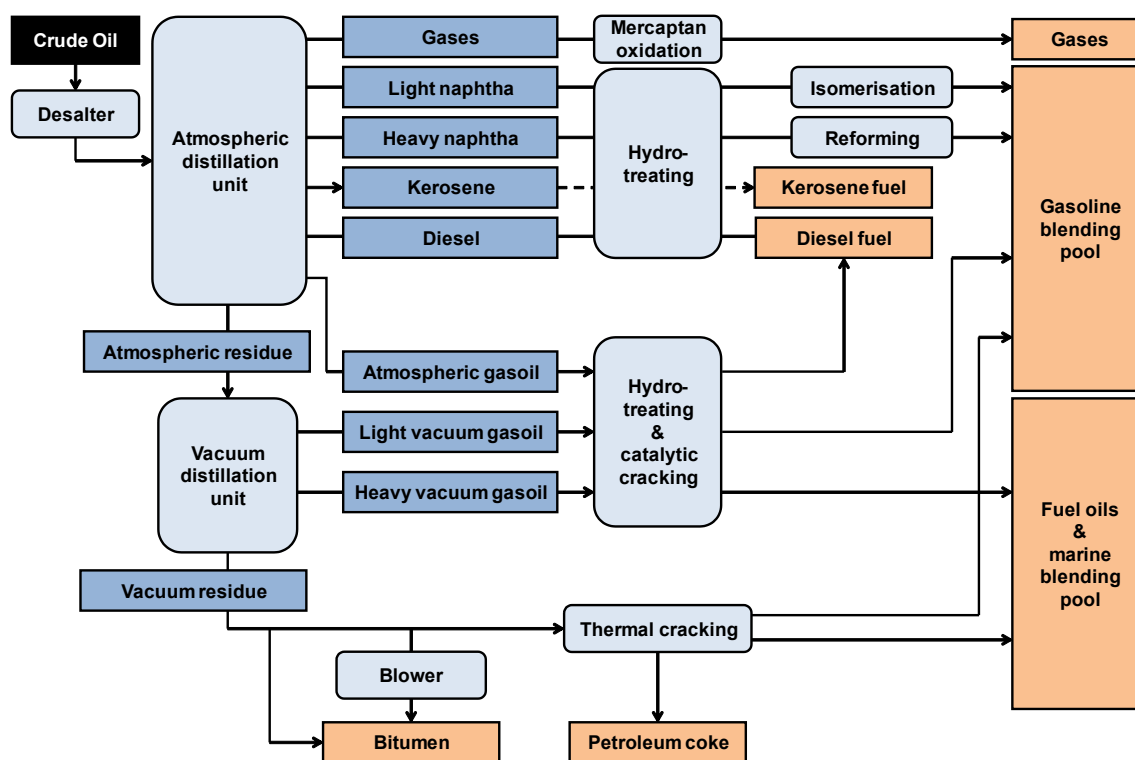
Figure 2. Simplified scheme of an exemplary, modern refinery; final products are marked in orange, intermediate fractions in blue. Adapted based on literature.[17,23]

The atmospheric residue can be further fractionated in the vacuum distillation process. The reduced pressure (10–50 mbar) leads to a reduction of the boiling points of substances, extending the range to higher boiling compounds. Two distillable fractions, light and heavy vacuum gasoil, and the non-distillable vacuum residue are obtained. Heavy, low-value products are often transformed into lighter, high-value products via cracking units. A distinction is made between thermal cracking and catalytic cracking. Another, yet similar technique, is coking, which can be used for the vacuum residue to produce fuel blending products and petroleum coke. However, coke formation on walls, pipes and catalysts, is unwanted and one of the main fouling reactions in refineries. All cracking units are prone to coke formation, as the high temperature always leads to carbonisation.

2.3 Pyrolysis in industry and analysis

Pyrolysis is defined as the thermal decomposition of materials at elevated temperatures in the absence of oxygen.[24] It involves a change of chemical composition, often towards smaller compounds, induced by chemical-bond scission. Some of the most important refining processes, such as cracking and coking, are accounted as pyrolysis processes.[25] Not only petroleum and coal can be thermally treated, also bio-based feedstock such as wood or bio-waste.[26] Prominent reactions of hydrocarbons are cleavage of alkanes into smaller alkanes and alkenes, cyclisation of alkanes into naphthenes, dehydrogenation of naphthenes into

aromatics, dehydration and decarboxylation.[27] The parameters of pyrolysis can be altered to shift the reaction to favorable products. The temperature, residence time, composition of feed, use of catalyst, concentration of educts and products, and the addition of inhibitors or reactants, such as steam or hydrogen respectively, have major influence. Different specialised, industrial cracking processes have emerged: steam cracking, fluid catalytic cracking, hydrocracking, visbreaking and coking.

Besides the importance to transform heavy feedstock into lighter fuels, cracking is essential for the production of short-chain olefins for polymer synthesis, for which steam cracking is particularly suited.[25] It is the principal industrial method for producing the lighter alkenes, including ethylene and propylene. A gaseous or liquid hydrocarbon feed like naphtha, liquefiable propane gas, or ethane is diluted with steam and briefly heated in a furnace. Typically, the temperature is very high at 750–900 °C and the residence time is in the order of milliseconds. A higher cracking temperature (also called severity) yields increased amounts of ethylene and benzene, whereas a lower severity favours propylene, C4 products (butane, butane, and butadiene) and liquid products. Light hydrocarbon feeds such as ethane, liquefied petroleum gas, or light naphtha give mainly lighter alkenes, including ethylene, propylene, and butadiene. Heavier hydrocarbon (full range and heavy naphtha as well as other refinery products) feeds give some of these same products, and also those rich in aromatic hydrocarbons and hydrocarbons suitable for inclusion in gasoline or fuel oil.

Pyrolysis is not only used for industrial processes, but also for analytical purposes. Some sophisticated methods rely on solubility (such as liquid chromatography or nuclear magnetic resonance) or volatility (such as gas chromatography), which hampers the analysis of insoluble and non-volatile samples.[28,29] Pyrolysis can be used to circumvent this, by breaking down the non-volatile material into smaller, volatile fragments.[30–34] For that reason, evolved gas analysis and specialised introduction systems, such as pyrolysis injectors, were developed. A distinction is made between slow and fast pyrolysis (also referred to as flash pyrolysis).

2.4 Polymers

A polymer is a chemical substance, which is composed of macro molecules. These macro molecules are made of one type (homopolymer) or several types (copolymer) of repeating structural units.[35] Bio-based polymers, such as DNA or proteins, synthesised in living organisms, are essential for life. Others, such as cellulose and lignin, can be used as material and feedstock. Synthetic or semi-synthetic polymers are the main component for the production of plastic materials. Polymers have become an integral part of our everyday life, because of their broad spectrum of excellent properties. Their large molecular mass produces unique physical properties including toughness, high elasticity, viscoelasticity, and a tendency to form amorphous and semi-crystalline structures rather than crystals.[36,37]

The reaction, in which many small, uniform molecules (monomers) are combined into a covalently bonded chain or network, is called polymerisation. Different types of polymerisation reaction are known: step-growth, chain-growth and photo polymerisation. And even for one type of polymerisation, such as chain-growth polymerisation, several approaches exist. Here, an initiation reaction (radical, ionic or coordinative) yields a reactive species, which then attacks a monomer. A bond between the reactive specie and the attacked monomer is formed, often by exploitation of a pre-existing functionality, and the newly formed end becomes reactive in the process. The propagation reaction repeats until a termination reaction occurs.[38]

Control of the polymerisation reaction enables access to differently composed polymers and thus properties. Polymers, even homopolymers, are not uniform at all. Differences can be present in the molecular weight distribution (MWD), branching, and for copolymers, in the copolymer content and sequence of comonomer units. There are even more possibilities to modify the properties of polymers: by use of additives, such as plasticisers or stabilisers, or post-processing, such as grafting.[25,39] Mankind became so good in producing and manipulating polymers that our age is sometimes referred to as 'the age of polymers'.[40]

But there are also problems associated with polymers, which often arise from their high resistance. High durability is desirable for many applications, but negative, when the material is deposited in a landfill or ends up otherwise in the environment. Many adverse effects on the environment and health, caused by synthetic polymers, were observed.[41] Only a small proportion is recycled, because of difficulties in the identification and separation of different types of polymers. Other promising approaches are the use of renewable and decomposable polymers, e.g. of bio-based origin, or the conversion of polymers back into monomers or usable oil by pyrolysis.[42–45] This way, separation might become unnecessary.

3 Fundamentals of the employed techniques

The fundamentals of the techniques employed in this PhD thesis are briefly explained and described in this section, focusing on thermal analysis, gas chromatography, mass spectrometry, and different ionisation techniques.

3.1 Thermal analysis

Thermal analysis (TA) is a group of different material-analytic methods, in which a property is measured under the influence of heating.[46] Methods are distinguished from one another by the property, that is measured. The coupling of subsequent chemical characterisation (infrared spectroscopy, gas chromatography, or mass spectrometry) of off-gasses after any TA technique is called evolved gas analysis (EGA).[47] When applying EGA, oxidation is often not wanted, because hydrocarbons are unspecifically transformed into carbon dioxide and water. Heating under inert atmosphere, however, enables access to evaporation and more specific

pyrolysis products. Some of the most commonly used TA methods in analytic chemistry are explained in the following chapters.

3.1.1 Thermogravimetry

Thermogravimetric analysis (TGA) is a method of thermal analysis in which the mass of a sample is measured over time as the temperature changes. This measurement provides information about physical phenomena, such as phase transitions, absorption, adsorption, and desorption; as well as chemical phenomena including chemisorption, thermal decomposition, and solid/liquid-gas reactions (e.g., oxidation or reduction).[48]

A thermogravimetric analyser consists of a precision balance with a sample pan located inside a furnace with a programmable control temperature. Heating can be dynamic or isothermal, or any combination of these two. The heating rate for dynamic heating or to achieve an isothermal temperature has great influence on the sensitivity and accuracy of TGA. In general, a higher heating rate lowers accuracy but increases sensitivity, and vice versa. Depending on the question of interest, the atmosphere can be chosen accordingly. Redox reactions (e.g., with oxygen or hydrogen), hydration (mixture of gaseous water/inert gas) or others, as well as under inert atmosphere (e.g., nitrogen or noble gas). When corrosive gasses are used or corrosive off-gasses are produced, the sensible parts of the balance need to be protected by an additional and sufficient flow rate of inert purge gas.

Two designs dominate the market: horizontal or vertical balance beam (**Figure 3**). The horizontal design is strongly influenced by buoyance, which lowers its accuracy, but also supports the transport of off-gasses away from the sample pan. The accuracy is higher for the vertical design, but a higher flow rate is needed for experiments with off-gassing. Flowrate and thus, the dilution, is an important factor in subsequent EGA.

3.1.2 Differential thermal analysis

Differential thermal analysis (DTA) enables qualitative and (semi-)quantitative investigation of all processes involved in enthalpy changes.[49] Two pans are installed in a symmetrical set-up, one for the sample and another for an inert reference. The reference material must not undergo any phase change in the investigated temperature range, which is why alumina (Al_2O_3) is often used. The temperature of each pan is measured precisely and the difference between both is determined. The DTA curve is obtained, when this differential temperature is plotted against time or temperature. During heating, heat flows identically into the sample and reference material. Changes in the sample cause either a temperature rise (exothermic) or temperature decrease (endothermic) relative to the inert reference. Thus, a DTA curve provides information on the transformations, such as glass transitions, crystallisation, phase change, and

decomposition. The on-set of phase change is a specific property of a substance and can be used for identification, while the peak area provides (semi-)quantitative information.
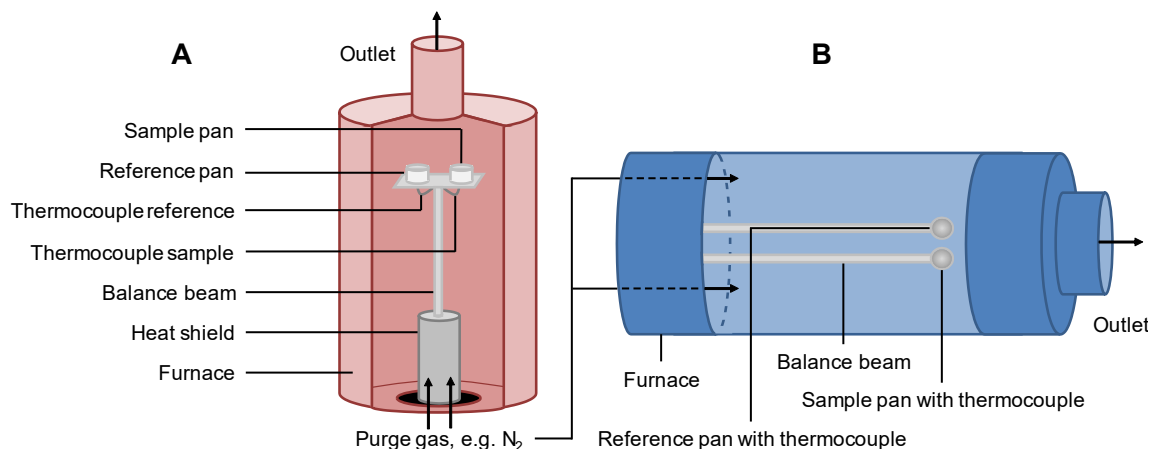
Figure 3. Scheme of two STA setups used in this PhD thesis: horizontal design, capable of TGA and DSC (**A**), and vertical design, capable of TGA and DTA (**B**). Additional parts for controlling, heating and computing are not depicted.

3.1.3 Differential scanning calorimetry

Differential scanning calorimetry (DSC) is a development of DTA. In principle, the differential temperature is also measured, but it is directly converted into the heat flow difference by calibration.[49] This way, transitions and calorimetric values, such as enthalpies or heat capacities, can be easily determined. There are two common set-ups for DSC devices: constant heat-flux and power compensated DSC. Constant heat flux is also the usual approach used for DTA and simultaneous thermal analysis (STA). Reference and sample pan are located in the same furnace and subjected to the same heat flux. In STA, TGA and DTA (or DSC) are measured simultaneously. Power compensating DSC is done in two separate, thermally insulated furnaces for reference and sample, respectively. The temperature is controlled, so that it is identical for both chambers. The power to achieve and maintain this status is recorded, instead of the temperature difference in heat flux DSC. DSC is a valuable tool for many applications, particularly in the field of polymer science.

3.2   Gas chromatography

Gas chromatography (GC) is a widely used separation technique for volatile and semi-volatile compounds within mixtures. It belongs to the group of adsorption and partition chromatography, in which different interactions of the individual components with the stationary and mobile phase are exploited.[50,51] A gas chromatograph is mainly composed of an inert gas supply, an injector, an oven equipped with a column, and a detector (**Figure 4**, **A**). The sample must be gaseous or volatilised prior to analysis. An inert gas (e.g., nitrogen, helium or hydrogen) is used as mobile phase and transports the gaseous mixture from the heated inlet

into and through the column. Different kinds of columns exist, but todays most used columns for complex hydrocarbon mixtures are probably wall-coated open tubular columns (WCOT). They are based on gas-liquid interactions and have the highest separation power.
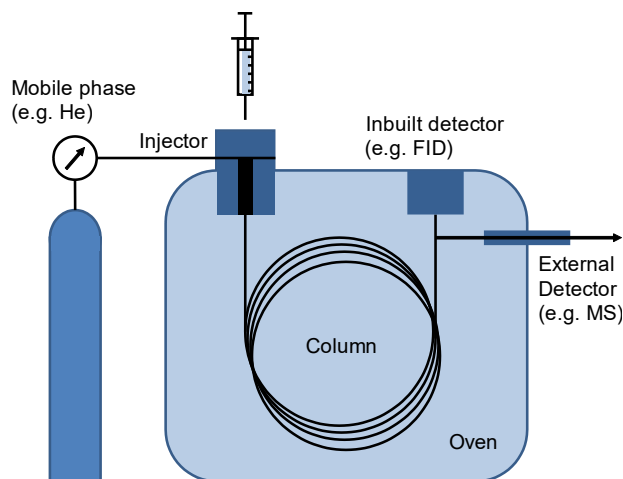
Figure 4. Scheme of a gas chromatograph; a syringe can be used to introduce liquid or gaseous samples into the depicted injector, while a pyrolysis injector can be used for solid samples. Different inbuilt or external detectors are available.

Liquid and gaseous samples are introduced into the injector by a syringe. The injection is the starting point of the measurement and, thus, has to be quick to avoid peak broadening. The inlet (or liner) in the injector is heated to guarantee total and immediate evaporation. The gaseous mixture is then transferred into the column. Solid samples can be analysed when a pyrolysis introduction unit is used. Different polysiloxanes and variations of their end-groups are used to produce a spectrum of phases with a variety of different polarities, thicknesses, and stabilities. A 100% polydimethylsiloxane (PDMS) phase can be used for nonpolar mixtures. Here, separation is mainly based on differences in the vapour pressures and weak van der Waals interactions. A slightly polar phase, which enables induced dipole and/or π-π interactions, is obtained when exchanging 5% of the methyl moieties by phenyl. The polarity can be increased by raising the ratio of phenyl groups, or by incorporation of other polar moieties.[52,53]

Besides, the choice of the mobile phase, its flow rate and the temperature programme are important as well. The temperature programme is chosen based on the volatility of the present analytes and the difficulty to separate them. Dynamic heating is often used with or without isothermal steps for complex mixtures with a range of different boiling points.

A detector records the eluting compounds at the end of the column. Different one-dimensional or structural elucidating techniques are available. The flame ionisation detector (FID), for example, is suited to register hydrocarbons, as it is sensitive towards C-H-bonds, but it does not yield any structural information.[54] The retention time is a measure of the time taken for a

substance to pass through a chromatography column. It is calculated as the time from injection to detection and can be used for identification. However, there are analytical problems, for which structural information are mandatory. These information can be provided by techniques such as infrared spectroscopy (IR) or mass spectrometry.

3.3   Mass spectrometry

The principle of mass spectrometry (MS) is to measure the mass of molecules.[55,56] Since single molecules cannot be handled and put on a balance, other means have to be applied for that purpose. Therefore, ionisation is used to transform the neutral molecules into ions, which can be easily controlled with help of magnetic and electric fields. Mass spectrometers are composed of an inlet, an ionisation source, a mass separator (mass analyser), and a detector. The mass analyser separates the ions according to their mass over charge ratio (*m/z*). Afterwards a detector records the intensity. Collisions of ions with other particles lead to charge transfer and should be avoided, for which reduced pressure is used. Though, ion sources and collision cells exist, in which collisions are tolerated or even wanted. Mass spectrometry developed into a powerful and diverse analytical tool. By now, it is possible to study a large quantity of samples in the gaseous, liquid and solid state. Even difficult samples, such as polymers, proteins or complex mixtures, are investigated. Couplings to other techniques, such as gas chromatography or liquid chromatography, produce valuable information. High-end devices, such as the Fourier-transform ion cyclotron resonance technique, have such high resolution, that not only highly complex mixtures are resolved, the sum formula of compounds can also be directly calculated based on the measured 'exact' mass.

3.3.1 Ionisation techniques

A wide variety of ionisation techniques exist. They can be divided by the pressure, under which they are operated, and their tendency to fragmentate the analytes.[55,57,58] Ionisation techniques operated at highly reduced pressure, belong to the vacuum ionisation techniques.[59] Samples have to be either introduced by a limited gaseous stream, or have to be placed inside prior to analysis (direct inlet probe) to avoid breaking the vacuum. As the name suggests, atmospheric pressure ionisation is operated under ambient pressure, which enhances the applicability of MS especially towards liquid samples. But in contrast to vacuum ionisation, collisions between ions and neutral particles can induce charge transfer to more stable ions, resulting in possible ion suppression of less stable ions. Another distinction is made between hard and soft ionisation.[55] An ion is generated, when the energy transferred to a molecule is exceeding its specific ionisation energy. Hard ionisation techniques strongly exceed the ionisation energy, which leads to heavy fragmentation of most molecules. Soft ionisation circumvents heavy fragmentation by use of less excess energy. This way, less fragments and more molecular ions are formed. The inlet and ionisation determine strongly, what is studied. It has to be guaranteed, that the compounds of interest are sufficiently introduced and ionised.

Electron ionisation

Electron ionisation (EI) was one of the first mass spectrometric ionisation techniques and is still very popular today. It belongs to the hard ionisation techniques, because of heavy fragmentation.[55] A hot cathode emits electrons, which are usually accelerated at 70 V ($\cong$ 70 eV). The analytes are introduced in a perpendicular orientation to the beam and pass through it. When a molecule gets hit by the beam, an electron of the molecule is expelled, leaving a positive charge and high excess energy on the molecule behind. Typically, the ionisation energy of organic molecules are in the range of 7–15 eV, which is substantially lower than 70 eV. At this value, however, the de Broglie wavelength of the accelerated electrons matches quite well with the typical bond lengths of organic molecules, maximising the probability of an energy transfer. In addition, the ionisation efficiency does not change much for small fluctuations in this region, resulting in very reproducible spectra of EI. The excess energy is dissipated by various processes, many of which can be fragmentation reactions. The fragmentation observed is defined by the chemical structure of the analyte and the resulting highly reproducible pattern of fragmentation can be used for structural elucidation and identification of unknowns.[60] This reproducibility has been exploited to develop user-generated and commercial libraries of spectra, which can be rapidly searched for comparable spectra. Electron ionisation is in particular helpful, when chromatographic separation is used and no or only little co-elution happens. In case of no pre-separation, the vast amount of fragments can hinder the interpretation of mass spectra of complex mixtures.

Single Photon Ionisation

Single photon ionisation (SPI) is a photo ionisation (PI) technique.[59] Photons with an energy equal to or higher than the ionisation energy of the analytes ($E_{photon} \geq E_{IE}$) are exploited for ionisation (**Figure 5**). Since the energy is usually adjusted to be just above the ionisation energy, SPI is accounted to the soft ionisation techniques. The photons are usually generated by lasers, lamps or at a beam line. One possibility for the generation of photons with a wavelength of 118 nm (= 10.5 eV) is to use a xenon-filled gas cell and a Nd:YAG laser (neodymium-doped yttrium aluminum garnet; $Nd:Y_3Al_5O_{12}$). Lasers produce pulses with high photon densities, while lamps (deuterium discharge or electron beam excimer lamps) are less sensitive but continuous and cheap. The best sensitivity and brilliance can be obtained at beam lines, but the measurement time at such facilities is highly limited.

Single photon ionisation is often considered a universal ionisation technique, because all substances with an ionisation energy less than that of the SPI photons are ionised.[59] This is true from the perspective of a petroleum analyst, but many inorganic substances, such as water (E_I = 12.6 eV), nitrogen (E_I = 15.6 eV) or carbon dioxide (E_I = 13.8 eV), are excluded. This can be quite advantageous, when evolved gas analysis is applied, where these gases would interfere with the analysis. While the cross section (probability for interactions between the molecule and the energy transmitting particle) of different substances is almost identical

for EI, it differs greatly for SPI.[61,62] This means for qualitative analysis, that the quantity cannot be directly estimated, and calibration curves or cross sections have to be determined. The overall lower cross section of SPI compared to EI explains why the photon density has such a huge effect on sensitivity. Too high photon densities however, can lead to multiple absorption and increased fragmentation.

The big advantage of soft ionisation is, that no or only a few fragments and mostly molecular ions are formed. Resulting spectra are clear, which is in particular useful when complex mixtures are analysed. When using EI, many different constituents yield the same fragments and cannot be distinguished from each other, which makes pre-separation necessary.

Resonance Enhanced Multi Photon Ionisation

Resonance enhanced multi photon ionisation (REMPI) belongs also to the PI techniques. Usually, photons with a lower wavelength (UV range) than those used for SPI (vacuum UV range) are used here.[55,63] And instead of a single photon absorption, multiple photons have to be absorbed to reach the ionisation energy (**Figure 5**). In contrast to photons with energies above the ionisation threshold, the first photon(s) can only be absorbed, if the molecule has a free energy level to which it can be promoted. The resulting excited state (M*) returns to the ground state over time by radiative or non-radiative relaxation. The processes and states differ for different molecules, as well as the life-times of these states. The probability to absorb (an)other photon(s) is higher for molecules, which can stabilise the excited state for longer times. The need of a molecule to meet all three criteria for ionisation (accessible, long-lived excited state and exceeding the ionisation energy), leads to selective ionisation.
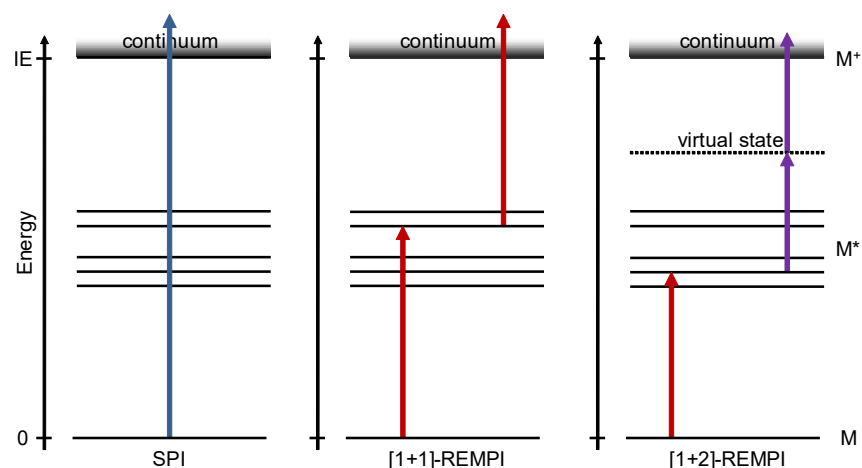
Figure 5. Scheme of different photo ionisation techniques; photons for SPI inhabit enough energy to reach the ionisation continuum in one step; [1+1]-REMPI is performed by two subsequent absorptions of photons of the same wavelength, while the example of [1+2]-REMPI is achieved by mixing two different wavelengths.

Very high photon densities are required to obtain a sufficient probability for a molecule to get hit multiple times, which is why REMPI is exclusively performed with help of lasers. By varying parameters like wavelength and pulse duration, the selectivity towards different compounds or compound classes can be controlled. By shortening the laser pulse, less long-lived states can be used. Altering the wavelength can be used to address the accessibility of the intermediate excited state, but also for reaching the ionisation continuum. Mixing of different wavelength enhances the possibilities, but also the instrumental requirements. One of the easiest setups is probably [1+1]-REMPI with a wavelength of 266 nm (fourth harmonic generation of a Nd:YAG laser) or 248 nm (krypton fluoride laser). Both wavelength are excellently suited to address aromatic and heteroaromatic compounds. The '[1+1]' suffix refers to the absorption of one photon for excitation and reaching the ionisation continuum respectively.

3.3.2 Mass analysers

Many different physical principles have been exploited to construct mass spectrometers. An ideal mass analyser does not exist, each and every one has its own advantages and drawbacks.[55,64] Characteristic properties of mass analyser are: resolution, mass range, spectra per second, transmission and duty cycle (and scan speed).

Sector field instruments use a static electric or magnetic sector (field) or some combination of the two (separately in space) as a mass analyser.[24,65] Ions passing through the field are forced on curved flight trajectories, which are dependent on their *m/z* ratio, by the Lorentz force. Usually, the magnetic field is altered to scan for different *m/z* values, or multiple ions are detected simultaneously by use of locally resolving detectors or use of multiple detectors.

Quadrupole mass spectrometers consist of four hyperbolic or cylindrical rods, which are arranged in a square (xy-plane) and extend into the z-plane. They are used for the generation of an electric field for the manipulation of ions, which travel between the rods. The opposite-faced rods are held at the same potential, which is composed of a direct current and an alternating current. For every *m/z* value (or a range of *m/z* values), certain conditions exist, under which a stable trajectory is achieved to pass through. All other ions cannot reach a stable trajectory and eventually hit a rod or wall. Therefore, quadrupoles need to scan over a selected mass window to obtain a mass spectrum and can be used as excellent mass filters for other purposes.

The best resolution power and mass accuracy can be attained with Fourier transform (FT) mass spectrometers. Fourier-transform ion cyclotron mass spectrometry (FTICR-MS) uses a homogeneous, static magnetic field, while the Orbitrap technology uses an inhomogeneous, static electric field. Common to both is the detection of the free induction decay (FID), subsequent Fourier transformation of the transient into the frequency domain and translation into the *m/z* scale afterwards. The high performance rests on the periodic detection of the image current. Ions, which pass by the detection electrodes on circular tracks, induce a charge

without getting destroyed. The two FT-MS analysers are classified as ion traps, because of their accumulation and storing behaviour. The destruction-free detection enables furthermore collision induced dissociation and subsequent MS/MS experiments. Different designs and concepts of ion traps exist, some are based on the FTICR (e.g., Penning trap), Orbitrap or quadrupole (e.g., linear quadrupole ion trap or quadrupole ion trap) technology and can be used for mass analysis. Others (such as RF multipole ion traps) are only used for transport, accumulation, storage and as collision cell prior to insertion into a mass analyser. Devices, which are composed of different ion storing and/or analysing techniques, are called hybrid devices. Ion traps are usually very sensitive towards the ion loading and benefit from controlled ion insertion. Another technique is time of flight mass spectrometry, which is explained in detail in the next chapter.

Time of flight mass spectrometry

The principle of time of flight (TOF) mass spectrometry is to uniformly accelerate ions into a field free drift region of a known length and measure the time for the ions to hit the detector at the end of it (**Figure 6**).[55] Either the ionisation or the ion extraction has to be pulsed for that purpose. Separation is achieved, because of the ions inertia: when applying the same amount of kinetic energy to each ion, the velocity varies depending on the respective *m/z* value. The acceleration of ions is achieved by use of an electric field, in which the potential energy is converted into kinetic energy in the process. In reality, the ions cannot be perfectly separated, because of fluctuations in their initial energy (e.g., thermal and kinetic energy) and location within the acceleration potential. The coulomb repulsion of like-charged ions leads to similar fluctuations. The local dispersion can be reduced, and thus the mass resolution improved, by refocusing, which can be achieved by use of an ion mirror (reflectron).
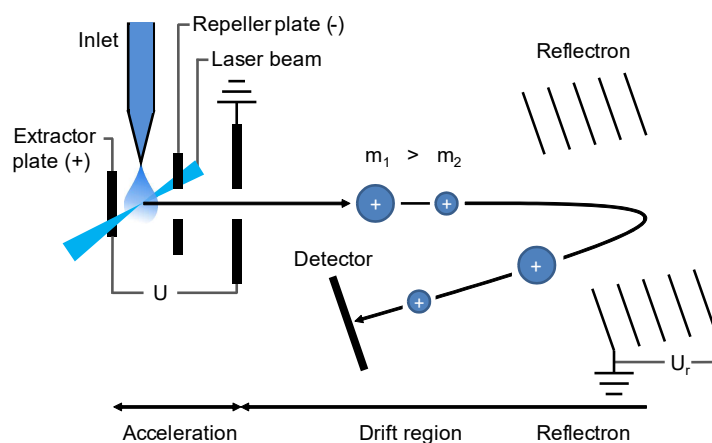
Figure 6. Scheme of a reflectron time of flight system, equipped with photo ionisation.[55]

The big advantages of TOF mass spectrometers are no limitation of the *m/z* range, a very fast duty cycle (and thus high repetition rates), high transmission and sensitivity, as well as relatively low cost and a compact design. They can be used for many purposes, such as accurate mass determination or MS/MS. The arrangement of multiple reflectrons in a multitude of V-shapes, enable measurements with high resolution, reaching above R = 50,000.

3.3.3 Detection

The earliest detection of ions was realised with the help of photo plates. Today, this rather unpractical method is substituted by electronic devices. The easiest detector for most mass spectrometers, which rely on ion counting, is the Faraday cup. A cup-shaped electrode is impinged by the mass-analysed ions, transferring their charge onto the electrode. The resulting current flows through a high resistor, creating a measureable voltage. Detectors used for FT-MS function in a different way and detect the image current, which is induced by ions passing by electrodes.[55]
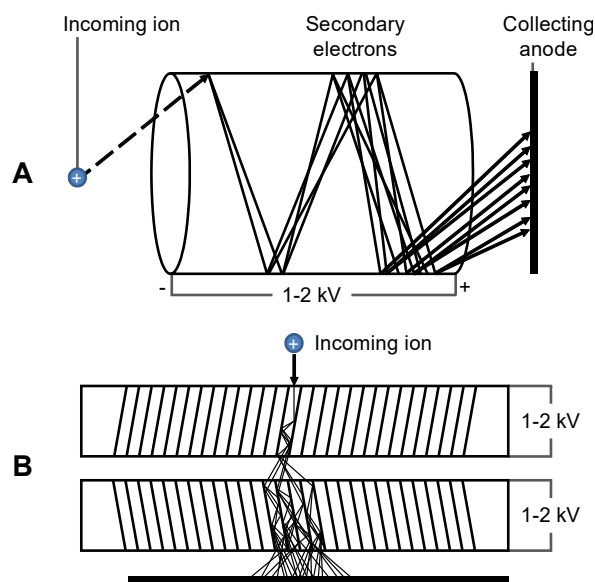
Figure 7. Scheme of a linear channeltron (**A**) and a microchannel plate (MCP) in a Chevron configuration (**B**).[55]

The principle of secondary electron multiplication is used by the secondary electron multiplier (SEM), channeltron and microchannel plate (MCP) detectors. In general, ions impinge on the surface of a charged metal or semiconductor electrode, which causes (secondary) electrons to be emitted. They are accelerated in a strong electric field, hitting similar surfaces and causing an electron cascade, which is ultimately detected by an anode. In a SEM this is usually realised by 12–18 discrete electrodes, each having a 100 V more positive potential than the electrode before. Channeltrons are composed of one continuous tube with an applied voltage, which continuously decreases over the length of the tube (**Figure 7**, **A**). Better results are

achieved with a horn-shaped tube. The curvature reduces the average free length of path of ions produced by collisions of residual gas and electron impact. The MCP detector is a direct development of the channeltron (**Figure 7**, **B**). In fact, modern MCPs are composed of millions of miniaturised linear channeltrons, symmetrically perforating a thin plate. The axis of these micro-canals is slightly tilted by a few degree in relation to the surface of the plate to avoid, that ions pass without colliding with the walls. The amplification of one plate is roughly 10^3–10^4, which is much lower than the amplification of a SEM or a channeltron (~10^6–10^8). By stacking two or three MCPs above each other in a V- or Z-configuration (each plate rotated by 180°), the amplification can be increased to 10^6–10^8. MCP detectors can be modified to yield spatial resolution. The signal from the electron-collecting anode is again amplified in a subsequent preamplifier by the factor of 10^6–10^9. Then, an analogue-to-digital converter translates the continuous values into discrete values, which is necessary when a computer is used for recording and data handling.

4   Concept of this work

Despite the existence of many different ionisation and introduction techniques, mass analysers and complementary analytical methods, samples and analytical problems remain, which cannot be handled well or even at all. Since many techniques rely on solubility (e.g., NMR, LC), volatility (e.g., GC, vacuum ionisation-MS) or polarity (e.g., atmospheric ionisation, MALDI), the analysis of especially non-volatile, insoluble and nonpolar substances remains challenging. In particular, when these substances are part of or completely make up complex mixtures.

Development of improved devices or new techniques can fill these analytical niches. Another approach is the combination of results of several techniques, or the hyphenation of different devices into one setup. Either way can yield more than just the sum of the information. Available information about the origin of the sample or bulk information (e.g., elemental analysis or IR) prior to analysis, help in choosing a suitable setup. A routine bulk method used for polymers is thermal analysis. Some polymers fulfil the above mentioned characteristics. They are composed of many similar yet different molecules and thus can be regarded as a complex mixture. Therefore, TA might be very well suited for other challenging samples as well. Beside transitions (glass transition, melting and evaporation), the decomposition of the material can be studied. By hyphenating TA to a molecular analyser (e.g., IR or MS), more valuable information can be obtained. However, decomposition reactions increase the complexity of a mixture. This is why either separation techniques or, in case of MS, soft ionisation approaches, such as SPI or REMPI, need to be employed. Photo ionisation enables time resolved, online measurement of the evolving gas (**Figure 8**). Consequently, this work aims to unravel the potential of thermal analysis and subsequent soft photo ionisation mass spectrometry for challenging petro-based samples from different stages of the process chain:

asphaltenes from within potential feed, fouling occurring during processing, polyethylene as an end product and recycling of polyethylene terephthalate by pyrolysis (**Figure 9**).
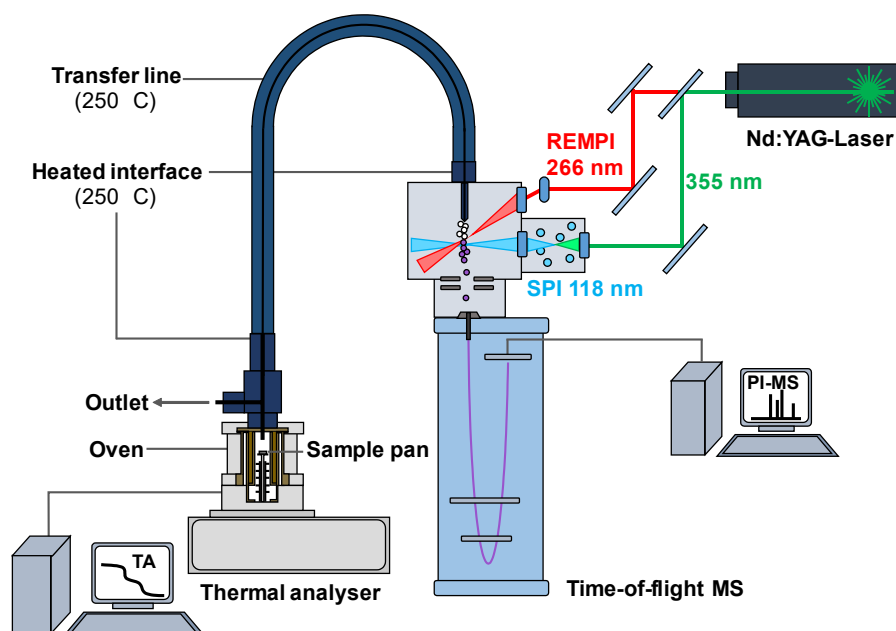
Figure 8. Setup of the thermal analysis–photo ionisation mass spectrometry (TA-PI-MS), equipped with SPI (118 nm = 10.5 eV) and REMPI (266 nm = 9.6 eV). Samples are heated within the thermal analyser and evaporate or decompose. The evolving gas is then transferred into the ion chamber of the TOF-MS and is subsequently ionised either by SPI or REMPI.

5   Results

During crude oil production and refining, several challenging fractions occur. In this work, asphaltenic fractions, fouling samples and polymers (polyethylene and polyethylene terephthalate) are studied by TA-PI-MS. In a sense, these samples simulate a real life scenario, in which crude oil fractions are used as feed for a steam cracking facility to produce light olefins for the subsequent production of polymers, which are recycled at the end of their life time. Asphaltenes within the crude oil fractions can cause trouble in up- and down-streams, such as fouling inside a steam cracker. The main product, ethylene, is transformed into different types of polyethylene materials, which structural elucidation is important to further understand and improve the adaptability of its properties.

Figure 9. Visualisation of the concept: four samples from different production sections.

Pyrolysis of polyethylene terephthalate to obtain reusable feed is one possibility of recycling. New findings about these samples and the evaluation of TA-PI-MS applicability is presented.

5.1 Analysis of asphaltenes

During oil production and refining, several problems such as flow assurance or processing issues are often triggered by asphaltenes. Therefore a molecular understanding of this highly intricate fraction is of particular interest.[16,66,67] Asphaltenes are defined as a fraction soluble in toluene, but insoluble in *n*-alkane (such as *n*-pentane, *n*-hexane or *n*-heptane). The composition and structure are still part of discussion and investigation, and only a few standardised analysis methods, concerning mainly sum or bulk parameters, exist.[16] Asphaltenic fractions are ultra-complex mixtures with high aromatic content, a variety of heteroelements and chemical functionalities, and a broad mass range. Over the last few decades, a lot of effort has gone into deciphering their molecular architecture, whereby two opposed models are discussed: island (a large aromatic core with side chains) and archipelago (several smaller aromatic cores connected by linkers) structure. A single analytical technique is not sufficient to provide throughout information, which is why several complementary methods are often used.[68,69] State-of the art techniques for the chemical characterisation of asphaltenes on the molecular level are mainly mass spectrometric approaches, such as direct infusion atmospheric pressure ionisation ultrahigh-resolution mass spectrometry.[66–68,70] In addition, high-field nuclear magnetic resonance (NMR) spectroscopy and absorption spectroscopic approaches, such as X-ray absorption near edge structure (XANES) as well as high-performance liquid chromatography, are deployed.[67,71–74] Thermal analysis, regarding evolved gas analysis, coupled to various analytical detectors has also become a powerful tool in petroleum analysis and other areas.[67,75–77] Besides spectroscopic approaches, such as infrared spectroscopy for fingerprint pattern or small-molecule quantification, mass spectrometry is the favoured coupling technique.[75–80] Pyrolysis gas chromatography was conducted extensively with low resolving mass analysers and hard ionisation to study thermal decomposition products.[81–86] Unfortunately, until now, no single mass spectrometric technique is capable of a comprehensive analysis of the complex pyrolysis effluent. Therefore, choosing an ionisation source is crucial, and different methods will cover different chemical spaces. For the thermal analysis of petroleum fractions, most often nominal resolving mass analysers with hard ionisation are used, which enable robust pattern information.[87] Nonetheless, soft ionisation techniques become more important in mass spectrometry and thermal analysis coupling. The generation of molecular ions, instead of an intense fragment pattern, reduces the complexity of the mass spectra and allows for an easier molecular assignment. With the selection of a particular soft ionisation technique, control of selectivity can be achieved. In case of REMPI, aromatic compounds are selectively ionised,[88,89] whereas atmospheric pressure photo ionisation (APPI) reveals a high ionisation efficiency for aromatic and sulphur containing species and atmospheric pressure chemical ionisation (APCI) has a high ionisation efficiency for medium-polar and polar constituents.[90,91] Asphaltene pyrolysis has not been studied before with photo ionisation techniques, with either vacuum PI or atmospheric pressure PI.[67]

In order to gain deeper insight of the asphaltene composition, the heptane (C7) asphaltene and its parent crude oil, distributed within the 'Asphaltene Characterization Interlaboratory Study for PetroPhase 2017', were characterised on the molecular level. Three different thermal analysis mass spectrometry hyphenations with five diverse ionisation techniques were deployed: (1) thermal desorption/pyrolysis gas chromatography electron ionisation (TD/Pyr-GC-EI-MS), (2/3) thermal analysis single photon ionisation/resonance enhanced multi photon ionisation (TA-SPI/REMPI-MS) and (4/5) thermogravimetry atmospheric pressure photo-/chemical ionisation ultra-high resolution mass spectrometry (TGA-APPI/APCI-FTICR-MS). As shown for pyrolysis gas chromatography in the literature, the thermal decomposition products of the macromolecular structure give information about the respective building blocks and add valuable information to the molecular architecture debate. The different ionisation techniques cover a particular molecular space and exhibit a certain part of the chemical signature of the evolving gas. TD/Pyr-GC-EI-MS provides structural information of the medium-sized evolving products, based on retention time and fragmentation pattern. The universal and soft ionisation character of TA-SPI-MS offers a general overview of evaporation and thermal decomposition over a very broad mass range. In particular small compounds, such as cleaved sidechains, can be easily tracked. Selective REMPI, APPI and APCI however, are used to investigate aromatics, aromatics and sulphur containing compounds, and medium-polar to polar compounds, respectively. In addition, the FTICR mass analyser enables determination of the exact mass (and thus of the elemental composition) of the constituents ionised by APCI/APPI. Combination of the five diverse data sets containing different comprehensive information yields a comprehensive image.

5.1.1 Results from TA-SPI/REMPI-MS

Bulk information such as thermal analysis data are usually the first to interpret. For the asphaltene, the mass loss curve shows no significant desorption step (<3.5 wt%) but a relatively sharp pyrolysis step with a maximum at 435–460 °C. About 47–49 wt% of the initial in-weight volatilises under nitrogen atmosphere. The remaining mass is oxidised at 820 °C, leaving no measurable residue behind. A look at the elemental analysis (EA) reveals, that about 0.1 wt% of the sample is made up by inorganics (i.e., mainly nickel and vanadium) and about 99.9 wt% are made up by carbon (81.5 wt%), hydrogen (7.4 wt%), sulphur (7.4 wt%), oxygen (1.5 wt%) and nitrogen (1.3 wt%). Thus, about 99.9 wt% are expected to volatilise under oxidative atmosphere at the latest and only a very small proportion forms non-volatile oxides (e.g., NiO or V_2O_5), which is below the limit of detection of the applied TGA methods.

The crude oil however, shows strong desorption over a broad range (~40 wt%, 50–300 °C), which transitions into pyrolysis (~53 wt%, 300–460 °C) and only ~5 wt% are oxidised at elevated temperatures. The definition of pyrolysis temperature is arbitrary here. It is dependent on the stability of the investigated compounds and probably higher for relatively stable petro-chemicals, as seen for the asphaltene (offset at ~400 °C). A more precise classification can

be undertaken, when considering the mass spectrometric data. Nonetheless, it can be stated, that the asphaltene is mainly made up by non-volatile constituents of the parent crude oil. In addition, the elemental composition of the crude oil differs and is as follows: carbon (83.9 wt%), hydrogen (12 wt%), sulphur (3.0 wt%), oxygen (<0.4 wt%) and nitrogen (3.5 wt%), and the inorganic content is roughly one order of magnitude lower. The less abundant hetero-atom content and aromaticity, compared to the asphaltene, is no wonder, when considering, that asphaltenic fractions are supposedly composed of highly aromatic cores and a high hetero-atom content.
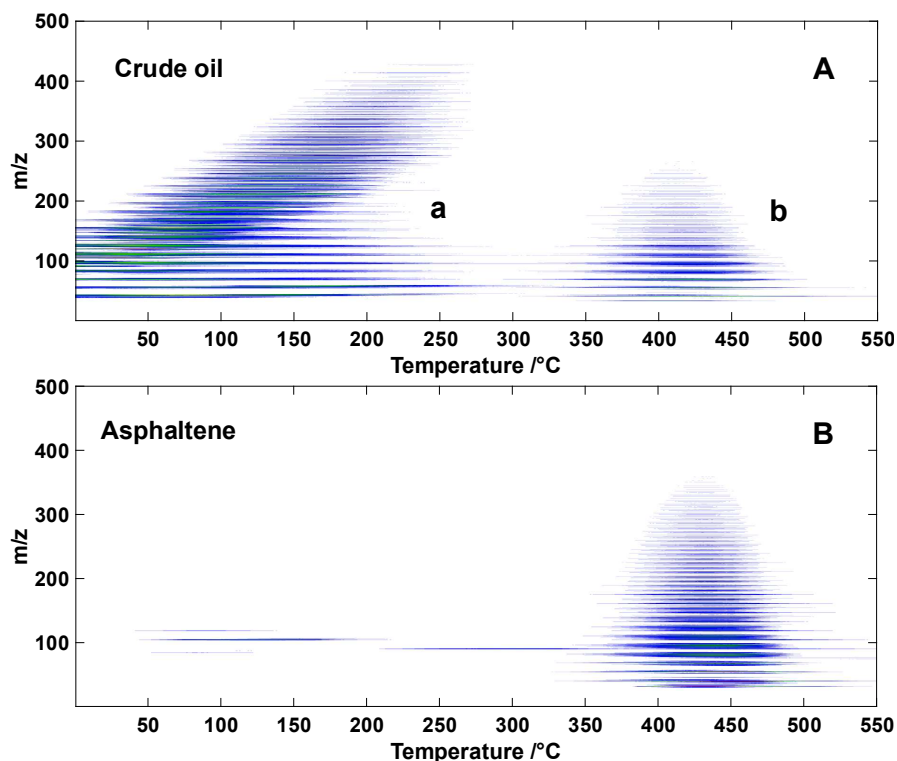
Figure 10. Survey plots of TA-SPI-MS measurements of the parent crude oil (**A**) and the respective heptane asphaltene (**B**).

Though thermal analysis has a low thermal separation power and constituents with similar vapour pressures appear simultaneously, compounds with high vapour pressure evaporate at lower temperatures than compounds with low vapour pressure, leading to the typical successive evaporation pattern (**Figure 10**, **A** [**a**]). With the beginning of pyrolysis processes, the pattern changes to the simultaneous detection of small and high m/z values (**Figure 10**, **A** [**b**]). As stated before, the asphaltene shows no significant signals during desorption (**Figure 10**, **B**). When examining the evaporation phase of the crude oil (not shown), the typical oil pattern can be recognised, ranging from m/z 34–400. Homologue series have a spacing of m/z 14 (CH_2-group), while a spacing of m/z 2 (H_2) indicates unsaturated or cyclised species. Nominal masses are assigned based on molecular ion information, general knowledge about petroleum and cross-verification by Pyr-GC-MS. Main substance classes are alkenes, (cyclo-

)alkanes and alkylated aromatics (benzenes, naphthalenes, anthracenes, phenanthrenes and many more). Cycloalkanes and alkenes share the same *m/z* values and cannot be distinguished by sole TA-PI-MS. But it is known from literature, that the signals occurring in the evaporation phase belong most certainly and exclusively to cycloalkanes. Alkenes are typically present during pyrolysis, when long chains or side-chains are cleaved.[92] Besides, a small proportion of hydrogen sulphide (H_2S, *m/z* 34) was found.
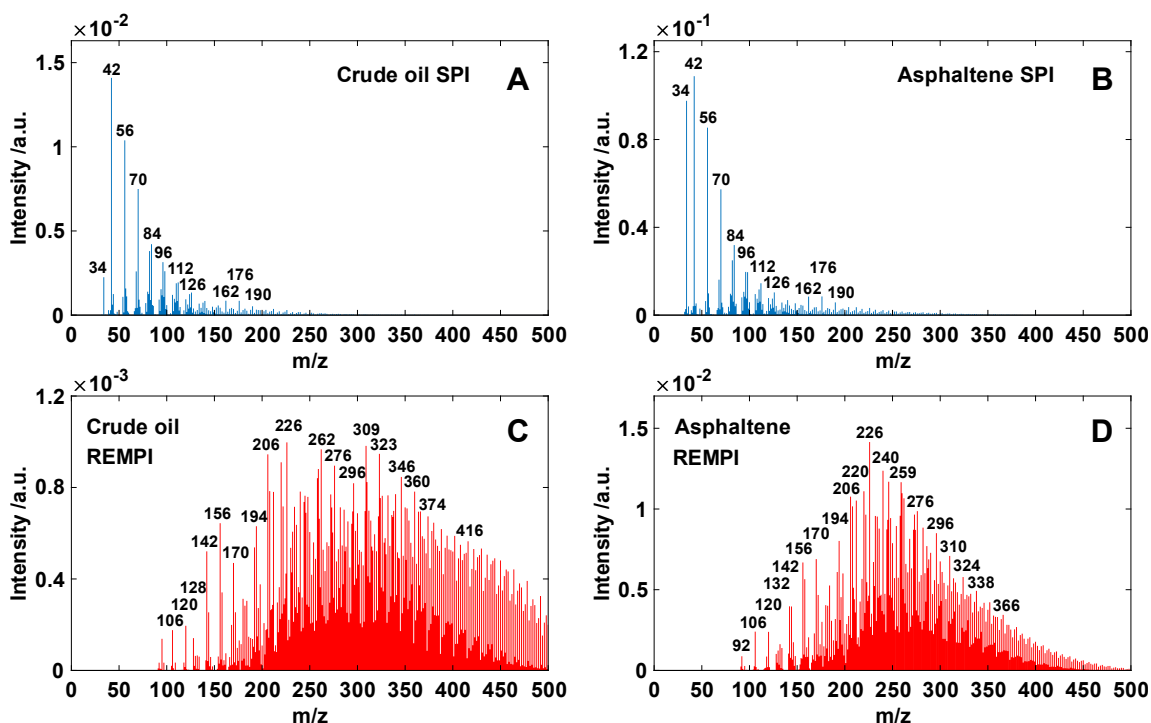
Figure 11. Summed mass spectra of TA-SPI-MS measurements of the parent crude oil and the respective heptane asphaltene during pyrolysis (400–550 °C). Adapted based on literature.[67]

When looking at the summed SPI-MS spectrum of the crude oil (**Figure 11**, **A**) during pyrolysis, high–medium signals of alkenes (*m/z* 42, 56, 70, 84, 98), dienes (*m/z* 68, 82, 96, 112, 126) and hydrogen sulphide and low signals of aromatics (*m/z* 106, 120, 134, 162, 176, 190) can be seen. The summed TA-SPI-MS spectrum of the asphaltene looks quite similar (**Figure 11**, **B**). The general signal intensities and relative signal of hydrogen sulphide are however higher. With REMPI, most of the before low abundant aromatic signals are strongly pronounced (**Figure 11**, **C** & **D**). REMPI is more sensitive than SPI for polycyclic aromatic hydrocarbons (PAH) and signals of highly abundant non-aromatics in general or non-aromatic isobars are discarded, leading to a better dynamic range for aromatics. Both samples reveal a strong and broad aromatic hump, ranging between *m/z* 92–500. The signal intensities found for the crude oil are however one order of magnitude lower than for the asphaltene. This is why overlapping signals originating from evaporation have a strong influence and lead to a broader distribution

especially in the high *m/z* region. Dealkylation of aromatics, which do not belong to the asphaltenes, can also distort REMPI and SPI spectra. Thus, clearer and more reliable results are obtained, when focusing on the asphaltene data. The average length of cleaved side-chains calculated from SPI-MS data is 9.1, which equals to *m/z* ~126. Evaluation of the REMPI pattern resulted in an average alkylation number of 2–3 for benzene, 8–9 for naphthalene and 6–8 for bigger condensed rings. The strong resemblance of both samples during pyrolysis arises from the fact that a big proportion of the contituents of the crude oil decomposing at high temperatures are probably asphaltenes. A few odd-numbered masses could be tentatively assigned to alkylated nitrogen containing aromatics, i.e. alkylated benzocarbazole (*m/z* 259, 273, 287 and 301). Pronounced *m/z* values of sulphur and oxygen containing aromatics were not found for different reasons: (1) the wavelength of 266 nm is not ideal for the ionisation of sulphur or oxygen containing aromatics, (2) highly abundant CH-isobars hamper the detection, (3) which is aggravated by the nominal mass resolution. Different strategies can be pursued to improve the utility of TA-PI-MS data. One is the additional application of chromatographic separation, either in-built (such as fast GC) or by an external, complementary technique (such as Pyr-GC-MS). A change in selectivity and an improvement in sensitivity for certain substance classes can be achieved by utilising other wavelengths (e.g. REMPI at 248 nm) or by other selective ionisation schemes such as APPI or APCI. Isobars can also be separated by high-resolution mass spectrometry. Both, more selective ionisation techniques and high-resolution MS are exploited in our applied TGA-APCI/APPI-FTICR-MS method.

5.1.2 Results from Pyr-GC-MS

Access to gas chromatographic separation of pyrolysis products was obtained by treating the asphaltene sample at 500 °C inside the introduction system of the TD/Pyr-GC-MS. Due to the broad distribution of very light to heavy products and the complex character of asphaltenes, separation is not ideal. Short constituents (≤C9) are not well resolved and are mainly detected as one hump. Evidence or indications, at least, of hydrocarbons down to C2, as well as hydrogen sulphide and small amounts of sulphur dioxide (SO$_2$, *m/z* 64) and carbon dioxide were found. Little contents of these oxygenated species come from residual oxygen introduced together with the sample or from within the sample and indicate nearly oxygen-free conditions. The hydrogen sulphide might be a product of thiol functions. A defined (cyclo-)alkane and alkene pattern becomes obvious between C10–C37. An average side-chain length of 8.2 is in good agreement with the average side-chain length obtained from SPI (9.1). Small differences arise mainly from the milder heating of TA and the slightly biased ionisation efficiency of SPI. Though the cross section of SPI diverges only by a factor of 2–3 within one compound class. It must be kept in mind that the detected products are not necessarily intact side-chains and the real side-chain length might be higher. When attached to an aromatic, side-chains do often not cleave directly at the core, so the remaining alkylation at the cores must be considered. Multiple cleavages on the same side-chain are unlikely, because dienes were found to only

minor extends. While primary pyrolysis signals are of aliphatic nature, an intricate pattern of CH and CHS aromatics exists. Alkylated benzenes, naphthalenes and benzothiophenes were assigned with good confidence, while low separation and signal height of higher aromatic constituents and heavier (especially branched) aliphatic compounds (>C18) hamper clear interpretation. Compared to the hydrogen sulphide signal, thiophenic signals exhibit a way higher intensity. The low ionisation efficiency dependence of EI is advantageous over chemical and photo ionisation, when comparing different classes, and (semi-)quantitative statements can be done more confidently.

5.1.3 Results from TGA-APCI/APPI-FTICR-MS

The big advantage of FTICR-MS is its very high mass resolution and the possibility of performing MS/MS. Isobars are separated from each other and sum formulas can be assigned to *m/z* values, because of the specific mass defect of each element. This way, about 800–1250 distinct chemical formulas in the mass range between *m/z* ~150–550 were assigned for APPI and APCI measurements of the asphaltene. These information are then summarised, plotted and interpreted. Both AP techniques found the CHS class to be the most prominent (58% of the respective TIC in both cases), followed by CH (25%$_{TIC}$ for APCI; 21%$_{TIC}$ for APPI) and CHS$_2$ (10%$_{TIC}$ for APCI; 18%$_{TIC}$ for APPI). Oxygen containing compounds are more pronounced by APCI than APPI, but still account only for ~5%$_{TIC}$ (CHSO: 2.5%$_{TIC}$; CHO: 1.9%$_{TIC}$). An overall low oxygen content for the asphaltene was proven by EA and is known by literature as well. Nitrogen containing compounds were only found to a minor extend (<1%$_{TIC}$). Under atmospheric pressure conditions, ions collide with neutral particles, resulting in possible charge transfer to an energetic more favourable partner. This way, certain compound classes such as CHS become overrepresented and others such as CH are suppressed. The limit of detection is therefore pushed down for the pronounced species at the cost of reliable detection of other classes and quantification in general. Nonetheless, detailed qualitative information about heavier unsaturated and aromatic species in particular are provided. An intensity-averaged ring number of 2–3 rings per aromatic core and an averaged alkylation grade of 8–14 was found. Both AP ionisation techniques ionise a similar chemical space, but APPI is shifted to higher *m/z* values, leading to slightly higher averaged values. Comparison of the asphaltene and the pyrolysis phase of the crude oil showed a great similarity, proving that asphaltenic species make up a high proportion of the pyrolysis of the crude oil by all applied techniques. CID experiments of aromatics with 7 double bond equivalents (DBE) revealed the presence of naphthenic structures bound to aromatic cores rather than alkenic side-chains. The CID data can also be used for planar limit-assisted structural interpretation of the aromatic building blocks, which showed that ring growth is dominated by benzene ring addition mainly by *cata*-condensation and a slight proportion of *peri*-condensation.

5.1.4 Combined data approach

Each data set revealed important information about parts of the asphaltene, which can be partly cross-validated by each other. Key features were the determination of average side-chain length by TA-SPI-MS and Pyr-GC-MS, average aromatic ring size and their respective alkylation degree by TA-REMPI-MS, in-depth analysis of aromatics by TGA-APCI/APPI-FTICR-MS and the mean molecular mass of intact asphaltene molecules by field desorption mass spectrometry. All of which culminate in the hypothesis that the investigated asphaltene has a predominant archipelago structure with an average number of three aromatic cores (which are composed of ~3 condensed rings) and ~14 CH_2-units as linkers or side-chains.

5.2   Description of steam cracker fouling

After production and pre-processing, the crude oil is subjected to a refinery. Different product streams are obtained and some are further processed. Steam cracking units can be used to crack compounds into smaller and more unsaturated products. However, asphaltenes present in the feed can be problematic here as well and are one potential source of fouling precursors. Besides, cracking products are also highly reactive. In refineries, fouling is defined as the deposition of material within a processing unit or on the solid surfaces of the unit to the detriment of function. It includes solid deposit formation, corrosion, and phase separation among others. The major effects are (1) loss of heat transfer as indicated by the decrease in charge outlet temperature and increase in pressure drop, (2) blocked process pipes, (3) under-deposit corrosion and pollution, and (4) hot spots in reactors. Increased maintenance costs and production losses of several million euros per year and cracker are the result.[93–95] A large part of the literature is focused on the coke formation in the hot section, but fouling can occur in almost all parts of a steam cracker facility.[93–96] Less investigated, organic fouling (i.e. soft fouling), can be found up- or downstream of the hot section at temperatures 80–200 °C. At these temperatures, dehydrogenation (i.e. coking) is not as pronounced as at higher temperatures so that radical polymerisation and Diels-Alder reactions play a more important role. This leads to complex mixtures with oligomeric and polymeric contents.[97–99] The reaction rates of both reactions increase with increasing temperature, though free-radical polymerisation already contributes significantly at temperatures >70 °C.[98] Radical polymerisation occurs, when unsaturated compounds are attacked by free radicals. Radicals can form due to heat, ingress of oxygen, catalyst activation (e.g. rust particles) or autopolymerisation of styrene.[98] Diels-Alder fouling occurs, when dienes such as butadiene and dienophiles such as acetaldehyde are present. Amphoteric species such as cyclopentadiene can react as diene as well as dienophile. Fouling reactions are often mitigated by dosing reagents into the feed stream. Free-radical inhibitors such as TEMPO are used to prevent radical polymerisation reactions, while dispersants are used to mitigate Diels-Alder reactions. Dosing has to be yet estimated, because of a lack of analytical methods for the description and quantification of fouling. Thus, novel and reliable methods have to be

developed. EGA proved to be an excellent tool in polymer and petroleum science.[75,76,78] And preliminary studies revealed promising results for the analysis of fouling as well, but the complexity of the evolving gas mixture hampered interpretability of data gathered by EI-MS and IR spectroscopy. When using soft ionisation however, this problem can be circumvented. The approach of EGA with soft ionisation was already successfully applied for crude oils, some of its fractions, polymers and solid fuels such as coal and biomass.[67,78,100–107]

5.2.1 Sample description and pretreatment

The two investigated fouling samples were received from Saudi Basic Industries Corporation (SABIC, Saudi Arabia) and were attained from different parts inside of a steam cracker facility during a turnover period. A sample (DS) was retrieved from downstream and the other (US) from upstream the hot section. One advantage of TA-PI-MS is that the technique itself needs no pretreatment. Small chunks of sample can be put into a pan, which is directly introduced and measured. The 'wet' appearance of the two samples and the first preliminary results revealed however a considerate amount of remaining feed/product from the operation of the steam cracker. Besides, both samples appeared to be very heterogeneous (brown, voluminous sponges with black dots). In order to obtain reproducible and representative results, it was necessary to develop a gentle grinding and drying procedure, which does not affect the underlying matrix. This was achieved by cryogenic grinding (in liquid nitrogen) and subsequent drying under mild conditions (40 °C, 96 h, 15 mbar). When comparing data from before and after pretreatment, differences during the evaporation phase become apparent, while at higher temperatures (>130 °C) the thermal behaviour and mass spectrometric pattern remains unchanged.

5.2.2 Thermal analysis of fouling materials

The flat TGA signal at the beginning of the thermal programme indicates the absence of remaining volatiles. Then, beginning at 130 °C, a slow mass loss of both samples can be recognised (**Figure 12**, **A**). Between 230–330 °C, two additional subtle but distinct mass loss steps can be seen for US, while DS reveals a single pronounced mass loss step. A minimum is reached for DS at ~330 °C. From there onwards, the mass loss rate increases drastically, peaking at ~420 °C. It decreases afterwards until all degradable constituents are expended. The mass loss rate of US remains almost constant and slowly decreases after 420 °C. The data has been normalised by the respective total mass loss to improve comparability between the samples. The remaining mass (62 wt% US; 29 wt% DS) results mainly from carbonation reactions (i.e., coke formation) and a substantial proportion of non-volatile inorganics, as shown by EA (**Table 3**). Sample US has a higher ash content (34.50 wt%) than DS (7.94 wt%). A very high proportion of it is made up iron (US, 31.56 wt%; DS, 3.29 wt%). Besides, many other hetero elements are found, the most abundant being nitrogen (US, 3.05 wt%; DS, 0.39

wt%) and sulphur (US, 3.19 wt%; DS, 0.09 wt%). Reversely, sample DS is much more organic and the ratio of hydrogen/carbon indicates further a higher aromaticity.
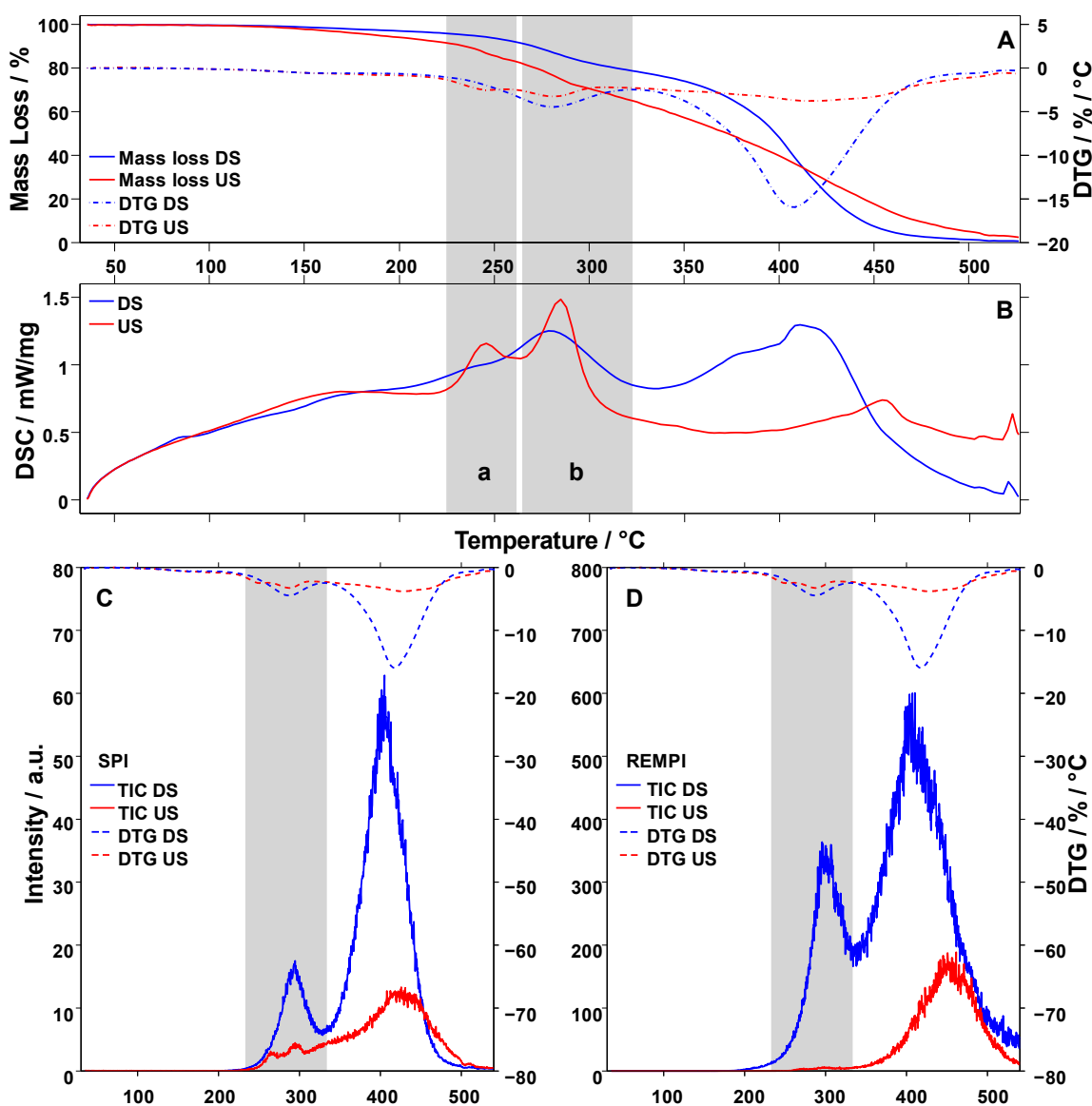
Figure 12. TGA (**A**) and DSC (**B**) data of DS and US reveal several different degradation processes with the most pronounced being between 230−330 °C (**a** and **b**) and 330−500 °C (not indicated). Panel (**C**) shows the evolved total ion current (TIC) obtained by more universal SPI and panel (**D**) shows the TIC during selective REMPI. The DTG (dashed line) is plotted for comparison and reveals a good correlation to the SPI TIC response. Adapted based on literature.[33]

Some of the above described mass loss processes can also be tracked by DSC (**Figure 12**, **B**), while the detection of enthalpy changes without mass loss are of particular interest. Clear but partially overlapping DSC signals are detected for the mass loss steps of US between 230–330 °C (**a** & **b**). The decomposition between 330–500 °C however, is hardly detected and

reveals only a relatively small peak at ~450 °C. The enthalpy change of DS shows a more overall congruent behaviour compared to the mass loss. The broad mass loss step between 230–330 °C as well as a similar trend between 330–500 °C are visible. The degradation of both samples is completely endothermic. Additional experiments with repetitive heating and cooling steps (ΔT ~100 °C) showed no signs of reversible reactions, which are common for intramolecular Diels-Alder reactions.

5.2.3 Mass spectrometric analysis of fouling materials

The detection of evolving gases is directly coupled to the mass loss. Thus, when applying a universal ionisation technique such as SPI, the total ion current (TIC) looks qualitatively similar to the TGA curve (**Figure 12**, **C** & **D**). In contrast to REMPI, which only selectively ionises aromatics. Nevertheless, the effluent of DS seems to be comprised of considerate amounts of aromatics in both phases, with a slight shift to a higher temperature of the first local maximum and a different ratio of both peak areas. US exhibits aromatic signals only at elevated temperatures (330–520 °C), peaking similar to the before described endothermic signal at ~450 °C. Though normalisation was conducted, the SPI-TIC and REMPI-TIC intensity of DS is much higher than of US (by a factor of 2.85 and 5.24, respectively). This indicates, that DS is composed of compounds with a higher cross section than US. The order of cross sections of different CH substance classes in SPI is in general: $\sigma_{aromatics} > \sigma_{alkenes} > \sigma_{alkanes}$.[61] This finding, together with EA, reveals that DS is much more aromatic than US.

Table 3. Elemental analysis and ash content of dried fouling samples.[33]

Sample	Elemental analysis /wt%					H/C /mol/mol	Ash content /wt%
	C	H	N	S	Fe		
DS	70.18	6.37	0.39	0.09	3.29	1.09	7.94
US	39.25	4.43	3.05	3.19	31.56	1.35	34.50

A very small mass loss with no mass spectrometric detection can be recognised for both samples until ~170 °C. An explanation might be, that non-ionisable compounds evolve. Two possible reactions with undetectable species are dehydration (IE_{H2O} = 12.6 eV) or decarboxylation (IE_{CO2} = 13.8 eV). Two phases were arbitrarily defined: phase 1 (<330 °C) and phase 2 (330–550 °C). Labile compounds such as Diels-Alder adducts are expected to break during phase 1, while C-C-bond cleavage of stabile compounds such as radical polymerised types should happen during phase 2. It was further shown by TA, that both samples can be roughly separated into these phases. Analysis of the molecular patterns is performed by summing the spectra for each phase. The signals are assigned based on the molecular weight information and data from Pyr-GC-MS.

Results

Qualitative description of downstream fouling

Small signals of hetero atom containing substances such as hydrogen sulphite (*m/z* 34), acetaldehyde (*m/z* 44), sulphur monoxide/methanethiol (*m/z* 48) and acetone (*m/z* 58) were found for DS in the first phase. Other lowly abundant signals (*m/z* 40, 42, 42, 54 and 70) can be assigned to alkynes, alkenes, or dienes such as butadiene. Highly abundant signals at m/z 66, 80 and 94 are assigned to cyclopentadiene, methylcyclopentadiene and C2-cyclopentadiene, respectively. Supportive Pyr-GC-MS measurements are used for cross verification. Several peaks with a molecular mass of *m/z* 92 were found and only a small peak can be accounted to toluene, while the other might be non-aromatic methylfulvene. A look on the summed REMPI spectrum reveals no signals at *m/z* 78 and 92, which supports the assignment to non-aromatic isomers.

Beginning with *m/z* 104 a transition towards aromatics can be seen. Some signals found by SPI and REMPI are identified as alkylated styrenes (*m/z* 104, 118, 132), alkylated indenes (*m/z* 116, 130) or alkenylbenzenes (*m/z* 130, 132, 146). Other strong signals can be identified as alkylated aromatics such as alkylated naphthalenes (*m/z* 128, 142, 156), acenaphthene (*m/z* 152), acenaphthylene (*m/z* 154), biphenyl (*m/z* 154), fluorene (*m/z* 166), anthracene/phenanthrene (*m/z* 178) and pyrene (*m/z* 202). Small signals of long, saturated hydrocarbons (C10–C17), which partly share the *m/z* values of aromatics and thus are hardly visible in SPI, were found as well.

The spectrum changes in phase 2 (330–550 °C) to an even more intense and complex aromatic pattern. While phase 1 contained a mono-modal distribution, phase 2 exhibits a multi-modal distribution, reaching up to *m/z* 380. Two modes are well detected by SPI and REMPI, while a third is only lowly abundant in SPI (peaking at *m/z* ~340). Multi modes can indicate a more or less regular structure of a chemical motif such as pyrolysis patterns of polymers (monomer subunits).[105] The difference between the maxima of two adjacent modes is about *m/z* 104, which might correspond to an alkylated styrenic motif. A few lowly abundant small *m/z* values appear, which might stem from side-chain cleavage. But compared to the extreme abundance of aromatics, these small *m/z* values including cyclic dienes are negligible.

The main structure of DS (~80 % of the total weight loss) can be described as an unregularly polystyrene-like type, which decomposes into alkylated styrenes, indenes and other similar aromatics above 330 °C (**Figure 13**, **A**). A very small and negligible part is made up by long alkanes or carboxylic acids, which might yield similar products during TA-PI-MS analysis. Most of the evolving constituents belong to the CH class, and only a few lowly abundant signals are assigned to hetero element containing substances, which is congruent with the little amounts found by EA. Moderate abundancies of cyclic dienes during phase 1 (<330 °C), indicate the presence of retro Diels-Alder reactions.
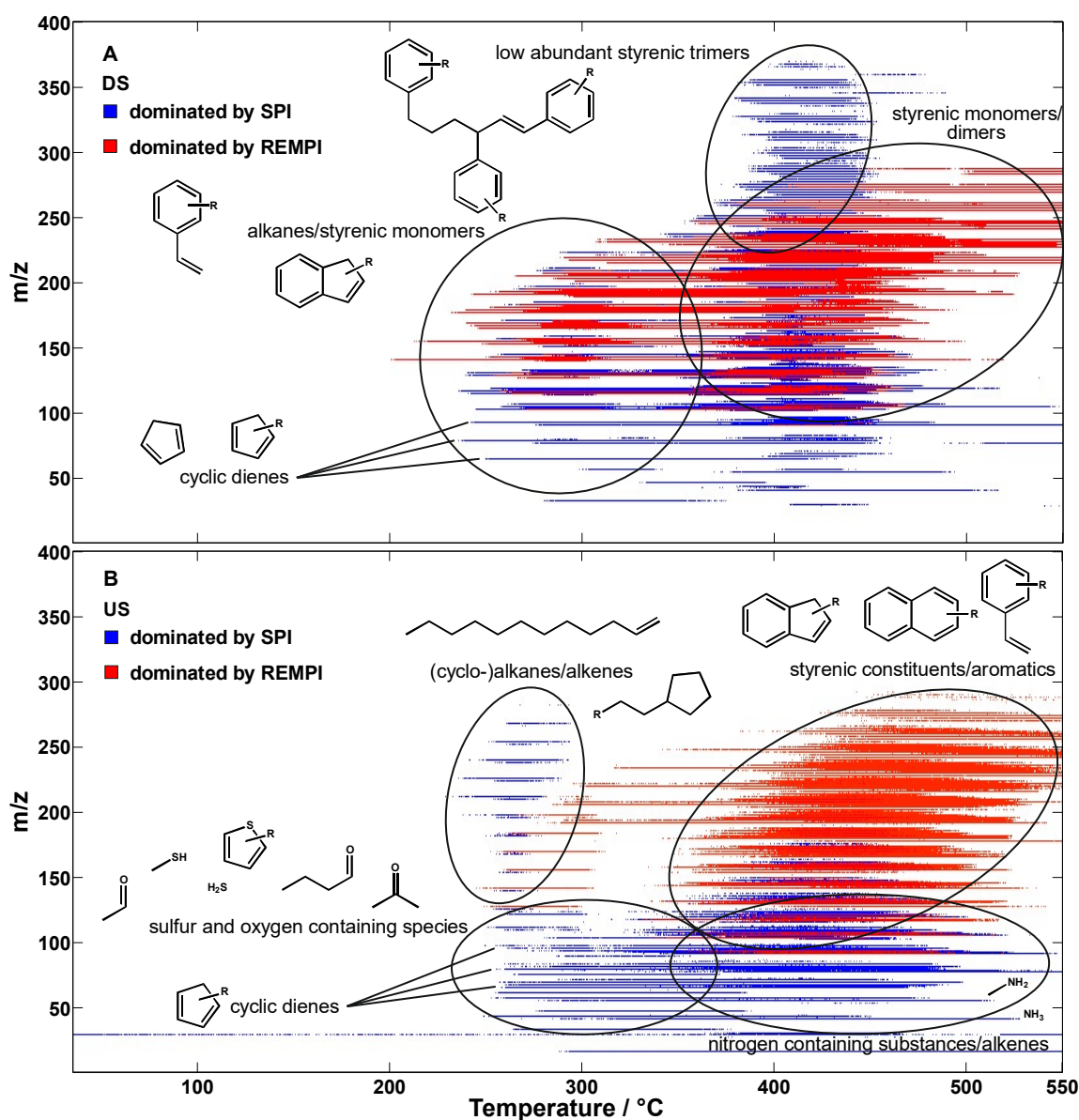
Figure 13. Simplified contour plot of DS (**A**) and US (**B**) illustrating the dominance of SPI (blue) and REMPI (red) for the ionization of evolving constituents during TA. Most abundant structural motives are indicated within the depiction. Adapted based on literature.[33]

Qualitative description of upstream fouling

Sample DS is summed over <330 °C as well, though at least two partly overlapping processes take place. A look into the time resolved data reveals the evolution of mid to heavy *m/z* values (peaking at ~250 °C) before an intricate pattern of small *m/z* values starts to appear at ~270 °C. The higher values can be assigned to (cyclo-)alkanes and alkenes (C_{10}–C_{30}, linear and branched), and the pattern of small *m/z* values is a mixture of different hetero atom containing compounds. Low to moderate intensities are found for ammonia (*m/z* 17), sulphur monoxide/methanethiol (*m/z* 48), sulphur dioxide (*m/z* 64), butanone (*m/z* 72), butanethiol (*m/z* 90), methylthiophene (*m/z* 98), pentanethiol (*m/z* 104) and diethyldisulfide (*m/z* 122). While

high abundancies of hydrogen sulphide (*m/z* 34), acetaldehyde (*m/z* 44), acetone (*m/z* 58), ethanethiol (*m/z* 62) and propanethiol/carbon disulphide (*m/z* 76) are identified. The *m/z* values 66 and 80 can be assigned to cyclopentadiene and methylcyclopentadiene, respectively. Similar compounds, but with at least one less double bond equivalent, are tentatively assigned for *m/z* 68, 70, 82 and 84. The summed REMPI spectrum revealed only little intensities of alkylated naphthalenes and other aromatics.

Phase 2 contains many of the above described hetero atom containing substances as well. Besides, a complex mixture of aromatics evolves, resulting in an intense pattern visible by REMPI. Similar to DS, many highly abundant signals of alkylated styrenes and moderate to high intensities of non-olefinic aromatics are visible. A multi-modal distribution however is not clearly visible. Furthermore, highly abundant signals of short alkenes (likely cleaved side-chains) and moderately abundant signals of phenols (*m/z* 94, 108, 122) are found. A sudden change of the hetero element containing compounds can be recognised in the time resolved data at around 370 °C. All sulphur containing substances disappear, whereas signals of ammonia and methylamine (*m/z* 31) increase/appear.

In general, the composition of US is much more diverse than of DS (**Figure 13**, **B**). The main structure of US (~60 % of the total weight loss) is somewhat similar to the polystyrene-like type of DS, but not as regular and shifted to higher alkylation degrees (as also indicated by the many small alkene signals). Cyclic dienes are found for US as well, but their abundancies during phase 1 are much lower, whereas the abundance of (cyclo-)alkanes/alkenes is pronounced. The staggered appearance of these products indicates a decomposition reaction rather than evaporation. A polyethylene-like type is however unlikely, because of the low temperature (~270 °C). Either decarboxylation reactions again or the detection of hetero element containing compounds with sulphur, oxygen or nitrogen might play a role here. The evolution of many small hetero element containing substances, in particular sulphur containing substances, indicates the existence of one or more chemical motifs such as polythioether-like ($[-S-(CH2)_n-]_m$) or polysulfide-like ($[-S-S-(CH2)_n-]_m$) structures.[108]

Quantification of Diels-Alder content

The optimal dosage of mitigation reagents is dependent on the extent of the respective fouling type, which is not yet accessible. Thus, quantification of the Diels-Alder content is attempted to improve chemical treatment of steam cracker facilities. Several possibilities exist to quantify with help of TA methods or PI-MS.[109] Mass loss, calorimetry and SPI-MS have been tested in the presented study. Dicyclopentadiene (DCPD) was used as a model substrate, which yields the monomer cyclopentadiene when heated above 150 °C.[110] All three data sets, obtained by TA-PI-MS, follow a linear regression quite well and might be suited for quantification. Taking into account, that fouling samples are complex matrices and several processes overlap mass loss and calorimetry might not yield accurate results. Whereas, SPI-MS can track several

masses very specifically and has a much lower limit of detection (theoretical LOD = 4×10^{-4} mg). Limitation of laser based PI-MS is however the fluctuation of the laser itself, which was reduced by normalisation based on standard gas measurements before and after each analysis. When attempting quantification of the two fouling samples, another problem occurs. It must be sure, that the tracked masses belong genuinely to Diel-Alder fouling. Evolution of Diels-Alder compounds (i.e., cyclic dienes) is seen at typical temperatures (phase 1) and at higher temperatures. An explanation might be, that cyclic dienes are incorporated by different mechanisms. Studies to further investigate this issue are advised. In summary, selective (semi-)quantification of Diels-Alder fouling can be achieved with TA-PI-MS, when (1) signals are identified unambiguously, (2) key signals can be assigned to the specific fouling, and (3) only one feature is tracked per signal (e.g., by selectivity or sufficient resolution/separation).[33]

5.3 Differentiation of differently branched polyethylene materials

After refining and steam cracking, the produced short-chain olefins can be used for the production of polymers, coatings, solvents and pesticides.[111] Polymers are widely applied advanced materials found almost everywhere in our daily life.[112] Natural polymers were used for quite some time without sophisticated knowledge about their composition. This changed with the discovery of synthetic polymers and Staudinger's structural elucidation of the nature of polymers.[113] Today, many different kinds of synthetic polymers with excellent properties exist. Manipulation of the respective composition enables control of said properties. One of the longest known and todays most produced synthetic polymer of the world is polyethylene (PE) with 116 Mt per year (2015, corresponds to ~29 % of total synthetic polymer production). It consists of a mixture of differently long and branched saturated hydrocarbons.[114] The molecular weight distribution (MWD) and branching are influenced by the synthesis conditions, in particular by the choice of catalyst and copolymer content.[115] The simplest polyethylene structure is completely linear, which leads to high crystallinity and thus density (high-density polyethylene, HDPE). Low-density polyethylene (LDPE) contains a high proportion of long- and short-chain branches and is synthesised by radical polymerisation. Linear low-density polyethylene (LLDPE) is obtained by usage of copolymers (1-olefins), yielding a large number of relatively regular, short branching. Besides, many different other polyethylene materials and mixtures (grafting) of these exist.[116] Branching has a strong influence on the materials' properties and thus its characterisation is essential for the understanding of the performance of different PE types.[115,117,118] The otherwise useful properties (nonpolar, non-volatile, inert and poorly soluble) of PE impede chemical analysis, which is often based on these characteristics.[118,119] Even typical mass spectrometric techniques used for polymers, such as matrix-assisted laser desorption (MALDI) or electrospray ionisation (ESI) are not applicable or only with difficulty.[120,121] Thus, methods aiming for bulk properties, such as melting behaviour or rheological properties, emerged. Though these information indicate indeed short- or long-chain branching, they are too shallow and ambiguous.[122,123] The total methyl group content can

be revealed by IR spectroscopy.[117] Information about short-chain and long-chain branching can be obtained by ^{13}C nuclear magnetic resonance (NMR) spectroscopy. Though valuable, it is limited by its inability to differentiate side chains with more than six carbon atoms and by sensitivity (≥1/1000 branched C atoms).[122,124] A sophisticated approach for polymers is the utilisation of fractionation methods. Size exclusion chromatography (SEC) or gel permeation chromatography (GPC) is well known for the elucidation of the MWD of polymers. Temperature rising elution fractionation (TREF) and crystallisation analysis fractionation (CRYSTAF) can be used to investigate branching.[115,125] The fractions can be individually analysed or online detection (IR, light scattering, UV/vis, viscosity, etc.) is applied.[115,125–128] Probably one of the most comprehensive analysis was achieved by using a triple detector GPC−TREF system.[129] Pyrolysis gas chromatography is a popular polymer scientific technique and is used to study additives or qualitatively analyse polymers.[127,130] Pyrolysis circumvents non-volatility by breaking the long chains into smaller fragments. Structural information can then be extracted from the pyrolysis pattern. Studies on the quantification of PE branching were conducted as well,[124,131] but reliable quantification is not accessible yet. Much effort has been put into understanding the pyrolysis of PE, which knowledge can be during analysis and recycling.[124,130–143] The aim of this study is to evaluate TA-PI-MS for the chemical characterisation of PE branching. Differently branched polyethylene materials (20 samples) are investigated. After evaluation of the melting and pyrolysis behaviour, the average decomposition pattern was examined by means of chemometric tools.

5.3.1 Thermal analysis data of differently branched polyethylene materials

The DSC curves of the differently branched PE materials exhibit two peaks. One between 110–130 °C for melting and another between 450–510 °C for degradation. With TGA, only the degradation can be seen, because of the related mass loss. The melting enthalpy however, contains valuable structural information. Branching, the MWD and former solidification conditions influence the crystallinity, which can be calculated by dividing the measured melting enthalpy by the melting enthalpy of a theoretically completely crystalline PE (293 J/g).[144] Very low and very high molecular weights are expected to interfere with the crystallisation process as well as fast cooling. Crystallinity is a measure of order and the ends of the polyethylene chains obstruct the regular arrangement of the chains. Short chains have an increased ratio of ends, relative to their length and thus reduce crystallinity. Longer chains exhibit a better end-to-length ratio, but are kinetically hindered to arrange. The faster the cooling, the more pronounced this effect becomes. Former solidification conditions can be negated and a higher reproducibility achieved by choosing a suitable experimental design (heating, controlled slow cooling and reheating).[145]
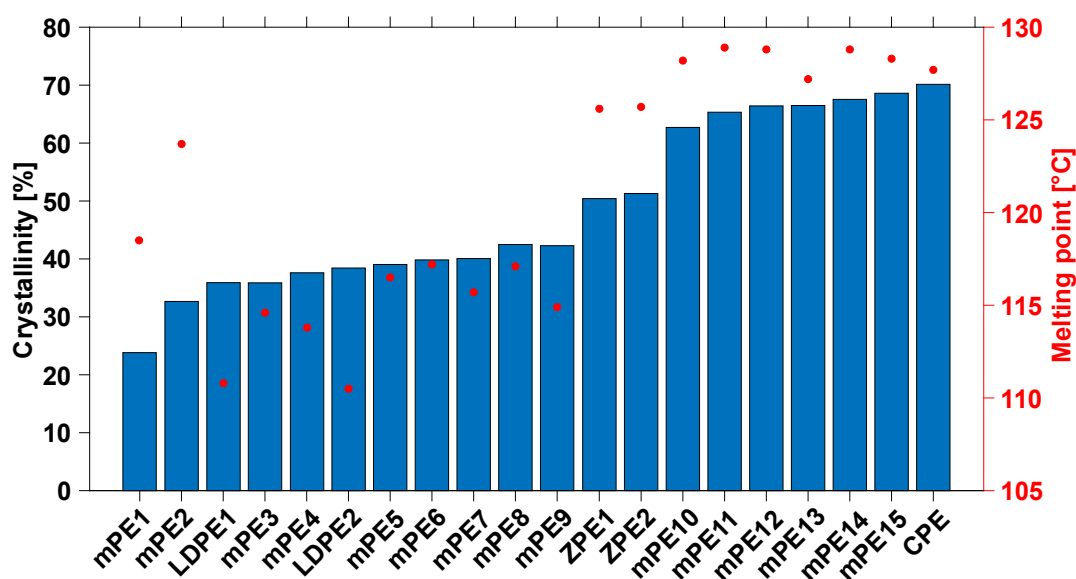
Figure 14. Crystallinity and melting point information obtained by DSC. Crystallinity can be calculated by dividing the measured value of a sample by the literature value for a completely crystalline PE.[144] Adapted based on literature.[34]

The offset of melting and the calculated crystallinity of the investigated samples are depicted in **Figure 14**. The crystallinity ranges between 24–70 % and the melting points between 111–129 °C. Samples are named after their respective synthesis route (mPE, metallocene catalyst; LDPE, radical polymerisation; ZPE, Ziegler-Natta catalyst; CPE, Phillips catalyst) and are sorted and numbered by ascending crystallinity. The densities of many mPE samples can be associated with LDPE (0.915–0.935 g/cm³) or LLDPE (0.87–0.94 g/cm³) and a few with HDPE (0.94–0.97 g/cm³). The mPE samples with low densities are most likely LLDPE, because of their synthesis route. A trend can be observed between the crystallinity and melting point, whereas the relation of MWD and melting point is not as clear due to its multiple dependencies. Nevertheless, when plotting crystallinity versus melting point, a grouping of similar samples is already obtained. The interpretability is however limited or at least hard to read.[34] The decomposition behaviour of the presented PE samples is very similar. Only the two LDPE samples behave significantly different. The beginning and maxima of the DTG curves are shifted to lower temperatures and the overall peaks slightly broader. Degradation reactions might be dependent on branching and MWD, but the applied method cannot resolve differences between the very similar samples (mPE, ZPE and CPE). The entire sample is volatilised at the end of the degradation process with no remaining detectable residue.[140]

5.3.2 Evolved gas analysis with SPI-MS of polyethylene

The curves of DTG and TIC look almost identical, but the summed mass spectra exhibit interesting structural information. Molecular ions in the range of *m/z* 42–390 were detected. Identification of the signals is performed based on the molecular weight information, literature

knowledge and by supportive Pyr-GC-MS data. High intensities of small alkenes and dienes are abundant (*m/z* 42–98), which level off in the medium-high region (*m/z* 98–180) and approach relatively constant values between *m/z* 180–360. Alkanes are lowly abundant between *m/z* 86–380. Investigation of the isomeric pattern of each signal, can be conducted by Pyr-GC-MS. Linear PE samples yield only linear constituents, whereas branched PE materials show branched species in addition and the ratio of branched to linear species increases with the branching degree of the PE. Even CPE, which has the highest crystallinity (70 %) of the herein investigated samples, exhibits signals of branched constituents. The data of Pyr-GC-MS shows further, that the double bonds of dienes and alkenes are always terminal (1-alkenes or α,ω-dienes). Unfortunately, the applied Pyr-GC-MS method does not resolve the full spectrum. Molecules with a carbon number ≥C10 are well resolved, but a lot of information is comprised in the smaller compounds as shown later.
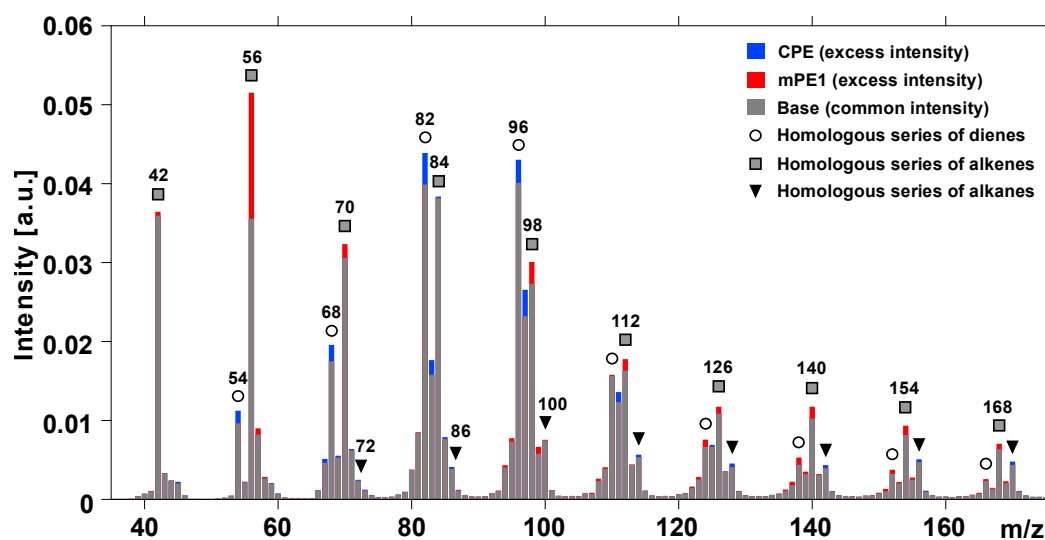
Figure 15. Difference plot of the summed spectra over the entire temperature range of TA-SPI-MS of highly crystalline CPE (blue) and lowly crystalline mPE1 (red). Differences between CPE and mPE1 can be seen mainly in the intensity of low *m/z* signals. In particular, butane (*m/z* 56), medium, and long alkenes are pronounced for mPE1, whereas several dienes (*m/z* 54, 68, 82 and 96) are pronounced for CPE. Adapted based on literature.[34]

When comparing summed SPI-MS spectra of the most extreme samples CPE (highly crystalline, 70 %) and mPE1 (lowly crystalline, 24 %), it becomes evident, that the signals are qualitatively the same. Differences can be found in the intensity of signals, in particular of small alkenes and dienes (**Figure 15**). Especially *m/z* 56 is highly pronounced for mPE1, which can be explained by the highly abundant side-chain content (9 wt% C6-). Besides, higher intensities for a lot of small–long alkenes (*m/z* 70, 98, 112, 126, etc.) can be seen. Sample CPE (no short-chain branching but long chain branched) however, exhibits high intensities of short dienes (*m/z* 54, 68, 82, 96) and medium–long alkanes. Both LDPE reveal high intensities of butene (*m/z* 56) and pentene (*m/z* 70). The back-biting mechanism (1-5 transfer and 1-6 transfer)

yielding these side-chains is typical for radical polymerisation reactions. Though structural features of the samples can be clearly uncovered by TA-SPI-MS, the partially small differences and large number of samples and observables (i.e., *m/z* values) complicates interpretation. Thus, chemometric tools were applied to reduce the complexity of data.

5.3.3 Exploratory data analysis

Because only limited quantitative information were available about the branching of samples, the use of an unsupervised data exploratory tool such as principal component analysis (PCA) is advised. Besides accurate measurements, careful data handling and testing have to be performed prior to applying PCA. When plotting the first two principal components (PC1–2), a distribution of the samples is seen (not shown). The third PC shows an additional spreading between LDPE1–2 and the other PE samples (10.0 % explained variance). Based on short-chain branching, four groups are defined: highly short-chain branched (red), medium short-chain branched (purple), no or little short-chain branched (yellow) and radical polymerised (green) PE.

The spreading within one group and the proximity of representatives of different groups can be explained by the dependency of SPI-MS signals of additional variables such as MWD or long-chain branching. The close proximity of CPE (0 wt% C6-, a lot of long-chain branching, 70 % crystallinity) and ZPE2 (1 wt% C6-, no long-chain branching, 51 % crystallinity) however, cannot be explained yet. One problem of unsupervised statistical methods is, that extreme samples can distort the overall outcome and the calculated principal components must not represent real underlying causes. But we can learn which observables have the most influence and try to comprehend their meaning (**Figure 16**, **A**). Alkenes, above all butene (*m/z* 56), pentene (*m/z* 70), and propene (*m/z* 42), and dienes, such as pentadiene (*m/z* 68), hexadiene (*m/z* 82) and heptadiene (*m/z* 96), have the strongest influence on the first four principal components.

A simple and robust grouping of the samples can also be achieved, when using the most influencing variables from PCA (*m/z* 42, 56, 68 and 70) as markers. By plotting the ratio of (56/42) against (70/68) a nice distribution is obtained (**Figure 16**, **B**). The representatives within each group move closer together and the groups are well separated from each other. Unfortunately, no trends concerning the MWD or long-chain branching are recognised by any of the applied tools (PCA nor marker ratios), assuming our estimates of long-chain branching are correct in the first place. Nevertheless, TA-PI-MS might be interesting in enhancing the range of quantifiable short-chains from state of the art 13C NMR (≤C6 side-chains) to longer chains.
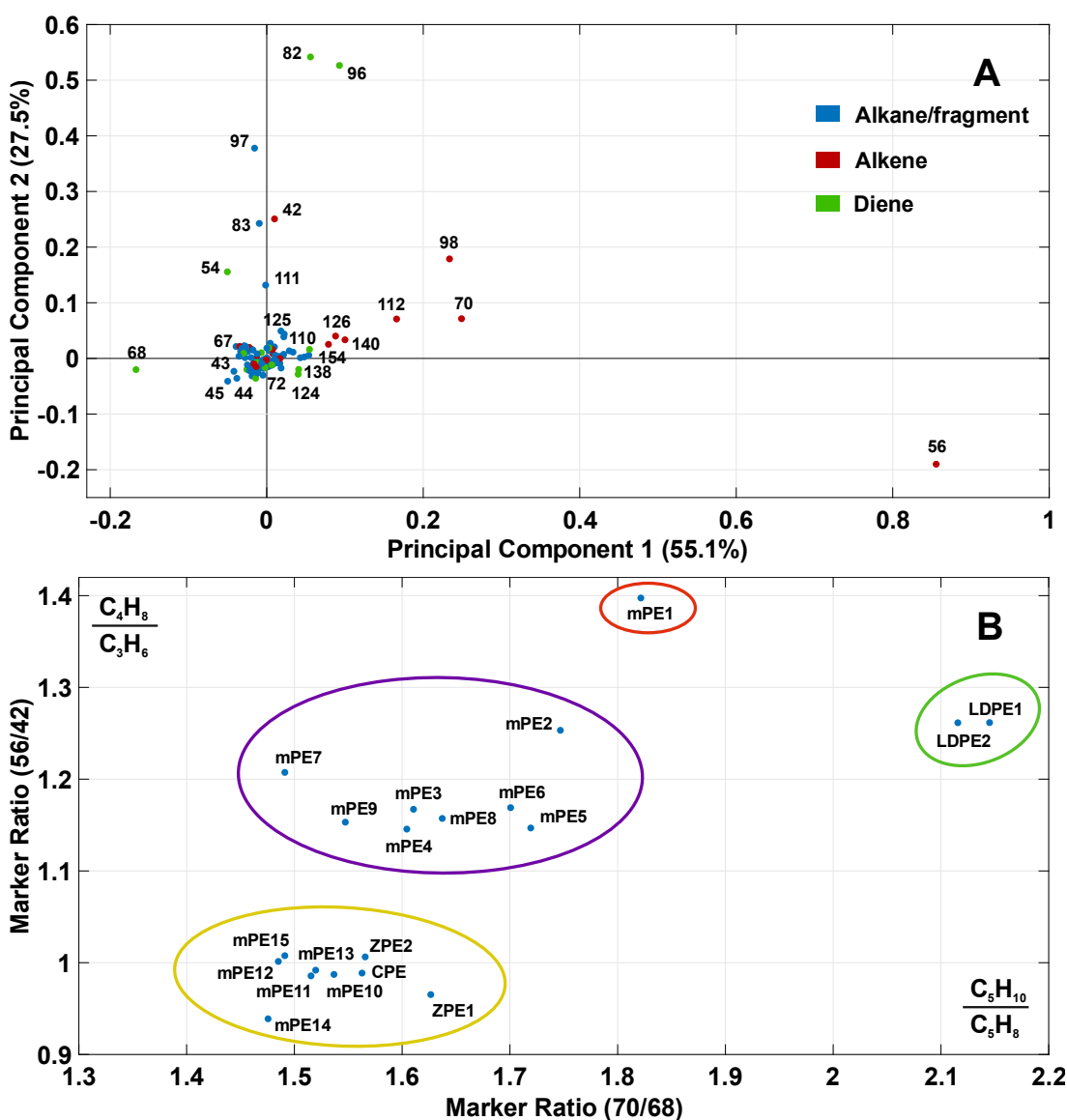
Figure 16. (**A**) Loading plot of the two first principal components of the PCA; (**B**) simple score plot shows grouping based on ratios of only four markers. Adapted based on literature.[34]

5.4 Pyrolysis of polyethylene terephthalate

The versatility and low cost of plastics such as polyethylene or polyethylene terephthalate (PET) has led to the production of vast amounts of these materials.[139,146] Adverse effects on the environment and health can arise from disposal, which is why different concepts for the valorisation and recycling of plastic waste are being deployed.[41] Some concepts are however problematic. Incineration with energy recovery generates highly toxic chlorinated organic compounds, which makes the operation controversial and expensive.[147] Growth potential of the already applied mechanical recycling (currently absorbing 13 wt% of all plastic waste generated in Western Europe) is already limited due to the low quality of the recycled plastic.[147,148] Thus, increased interest can be recognised for feedstock recycling, which has the

potential to absorb large quantities of waste plastic. Different processes, such as pyrolysis, gasification, catalytic cracking, depolymerisation or hydrogenation, can be used to convert plastic waste into petrochemical feedstock for use in the production of refined chemicals or fuels.[139,148] The third most produced plastic is PET (56 Mt per year, 2016), which makes the understanding of its decomposition reactions crucial.[146]

5.4.1 Identification of evolving constituents

Similar to PE and the asphaltene, PET shows a single mass loss step during degradation (350–500 °C) leaving a small residue behind (~17 wt%). The SPI-TIC coincidences quite well with DTG, though some major products such as CO and CO_2 are excluded by SPI. Both curves peak at 435 °C. Different patterns were obtained by summing over different temperature regions. In the beginning (350–400 °C), m/z 44 (acetaldehyde), 122 (benzoic acid), 149 (photo fragment of vinyl terephthalate) and other small abundant signals are recorded. The intensity of this pattern increases with temperature (400–450 °C), revealing even more small signals such as m/z 105 (fragment of vinylbenzoate), 150 (4-ethylbenzoate), 166 (terephthalic acid), 175 (fragment of divinyl terephthalate) and 198 (biphenyl-4-carboxylic acid). After 435 °C most intensities of signals decrease, whereas the maximum of terephthalic acid (m/z 166) is located at 440 °C and benzene (m/z 78) shows two maxima at 427 °C and 447 °C, as well as an increasing signal at >500 °C. The two maxima of benzene could be from decarboxylation of benzoic acid and terephthalic acid, respectively.

The summed REMPI spectra of the corresponding temperature regions look quite complex, revealing the before lowly abundant aromatic fingerprint, because of a higher sensitivity for most aromatics. Some signals are however excluded such as benzoic acid (m/z 122) or terephthalic acid (m/z 166) due to too high ionisation energies. Two partly overlapping peaks of evolving aromatics can be seen in the REMPI-TIC, indicating the existence of two different mechanisms for the formulation of aromatics. At first, high mass low intensity peaks of m/z 264, 274, 288 and 298 appear (300–350 °C). Signals at m/z 94 (phenol), 144, 148 (vinyl benzoate), 162 (vinyl 4-methylbenzoate), 188 and 192 (vinyl terephthalate) are detected between 350–400 °C. With REMPI, vinyl ester do not fragment in contrast to SPI. The highest signal intensities of m/z 162 (vinyl 4-methylbenzoate), 172, 188 and 198 (biphenyl-4-carboxylic acid) are recorded between 400–450 °C, corresponding to the main part of the first REMPI-TIC peak. During the second peak (450–500 °C) mainly polycyclic aromatic hydrocarbons (PAH) evolve. Signals of m/z 154 (biphenyl/acenaphthene, 166 (fluorene), 178 (anthracene/phenanthrene), 228 (benzo[a]anthracene), 230 (terphenyle) and 254 (1,2'-binaphthalene) are found. Some of the above described species were also found by TGA-APCI-FTICR-MS.
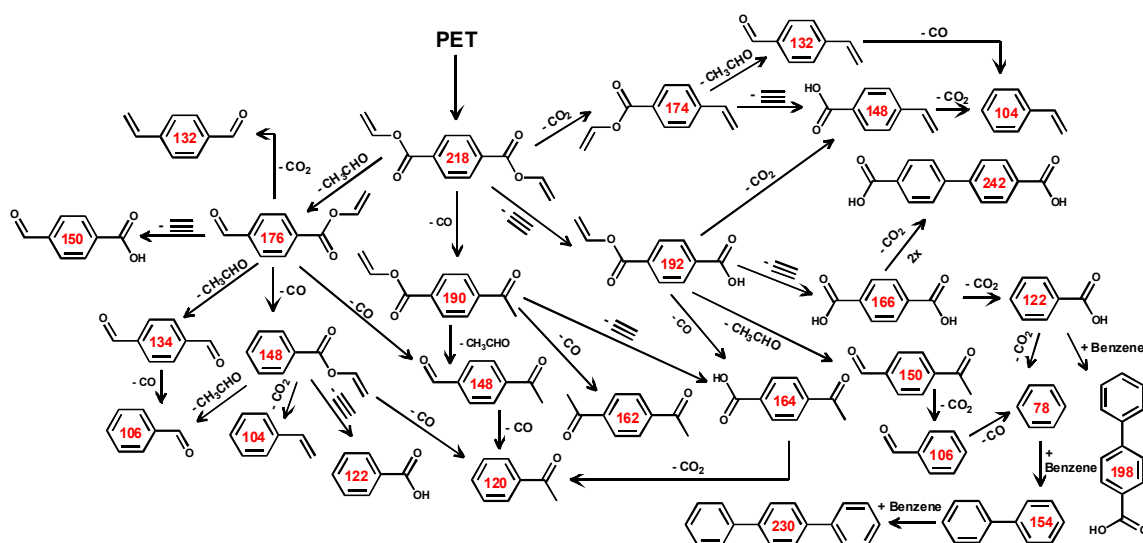
Figure 17. Proposed reaction pathways for the degradation and occurrence of major products. Adapted based on literature.[149]

Based on the assigned products and knowledge from literature, different reactions can be proposed (**Figure 17**). At relatively low temperatures (~300 °C) the formation of cyclic products (e.g., cyclic dimers) plays a major role, which then further decompose at higher temperatures. Several reactions leading to hydroxyl or vinyl end groups are more energetically favourable than decarboxylation reactions, which might be why vinyl/hydroxy products occur in the first and PAHs in the second peak.

6 Summary and outlook

In the presented work, thermal analysis hyphenated to photo ionisation mass spectrometry was used on four challenging petrochemical samples from different parts of the process chain to evaluate its applicability and generate new knowledge.

Asphaltenes within crude oil or feed fractions can cause many problems and are a potential reason for fouling. The combination of data obtained by TA-PI-MS and complementary thermal analysis techniques enabled a detailed chemical description of an exemplary asphaltene sample. The chemical spaces unravelled by single photon ionisation and resonance-enhanced multiphoton ionisation cover very well main features of the pyrolysed asphaltene sample. In addition, vacuum photo ionisation yields less biased molecular information than e.g. atmospheric pressure ionisation techniques.

Our analysis of steam cracker fouling samples yielded the identification of various chemical motifs as main components. Despite the low thermal resolution of thermal analysis, the different patterns could be sufficiently separated. In addition, first attempts and theoretical considerations were made to quantify the Diels-Alder content of fouling samples. Polyethylene is a potential end-product from short-chain olefin generation and also a challenging sample for many analytical methods.

It was tested if the branching of different polyethylene materials can be differentiated or even quantified. It was shown that TA-SPI-MS reveals differences quite sensitive. DSC data and principal component analysis were used to achieve a grouping of similar samples and reduce the high amount of variables to a small number of markers. First results suggest a robust and at least semi-quantitative method, which could enhance the quantifiable chain-length.

An efficient way of plastic waste recycling might be the waste to oil concept, in which polymers are pyrolysed into reusable feed. For this purpose, the pyrolysis of polyethylene terephthalate was studied in-depth by TA-PI-MS and APCI-FTICR-MS. New findings about the temperature depending product spectrum allowed the postulation of possible decomposition reactions.

In summary, it was shown that TA-PI-MS can be used for many different applications. The value of information is however dependent on the type and extent of complexity. Analysis of samples bearing highly isomeric and isobaric complexity such as asphaltenes yields only shallow information on many aspects, but side-chain cleavage. Whereas analysis of polymers or polymer-like structures (i.e. fouling) can be conducted quite well. For future applications, a higher resolution on the used mass analyser and improvements of the light generating system can significantly improve the quality of data, probably resulting in the omission of supportive techniques.

7 References

(1) EKT Interactive. History of Oil. https://ektinteractive.com/history-of-oil/ (accessed Jan.13, 2021).

(2) Horn, J.; Rosenband, L. N.; Smith, M. R., Eds. *Reconceptualizing the Industrial Revolution*; MIT Press, 2010.

(3) Wrigley, E. A. Reconsidering the Industrial Revolution: England and Wales. *Journal of Interdisciplinary History* **2018**, *49* (1), 9–42. DOI: 10.1162/jinh_a_01230.

(4) Landes, D. S. *The unbound Prometheus*:*Technological change and industrial development in Western Europe from 1750 to the present*; Cambridge University Press, 1969.

(5) Gordon, R. B. *American iron 1607-1900*, Paperback ed.; Johns Hopkins studies in the history of technology; Johns Hopkins University Press, 2001.

(6) Russell, L. S. *A heritage of light*:*Lamps and lighting in the early Canadian home*; University of Toronto Press, 2003.

(7) Maugeri, L. *The age of oil*:*The mythology, history, and future of the world's most controversial resource*; Lyons Press, 2006.

(8) BP. Statistical Review of World Energy. https://www.bp.com/en/global/corporate/energy-economics/statistical-review-of-world-energy.html (accessed Jan.13, 2021).

(9) *Key World Energy Statistics 2014*; OECD, 2014. DOI: 10.1787/key_energ_stat-2014-en.

(10) Simanženkov, V.; Idem, R. *Crude oil chemistry*; Dekker, 2003.

(11) Ceriþc, E. *Crude oil, processes and products*; IBC d.o.o, 2012.

(12) Hyne, N. J. *Nontechnical guide to petroleum geology, exploration, drilling, and production*, 2. ed.; Penn Well Corp, 2001.

(13) Speight, J. G. *The chemistry and technology of petroleum*, 3. ed.; Chemical industries, Vol. 76; Dekker, 1999.

(14) Murray, J.; King, D. Climate policy: Oil's tipping point has passed. *Nature* **2012**, *481* (7382), 433–435. DOI: 10.1038/481433a.

(15) Stocker, T.; Alexander, L.; Allen, M. *Climate change 2013*:*The physical science basis ; Working Group I contribution to the fifth assessment report of the Intergovernmental Panel on Climate Change*, WMO IPCC, 2014. DOI: 10.1017/CBO9781107415324.

(16) Mullins, O. C. *Asphaltenes, heavy oils and petroleomics*; Springer, 2007. DOI: 10.1007/0-387-68903-6.

(17) Fahim, M. A.; Alsahhaf, T. A.; Elkilani, A. S. *Fundamentals of petroleum refining*, 1. ed.; Elsevier, 2010.

(18) Kharrat, A. M.; Zacharia, J.; Cherian, V. J.; Anyatonwu, A. Issues with Comparing SARA Methodologies. *Energy Fuels* **2007**, *21* (6), 3618–3621. DOI: 10.1021/ef700393a.

(19) Fan, T.; Wang, J.; Buckley, J. S. Evaluating Crude Oils by SARA Analysis. *SPE/DOE Improved Oil Recovery Symposium*; Society of Petroleum Engineers, 2002. DOI: 10.2118/75228-MS.

(20) Qiao, P.; Harbottle, D.; Tchoukov, P.; Masliyah, J.; Sjoblom, J.; Liu, Q.; Xu, Z. Fractionation of Asphaltenes in Understanding Their Role in Petroleum Emulsion Stability and Fouling. *Energy Fuels* **2017**, *31* (4), 3330–3337. DOI: 10.1021/acs.energyfuels.6b02401.

(21) Bissada, K. K.; Tan, J.; Szymczyk, E.; Darnell, M.; Mei, M. Group-type characterization of crude oil and bitumen. Part I: Enhanced separation and quantification of saturates, aromatics, resins and asphaltenes (SARA). *Organic Geochemistry* **2016**, *95*, 21–28. DOI: 10.1016/j.orggeochem.2016.02.007.

(22) Baerns, M.; Behr, A.; Brehm, A.; Gmehling, J.; Hinrichsen, K.-O.; Hofmann, H.; Palkovits, R.; Onken, U.; Renken, A. *Technische Chemie*, 2. ed.; Wiley-VCH, 2013.

(23) Lucas, A. G. *Modern petroleum technology*, 6th ed.; Wiley, 2002.

(24) Nič, M.; Jirát, J.; Košata, B.; Jenkins, A.; McNaught, A., Eds. *IUPAC Compendium of Chemical Terminology*; IUPAC, 2009. DOI: 10.1351/goldbook.

(25) *Ullmann's Encyclopedia of Industrial Chemistry:Electronic Release. CD*; Wiley-VCH, 2003.

(26) Ramirez, J.; Brown, R.; Rainey, T. A Review of Hydrothermal Liquefaction Bio-Crude Properties and Prospects for Upgrading to Transportation Fuels. *Energies* **2015**, *8* (7), 6765–6794. DOI: 10.3390/en8076765.

(27) Speight, J. G. *The refinery of the future*; William Andrew; Elsevier Science distributor, 2011.

(28) Dutriez, T.; Courtiade, M.; Thiébaut, D.; Dulot, H.; Borras, J.; Bertoncini, F.; Hennion, M.-C. Advances in Quantitative Analysis of Heavy Petroleum Fractions by Liquid Chromatography−High-Temperature Comprehensive Two-Dimensional Gas Chromatography: Breakthrough for Conversion Processes. *Energy Fuels* **2010**, *24* (8), 4430–4438. DOI: 10.1021/ef1002809.

(29) Dutriez, T.; Courtiade, M.; Thiébaut, D.; Dulot, H.; Hennion, M.-C. Improved hydrocarbons analysis of heavy petroleum fractions by high temperature comprehensive two-dimensional gas chromatography. *Fuel* **2010**, *89* (9), 2338–2345. DOI: 10.1016/j.fuel.2009.11.041.

(30) Kok, M. V. Characterization of medium and heavy crude oils using thermal analysis techniques. *Fuel Processing Technology* **2011**, *92* (5), 1026–1031. DOI: 10.1016/j.fuproc.2010.12.027.

(31) Rüger, C. P.; Miersch, T.; Schwemer, T.; Sklorz, M.; Zimmermann, R. Hyphenation of Thermal Analysis to Ultrahigh-Resolution Mass Spectrometry (Fourier Transform Ion Cyclotron Resonance Mass Spectrometry) Using Atmospheric Pressure Chemical Ionization For Studying Composition and Thermal Degradation of Complex Materials. *Analytical chemistry* **2015**, *87* (13), 6493–6499. DOI: 10.1021/acs.analchem.5b00785.

(32) Trejo, F.; Rana, M. S.; Ancheyta, J. Thermogravimetric determination of coke from asphaltenes, resins and sediments and coking kinetics of heavy crude asphaltenes. *Catalysis Today* **2010**, *150* (3-4), 272–278. DOI: 10.1016/j.cattod.2009.07.091.

(33) Grimmer, C.; Rüger, C. P.; Streibel, T.; Cuoq, F.; Kwakkenbos, G.; Cordova, M.; Peñalver, R.; Zimmermann, R. Description of Steam Cracker Fouling and Coking Residues by Thermal Analysis-Photoionization Mass Spectrometry. *Energy Fuels* **2019**, *33* (11), 11592–11602. DOI: 10.1021/acs.energyfuels.9b02886.

(34) Grimmer, C.; Friederici, L.; Streibel, T.; Naim, A.; Cirriez, V.; Giusti, P.; Afonso, C.; Rüger, C. P.; Zimmermann, R. Characterization of Polyethylene Branching by Thermal Analysis-Photoionization Mass Spectrometry. *Journal of the American Society for Mass Spectrometry* **2020**, *31* (11), 2362–2369. DOI: 10.1021/jasms.0c00291.

(35) The Editors of Encyclopaedia Britannica. *Polymer*. https://www.britannica.com/science/polymer (accessed Jan.13, 2021).

(36) Painter, P. C.; Coleman, M. M. *Fundamentals of polymer science:An introductory text*, 2. ed.; Technomic Publ. Co, 1997.

(37) MacCrum, N. G.; Buckley, C. P.; Bucknall, C. B. *Principles of polymer engineering*, 2. ed.; Oxford Univ. Press, 1997.

(38) Young, R. J. *Introduction to polymers*; Chapman and Hall, 1981.

(39) Feldman, D. Polymer History. *Designed Monomers and Polymers* **2008**, *11* (1), 1–15. DOI: 10.1163/156855508X292383.

(40) Kumaraswamy, G. Living in the Polymer Age. *Reson* **2017**, *22* (4), 333–334. DOI: 10.1007/s12045-017-0472-3.

(41) Proshad, R.; Kormoker, T.; Islam, M. S.; Haque, M. A.; Rahman, M. M.; Mithu, M. M. R. Toxic effects of plastic on human health and environment : A consequences of health risk assessment in Bangladesh. *IJH* **2017**, *6* (1), 1. DOI: 10.14419/ijh.v6i1.8655.

(42) Zhou, H. *Combustible Solid Waste Thermochemical Conversion:A Study of Interactions and Influence Factors*; Springer Theses; Springer Singapore, 2017.

(43) Zhou, H.; Long, Y.; Meng, A.; Li, Q.; Zhang, Y. Thermogravimetric characteristics of typical municipal solid waste fractions during co-pyrolysis. *Waste management (New York, N.Y.)* **2015**, *38*, 194–200. DOI: 10.1016/j.wasman.2014.09.027.

(44) Zhou, H.; Long, Y.; Meng, A.; Li, Q.; Zhang, Y. Interactions of three municipal solid waste components during co-pyrolysis. *Journal of Analytical and Applied Pyrolysis* **2015**, *111*, 265–271. DOI: 10.1016/j.jaap.2014.08.017.

(45) Zhou, H.; Long, Y.; Meng, A.; Li, Q.; Zhang, Y. The pyrolysis simulation of five biomass species by hemi-cellulose, cellulose and lignin based on thermogravimetric curves. *Thermochimica Acta* **2013**, *566*, 36–43. DOI: 10.1016/j.tca.2013.04.040.

(46) Haines, P. J., Ed. *Principles of thermal analysis and calorimetry*; RSC paperbacks; Royal Soc. of Chemistry, 2002.

(47) Wendlandt, W. W. *Thermal methods of analysis*, 2. ed.; Chemical analysis, Vol. 19; Wiley, 1974.

(48) Coats, A. W.; Redfern, J. P. Thermogravimetric analysis. A review. *Analyst* **1963**, *88* (1053), 906. DOI: 10.1039/AN9638800906.

(49) Hemminger, W. F.; Cammenga, H. K. *Methoden der thermischen Analyse*; Anleitungen für die chemische Laboratoriumspraxis, Vol. 24; Springer, 1989.

(50) James, A. T.; Martin, A. J. P. Gas-liquid partition chromatography; the separation and micro-estimation of volatile fatty acids from formic acid to dodecanoic acid. *The Biochemical journal* **1952**, *50* (5), 679–690. DOI: 10.1042/bj0500679.

(51) Bartle, K. D.; Myers, P. History of gas chromatography. *TrAC Trends in Analytical Chemistry* **2002**, *21* (9-10), 547–557. DOI: 10.1016/S0165-9936(02)00806-3.

(52) McNair, H. M.; Miller, J. M. *Basic gas chromatography*, 2. ed.; Wiley, 2009. DOI: 10.1002/9780470480106.

(53) Dettmer-Wilde, K.; Engewald, W.; Adahchour, M. *Practical gas chromatography*:*A comprehensive reference*; Springer, 2014.

(54) Otto, M. *Analytische Chemie*, 3. ed.; Wiley-VCH, 2006.

(55) Gross, J. H. *Mass spectrometry*:*A textbook*, 2. ed.; Springer, 2011.

(56) Hoffmann, E. de; Stroobant, V. *Mass spectrometry*:*Principles and applications*, 3. ed.; Wiley, 2007.

(57) Alberici, R. M.; Simas, R. C.; Sanvido, G. B.; Romão, W.; Lalli, P. M.; Benassi, M.; Cunha, I. B. S.; Eberlin, M. N. Ambient mass spectrometry: bringing MS into the "real world". *Analytical and bioanalytical chemistry* **2010**, *398* (1), 265–294. DOI: 10.1007/s00216-010-3808-3.

(58) Schröder, E. *Massenspektrometrie*:*Begriffe und Definitionen*; Heidelberger Taschenbücher, Vol. 260; Springer, 1991. DOI: 10.1007/978-3-642-76206-2.

(59) Hanley, L.; Zimmermann, R. Light and molecular ions: the emergence of vacuum UV single-photon ionization in MS. *Analytical chemistry* **2009**, *81* (11), 4174–4182. DOI: 10.1021/ac8013675.

(60) Hocart, C. H. Mass Spectrometry: An Essential Tool for Trace Identification and Quantification. In *Comprehensive Natural Products II*; Elsevier, 2010; pp 327–388. DOI: 10.1016/B978-008045382-8.00187-8.

(61) Adam, T.; Zimmermann, R. Determination of single photon ionization cross sections for quantitative analysis of complex organic mixtures. *Analytical and bioanalytical chemistry* **2007**, *389* (6), 1941–1951. DOI: 10.1007/s00216-007-1571-x.

(62) Eschner, M. S.; Zimmermann, R. Determination of photoionization cross-sections of different organic molecules using gas chromatography coupled to single-photon ionization (SPI) time-of-flight mass spectrometry (TOF-MS) with an electron-beam-pumped rare gas excimer light source (EBEL): influence of molecular structure and analytical implications. *Applied spectroscopy* **2011**, *65* (7), 806–816. DOI: 10.1366/11-06233.

(63) Heger, H. J.; Zimmermann, R.; Dorfner, R.; Beckmann, M.; Griebel, H.; Kettrup, A.; Boesl, U. On-Line Emission Analysis of Polycyclic Aromatic Hydrocarbons down to pptv Concentration Levels in the Flue Gas of an Incineration Pilot Plant with a Mobile Resonance-Enhanced Multiphoton Ionization Time-of-Flight Mass Spectrometer. *Analytical chemistry* **1999**, *71* (1), 46–57. DOI: 10.1021/ac980611y.

(64) Brunnée, C. The ideal mass analyzer: Fact or fiction? *International Journal of Mass Spectrometry and Ion Processes* **1987**, *76* (2), 125–237. DOI: 10.1016/0168-1176(87)80030-7.

(65) Electric sector in mass spectrometry. In *IUPAC Compendium of Chemical Terminology*; Nič, M., Jirát, J., Košata, B., Jenkins, A., McNaught, A., Eds.; IUPAC, 2009. DOI: 10.1351/goldbook.E01938.

(66) Marshall, A. G.; Rodgers, R. P. Petroleomics: the next grand challenge for chemical analysis. *Accounts of chemical research* **2004**, *37* (1), 53–59. DOI: 10.1021/ar020177t.

(67) Rüger, C. P.; Grimmer, C.; Sklorz, M.; Neumann, A.; Streibel, T.; Zimmermann, R. Combination of Different Thermal Analysis Methods Coupled to Mass Spectrometry for the Analysis of Asphaltenes and Their Parent Crude Oils: Comprehensive Characterization of the Molecular Pyrolysis Pattern. *Energy Fuels* **2018**, *32* (3), 2699–2711. DOI: 10.1021/acs.energyfuels.7b02762.

(68) Rodgers, R. P.; Schaub, T. M.; Marshall, A. G. Petroleomics: MS Returns to Its Roots. *Anal. Chem.* **2005**, *77* (1), 20 A-27 A. DOI: 10.1021/ac053302y.

(69) Nizio, K. D.; McGinitie, T. M.; Harynuk, J. J. Comprehensive multidimensional separations for the analysis of petroleum. *Journal of chromatography. A* **2012**, *1255*, 12–23. DOI: 10.1016/j.chroma.2012.01.078.

(70) Marshall, A. G.; Rodgers, R. P. Petroleomics: chemistry of the underworld. *Proceedings of the National Academy of Sciences of the United States of America* **2008**, *105* (47), 18090–18095. DOI: 10.1073/pnas.0805069105.

(71) George, G. N.; Gorbaty, M. L. Sulfur K-edge x-ray absorption spectroscopy of petroleum asphaltenes and model compounds. *J. Am. Chem. Soc.* **1989**, *111* (9), 3182–3186. DOI: 10.1021/ja00191a012.

(72) Mitra-Kirtley, S.; Mullins, O. C.; van Elp, J.; George, S. J.; Chen, J.; Cramer, S. P. Determination of the nitrogen chemical structures in petroleum asphaltenes using XANES spectroscopy. *J. Am. Chem. Soc.* **1993**, *115* (1), 252–258. DOI: 10.1021/ja00054a036.

(73) Pomerantz, A. E.; Seifert, D. J.; Bake, K. D.; Craddock, P. R.; Mullins, O. C.; Kodalen, B. G.; Mitra-Kirtley, S.; Bolin, T. B. Sulfur Chemistry of Asphaltenes from a Highly Compositionally Graded Oil Column. *Energy Fuels* **2013**, *27* (8), 4604–4608. DOI: 10.1021/ef400773f.

(74) Podgorski, D. C.; Corilo, Y. E.; Nyadong, L.; Lobodin, V. V.; Bythell, B. J.; Robbins, W. K.; McKenna, A. M.; Marshall, A. G.; Rodgers, R. P. Heavy Petroleum Composition. 5. Compositional and Structural Continuum of Petroleum Revealed. *Energy Fuels* **2013**, *27* (3), 1268–1276. DOI: 10.1021/ef301737f.

(75) Materazzi, S.; Risoluti, R. Evolved Gas Analysis by Mass Spectrometry. *Applied Spectroscopy Reviews* **2014**, *49* (8), 635–665. DOI: 10.1080/05704928.2014.887021.

(76) Materazzi, S.; Vecchio, S. Recent Applications of Evolved Gas Analysis by Infrared Spectroscopy (IR-EGA). *Applied Spectroscopy Reviews* **2013**, *48* (8), 654–689. DOI: 10.1080/05704928.2013.786722.

(77) Materazzi, S.; Gentili, A.; Curini, R. Applications of evolved gas analysis Part 2: EGA by mass spectrometry. *Talanta* **2006**, *69* (4), 781–794. DOI: 10.1016/j.talanta.2005.12.007.

(78) Materazzi, S.; Vecchio, S. Evolved Gas Analysis by Mass Spectrometry. *Applied Spectroscopy Reviews* **2011**, *46* (4), 261–340. DOI: 10.1080/05704928.2011.565533.

(79) Huang, J. Thermal Degradation of Asphaltene and Infrared Characterization of Its Degraded Fractions. *Petroleum Science and Technology* **2006**, *24* (9), 1089–1095. DOI: 10.1081/LFT-200056601.

(80) Alosmanov, R.; Wolski, K.; Matuschek, G.; Magerramov, A.; Azizov, A.; Zimmermann, R.; Aliyev, E.; Zapotoczny, S. Effect of functional groups on the thermal degradation of phosphorus- and phosphorus/nitrogen-containing functional polymers. *J Therm Anal Calorim* **2017**, *130* (2), 799–812. DOI: 10.1007/s10973-017-6464-4.

(81) Riley, B. J.; Lennard, C.; Fuller, S.; Spikmans, V. Pyrolysis-GC-MS analysis of crude and heavy fuel oil asphaltenes for application in oil fingerprinting. *Environmental Forensics* **2018**, *19* (1), 14–26. DOI: 10.1080/15275922.2017.1408163.

(82) Garg, A. K.; Philp, R. P. Pyrolysis-gas chromatography of asphaltenes/kerogens from source rocks of the Gandhar Field, Cambay Basin, India. *Organic Geochemistry* **1994**, *21* (3-4), 383–392. DOI: 10.1016/0146-6380(94)90200-3.

(83) Mascherpa, A.; Casalini, A. Pyrolysis GC-MS of asphaltenes from straight-run and visbreaker bitumens. *J. High Resol. Chromatogr.* **1988**, *11* (3), 296–299. DOI: 10.1002/jhrc.1240110317.

(84) Nali, M.; Corana, F.; Montanari, L. Pyrolysis/gas chromatography/mass spectrometry in the analysis of asphaltenes. *Rapid Commun. Mass Spectrom.* **1993**, *7* (7), 684–687. DOI: 10.1002/rcm.1290070728.

(85) Solli, H.; Leplat, P. Pyrolysis-gas chromatography of asphaltenes and kerogens from source rocks and coals—A comparative structural study. *Organic Geochemistry* **1986**, *10* (1-3), 313–329. DOI: 10.1016/0146-6380(86)90032-X.

(86) Speight, J. G.; Pancirov, R. J. STRUCTURAL TYPES IN PETROLEUM ASPHALTENES AS DEDUCED FROM PYROLYSIS/GAS CHROMATOGRAPHY/MASS SPECTROMETRY. *Liquid Fuels Technology* **1984**, *2* (3), 287–305. DOI: 10.1080/07377268408915354.

(87) Kök, M. V. Thermal analysis applications in fossil fuel science: Literature survey. *J Therm Anal Calorim* **2002**, *68* (3), 1061–1077. DOI: 10.1023/A:1016119428815.

(88) Streibel, T.; Zimmermann, R. Resonance-enhanced multiphoton ionization mass spectrometry (REMPI-MS): applications for process analysis. *Annual review of analytical chemistry (Palo Alto, Calif.)* **2014**, *7*, 361–381. DOI: 10.1146/annurev-anchem-062012-092648.

(89) Zimmermann, R. Photo ionisation in mass spectrometry: light, selectivity and molecular ions. *Analytical and bioanalytical chemistry* **2013**, *405* (22), 6901–6905. DOI: 10.1007/s00216-013-7187-4.

(90) Li, D.-X.; Gan, L.; Bronja, A.; Schmitz, O. J. Gas chromatography coupled to atmospheric pressure ionization mass spectrometry (GC-API-MS): review. *Analytica chimica acta* **2015**, *891*, 43–61. DOI: 10.1016/j.aca.2015.08.002.

(91) Himmelsbach, M.; Buchberger, W.; Reingruber, E. Determination of polymer additives by liquid chromatography coupled with mass spectrometry. A comparison of atmospheric pressure photoionization (APPI), atmospheric pressure chemical ionization (APCI), and electrospray ionization (ESI). *Polymer Degradation and Stability* **2009**, *94* (8), 1213–1219. DOI: 10.1016/j.polymdegradstab.2009.04.021.

(92) Calemma, V.; Rausa, R. Thermal decomposition behaviour and structural characteristics of asphaltenes. *Journal of Analytical and Applied Pyrolysis* **1997**, *40-41*, 569–584. DOI: 10.1016/S0165-2370(97)00016-8.

(93) Speight, J. *Fouling in refineries*; Gulf Professional Publishing an imprint of Elsevier, 2015.

(94) Hancock, J. M.; van Zijl, A. W.; Robson, I.; Vachon, J.; Hashmi, A. A chemist's perspective on organic fouling in ethylene operations. *Hydrocarbon Process.* **2014**, *96* (6), 61–66.

(95) Cuoq, F.; Vachon, J.; Jordens, J.; Kwakkenbos, G. Red-oils in ethylene plants: formation mechanisms, structure and emulsifying properties. *Appl Petrochem Res* **2016**, *6* (4), 397–402. DOI: 10.1007/s13203-016-0171-0.

(96) Cai, H.; Krzywicki, A.; Oballa, M. C. Coke formation in steam crackers for ethylene production. *Chemical Engineering and Processing: Process Intensification* **2002**, *41* (3), 199–214. DOI: 10.1016/S0255-2701(01)00135-0.

(97) Vachon, J.; Hancock, J. M.; Robson, I. A chemist's perspective on organic fouling in ethylene operations: update. *Hydrocarbon Process.* **2015**, *94* (10), 49.

(98) Khuong, K. S.; Jones, W. H.; Pryor, W. A.; Houk, K. N. The mechanism of the self-initiated thermal polymerization of styrene. Theoretical solution of a classic problem. *J. Am. Chem. Soc.* **2005**, *127* (4), 1265–1277. DOI: 10.1021/ja0448667.

(99) Nohara, D.; Sakai, T. Kinetic study of model reactions in the gas phase at the early stage of coke formation. *Ind. Eng. Chem. Res.* **1992**, *31* (1), 14–19. DOI: 10.1021/ie00001a003.

(100) Streibel, T.; Weh, J.; Mitschke, S.; Zimmermann, R. Thermal desorption/pyrolysis coupled with photoionization time-of-flight mass spectrometry for the analysis of molecular organic compounds and oligomeric and polymeric fractions in urban particulate matter. *Anal. Chem.* **2006**, *78* (15), 5354–5361. DOI: 10.1021/ac060227y.

(101) Zhou, Z.; Chen, X.; Ma, H.; Liu, C.; Zhou, C.; Qi, F. Real-time monitoring biomass pyrolysis via on-line photoionization ultrahigh-resolution mass spectrometry. *Fuel* **2019**, *235*, 962–971. DOI: 10.1016/j.fuel.2018.08.098.

(102) Fendt, A.; Geissler, R.; Streibel, T.; Sklorz, M.; Zimmermann, R. Hyphenation of two simultaneously employed soft photo ionization mass spectrometers with thermal analysis of

biomass and biochar. *Thermochimica Acta* **2013**, *551*, 155–163. DOI: 10.1016/j.tca.2012.10.002.

(103) Zimmermann, R.; Saraji-Bozorgzad, M.; Grimmer, C.; Ulbrich, A.; Streibel, T. Erdöl in seine Bestandteile zerlegen und charakterisieren. *Nachr. Chem.* **2016**, *64* (7-8), 751–754. DOI: 10.1002/nadc.20164051750.

(104) Geißler, R.; Saraji-Bozorgzad, M.; Streibel, T.; Kaisersberger, E.; Denner, T.; Zimmermann, R. Investigation of different crude oils applying thermal analysis/mass spectrometry with soft photoionisation. *J Therm Anal Calorim* **2009**, *96* (3), 813–820. DOI: 10.1007/s10973-009-0034-3.

(105) Saraji-Bozorgzad, M. R.; Streibel, T.; Eschner, M.; Groeger, T. M.; Geissler, R.; Kaisersberger, E.; Denner, T.; Zimmermann, R. Investigation of polymers by a novel analytical approach for evolved gas analysis in thermogravimetry. *J Therm Anal Calorim* **2011**, *105* (3), 859–866. DOI: 10.1007/s10973-011-1720-5.

(106) Geissler, R.; Saraji-Bozorgzad, M. R.; Gröger, T.; Fendt, A.; Streibel, T.; Sklorz, M.; Krooss, B. M.; Fuhrer, K.; Gonin, M.; Kaisersberger, E.; Denner, T.; Zimmermann, R. Single Photon Ionization Orthogonal Acceleration Time-of-Flight Mass Spectrometry and Resonance Enhanced Multiphoton Ionization Time-of-Flight Mass Spectrometry for Evolved Gas Analysis in Thermogravimetry: Comparative Analysis of Crude Oils. *Anal. Chem.* **2009**, *81* (15), 6038–6048. DOI: 10.1021/ac900216y.

(107) Streibel, T.; Fendt, A.; Geißler, R.; Kaisersberger, E.; Denner, T.; Zimmermann, R. Thermal analysis/mass spectrometry using soft photo-ionisation for the investigation of biomass and mineral oils. *J Therm Anal Calorim* **2009**, *97* (2), 615–619. DOI: 10.1007/s10973-008-9769-5.

(108) Platzer, N. Encyclopedia of polymer science and engineering, 2. ed., volume 6; Interscience, New York, 1986.

(109) Slager, T. L.; Prozonic, F. M. Simple methods for calibrating IR in TGA/IR analyses. *Thermochimica Acta* **2005**, *426* (1-2), 93–99. DOI: 10.1016/j.tca.2004.07.022.

(110) Herndon, W. C.; Grayson, C. R.; Manion, J. M. Retro-Diels-Alder reactions. III. Kinetics of the thermal decompositions of exo- and endo-dicyclopentadiene. *J. Org. Chem.* **1967**, *32* (3), 526–529. DOI: 10.1021/jo01278a003.

(111) Zimmermann, H.; Walzl, R. Ethylene. In *Ullmann's Encyclopedia of Industrial Chemistry*; Wiley-VCH Verlag GmbH & Co. KGaA, 2000. DOI: 10.1002/14356007.a10_045.pub3.

(112) Namazi, H. Polymers in our daily life. *BioImpacts : BI* **2017**, *7* (2), 73–74. DOI: 10.15171/bi.2017.09.

(113) Mülhaupt, R. Hermann Staudinger and the origin of macromolecular chemistry. *Angewandte Chemie (International ed. in English)* **2004**, *43* (9), 1054–1063. DOI: 10.1002/anie.200330070.

(114) Kaminsky, W., Ed. *Polyolefins: 50 years after Ziegler and Natta I*; Advances in Polymer Science; Springer Berlin Heidelberg, 2013. DOI: 10.1007/978-3-642-40808-3.

(115) Monrabal, B.; Blanco, J.; Nieto, J.; Soares, J. B.P. Characterization of homogeneous ethylene/1-octene copolymers made with a single-site catalyst. CRYSTAF analysis and calibration. *J. Polym. Sci. A Polym. Chem.* **1999**, *37* (1), 89–93. DOI: 10.1002/(SICI)1099-0518(19990101)37:1<89:AID-POLA10>3.0.CO;2-%23.

(116) Eselem Bungu, P. S.; Pflug, K.; Busch, M.; Pasch, H. Comprehensive analysis of novel grafted polyethylenes using multidimensional fractionation methods. *Polym. Chem.* **2018**, *9* (40), 5051–5065. DOI: 10.1039/C8PY01122B.

(117) Cudby, M.E.A.; Bunn, A. Determination of chain branching in low density polyethylene by 13C nuclear magnetic resonance and infra-red spectroscopy. *Polymer* **1976**, *17* (4), 345–347. DOI: 10.1016/0032-3861(76)90193-2.

(118) Macko, T.; Brüll, R.; Zhu, Y.; Wang, Y. A review on the development of liquid chromatography systems for polyolefins. *Journal of separation science* **2010**, *33* (22), 3446–3454. DOI: 10.1002/jssc.201000516.

(119) Malik, M. I.; Pasch, H. Field-flow fractionation: New and exciting perspectives in polymer analysis. *Progress in Polymer Science* **2016**, *63*, 42–85. DOI: 10.1016/j.progpolymsci.2016.03.004.

(120) Drzeżdżon, J.; Jacewicz, D.; Sielicka, A.; Chmurzyński, L. MALDI-MS for polymer characterization – Recent developments and future prospects. *TrAC Trends in Analytical Chemistry* **2019**, *115*, 121–128. DOI: 10.1016/j.trac.2019.04.004.

(121) Moscato, B.; Landis, C. Are carbodiimide-quenched polyethylene distributions representative of bulk polymer samples? Analysis of metallocene-catalyzed ethylene polymerization by ESI-MS, MALDI, GPC and NMR. *Chemical communications (Cambridge, England)* **2008** (44), 5785–5787. DOI: 10.1039/B812133H.

(122) van Ruymbeke, E.; Stéphenne, V.; Daoust, D.; Godard, P.; Keunings, R.; Bailly, C. A sensitive method to detect very low levels of long chain branching from the molar mass distribution and linear viscoelastic response. *Journal of Rheology* **2005**, *49* (6), 1503–1520. DOI: 10.1122/1.2048743.

(123) Zhang, M.; Wanke, S. E. Quantitative determination of short-chain branching content and distribution in commercial polyethylenes by thermally fractionated differential scanning calorimetry. *Polym. Eng. Sci.* **2003**, *43* (12), 1878–1888. DOI: 10.1002/pen.10159.

(124) Eckerle, P.; Pursch, M.; Cortes, H. J.; Sun, K.; Winniford, B.; Luong, J. Determination of short-chain branching content in polyethylene by pyrolysis comprehensive multidimensional gas chromatography using low thermal mass column technology. *Journal of separation science* **2008**, *31* (19), 3416–3422. DOI: 10.1002/jssc.200800218.

(125) Wild, L.; Ryle, T. R.; Knobeloch, D. C.; Peat, I. R. Determination of branching distributions in polyethylene and ethylene copolymers. *J. Polym. Sci. Polym. Phys. Ed.* **1982**, *20* (3), 441–455. DOI: 10.1002/pol.1982.180200307.

(126) Monrabal, B. Polyolefin Characterization: Recent Advances in Separation Techniques. In *Polyolefins: 50 years after Ziegler and Natta I*; Kaminsky, W., Ed.; Advances in Polymer Science; Springer Berlin Heidelberg, 2013; pp 203–251. DOI: 10.1007/12_2013_216.

(127) Pasch, H. Recent developments in polyolefin characterization. *Macromol. Symp.* **2001**, *165* (1), 91–98. DOI: 10.1002/1521-3900(200103)165:1<91:AID-MASY91>3.0.CO;2-2.

(128) DesLauriers, P. J.; Rohlfing, D. C.; Hsieh, E. T. Quantifying short chain branching microstructures in ethylene 1-olefin copolymers using size exclusion chromatography and Fourier transform infrared spectroscopy (SEC–FTIR). *Polymer* **2002**, *43* (1), 159–170. DOI: 10.1016/S0032-3861(01)00574-2.

(129) Yau, W. W.; Gillespie, D. New approaches using MW-sensitive detectors in GPC–TREF for polyolefin characterization. *Polymer* **2001**, *42* (21), 8947–8958. DOI: 10.1016/S0032-3861(01)00392-5.

(130) Tsuge, S.; Ohtani, H. Structural characterization of polymeric materials by Pyrolysis—GC/MS. *Polymer Degradation and Stability* **1997**, *58* (1-2), 109–130. DOI: 10.1016/S0141-3910(97)00031-1.

(131) Ohtani, H.; Tsuge, S.; Usami, T. Determination of short-chain branching up to C6 in low-density polyethylenes by high-resolution pyrolysis-hydrogenation gas chromatography. *Macromolecules* **1984**, *17* (12), 2557–2561. DOI: 10.1021/ma00142a016.

(132) Cody, R. B.; Fouquet, T. N. J.; Takei, C. Thermal desorption and pyrolysis direct analysis in real time mass spectrometry for qualitative characterization of polymers and polymer additives. *Rapid Commun. Mass Spectrom.* **2020**, *34 Suppl 2*, e8687. DOI: 10.1002/rcm.8687.

(133) Farenc, M.; Witt, M.; Craven, K.; Barrère-Mangote, C.; Afonso, C.; Giusti, P. Characterization of Polyolefin Pyrolysis Species Produced Under Ambient Conditions by Fourier Transform Ion Cyclotron Resonance Mass Spectrometry and Ion Mobility-Mass Spectrometry. *Journal of the American Society for Mass Spectrometry* **2017**, *28* (3), 507–514. DOI: 10.1007/s13361-016-1572-0.

(134) Kiran, E.; Gillham, J. K. Pyrolysis-molecular weight chromatography: A new on-line system for analysis of polymers. II. Thermal decomposition of polyolefins: Polyethylene, polypropylene, polyisobutylene. *J. Appl. Polym. Sci.* **1976**, *20* (8), 2045–2068. DOI: 10.1002/app.1976.070200803.

(135) Poutsma, M. L. Reexamination of the Pyrolysis of Polyethylene: Data Needs, Free-Radical Mechanistic Considerations, and Thermochemical Kinetic Simulation of Initial Product-Forming Pathways. *Macromolecules* **2003**, *36* (24), 8931–8957. DOI: 10.1021/ma0303768.

(136) Ratkiewicz, A. Kinetics of the C-C bond beta scission reactions in alkyl radicals. *Physical chemistry chemical physics : PCCP* **2011**, *13* (33), 15037–15046. DOI: 10.1039/C1CP21229J.

(137) Bockhorn, H.; Hornung, A.; Hornung, U.; Schawaller, D. Kinetic study on the thermal degradation of polypropylene and polyethylene. *Journal of Analytical and Applied Pyrolysis* **1999**, *48* (2), 93–109. DOI: 10.1016/S0165-2370(98)00131-4.

(138) Murata, K.; Sato, K.; Sakata, Y. Effect of pressure on thermal degradation of polyethylene. *Journal of Analytical and Applied Pyrolysis* **2004**, *71* (2), 569–589. DOI: 10.1016/j.jaap.2003.08.010.

(139) Serrano, D. P.; Aguado, J.; Escola, J. M.; Rodríguez, J. M.; San Miguel, G. An investigation into the catalytic cracking of LDPE using Py–GC/MS. *Journal of Analytical and Applied Pyrolysis* **2005**, *74* (1-2), 370–378. DOI: 10.1016/j.jaap.2004.11.026.

(140) Ueno, T.; Nakashima, E.; Takeda, K. Quantitative analysis of random scission and chain-end scission in the thermal degradation of polyethylene. *Polymer Degradation and Stability* **2010**, *95* (9), 1862–1869. DOI: 10.1016/j.polymdegradstab.2010.04.020.

(141) Tsuchiya, Y.; Sumi, K. Thermal decomposition products of polyethylene. *J. Polym. Sci. A-1 Polym. Chem.* **1968**, *6* (2), 415–424. DOI: 10.1002/pol.1968.150060211.

(142) Madorsky, S. L. Rates of thermal degradation of polystyrene and polyethylene in a vacuum. *J. Polym. Sci.* **1952**, *9* (2), 133–156. DOI: 10.1002/pol.1952.120090203.

(143) Kuroki, T.; Sawaguchi, T.; Niikuni, S.; Ikemura, T. Mechanism for long-chain branching in the thermal degradation of linear high-density polyethylene. *Macromolecules* **1982**, *15* (6), 1460–1464. DOI: 10.1021/ma00234a002.

(144) Wunderlich, B.; Czornyj, G. A Study of Equilibrium Melting of Polyethylene. *Macromolecules* **1977**, *10* (5), 906–913. DOI: 10.1021/ma60059a006.

(145) Gopalan, M. R.; Mandelkern, L. Effect of crystallization temperature and molecular weight on the melting temperature of linear polyethylene. *J. Phys. Chem.* **1967**, *71* (12), 3833–3841. DOI: 10.1021/j100871a018.

(146) Yoshida, S.; Hiraga, K.; Takehana, T.; Taniguchi, I.; Yamaji, H.; Maeda, Y.; Toyohara, K.; Miyamoto, K.; Kimura, Y.; Oda, K. A bacterium that degrades and assimilates poly(ethylene terephthalate). *Science (New York, N.Y.)* **2016**, *351* (6278), 1196–1199. DOI: 10.1126/science.aad6359.

(147) Tukker, A. *Plastics Wastes - Feestock Recycling, Chemical Recycling and Incineration*; Rapra Review Reports; Rapra Technology Ltd, 2002.

(148) Aguado, J., Serrano, D. P., Clark, J. H. *Feedstock Recycling of Plastic Wastes*; Royal Society of Chemistry, 1999. DOI: 10.1039/9781847550804.

(149) Dhahak, A.; Grimmer, C.; Neumann, A.; Rüger, C.; Sklorz, M.; Streibel, T.; Zimmermann, R.; Mauviel, G.; Burkle-Vitzthum, V. Real time monitoring of slow pyrolysis of polyethylene terephthalate (PET) by different mass spectrometric techniques. *Waste management (New York, N.Y.)* **2020**, *106*, 226–239. DOI: 10.1016/j.wasman.2020.03.028.

8 Appendix: Scientific publications

8.1 Publication 1

Combination of Different Thermal Analysis Methods Coupled to Mass Spectrometry for the Analysis of Asphaltenes and Their Parent Crude Oils: Comprehensive Characterization of the Molecular Pyrolysis Pattern

by

Christopher. P. Rüger, Christoph Grimmer, Martin Sklorz, Anika Neumann, Thorsten Streibel, Ralf Zimmermann

energy&fuels

Combination of Different Thermal Analysis Methods Coupled to Mass Spectrometry for the Analysis of Asphaltenes and Their Parent Crude Oils: Comprehensive Characterization of the Molecular Pyrolysis Pattern

Christopher P. Rüger,*,[†] Christoph Grimmer,[†] Martin Sklorz,[†] Anika Neumann,[†] Thorsten Streibel,[†,‡] and Ralf Zimmermann[†,‡,§]

[†]Joint Mass Spectrometry Centre/Chair of Analytical Chemistry, University of Rostock, 18051 Rostock, Germany

[‡]Joint Mass Spectrometry Centre/Cooperation Group Comprehensive Molecular Analytics, Helmholtz Zentrum München, 85764 Neuherberg, Germany

[§]Aerosols and Health, Helmholtz Virtual Institute of Complex Molecular Systems in Environmental Health (HICE), 85764 Neuherberg, Germany

S *Supporting Information*

ABSTRACT: In this study, the asphaltene and corresponding crude oil, distributed within the Asphaltene Characterization Interlaboratory Study for PetroPhase 2017, were characterized on the molecular level. For this purpose, three different thermal analysis mass spectrometry hyphenations with five diverse ionization techniques varying in selectivity were deployed: (1) thermal desorption/pyrolysis gas chromatography electron ionization (TD/Pyr−GC−EI−QMS), (2/3) thermogravimetry single-photon/resonance-enhanced multiphoton ionization time-of-flight (TG SPI/REMPI TOF−MS), and (4/5) thermogravimetry atmospheric pressure photo-/chemical ionization ultrahigh-resolution mass spectrometry (TG APPI/APCI FT−ICR MS). For the investigated C_7 asphaltene, no mass loss was detected at <300 °C and the pyrolysis phase was dominant, whereas the parent crude oil exhibits a high abundant desorption phase. At roughly 330 °C, pyrolysis begins and mass loss as well as complex mass spectrometric patterns were recorded. The resulting information on the effluent gained by the different soft ionization mass spectrometric approaches was combined with the GC−EI−MS data for structural cross-evaluation. We showed that the combination of the applied techniques leads to a more comprehensive chemical characterization. For the asphaltene, TG SPI TOF−MS shows high abundances of alkanes, alkenes, and hydrogen sulfide during pyrolysis. TG REMPI TOF−MS is selective toward aromatics and reveals clear patterns of polyaromatic hydrocarbons (PAHs) and minor amounts of nitrogen-containing aromatics tentatively identified as acridine- or carbazol-like structures. GC−EI−MS provides information on the average chain length of alkanes, alkenes, and PA(S)H. Both atmospheric pressure ionization techniques (APPI and APCI) hyphenated to FT−MS showed CHS (in particular, benzothiophenes) and CH as dominant compound classes, with an average number of condensed aromatic rings of 2−4. Combining the information of all techniques, including the average asphaltene mass obtained by field desorption experiments and aromatic core size received by collision-induced dissociation, the archipelago-type molecular structure seems to be dominant for the investigated asphaltene.

■ INTRODUCTION

The chemical composition of petroleum and petrochemical products is crucial for their processing and economic utilization.[1−3] Even with state-of-the-art analytical instrumentation, the analysis of heavy petroleum and its fractions as well as from unconventional petroleum sources, such as oil sands, is still a challenge.[4,5] Especially, for the asphaltene fraction, a part of the petroleum that is soluble in toluene and insoluble in a small paraffin, such as *n*-heptane, only a few standardized analysis methods exist.[6] These ultracomplex mixtures with high aromatic content, besides other heavy constituents, cause particular problems for traditional approaches, e.g., chromatographic and high-resolution mass spectrometric techniques. A molecular understanding of the asphaltene fraction is however of particular interest because these species are known to cause flow assurance and processing issues in up- and downstream processes.[6,7]

State-of the art techniques for the chemical characterization of asphaltenes on the molecular level are mainly mass spectrometric approaches, such as direct infusion atmospheric pressure ionization ultrahigh-resolution mass spectrometry.[4,8,9] In addition, high-field nuclear magnetic resonance (NMR) spectroscopy and absorption spectroscopic approaches, such as X-ray absorption near edge structure (XANES)[10−12] as well as high-performance liquid chromatography, are deployed.[13] Thermal analysis (TA), regarding evolved gas analysis, coupled to various analytical detectors has also become a powerful tool in petroleum analysis and other areas.[14−19]

Besides spectroscopic approaches, such as infrared spectroscopy for fingerprint pattern or small-molecule quantification,[15,20,21] mass spectrometry is the favored coupling technique.[14,16,18] For heavy petroleum, thermal analysis is primarily applied for studying the evaporation pattern as well as the thermal decomposition products at an elevated temperature during pyrolysis.[22−24] Pyrolysis gas chromatography was conducted extensively with low resolving mass analyzers and hard ionization to study thermal decomposition products since the 1980s.[25−31]

Unfortunately, until now, no single mass spectrometric technique is capable of a comprehensive analysis of the complex pyrolysis effluent. Therefore, choosing an ionization source is crucial, and different methods will cover different chemical spaces.[32] For the thermal analysis of petroleum fractions, most often nominal resolving mass analyzers with hard ionization are used, which enable robust pattern information.[15,33] Nonetheless, soft ionization techniques become more important in mass spectrometry and thermal analysis coupling. The generation of molecular ions, instead of an intense fragment pattern, reduces the complexity of the mass spectra and allows for an easier molecular assignment. In previous studies, we applied various soft ionization techniques for thermal analysis, such as photoionization[23,34−37] and chemical ionization.[38−41] With the selection of a particular soft ionization technique, control of selectivity can be achieved. In the case of resonance-enhanced multiphoton ionization (REMPI), aromatic compounds are selectively ionized,[42,43] whereas atmospheric pressure photoionization (APPI) reveals a high ionization efficiency for aromatic and sulfur-containing species and atmospheric pressure chemical ionization (APCI) reveals a high ionization efficiency for medium-polar and polar constituents.[32,44−47] We applied TA with soft ionization mass spectrometric detection for a wide range of applications, e.g., nut and coffee roasting,[36,48,49] crude oils,[23,24,37] biomass/tobacco pyrolysis,[34,35,41] elemental sulfur evaporation,[50] polymers,[37] and dissolved organic matter.[51] Asphaltene pyrolysis has not been studied before with photoionization (PI) techniques, with either vacuum PI or atmospheric pressure PI.

All ionization techniques cover a particular molecular space and exhibit a certain part of the chemical signature of a complex mixture. In this study, the results of three different thermal analysis approaches equipped with five different ionization techniques are combined for a more comprehensive analysis of the effluent of an asphaltene and its parent crude oil. For this purpose, the heptane (C_7) asphaltene and parent crude oil of the Asphaltene Characterization Interlaboratory Study for PetroPhase 2017 were investigated. Asphaltenes are one of the most complex natural mixtures with a variety of heteroelements and chemical functionalities, spanning a broad mass range. Over the last few decades, a lot of effort has gone into deciphering their molecular architecture, whereby two opposed models are discussed: island (large aromatic core with side chains) and archipelago (linker connected smaller aromatic cores). As shown for pyrolysis gas chromatography in the literature, the thermal decomposition products of the macromolecular structure should give information about the respective building blocks and add valuable information to the molecular architecture debate.

Five different ionization schemes were applied with electron ionization (EI) as a hard and universal technique, single-photon ionization (SPI) as a soft and universal method, REMPI as an aromatic-selective and soft technique, as well as atmospheric pressure chemical and photoionization (APCI/APPI). This study

aims to show the advantages and limitations of the individual methods and the potential of combining their results. High-resolution mass spectrometry will give information about the elemental composition, whereas pyrolysis gas chromatography will add structural aspects and SPI will provide information on the thermally cracked side chains. We hypothesize that thermal analysis mass spectrometry can contribute significantly to unravel asphaltene composition and structure when several techniques are combined, with the interlaboratory asphaltene study as an ideal case study as a result of the extensive research conducted on the same asphaltene sample.

■ MATERIALS AND METHODS

Material. In this study, a heptane (C_7) asphaltene and the corresponding parent crude oil (a Columbian heavy crude oil, with an American Petroleum Institute (API) gravity of 12°)[52] were investigated. The samples were received within the Asphaltene Characterization Interlaboratory Study for PetroPhase 2017 and had been prepared by the group of Marianny Y. Comariza at the Industrial University of Santander (Colombia).[52] In brief, asphaltenes are precipitated using the ASTM D6560-12 procedure with *n*-heptane under sonication (110 W and 40 kHz), which decreased co-precipitants significantly. Four Soxhlet extraction steps were deployed as an additional cleaning procedure for an efficient removal of occluded compounds of the maltene fraction to receive the final cleaned asphaltene sample. Additional information on the elemental composition is given in Table S1 of the Supporting Information.

Instrumentation. Three thermal analysis setups coupled to different mass spectrometric systems were deployed within this study: (1) thermal desorption/pyrolysis gas chromatography with electron ionization and quadrupole mass spectrometric detection (TD/Pyr−GC−EI−QMS); (2/3) thermogravimetry photoionization [single-photon ionization (SPI) and resonance-enhanced multiphoton ionization (REMPI)] with time-of-flight mass spectrometric detection (TG SPI/REMPI TOF−MS), and (4/5) thermogravimetry atmospheric pressure photo- and atmospheric pressure chemical ionization ultrahigh-resolution mass spectrometry (TG APPI/APCI FT-ICR MS). The schematic setup of the three mass spectrometric hyphenations and their corresponding ionization techniques is given in Figure 1. Additionally, the figure depicts survey diagrams of the associated asphaltene measurements.

For the (1) thermal desorption/pyrolysis gas chromatographic analysis, 10 μL of the diluted parent crude oil (1:100 in dichloromethane) and roughly 0.5−0.9 mg of the solid asphaltene were injected into the pyrolyzer (model PY-2020iD, double-shot pyrolyzer, Frontier Laboratories) mounted onto a HP 6890 gas chromatograph.[53,54] The sample material undergoes two steps: (1) a thermal desorption process at 300 °C and (2) a pyrolysis step at 500 °C, each held for 1 min. To separate the evolved gas mixture, a 30 m SGE-BPX5 column (250 μm inner diameter, 0.25 μm film, helium at 99.999%, and head pressure at 0.4 bar) was used with the following temperature program: hold for 10 min at 50 °C, ramp to 330 °C with 10 K/min, and hold for 20 min. The effluent from the column was ionized by a 70 eV electron ionization source and analyzed by a quadrupole mass spectrometer. Mass spectra were recorded in scan mode from m/z 10 to 500. Data were analyzed by AMDIS version 2.62 and Bruker DataAnalysis 4.0 SP 1. In brief, Bruker DataAnalysis was used for fast assessment of the data and obtaining a qualitative overview, e.g., survey view, extracted ion chromatograms, and averaging of time segments. Afterward, AMDIS was used for finding chromatographic features (deconvolution) and validation of fragment spectra with the National Institute of Standards and Technology (NIST) database (NIST MS Search 2.0).

For setup 2/3, the volatile and semi-volatile constituents of the effluent from a thermal balance were analyzed by single- and resonance-enhanced multiphoton ionization (SPI/REMPI). For this purpose, a thermobalance (STA 409, Netzsch Gerätebau, Selb, Germany) was directly hyphenated to the ionization source of the mass spectrometer
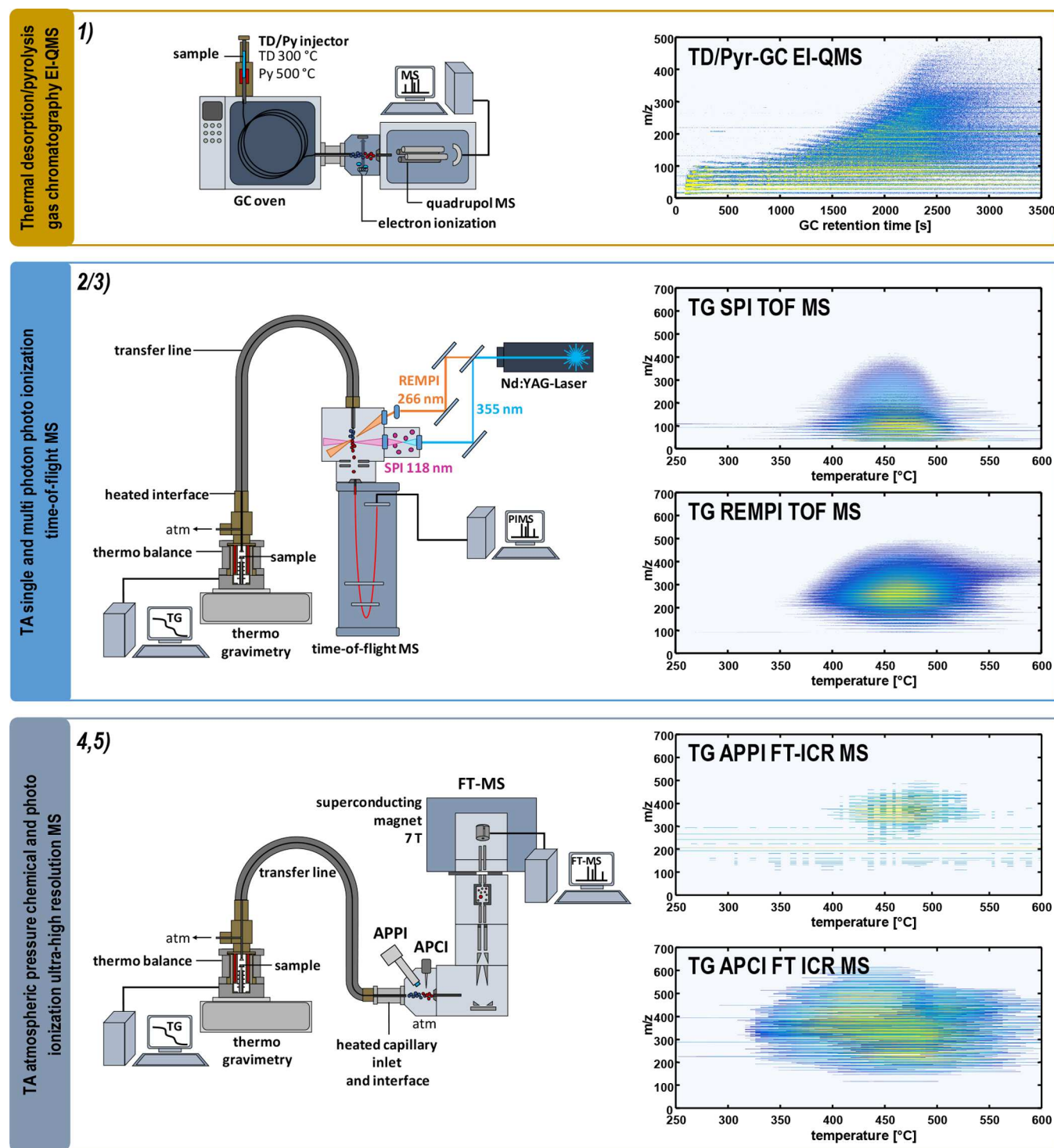
Figure 1. Schematic overview of the deployed thermal analysis mass spectrometry hyphenations: (1) thermal desorption/pyrolysis gas chromatography with electron ionization quadrupole mass spectrometric detection (TD/Pyr−GC−EI−QMS); (2/3) thermogravimetry photoionization with time-of-flight mass spectrometric detection (TG SPI/REMPI TOF−MS), and (4/5) thermogravimetry atmospheric pressure photo-/chemical ionization ultrahigh-resolution mass spectrometry (TG APPI/APCI FT-ICR MS). Survey views (retention time/temperature versus m/z) are given on the right-hand side for each applied technique on the analysis of the Asphaltene Characterization Interlaboratory Study for PetroPhase 2017 asphaltene sample.

via a heated interface and transfer line (l 2.25 m, 280 μm inner diameter, and 280 °C).[55,56] A few milligrams of the sample material were placed on an aluminum oxide crucible without any sample pretreatment. Thermal analysis was carried out with a heating rate of 10 K/min under a nitrogen atmosphere (60 mL/min) from 30 to 800 °C. At 800 °C, nitrogen is partially replaced by air (40 mL/min synthetic air

and 20 mL/min nitrogen), yielding an oxidative atmosphere. Evolved gas was sampled as a result of the pressure difference between the balance at atmospheric pressure and the ion source at vacuum (roughly 3×10^{-4} mbar). The subsequent SPI and REMPI TOF−MS analysis is described in detail elsewhere.[23,34,57] In brief, for SPI, 355 nm laser pulses (25 mJ pulse energy, 10 Hz repetition rate, and 5 ns

pulse width), generated from a Nd:YAG laser (Surelite III, Continuum, Inc., Santa Clara, CA, U.S.A.), were sent through a xenon-filled gas cell (Xe 4.0, 12 mbar), yielding vacuum ultraviolet photons (118 nm and 10.5 eV). For REMPI, the Nd:YAG fundamental wavelength is frequency-quadrupled (4.7 eV and 266 nm). The molecular ions formed by either REMPI or SPI are recorded from m/z 5 to 500 with TOF−MS using a multichannel plate detector. Data processing and analysis were carried out with the instrument-specific LabView graphical user interface and self-written MATLAB scripts.

The third mass spectrometric setup (4/5) is composed of a thermobalance (TG 209, Netzsch Gerätebau, Selb, Germany) coupled to a modified Bruker GC-APCI II source, which allows us to carry out APCI with a stainless-steel corona needle (3 μA corona current) as well as APPI with a Kr vacuum ultraviolet (VUV) lamp (10/10.6 eV and 124/117 nm).[58] The temperature program of the thermobalance with a constant flow of 200 mL/min nitrogen was 2 min isothermal at 20 °C, ramp to 600 °C with 10 K/min, and hold for 10 min at 600 °C. The evolved mixture was sampled via a 300 °C interface and 280 °C transfer line into the ion source. In contrast to setup 2/3, the gas sampling was achieved by a slight overpressure of 8−10 mbar in the thermobalance compared to the atmospheric pressure in the ionization source. For mass spectrometric detection, a Bruker Apex II ultra FT−MS equipped with a 7 T superconducting magnet was used. Mass spectra were recorded from m/z 100 to 2000 with a four megaword transient, resulting in a resolving power of roughly 300 000 at m/z 400. A broad band spectrum with five microscans was recorded, alternating with a collision-induced dissociation (CID) spectrum of the whole mass range at 30 V with five microscans, resulting in an overall acquisition rate of 0.2 Hz. A detailed description of the APCI setup can be found elsewhere.[41] Atmospheric pressure chemical and photo-ionization were deployed in positive ion mode. For APCI, roughly 1−2 mg of the parent crude oil and asphaltene were analyzed, whereas for APPI, 3−5 mg of the sample was placed into the aluminum crucible. Please note that the source was optimized for gas chromatography APCI, leading to a lower sensitivity in APPI mode.

■ RESULTS AND DISCUSSION

All of the applied techniques exhibit certain characteristics, such as high mass resolving power and accuracy for the hyphenation of thermogravimetry to atmospheric pressure ionization FT−MS, vacuum ionization avoiding matrix effects, or additional gas chromatographic information from the two-step desorption/pyrolysis system. This diversity results in five complex and diverse data sets (see Figure 1), and their information has to be efficiently combined to allow for a comprehensive description of the effluent. In Figure 2, a simplified schematic of one possible data analysis route is given as a roadmap for the analysis throughout this study.

One advantage of the thermogravimetric assemblies (2/3 and 4/5) is the recording of the temperature-dependent mass loss curve, which reveals quantitative information on the volatility and decomposition, which is not accessible with the TD/Pyr−GC setup. The mass loss curves showed no significant desorption step and a relatively sharp pyrolysis signal peaking at 435−460 °C with
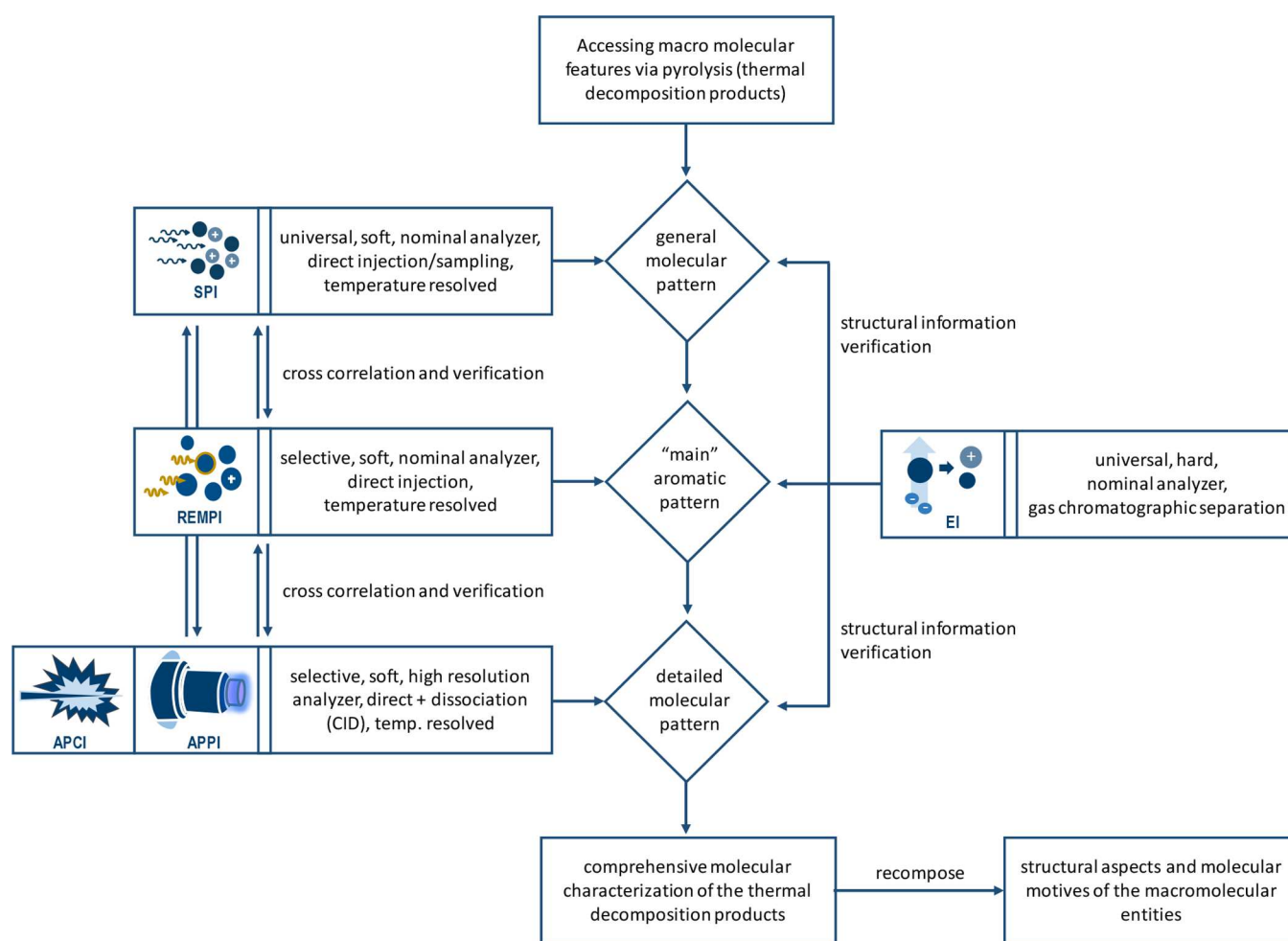
Figure 2. Flowchart for the evaluation of the applied thermal analysis mass spectrometric data sets. The data from techniques not involving chromatographic separation are backed up partially with information from GC and among themselves.
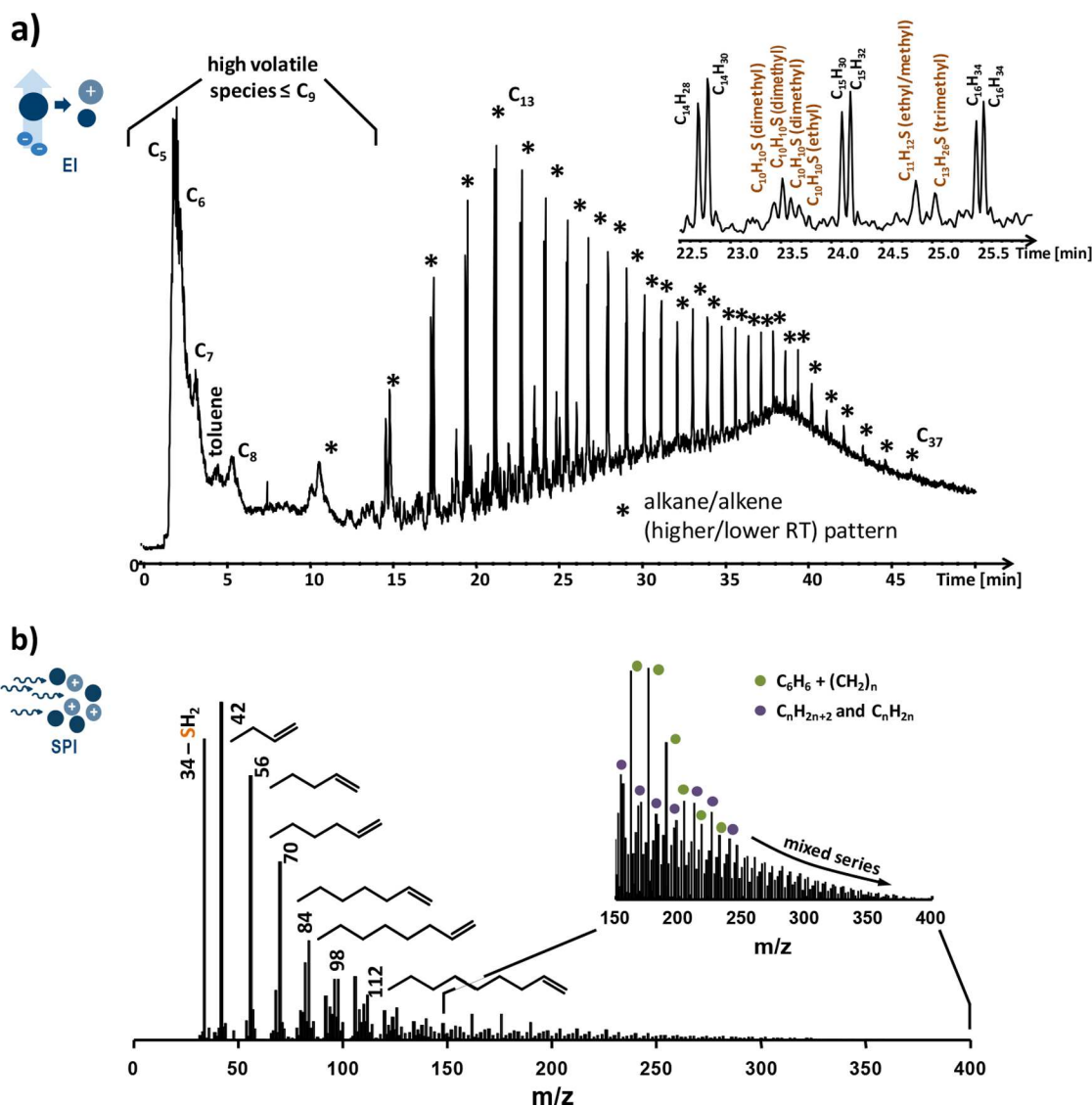
Figure 3. (a) Total ion count gas chromatogram for the 500 °C pyrolysis EI–QMS measurement of the asphaltene. Low mass hydrocarbons down to C_2 were detected, but chromatographic separation was insufficient. Starting with C_{10}, a defined alkane and alkene pattern is observed, whereas the enlarged section reveals alkylated benzothiophene isomers. (b) Averaged SPI mass spectrum for the asphaltene pyrolysis with a high abundance alkene pattern. Within the expanded part of the SPI mass spectrum, a continuing benzene, alkane, and alkene pattern can be observed.

a mass loss of 47–49 wt % (Figure S1 of the Supporting Information). The thermal behavior is in good agreement with the chemical evolved gas analysis data from TD/Pyr–GC as well as with the mass spectrometric response of the TG-coupled spectrometer. In contrast, the parent crude oil exhibits an intense desorption phase with a mass loss of roughly 60 wt % before 300 °C and a further mass loss of approximately 30 wt % in the pyrolysis phase (300–600 °C). An amount of approximately 49 wt % for the asphaltene and 5 wt % for the parent crude oil remained as a deposit and is rapidly decomposed under an oxidative atmosphere at 800 °C. This deposit can be assigned to carbonized species formed during pyrolysis, e.g., graphite. Literature shows that the yield of volatile matter in the pyrolysis phase correlates with the aliphatic content in petrochemicals, and therefore, a high proportion of the mass loss will be caused by dealkylation of aromatic species.[59] In summary, the hypothesis that the interlaboratory asphaltene sample does not contain significant amounts of volatile

or semi-volatile species can be stated and is in agreement with the literature for other asphaltenes.[60]

Pyrolysis Gas Chromatography. The pyrograms obtained by pyrolysis gas chromatography at 500 °C were analyzed as shown in the literature to obtain the average side-chain length, sulfur compounds versus aliphatic compounds, and to indicate the presence of SO_2 as well as CO_2.[28,61] The low ionization efficiency dependence of the EI concerning the molecular structure and size is a useful advantage compared to chemical and photoionization. Primary pyrolysis signals were aliphatic side chains up to a length of 37 carbons (C_{37}). SO_2 (m/z 64) was found to a very low extent compared to H_2S (m/z 34). This finding indicates nearly oxygen-free conditions. Thiophenic species were found to be more abundant than H_2S, indicating thiophene sulfur constituents dominant compared to thiols. The comparison between sulfur compounds and aliphatic species revealed a strong dominance of aliphatic species, with 2 orders of magnitude higher abundance. The average aliphatic side-chain length turned out to be 8.2 (m/z ~120), identified by
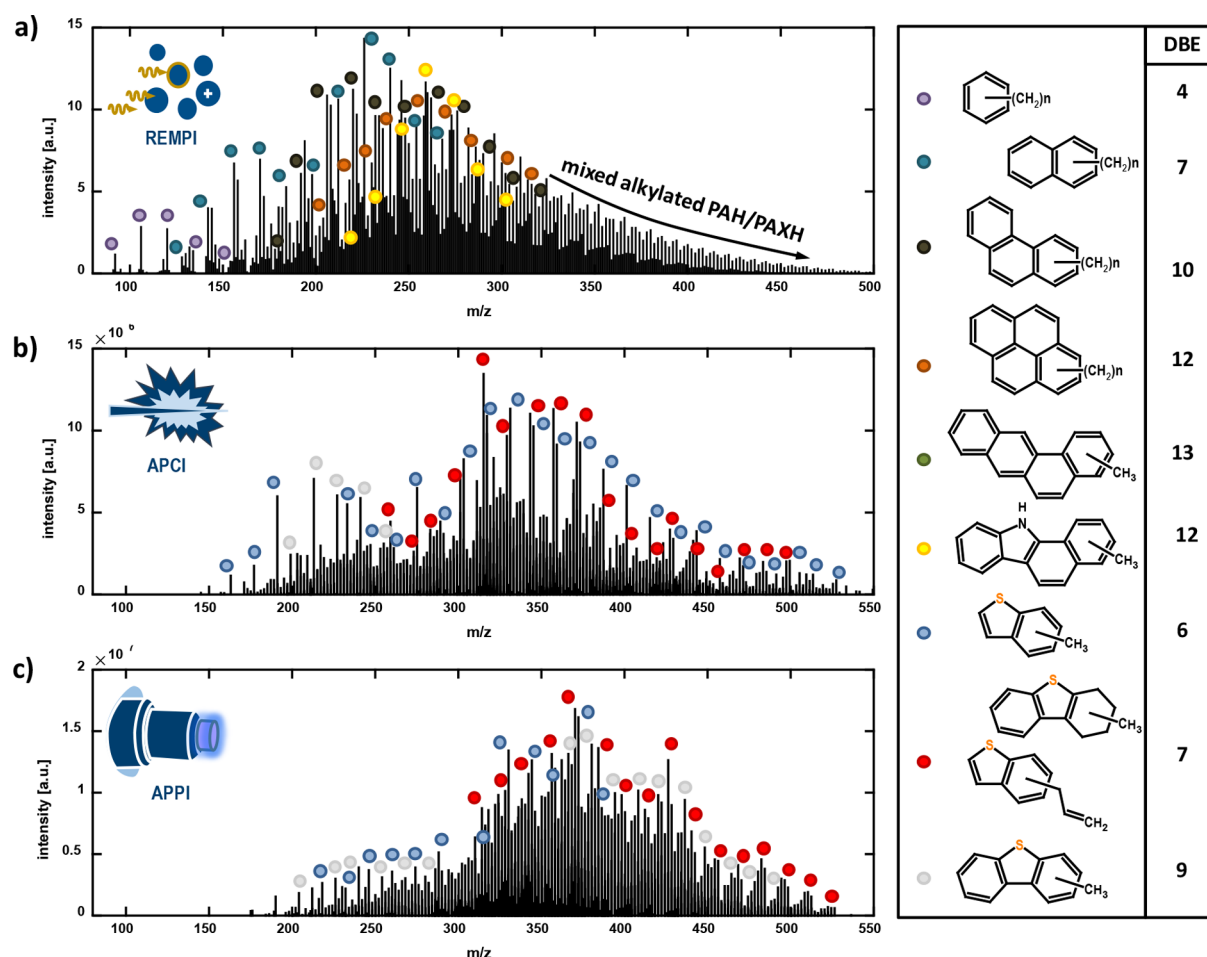
Figure 4. Average mass spectra of the asphaltene pyrolysis for (a) REMPI TOF−MS, (b) APCI, and (c) APPI FT-ICR MS. Tentative assignments of selected aromatic alkylated series as well as their structure and DBE are given on the right side. PAXH = heteroatom (X = N, S, and O)-containing polycyclic aromatic hydrocarbons (PAHs).

the alkane and alkene main fragments m/z 55 and 57, which is slightly higher than values from the literature (Figures S2−S5 of the Supporting Information).[28,61] Branched alkane/alkene species were only present in minor abundance in the effluent compared to the *n*-isomeric species. Nonetheless, for larger carbon numbers, the separation power is insufficient for a complete separation and no clear isomeric information can be given on species larger than C_{18}. They may have a higher proportion of branched isomers as the ratio of branched/linear species increases with increasing m/z. The investigation of the aromatics on the basis of m/z 91 for the alkyl benzene species and m/z 162 and 176 for benzo- and dibenzothiophenes revealed an intricate pattern of sulfur species, captured in more detail with APPI and APCI. Furthermore, the thiophene species with the lowest molecular weight were found to be 2-ring benzothiophenes, whereas for hydrocarbons, alkylated benzene species (1 ring) were found. These 1-ring aromatics can be eventually formed during pyrolysis from naphthenic derivatives and, moreover, might be overrepresented as a result of their GC optimal volatility range. The fragmentation of the EI hinders the detection of the molecular ion and, in addition to that, a more detailed assignment, e.g., of naphthenic constituents.

Single-Photon Ionization. For the single-photon ionization, a universal and soft ionization technique,[43,62] typical petroleum patterns with homologue series of m/z 14 (CH_2) and m/z 2 (H_2) spacing were observed for the parent crude oil

as well as asphaltene. The spectra (Figure S6 of the Supporting Information and Figure 3b) covered a mass range from m/z 34 to approximately 450. The higher contribution of intact desorbed species in the total average parent crude oil spectra (89% TIC < 350 °C) leads to a higher intensity-weighted molecular weight (m/z 147.9), whereas the asphaltene spectrum is dominated by thermally induced dealkylation products (average m/z 100.8, 97.3% TIC > 350 °C) partially identified by pyrolysis GC. The asphaltene pattern peaks at m/z 42 (C_3-alkene and propene), with m/z 34 (H_2S) the second dominant, whereas the crude oil pattern peaks at m/z 120 (C_3-alkylated benzene) with m/z 156 (C_3-alkylated benzene) as the second dominant. Comparing only the pyrolysis pattern of the parent crude oil and the asphaltene, SPI shows a high similarity. In more detail, the abundance of the alkene pattern in the asphaltene spectra exponentially decreases for heavier alkenes. This finding is in good agreement with the pyrolysis GC, for which the C_5 alkene was found to be the most abundant alkene (because C_4 was too volatile for detection). Assuming an alkylated homologous series starting at m/z 42 (m/z 42 + $n \times$ 14) for the alkenes and isobaric cycloalkanes, an average alkene length of $C_{9.1}$ can be calculated for the asphaltene. Isobaric species for this series can be alkylated cycloalkanes with 1 saturated ring, which were found only in minor abundance in the GC pyrograms and are less common as stable products in pyrolysis.[59,63] The average alkene length

estimated with the universal soft SPI is congruent to the pyrolysis GC data obtained with the universal hard electron ionization, although the photoionization cross section has to be taken into account. Fortunately, in SPI, the cross sections range only between a factor of 2 and 3 within one compound class.[64] The substantial occurrence of H_2S is caused by the decomposition of organic sulfur constituents, mainly thiols. On the basis of this signal, the sulfur content of the asphaltene is far higher compared to the parent crude oil, which was also found in the respective GC data. Pyrolysis GC−EI−QMS was optimized for larger constituents; hence, species below C_9 do not reveal a good peak shape (Figure 3). Nonetheless, the main effluent components can be verified by the electron ionization fragment spectrum as starting from the C_5 alkane/alkene at a retention time of roughly 2 min. As of a retention time of 15 min, the gas chromatogram exhibits a clear pattern for alkanes and alkenes, peaking at C_{13}. Pyrolysis of the macromolecular asphaltene structures results to a large extent in the release of smaller alkyl chains below C_7 by cracking as well as notable amounts of larger alkenes above C_{10}. Nonetheless, also very long alkyl chains, which can either originate from a linker or more likely from a core structure alkylation side, can be found (up to C_{37}, $m/z \sim 520$). The cracking process during pyrolysis is a complex mixture of reactions economically used by refineries (thermal cracking/visbreaking, 450−750 °C, usually at high pressures around 70 bar). Carbon−carbon single bonds are broken, and free radicals are formed. A series of reactions then lead to a high proportion of terminal alkenes. We can assume that long side chains more readily undergo cracking than sterically hindered linker sites. Besides the dominant alkene pattern, a less abundant distribution pattern of thermal decomposition products with higher m/z can be seen in the survey view of SPI TOF−MS (Figure 1). These patterns can be partially attributed to aromatic species, which were already briefly discussed in the pyrolysis GC data. A more specific approach, such as REMPI, which is highly selective for aromatic constituents, can be beneficial, particularly because the m/z values of alkane and alkene/cycloalkane species coincide with aromatic alkylation series. Alkenes formed by cracking are highly abundant. Thus, as a result of dynamic range aspects, a more selective technique is advantageous too.

Resonance-Enhanced Multiphoton Ionization. Figure 4 provides a more selective view on the complex asphaltene pyrolysis mixture. The two-photon process in REMPI ionizes species with an ionization energy (IE) below 9.32 eV (2 × 4.66 eV) and a stable intermediate state. Consequently, solely aromatics can be found. A pattern with the same characteristic CH_2 group spacing as with SPI can be observed. The spectrum peaks at m/z 226, most likely C_7-alkylated naphthalenes. The 2−4-ring polycyclic aromatic hydrocarbons dominate the spectrum. At higher masses, the series overlap and no clear assignments are possible. It must be kept in mind that REMPI ionization efficiencies span orders of magnitude;[65,66] in comparison to, e.g., naphthalene, sulfur-containing benzothiophenes are ionized with a 100-fold lower efficiency, whereas alkanes overlapping the aromatic alkylation series are not ionized at all. Nitrogen-containing species will be found on odd m/z values (nitrogen rule), and carbazole and acridine homologue alkylation rows were tentatively identified. With the relative measured abundances, an aromatic ring size of 3−4 with a main alkylation length of C_{3-10} can be revealed for the asphaltene. The average alkylation length of the individual ring sizes was found to be 2−3 for benzene, 8−9 for naphthalene, and slightly

lower for condensed aromatics, with 3−5 rings (6−8). The relatively low average alkylation length results from the cracking process during the pyrolysis.

Atmospheric Pressure Ionization. For REMPI, assignments of probable chemical structures rely on literature knowledge and the ionizable chemical space, e.g., selectivity to aromatics and cross sections. Ultrahigh mass resolution and mass accuracy, as routinely delivered by FT−MS instruments, allow for a mathematical calculation of the elemental composition. Assignment to the summed APPI and APCI FT-ICR MS spectra revealed roughly 800 and 1250 distinct chemical formulas. Grouped into compound classes, it was found for both techniques that CHS species are most dominant (APCI, 58% TIC; APPI, 58% TIC), whereas the CH class is the second dominant (APCI, 25% TIC; APPI, 21% TIC), followed by the CHS_2 class (APCI, 10% TIC; APPI, 18% TIC). In APCI, oxygenated species are present with a higher abundance compared to APPI but still only account for approximately 5% TIC (CHSO, 2.5% TIC; CHO, 1.9% TIC). The low abundance of oxygenated species in asphaltene analysis was also reported in the literature.[45,67] In both spectra, $CHS_{0-2}O_{0-3}$ class species account for more than 97% of the overall intensity. CHN class species were only found with a very low abundance (<1% TIC). This phenomenon can be explained by the high ionization efficiency of CH and CHS class constituents in positive polarity mode. In comparison to the complete temperature range of the parent crude oil, the asphaltene exhibits a higher abundance of sulfur species and a decreased proportion of CH, CHSO, and CHO_{1-2} (Figure S7 of the Supporting Information). Nonetheless, if only the pyrolysis phase of the parent crude oil is taken into account, the data are consistent with the asphaltene compound class pattern.

Aside from that, the elemental composition assignment allows for an assessment of the aromaticity by the double bond equivalent (DBE) value.[68] For APCI, an intensity-averaged DBE of roughly 7.8 was detected, whereas for APPI, the value is 9.1, corresponding to a 2−3-ring system. Figure 4 visualizes the dominant homologue row of three selected CHS class members. Both API spectra reveal a pattern peaking at m/z 320−360, corresponding to an alkylation grade of 8−14. The average DBE is slightly higher for the CHS_2 class and similar between CHS and CH constituents. The deviation in average DBE between the API techniques is caused by the slightly shifted observed chemical space. Furthermore, the biased molecular weight distribution of FT−MS compared to TOF data has to be mentioned. A longer storage time for the CID experiments revealed the presence of larger aromatic moieties, with an average DBE value of 13 and 11.7 for APCI and APPI, respectively. With CID, the different tentative assignments, i.e., (1) small aromatics with alkene side chains versus (2) larger ring systems with saturated positions, can be proven. If the double bond is located in the side chain (case 1), the DBE 7 homologous row should decrease significantly in the fragmented spectra compared to the DBE 6 or 9 row. This reduction was not observed, leading to the hypothesis that a large proportion is given by partially saturated ring systems (case 2) rather than the particular alkene isomer (case 1). The DBE patterns of asphaltene pyrolysis are similar to those from the pyrolysis phase of the parent crude oil. The similarity between the pyrolysis phases of the asphaltene and the parent crude oil shown by all techniques suggests that asphaltenic species cause a high proportion of the pyrolysis of the crude oil. Figure 5 visualizes the revealed chemical space by example of
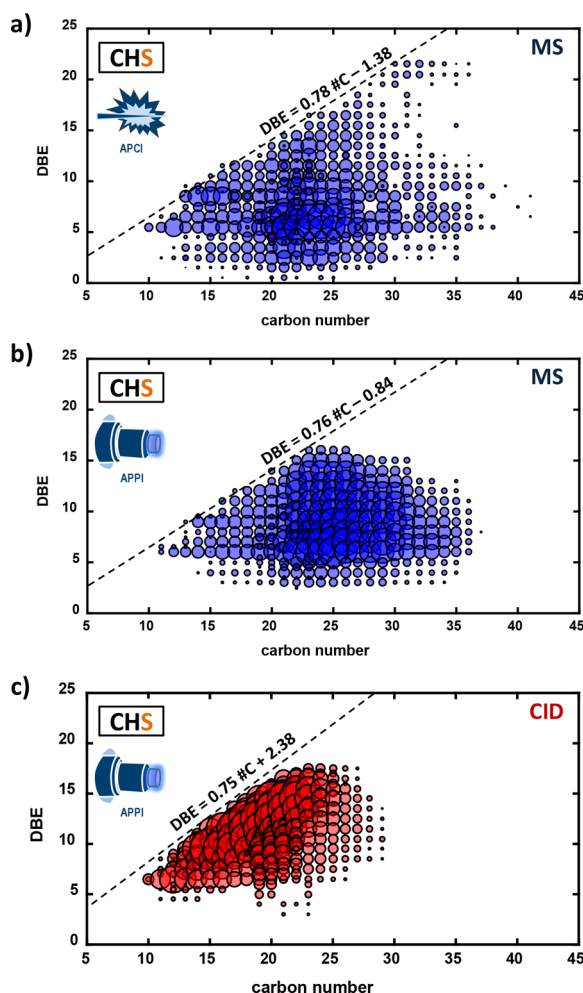
Figure 5. Carbon number versus DBE visualization for the (a) APCI and (b) APPI assignments of the CHS₁ class as well as for the (c) CHS₁ class assignments observed for the asphaltene sample via APPI−CID. Additionally, the results of the planar limit-assisted calculation are given.

the CHS class and carbon number versus DBE diagram. Elemental compositions with a carbon number up to 37 were found ($m/z \sim 520-550$) spanning a DBE range from 2 to 22 in APCI, whereas APPI reveals a narrower DBE spread from 3 to 16. Interestingly, thermal decomposition products identified with SPI and GC are in the same m/z range. Furthermore, the elemental composition assignments received by the high-resolution FT−MS CID spectra can be used for planar limit-assisted structural interpretation of the aromatic building blocks, which give information on how the rings are arranged.[69,70] For this purpose, the lower carbon number limit of the distribution is fitted linearly. A slope of 0.78 for APCI and 0.76 for APPI was found, corresponding to a linear benzene ring addition (*cata*-condensed, e.g., anthracene, naphthalene, and biphenylene) with a slight proportion of nonlinear addition (*peri*-condensed, e.g., pyrene, perylene, and coronene). These values are in good agreement with the fittings observed for the CID spectra. The CHS₂ class revealed the highest slope, which indicates condensed aromatic ring systems as a more dominant structural motive.

The carbon number versus DBE diagrams show a horizontal shift for the CID spectra compared to the non-fragmented as a result of (neutral loss) dealkylation with preservation of the

parent aromatic structure. This finding proves that the observed thermal decomposition products have a single aromatic core architecture, which is alkylated by side chains containing no additional ring systems. An average dealkylation, as calculated by the difference of the intensity-weighted average m/z of the parent and CID spectra divided by 14 (m/z of CH_2), of 2.1 for APCI and 6 for APPI was found. A more precise estimation of the average alkylation length can be performed by subtraction of the mean carbon number determined for the non-fragmented spectra and the lowest carbon number found in the CID experiment for each DBE value. This approach results in an average alkylation length of 6−10. The CID voltage was kept rather low to prevent other fragmentation processes. Nonetheless, this precaution will not lead to a complete dealkylation, and alkylated constituents are still observed in the CID pattern. Thus, the real average alkylation length may be somewhat higher. With this in mind and assuming the structures proposed in Figure 4, an average alkylation state of 10−13 is more realistic. The parent crude oil reveals a higher value with the same approach. This finding agrees with the literature that the alkyl chain length decreases in the order of saturates > aromatics > resins > asphaltenes.[69] Furthermore, it has to be kept in mind that, in this study, thermal decomposition products were investigated and the intact asphaltene molecules might consist of several of the observed aromatic cores and alkyl chains.

Data Combination. In the Asphaltene Characterization Interlaboratory Study for PetroPhase 2017, among many other techniques, field desorption mass spectrometry (FD−MS), a universal and soft ionization approach, was conducted with the same sample (Figure S8 of the Supporting Information). A mean molecular mass (M_w) of m/z 1267 and an intensity-weighted molecular mass (M_n) of m/z 974 with a polydispersity (M_w/M_n) of 1.30 was revealed with this approach. Less stable molecules can undergo a certain degree of dissociation in FD−MS. Therefore, the prediction of the mean intact mass is a rather conservative assumption and might be higher. Nonetheless, field ionization mass spectrometric investigations as well as fluorescence depolarization techniques on asphaltenes obtained an average molecular weight of m/z 700−750,[71−73] which is in the same order of magnitude, and the dissociation effect might be very small. Dependent upon the type of applied ionization techniques, the following intensity-weighted average mass for the thermal decomposition product were obtained: m/z 100, 270, 366, and 337 for SPI, REMPI, APPI, and APCI. DBE can be calculated from the molecular weight, given by FD−MS, and elemental analysis.[68] This calculation results in an average DBE value of 31.6 for an average intact molecular weight of m/z 974, a carbon content of 81.5 wt %, a hydrogen content of 7.4 wt %, and a nitrogen content of 1.3 wt %. If we assume an average DBE of 10 (3 condensed aromatic rings) and m/z of 270 (taken from the REMPI TOF data) for the aromatic pyrolysis products, and an average DBE of 1 (taken from SPI TOF, representing mainly non-polyaromatic products), the intact macromolecular asphaltene structure is composed of roughly three aromatic cores (Figure 6 and Figure S9 of the Supporting Information). A remaining mass of approximately m/z 200 (∼14 CH_2-units) is contributed by additional alkylation sites and linkers. As mentioned above, the intact mass assumption might be higher, consequently contributing to alkylation sites and saturated linker motives. Figure 6 summarizes the findings of the individual soft ionization techniques, indicating their overlap
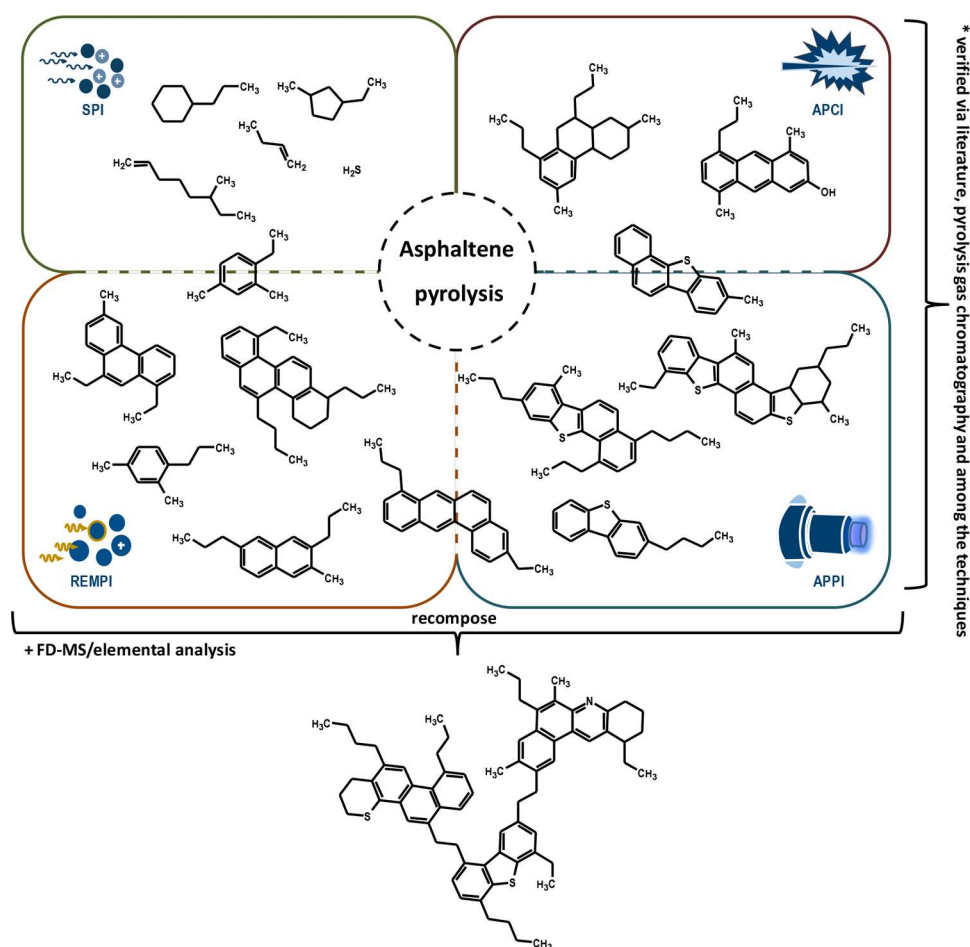
Figure 6. Schematic representation of the most likely tentative assignments and the chemical space, which is covered by the individual techniques as well as their overlap. The molecular structures and moieties can be recomposed to an exemplary asphaltene structure.

as well as giving a tentative asphaltene structure as revealed here by the presented pyrolysis approach and FD−MS.

The chemical nature of asphaltene linker sites has been extensively discussed in the literature. It was stated: "If the archipelago structures are bridged by cycloalkane rather than linear alkane linkages much of the controversy between the molecular architecture models would be resolved".[13] Unfortunately, naphthenes/cycloalkanes cannot be distinguished from the corresponding alkenes via the soft ionization techniques, but the cycloalkanes were detected by GC−EI−QMS only with a minor abundance (in comparison to alkane pyrolytic fragments). Moreover, taking into account the dominance of alkenes, as a product of the thermal cracking of alkylation side chains, the presence of cycloalkane bridging might be a less common structural motive.

According to the mass loss curves discussed above, roughly 40 wt % of the asphaltene sample remains after 600 °C treatment. During pyrolysis, high aromatic island structures can release hydrogen and form a stable coke residue. This carbonization will involve various reactions.[74] It was shown that aliphatic moieties reveal a higher alteration degree compared to the relatively stable aromatic core.[75] In this study, the evolved gas is analyzed, and the exact nature of the residue is not a relevant hindering. Furthermore, the reaction parameter, e.g., pressure, reaction time, etc., for which these pathways were shown to be significant, i.e., visbreaking/coking in the refinery, are much harsher than the conditions applied in this study.[76,77]

Thermal decomposition in thermogravimetry of asphaltenes was reported to be a first-order reaction and relatively quick at temperatures above 440 °C. These complex thermal degradation pathways potentially limit the thermal analysis approach applied upon asphaltenes. Nonetheless, direct infusion APPI FT−MS of the exact same asphaltene within the Asphaltene Characterization Interlaboratory Study for PetroPhase 2017 revealed DBE values of 25−30 for the intact molecules and a loss of DBE during CID, which consolidates the presented interpretation and supports our molecular architecture hypothesis. The findings of thin-film pyrolysis on asphaltenes also suggest bridged structures present in a significant concentration.[78]

Table 1 summarizes the main aspects of the individual techniques and their respective findings. SPI revealed a dominant alkene/alkane pattern, caused by cracking of alkylation sites and verified with Pyr−GC. REMPI exhibits the PAH pattern selectively and even-numbered m/z homologue series as well as tentatively assigned carbazole and acridine derivatives, indicated by even m/z values. Sulfur-containing aromatic structures are detectable, but the short lifetime of their first excited state required for REMPI leads to a very low signal intensity. For polycyclic aromatic sulfur hydrocarbon (PASH) detection, APPI is the method of choice, and the sulfur species could be easily identified, as shown above. APCI is sensitive toward oxygenated compounds, but only a minor proportion of thermally stable oxygen-containing species was observed in the asphaltene pyrolysis effluent. APCI, APPI, and REMPI enable a sensitive

Table 1. Compilation of the Applied Techniques, Their Essential Characteristics, and the Most Significant Results of the Investigation of the PetroPhase 2017 Asphaltene and Parent Crude Oil

	method	(1) TD/Pyr−GC−EI−QMS	(2) TG SPI TOF−MS	(3) TG REMPI TOF−MS	(4) TG APPI FT-ICR MS	(5) TG APCI FT-ICR MS
full name		thermal desorption/pyrolysis gas chromatography electron ionization quadrupole mass spectrometry	thermogravimetry single-photon ionization time-of-flight mass spectrometry	thermogravimetry resonance-enhanced multiphoton ionization time-of-flight mass spectrometry	thermogravimetry atmospheric pressure photon ionization Fourier transform ion cyclotron resonance mass spectrometry	thermogravimetry atmospheric pressure chemical ionization Fourier transform ion cyclotron resonance mass spectrometry
concept	ionization	70 eV electron impact, hard	118 nm single-photon ionization, soft	266 nm resonance-enhanced multiphoton ionization, soft	Kr VUV lamp with 10/10.6 eV (124/117 nm), soft	corona discharge chemical ionization at a 3000 μA stainless-steel needle, soft
	analyzer	nominal resolution quadrupole with secondary electron multiplier, gas chromatography with separation and retention time information (structure)	reflectron time-of-flight with multichannel plate detection, nominal resolving power, high acquisition rate	reflectron time-of-flight with multichannel plate detection, nominal resolving power, high acquisition rate	ion cyclotron resonance with 7 T magnet (ParaCell, Bruker), ultrahigh resolution (260000 at m/z 400)	ion cyclotron resonance with 7 T magnet (ParaCell, Bruker), ultrahigh resolution (260000 at m/z 400)
detectable compounds		ionization of all organic and inorganic species (universal), gas chromatographic limitation in volatility	species with ionization energy below 10.5 eV, universal for most hydrocarbons	aromatic hydrocarbons with stable intermediate state	semi-polar and nonpolar components, highly efficient for sulfur-containing species	polar and semi-polar constituents, sensitive toward oxygenated species
what was found?	PetroPhase C_7 asphaltene	no signal in the thermal desorption (at 300 °C), dominant alkene and alkane pattern, mainly side-chain information, less abundant	intense alkene pattern (C_{3-35}) peaking at propane and an exponential decrease, high abundant H_2S	1−5-ring aromatics and their alkylated species up to m/z 500 peaking at m/z 224, 2−3 ring with 3−10 alkylation on average	intense homologue series of benzothiophene with alkane and alkene side chains	intense homologue series of benzothiophene with alkane and alkene side chains, oxygenated species, e.g., CHO and CHSO

detection of aromatic hydrocarbon structures. All three techniques found 2−4-ring PAHs with a DBE of 6−13 as the most abundant constituents of the asphaltene thermal degradation.

CONCLUSION

The thermal analysis of a C_7 asphaltene as well as its parent crude oil and the comprehensive molecular description of the evolved gas mixture were successfully conducted deploying three different couplings and five different ionization techniques. We showed that no significant amount of material evaporates in the desorption phase (<300 °C), whereas in the pyrolysis phase (> ∼320 °C) a complex variety of thermal decomposition products was detected. A residue of roughly 50 wt % remains after pyrolysis and can be evaporated nearly completely under an oxidative atmosphere at 800−1000 °C. Thus, the asphaltene sample, distributed within the Asphaltene Characterization Interlaboratory Study for PetroPhase 2017, was proven to be carefully prepared and devoid of desorbable co-precipitates.

The combination of different ionization schemes and mass spectrometric analyzers allowed for a more comprehensive chemical description and validation of the pyrolysis effluent. APCI as well as the photoionization techniques allow for a fragment-free characterization, whereas GC−EI partially allows for the validation of structural motives. Side-chain loss dominates the pyrolysis pattern, revealed as alkenes and alkanes via EI and SPI as well as aromatics detected via REMPI, APPI, and APCI. The thermal fragments and field desorption mass spectrometric results were used for an indirect assessment of the molecular architecture. The findings strongly indicate a molecular structure type with several aromatic cores (mainly 2−4-ring systems) linked by aliphatic side chains. Thermal decomposition

of the aromatic core in the proposed island structure type can happen, e.g., along partially saturated ring systems, but is less favorable. Therefore, we suggest archipelago-type asphaltenes be dominant in the PetroPhase 2017 asphaltene. Direct infusion measurements with APPI and CID on an ultrahigh-resolution mass spectrometer on the same sample give evidence for this hypothesis as well.

We have proven that soft ionization is crucial for the specification of the effluent obtained from asphaltene and parent crude oil thermal analysis. Conventional TD/Pyr−GC−EI−QMS delivers valuable information that is, however, not sufficient for the molecular characterization of these ultra-complex sample materials. Investigation of the thermal behavior of standard substances, which mimic each of the suggested architecture types, will be performed in future work, e.g., to address residue and coke formation. Additional information on nitrogen-containing species is obtainable by applying electrospray ionization. Nonetheless, direct infusion experiments most often struggle with the high dynamic range and ultrahigh complexity of these sample materials, and substantial effort has to be taken to generate valuable spectra, e.g., by deploying high-field magnets, acquisition of narrow m/z bands, or chromatographic separation. As for the thermal analysis approaches used in this study, the sample can be used directly without any pretreatment.

The high potential of evolved gas analysis coupled to mass spectrometry and, in particular, the combination of several ionization techniques will stimulate further studies on troublemakers in the petrochemical industry, such as resins, naphthenates, and other deposits, as well as on asphaltenes from a different origin. Additionally, analyzing the residue formed at 600 °C thermal treatment, e.g., via direct infusion or laser desorption high-resolution mass spectrometric techniques, will

increase the understanding of the thermal behavior and allow for further structural assignments.

■ ASSOCIATED CONTENT

Ⓢ Supporting Information

The Supporting Information is available free of charge on the ACS Publications website at DOI: 10.1021/acs.energyfuels.7b02762.

> Mass loss curves for the investigation of the parent crude oil and asphaltene with the two deployed thermogravimetric systems (Figure S1), chromatograms (TIC and EIC for m/z 55 and 57) and survey view (m/z versus retention time) of the desorption and pyrolysis gas chromatographic measurements (Figures S2−S5), average mass spectra of the crude oil and asphaltene for the photoionization TOF−MS analysis (Figure S6), average CID APCI and APPI mass spectra for the asphaltene pyrolysis (Figure S7), average field desorption mass spectrum (Figure S8), and schematic concept of the thermal decomposition products assembled to the intact molecular weight given by FD−MS (Figure S9) (PDF)

■ AUTHOR INFORMATION

Corresponding Author

*E-mail: christopher.rueger@uni-rostock.de.

ORCID ⊙

Christopher P. Rüger: 0000-0001-9634-9239
Ralf Zimmermann: 0000-0002-6280-3218

Notes

The authors declare no competing financial interest.

■ ACKNOWLEDGMENTS

■ REFERENCES

(1) Fahim, M. A.; Alsahhaf, T. A.; Elkilani, A. S. *Fundamentals of Petroleum Refining*, 1st ed.; Elsevier: Amsterdam, Netherlands, 2010.

(2) Kandiyoti, R. *Solid Fuels and Heavy Hydrocarbon Liquids: Thermal Characterization and Analysis*, 2nd ed.; Elsevier Science: Kent, U.K., 2017.

(3) Speight, J. G. *The Chemistry and Technology of Petroleum*, 4th ed.; CRC Press (Taylor & Francis Group): Boca Raton, FL, 2007.

(4) Rodgers, R. P.; Schaub, T. M.; Marshall, A. G. Petroleomics: MS Returns to Its Roots. *Anal. Chem.* **2005**, *77* (1), 20 A−27 A.

(5) Nizio, K. D.; McGinitie, T. M.; Harynuk, J. J. Comprehensive multidimensional separations for the analysis of petroleum. *Journal of chromatography. A* **2012**, *1255*, 12−23.

(6) *Asphaltenes, Heavy Oils, and Petroleomics*; Mullins, O. C., Sheu, E. Y., Hammami, A., Marshall, A. G., Eds.; Springer: New York, 2007; DOI: 10.1007/0-387-68903-6.

(7) Mullins, O. C.; Pomerantz, A. E.; Zuo, J. Y.; Dong, C. Downhole fluid analysis and asphaltene science for petroleum reservoir evaluation. *Annu. Rev. Chem. Biomol. Eng.* **2014**, *5*, 325−345.

(8) Marshall, A. G.; Rodgers, R. P. Petroleomics: The next grand challenge for chemical analysis. *Acc. Chem. Res.* **2004**, *37* (1), 53−59.

(9) Marshall, A. G.; Rodgers, R. P. Petroleomics: Chemistry of the underworld. *Proc. Natl. Acad. Sci. U. S. A.* **2008**, *105* (47), 18090−18095.

(10) George, G. N.; Gorbaty, M. L. Sulfur K-edge x-ray absorption spectroscopy of petroleum asphaltenes and model compounds. *J. Am. Chem. Soc.* **1989**, *111* (9), 3182−3186.

(11) Mitra-Kirtley, S.; Mullins, O. C.; van Elp, J.; George, S. J.; Chen, J.; Cramer, S. P. Determination of the nitrogen chemical structures in petroleum asphaltenes using XANES spectroscopy. *J. Am. Chem. Soc.* **1993**, *115* (1), 252−258.

(12) Pomerantz, A. E.; Seifert, D. J.; Bake, K. D.; Craddock, P. R.; Mullins, O. C.; Kodalen, B. G.; Mitra-Kirtley, S.; Bolin, T. B. Sulfur Chemistry of Asphaltenes from a Highly Compositionally Graded Oil Column. *Energy Fuels* **2013**, *27* (8), 4604−4608.

(13) Podgorski, D. C.; Corilo, Y. E.; Nyadong, L.; Lobodin, V. V.; Bythell, B. J.; Robbins, W. K.; McKenna, A. M.; Marshall, A. G.; Rodgers, R. P. Heavy Petroleum Composition. 5. Compositional and Structural Continuum of Petroleum Revealed. *Energy Fuels* **2013**, *27* (3), 1268−1276.

(14) Materazzi, S.; Risoluti, R. Evolved Gas Analysis by Mass Spectrometry. *Appl. Spectrosc. Rev.* **2014**, *49* (8), 635−665.

(15) Materazzi, S.; Vecchio, S. Recent Applications of Evolved Gas Analysis by Infrared Spectroscopy (IR-EGA). *Appl. Spectrosc. Rev.* **2013**, *48* (8), 654−689.

(16) Materazzi, S.; Gentili, A.; Curini, R. Applications of evolved gas analysis Part 2: EGA by mass spectrometry. *Talanta* **2006**, *69* (4), 781−794.

(17) Rustschev, D. D. Application of thermal analysis for investigating liquid fuels, petroleum- and coke-chemical products. *Thermochim. Acta* **1990**, *168*, 261−271.

(18) Materazzi, S.; Vecchio, S. Evolved Gas Analysis by Mass Spectrometry. *Appl. Spectrosc. Rev.* **2011**, *46* (4), 261−340.

(19) Holdiness, M. R. Evolved gas analysis by mass spectrometry: A review. *Thermochim. Acta* **1984**, *75* (3), 361−399.

(20) Huang, J. Thermal Degradation of Asphaltene and Infrared Characterization of Its Degraded Fractions. *Pet. Sci. Technol.* **2006**, *24* (9), 1089−1095.

(21) Alosmanov, R.; Wolski, K.; Matuschek, G.; Magerramov, A.; Azizov, A.; Zimmermann, R.; Aliyev, E.; Zapotoczny, S. Effect of functional groups on the thermal degradation of phosphorus- and phosphorus/nitrogen-containing functional polymers. *J. Therm. Anal. Calorim.* **2017**, *109*, 130−799.

(22) Streibel, T.; Geißler, R.; Saraji-Bozorgzad, M.; Sklorz, M.; Kaisersberger, E.; Denner, T.; Zimmermann, R. Evolved gas analysis (EGA) in TG and DSC with single photon ionisation mass spectrometry (SPI-MS): Molecular organic signatures from pyrolysis of soft and hard wood, coal, crude oil and ABS polymer. *J. Therm. Anal. Calorim.* **2009**, *96* (3), 795−804.

(23) Geissler, R.; Saraji-Bozorgzad, M. R.; Gröger, T.; Fendt, A.; Streibel, T.; Sklorz, M.; Krooss, B. M.; Fuhrer, K.; Gonin, M.; Kaisersberger, E.; Denner, T.; Zimmermann, R. Single Photon Ionization Orthogonal Acceleration Time-of-Flight Mass Spectrometry and Resonance Enhanced Multiphoton Ionization Time-of-Flight Mass Spectrometry for Evolved Gas Analysis in Thermogravimetry: Comparative Analysis of Crude Oils. *Anal. Chem.* **2009**, *81* (15), 6038−6048.

(24) Wohlfahrt, S.; Fischer, M.; Saraji-Bozorgzad, M.; Matuschek, G.; Streibel, T.; Post, E.; Denner, T.; Zimmermann, R. Rapid comprehensive characterization of crude oils by thermogravimetry coupled to fast modulated gas chromatography-single photon ionization time-of-flight mass spectrometry. *Anal. Bioanal. Chem.* **2013**, *405* (22), 7107−7116.

(25) Béhar, F.; Pelet, R. Pyrolysis-gas chromatography applied to organic geochemistry. *J. Anal. Appl. Pyrolysis* **1985**, *8*, 173−187.

(26) Garg, A. K.; Philp, R. P. Pyrolysis-gas chromatography of asphaltenes/kerogens from source rocks of the Gandhar Field, Cambay Basin, India. *Org. Geochem.* **1994**, *21* (3−4), 383−392.

(27) Mascherpa, A.; Casalini, A. Pyrolysis GC-MS of asphaltenes from straight-run and visbreaker bitumens. *J. High Resolut. Chromatogr.* **1988**, *11* (3), 296−299.

(28) Nali, M.; Corana, F.; Montanari, L. Pyrolysis/gas chromatography/mass spectrometry in the analysis of asphaltenes. *Rapid Commun. Mass Spectrom.* **1993**, *7* (7), 684−687.

(29) Sarmah, M. K.; Borthakur, A.; Dutta, A. Pyrolysis of petroleum asphaltenes from different geological origins and use of methylnaphthalenes and methylphenanthrenes as maturity indicators for asphaltenes. *Bull. Mater. Sci.* **2010**, *33* (4), 509−515.

(30) Solli, H.; Leplat, P. Pyrolysis-gas chromatography of asphaltenes and kerogens from source rocks and coals—A comparative structural study. *Org. Geochem.* **1986**, *10* (1−3), 313−329.

(31) Speight, J. G.; Pancirov, R. J. Structural types in petroleum asphaltenes as deduced from pyrolysis/gas chromatography/mass spectrometry. *Liq. Fuels Technol.* **1984**, *2* (3), 287−305.

(32) Li, D.-X.; Gan, L.; Bronja, A.; Schmitz, O. J. Gas chromatography coupled to atmospheric pressure ionization mass spectrometry (GC-API-MS): Review. *Anal. Chim. Acta* **2015**, *891*, 43−61.

(33) Kök, M. V. Thermal analysis applications in fossil fuel science: Literature survey. *J. Therm Anal Calorim* **2002**, *68* (3), 1061−1077.

(34) Fendt, A.; Geissler, R.; Streibel, T.; Sklorz, M.; Zimmermann, R. Hyphenation of two simultaneously employed soft photo ionization mass spectrometers with thermal analysis of biomass and biochar. *Thermochim. Acta* **2013**, *551*, 155−163.

(35) Fischer, M.; Wohlfahrt, S.; Saraji-Bozorgzad, M.; Matuschek, G.; Post, E.; Denner, T.; Streibel, T.; Zimmermann, R. Thermal analysis/evolved gas analysis using single photon ionization. *J. Therm. Anal. Calorim.* **2013**, *113* (3), 1667−1673.

(36) Hölzer, J.; Fischer, M.; Gröger, T.; Streibel, T.; Saraji-Bozorgzad, M.; Wohlfahrt, S.; Matuschek, G.; Zimmermann, R. Hyphenation of thermogravimetry and soft single photon ionization− ion trap mass spectrometry (TG−SPI−ITMS) for evolved gas analysis. *J. Therm. Anal. Calorim.* **2014**, *116* (3), 1471−1479.

(37) Streibel, T.; Fendt, A.; Geißler, R.; Kaisersberger, E.; Denner, T.; Zimmermann, R. Thermal analysis/mass spectrometry using soft photo-ionisation for the investigation of biomass and mineral oils. *J. Therm. Anal. Calorim.* **2009**, *97* (2), 615−619.

(38) Dyszel, S. M. Thermogravimetry coupled with atmospheric pressure ionization mass spectrometry. A new combined technique. *Thermochim. Acta* **1983**, *61* (1−2), 169−183.

(39) Dyszel, S. M. Characterization of green coffee beans by combined thermogravimetric analysis/atmospheric pressure chemical ionization mass spectrometry. *Thermochim. Acta* **1985**, *87*, 89−98.

(40) Prime, R. B.; Shushan, B. Thermogravimetric analyzer/atmospheric pressure chemical ionization tandem triple quadrupole mass spectrometer system for evolved gas analysis. *Anal. Chem.* **1989**, *61* (11), 1195−1201.

(41) Rüger, C. P.; Miersch, T.; Schwemer, T.; Sklorz, M.; Zimmermann, R. Hyphenation of Thermal Analysis to Ultrahigh-Resolution Mass Spectrometry (Fourier Transform Ion Cyclotron Resonance Mass Spectrometry) Using Atmospheric Pressure Chemical Ionization For Studying Composition and Thermal Degradation of Complex Materials. *Anal. Chem.* **2015**, *87* (13), 6493−6499.

(42) Streibel, T.; Zimmermann, R. Resonance-enhanced multiphoton ionization mass spectrometry (REMPI-MS): Applications for process analysis. *Annu. Rev. Anal. Chem.* **2014**, *7*, 361−381.

(43) Zimmermann, R. Photo ionisation in mass spectrometry: Light, selectivity and molecular ions. *Anal. Bioanal. Chem.* **2013**, *405* (22), 6901−6905.

(44) Himmelsbach, M.; Buchberger, W.; Reingruber, E. Determination of polymer additives by liquid chromatography coupled with mass spectrometry. A comparison of atmospheric pressure photoionization (APPI), atmospheric pressure chemical ionization (APCI), and electrospray ionization (ESI). *Polym. Degrad. Stab.* **2009**, *94* (8), 1213−1219.

(45) Gaspar, A.; Zellermann, E.; Lababidi, S.; Reece, J.; Schrader, W. Impact of different ionization methods on the molecular assignments

of asphaltenes by FT-ICR mass spectrometry. *Anal. Chem.* **2012**, *84* (12), 5257−5267.

(46) Farenc, M.; Corilo, Y. E.; Lalli, P. M.; Riches, E.; Rodgers, R. P.; Afonso, C.; Giusti, P. Comparison of Atmospheric Pressure Ionization for the Analysis of Heavy Petroleum Fractions with Ion Mobility-Mass Spectrometry. *Energy Fuels* **2016**, *30* (11), 8896−8903.

(47) Cai, S.-S.; Syage, J. A. Comparison of atmospheric pressure photoionization, atmospheric pressure chemical ionization, and electrospray ionization mass spectrometry for analysis of lipids. *Anal. Chem.* **2006**, *78* (4), 1191−1199.

(48) Fischer, M.; Wohlfahrt, S.; Varga, J.; Matuschek, G.; Saraji-Bozorgzad, M. R.; Walte, A.; Denner, T.; Zimmermann, R. Evolution of Volatile Flavor Compounds During Roasting of Nut Seeds by Thermogravimetry Coupled to Fast-Cycling Optical Heating Gas Chromatography-Mass Spectrometry with Electron and Photoionization. *Food Anal. Methods* **2017**, *10* (1), 49−62.

(49) Fischer, M.; Wohlfahrt, S.; Varga, J.; Saraji-Bozorgzad, M.; Matuschek, G.; Denner, T.; Zimmermann, R. Evolved gas analysis by single photon ionization-mass spectrometry. *J. Therm. Anal. Calorim.* **2014**, *116* (3), 1461−1469.

(50) Varga, J.; Wohlfahrt, S.; Fischer, M.; Saraji-Bozorgzad, M. R.; Matuschek, G.; Denner, T.; Reller, A.; Zimmermann, R. An evolved gas analysis method for the characterization of sulfur vapor. *J. Therm. Anal. Calorim.* **2017**, *127* (1), 955−960.

(51) Otto, S.; Erdmann, S.; Streibel, T.; Herlemann, D. P. R.; Schulz-Bull, D.; Zimmermann, R. Pyrolysis-gas chromatography-mass spectrometry with electron-ionization and resonance-enhanced-multi-photon-ionization for the characterization of terrestrial dissolved organic matter in the Baltic Sea. *Anal. Methods* **2016**, *8* (12), 2592−2603.

(52) Chacón-Patiño, M. L.; Vesga-Martínez, S. J.; Blanco-Tirado, C.; Orrego-Ruiz, J. A.; Gómez-Escudero, A.; Combariza, M. Y. Exploring Occluded Compounds and Their Interactions with Asphaltene Networks Using High-Resolution Mass Spectrometry. *Energy Fuels* **2016**, *30* (6), 4550−4561.

(53) Otto, S.; Streibel, T.; Erdmann, S.; Sklorz, M.; Schulz-Bull, D.; Zimmermann, R. Application of pyrolysis-mass spectrometry and pyrolysis-gas chromatography-mass spectrometry with electron-ionization or resonance-enhanced-multi-photon ionization for characterization of crude oils. *Anal. Chim. Acta* **2015**, *855*, 60−69.

(54) Otto, S.; Streibel, T.; Erdmann, S.; Klingbeil, S.; Schulz-Bull, D.; Zimmermann, R. Pyrolysis-gas chromatography-mass spectrometry with electron-ionization or resonance-enhanced-multi-photon-ionization for characterization of polycyclic aromatic hydrocarbons in the Baltic Sea. *Mar. Pollut. Bull.* **2015**, *99* (1−2), 35−42.

(55) Streibel, T.; Mitschke, S.; Adam, T.; Weh, J.; Zimmermann, R. Thermal desorption/pyrolysis coupled with photo ionisation time-of-flight mass spectrometry for the analysis and discrimination of pure tobacco samples. *J. Anal. Appl. Pyrolysis* **2007**, *79* (1−2), 24−32.

(56) Zimmermann, R.; Saraji-Bozorgzad, M.; Grimmer, C.; Ulbrich, A.; Streibel, T. Erdöl in seine Bestandteile zerlegen und charakterisieren. *Nachr. Chem.* **2016**, *64* (7−8), 751−754.

(57) Mühlberger, F.; Hafner, K.; Kaesdorf, S.; Ferge, T.; Zimmermann, R. Comprehensive on-line characterization of complex gas mixtures by quasi-simultaneous resonance-enhanced multiphoton ionization, vacuum-UV single-photon ionization, and electron impact ionization in a time-of-flight mass spectrometer: Setup and instrument characterization. *Anal. Chem.* **2004**, *76* (22), 6753−6764.

(58) Schiewek, R.; Lorenz, M.; Giese, R.; Brockmann, K.; Benter, T.; Gäb, S.; Schmitz, O. J. Development of a multipurpose ion source for LC-MS and GC-API MS. *Anal. Bioanal. Chem.* **2008**, *392* (1−2), 87−96.

(59) Calemma, V.; Rausa, R. Thermal decomposition behaviour and structural characteristics of asphaltenes. *J. Anal. Appl. Pyrolysis* **1997**, *40−41*, 569−584.

(60) Gonçalves, M. L. A.; Teixeira, M. A. G.; Pereira, R. C. L.; Mercury, R. L. P.; Matos, J. R. Contribution of thermal analysis for characterization of asphaltenes from Brazilian crude oil. *J. Therm Anal Calorim* **2001**, *64* (2), 697−706.

(61) Nali, M.; Calemma, V.; Montanari, L. Pyrolysis/gas chromatography/mass spectrometry of asphaltene fractions. *Org. Mass Spectrom.* **1994**, *29* (11), 607−614.

(62) Hanley, L.; Zimmermann, R. Light and molecular ions: The emergence of vacuum UV single-photon ionization in MS. *Anal. Chem.* **2009**, *81* (11), 4174−4182.

(63) Islas, C. A.; Suelves, I.; Carter, J. F.; Herod, A. A.; Kandiyoti, R. Pyrolysis-gas chromatography/mass spectrometry of a coal extract and its fractions separated by planar chromatography: Correlation of structural features with molecular mass. *Rapid Commun. Mass Spectrom.* **2000**, *14* (19), 1766−1782.

(64) Eschner, M. S.; Zimmermann, R. Determination of photo-ionization cross-sections of different organic molecules using gas chromatography coupled to single-photon ionization (SPI) time-of-flight mass spectrometry (TOF-MS) with an electron-beam-pumped rare gas excimer light source (EBEL): Influence of molecular structure and analytical implications. *Appl. Spectrosc.* **2011**, *65* (7), 806−816.

(65) Boesl, U.; Neusser, H. J.; Schlag, E. W. Multi-photon ionization in the mass spectrometry of polyatomic molecules: Cross sections. *Chem. Phys.* **1981**, *55* (2), 193−204.

(66) Adam, T. W.; Clairotte, M.; Streibel, T.; Elsasser, M.; Pommeres, A.; Manfredi, U.; Carriero, M.; Martini, G.; Sklorz, M.; Krasenbrink, A.; Astorga, C.; Zimmermann, R. Real-time analysis of aromatics in combustion engine exhaust by resonance-enhanced multiphoton ionisation time-of-flight mass spectrometry (REMPI-TOF-MS): A robust tool for chassis dynamometer testing. *Anal. Bioanal. Chem.* **2012**, *404* (1), 273−276.

(67) Pereira, T. M. C.; Vanini, G.; Tose, L. V.; Cardoso, F. M. R.; Fleming, F. P.; Rosa, P. T. V.; Thompson, C. J.; Castro, E. V. R.; Vaz, B. G.; Romão, W. FT-ICR MS analysis of asphaltenes: Asphaltenes go in, fullerenes come out. *Fuel* **2014**, *131*, 49−58.

(68) Korsten, H. Characterization of hydrocarbon systems by DBE concept. *AIChE J.* **1997**, *43* (6), 1559−1568.

(69) Cho, Y.; Kim, Y. H.; Kim, S. Planar limit-assisted structural interpretation of saturates/aromatics/resins/asphaltenes fractionated crude oil compounds observed by Fourier transform ion cyclotron resonance mass spectrometry. *Anal. Chem.* **2011**, *83* (15), 6068−6073.

(70) Rüger, C. P.; Sklorz, M.; Schwemer, T.; Zimmermann, R. Characterisation of ship diesel primary particulate matter at the molecular level by means of ultra-high-resolution mass spectrometry coupled to laser desorption ionisation-comparison of feed fuel, filter extracts and direct particle measurements. *Anal. Bioanal. Chem.* **2015**, *407* (20), 5923−5937.

(71) Badre, S.; Carla Goncalves, C.; Norinaga, K.; Gustavson, G.; Mullins, O. C. Molecular size and weight of asphaltene and asphaltene solubility fractions from coals, crude oils and bitumen. *Fuel* **2006**, *85* (1), 1−11.

(72) Groenzin, H.; Mullins, O. C. Asphaltene Molecular Size and Structure. *J. Phys. Chem. A* **1999**, *103* (50), 11237−11245.

(73) Groenzin, H.; Mullins, O. C. Molecular Size and Structure of Asphaltenes from Various Sources. *Energy Fuels* **2000**, *14* (3), 677−684.

(74) Zhao, Y.; Wei, F.; Yu, Y. Effects of reaction time and temperature on carbonization in asphaltene pyrolysis. *J. Pet. Sci. Eng.* **2010**, *74* (1−2), 20−25.

(75) Douda, J.; Alvarez, R.; Navarrete Bolaños, J. Characterization of Maya Asphaltene and Maltene by Means of Pyrolysis Application. *Energy Fuels* **2008**, *22* (4), 2619−2628.

(76) Alshareef, A. H.; Scherer, A.; Tan, X.; Azyat, K.; Stryker, J. M.; Tykwinski, R. R.; Gray, M. R. Formation of Archipelago Structures during Thermal Cracking Implicates a Chemical Mechanism for the Formation of Petroleum Asphaltenes. *Energy Fuels* **2011**, *25* (5), 2130−2136.

(77) Yasar, M.; Trauth, D. M.; Klein, M. T. Asphaltene and Resid Pyrolysis. 2. The Effect of Reaction Environment on Pathways and Selectivities. *Energy Fuels* **2001**, *15* (3), 504−509.

(78) Karimi, A.; Qian, K.; Olmstead, W. N.; Freund, H.; Yung, C.; Gray, M. R. Quantitative Evidence for Bridged Structures in

Asphaltenes by Thin Film Pyrolysis. *Energy Fuels* **2011**, *25* (8), 3581−3589.

8.2   Publication 2

Description of Steam Cracker Fouling and Coking Residue by Thermal Analysis-Photoionization Mass Spectrometry

by

Christoph Grimmer, Christopher P. Rüger, Thorsten Streibel, Fabrice Cuoq, Gerard Kwakkenbos, Miguel Cordova, Rosa Peñalver, Ralf Zimmermann

Description of Steam Cracker Fouling and Coking Residues by Thermal Analysis-Photoionization Mass Spectrometry

Christoph Grimmer,[†] Christopher P. Rüger,[†] Thorsten Streibel,[*,†,‡] Fabrice Cuoq,[§] Gerard Kwakkenbos,[§] Miguel Cordova,[§] Rosa Peñalver,[∥] and Ralf Zimmermann[†,‡]

[†]Joint Mass Spectrometry Centre/Chair of Analytical Chemistry, University of Rostock, 18059 Rostock, Germany

[‡]Joint Mass Spectrometry Centre/Cooperation Group Comprehensive Molecular Analytics, Helmholtz Zentrum München, 85764 Neuherberg, Germany

[§]Saudi Basic Industries Corporation (SABIC), SABIC Technology Center Geleen, Urmonderbaan 22, P.O. Box 319, 6167 RD Geleen, Netherlands

[∥]Saudi Basic Industries Corporation (SABIC), SABIC Technology Cartagena, Ctra. de Cartagena, Alhama de Murcia Km 13, La Aljorra, Murcia, 30390, Spain

S *Supporting Information*

ABSTRACT: Two organic fouling samples obtained from downstream the cracking oven (DS) and from upstream the hot zone (US) of a steam cracker facility were characterized. For this purpose, a simultaneous thermal analyzer coupled to a photoionization mass spectrometer (STA-PI-MS) and a thermal desorption/pyrolysis gas chromatograph (TD/Py-GC-EI-MS) were used. Mass loss and differential scanning calorimetry information revealed the degradation of the materials beginning at 130 °C with two distinct maxima for US and one for DS (230−330 °C) as well as broad signals (330−500 °C) for both. Structural motives of different polymeric-like structures were assigned based on PI-MS of the effluent and separately conducted TD/Py-GC-EI-MS. The advantage of soft photoionization over hard ionization techniques such as electron ionization is the considerable reduction of fragmentation, yielding higher abundancies of molecular ions. Thus, even though complex samples are studied, evolving constituents can often be easily tracked in a time-resolved manner (1 Hz). While single photon ionization (SPI, 118 nm = 10.5 eV) ionizes most organic molecules, resonance-enhanced multiphoton ionization (REMPI, 2 × 266 nm = 9.4 eV) selectively addresses aromatic species. Differentiation of polymeric-like structures was achieved by exploiting this selectivity (SPI vs REMPI) and comparison of molecular patterns with GC-EI-MS data, which supports the identification of compounds by providing fragmentation patterns and chemical information based on retention time. US shows high inorganic content (~50%) and more diversity in its organic part, as indicated by four types of patterns: polyethylene-like, Diels−Alder-like, polythioether/polysulfide-like, and polystyrene-like motives. In contrast, DS exhibits almost only signals of Diels−Alder-like and polystyrene-like structures and contains a less inorganic material (~23%). Additionally, first attempts to quantify the Diels−Alder content by STA-SPI-MS were successfully conducted.

INTRODUCTION

Petroleum and petrochemical product-related analysis remains a challenging task for state-of-the-art instrumental analysis. In particular, heavy fractions are challenging, on the one hand, due to low volatility, which makes them inaccessible for gas chromatography, and on the other hand, due to lower solubility in common solvents for liquid chromatography–mass spectrometry analysis. Moreover, an increasing isomeric complexity impedes separation and data handling. The same problems usually occur when approaching solid residues from petroleum refineries such as fouling from steam cracker facilities.

Fouling, in refineries, is the accumulation of unwanted materials within a processing unit or on the solid surfaces of the unit to the detriment of function. It includes solid deposit formation, corrosion, and phase separation among others. The major effects are (1) loss of heat transfer as indicated by the decrease in charge outlet temperature and increase in pressure drop, (2) blocked process pipes, (3) underdeposit corrosion and pollution, and (4) hot spots in reactors. All of these effects

culminate in production losses and increased maintenance costs of several million euros per year and cracker.[1−3]

Fouling can occur in almost all parts of a steam cracker facility, but a large part of the literature is focused on the coke formation in the coils and transfer line exchangers of the hot section.[1−4] This type of fouling (i.e., coke) is however not investigated in this study. The focus of this study is on less investigated organic fouling that occurs downstream or upstream of the hot section at temperatures ranging from 80 to 200 °C. At these temperatures, both radical polymerization and Diels−Alder reactions take place leading to a very complex mixture of oligomeric and polymeric adducts.[5−7] A higher temperature will lead to higher rates of fouling formation (via Diels−Alder or radical polymerization) even though it is generally admitted that free-radical polymerization significantly contributes to fouling at temperatures above 70 °C.[6] Diels−

Alder reactions require the presence of a dienophile and a diene, for example, acetaldehyde and butadiene, respectively, or amphoteric monomers such as cyclopentadiene.[7,8] Radical polymerization can either be initiated by autopolymerization of styrene[6] or by the formation of radicals on free unsaturated monomers catalyzed by for example inorganic particles such as rust or due to the ingress of oxygen in the system. Radical fouling is often mitigated by dosing free-radical inhibitors such as TEMPO, whereas Diels−Alder fouling is mitigated by dosing a dispersant. However, the optimal dosage of reagents for chemical treatment of fouling is not accessible by any means so far and is yet to be estimated.

Previous studies of the authors, with direct insertion probe−mass spectrometry (DIP−MS) and thermogravimetric analysis (TGA) coupled to an IR detector (TGA−IR) of similar samples revealed a highly heterogeneous polymeric character and the abundance of typical Diels−Alder and radical fouling monomers.[9] Evolved gas analysis (EGA) techniques, such as direct insert probe (DIP) or thermal analysis (TA) coupled to MS or spectroscopy, offer access to desorption of intact molecules as well as to the evolution of thermally degraded pyrolysis products. Therefore, solid samples such as polymers,[10] asphaltenes,[11] or solid fuels[10,12−16] can be investigated. EGA approaches have been widely used in industrial analytical research for different applications, for example, investigation of thermal decomposition pathways of polymers, chemical oils, complex mixture characterization, and understanding of reaction mechanisms.[16−21]

Though thermal separation of retro-Diels−Alder reactions (∼150−300 °C) and the decomposition of the radical polymer (>300 °C) was previously achieved by DIP−MS, the high complexity of evolving constituents and strong fragmentation (EI-MS) hampers more in-depth investigations. Similar problems were encountered during TGA−IR measurements.

The hyphenation of TGA to mass spectrometry with soft photoionization methods could circumvent such problems and shed more light on the chemical composition of solid deposits. This analytical method has been successfully applied for the detection of crude oils, its refined products, and solid fuels such as coal and biomass.[11,22−28] Photoionization exhibits not only the advantage of keeping the molecular profile of the evolved gas mixture intact but provides additional information via its selective ionization. The latter is especially helpful with low-resolution mass spectrometers. For instance, resonance-enhanced multiphoton ionization (REMPI) with 266 nm photons addresses only aromatic species, while single photon ionization (SPI) ionizes all compounds with ionization energies below the used photon energy. Hence, the combined application of both ionization methods for the investigation of fouling samples by means of EGA with TGA thus constitutes a novel approach for the characterization of such a material. Especially the possibility of distinguishing between aromatic and nonaromatic components of the fouling samples by switching the ionization technique offers a straightforward route to get new insights into their composition.

In this study, we deployed a simultaneous thermal analyzer (STA) coupled to soft photoionization time-of-flight mass spectrometry to demonstrate the feasibility of this hyphenated method for the description of two representative steam cracker fouling residues. Because only little literature is found on soft fouling, we present useful qualitative information as well as first attempts to quantify the Diels−Alder content to improve chemical treatment of the ethylene steam cracker. Supporting

analyses were performed by classical TD/pyrolysis gas chromatography electron ionization mass spectrometry.

■ MATERIALS AND METHODS

Materials. The investigated fouling samples were received from Saudi Basic Industries Corporation (SABIC, Saudi Arabia) and originate from different parts inside a steam cracker facility. In order to increase result reproducibility, it was necessary to remove the residual solvent and achieve a homogenous sample by setting a grinding and drying procedure, which does not affect the underlying matrix. This was achieved by cryogenic grinding (in liquid nitrogen, −196 °C, 2 min at 10 Hz, 6750 Freezer/Mill, SPEX CertiPrep) and successively drying under mild conditions (40 °C, 96 h, 15 mbar) in a rotary evaporator. Dicyclopentadiene (DCPD) (purity ≥ 96%, Sigma-Aldrich) was used as a model substrate. For mass calibration and signal intensity standardization of the simultaneous thermal analyzer coupled to a photoionization mass spectrometer (STA-PI-MS), a gas container filled with nitrogen and benzene (10 ppm), toluene (10 ppm), xylene (10 ppm), and mesitylene (10 ppm) was acquired from Linde AG, Germany. Several additional substances for the identification of gas chromatographic signals were purchased and used as delivered. Details can be found in the supplementary material (Table S1).

Elemental Analysis. Elemental analysis was performed by means of quantitative CHNS, semi-quantitative WDXRF, and ash content analysis of the dried sample material. The CHNS content was determined with the help of an elemental analyzer (LECO TruSpec Micro CHNS). Other elements (with atomic numbers ≥11) were measured by X-ray fluorescence spectroscopy (XRF) with a wavelength dispersive X-ray fluorescence spectrometer (AXIOS WDXRF spectrometer) using an externally validated, fully automated method (semi-quantitative without standard). Quantification is based on theoretical properties of the elements and their spectra. The method has an excellent reproducibility, but the absolute level may differ from the level as measured by other methods. Ash content is measured by an in-house method, in which the sample is completely incinerated at 900 °C and then the residue is weighed.

Simultaneous Thermal Analyzer Coupled to a Photo-ionization Mass Spectrometer. A simultaneous thermal analyzer (STA 409, Netzsch Gerätebau, Selb, Germany) was coupled to a custom photoionization time-of-flight mass spectrometer (PI-MS), which utilizes either SPI or REMPI. Evolving constituents of the effluent from the thermal analyzer were sampled via a heated interface and transfer line (length 2.25 m, 200 μm inner diameter, at 280 °C).[25,29] A few milligrams (5−10 mg) of the prepared sample material were placed in an aluminum crucible, which was sealed by a lid (pinhole 50 μm diameter). Thermal analysis was carried out with a heating rate of 20 K/min under nitrogen atmosphere (60 mL/min) from 35 to 525 °C. At 525 °C, nitrogen is partially replaced by air (40 mL/min synthetic air and 20 mL/min nitrogen), yielding an oxidative atmosphere. Evolved gas was sampled as a result of the pressure difference between the balance at atmospheric pressure and the ion source at reduced pressure (roughly 3×10^{-5} mbar). Subsequent SPI and REMPI TOF-MS analysis is described in detail elsewhere.[30−32] In brief, for SPI, 355 nm laser pulses (25 mJ pulse energy, 10 Hz repetition rate, and 5 ns pulse width), generated from a Nd:YAG laser (Surelite III, Continuum, Inc., Santa Clara, CA, U.S.A.), were sent through a xenon-filled gas cell (Xe 4.0, 12 mbar), yielding vacuum ultraviolet photons by nonlinear frequency tripling (118 nm = 10.5 eV). For REMPI, the Nd:YAG fundamental wavelength is frequency-quadrupled (266 nm = 4.7 eV). The molecular ions formed by either REMPI or SPI are recorded with an acquisition frequency of 10 Hz from m/z 5 to 500 with a reflectron TOF-MS using a multichannel plate detector. Averaging over 10 spectra yields a time-resolution of 1 Hz. Data processing and analysis were carried out with an instrument-specific LabView graphical user interface and self-written MATLAB (2010b) scripts.

TD/Py-GC-EI-MS. For thermal desorption/pyrolysis gas chromatographic analysis, 0.3−4.0 mg of the prepared sample was injected into
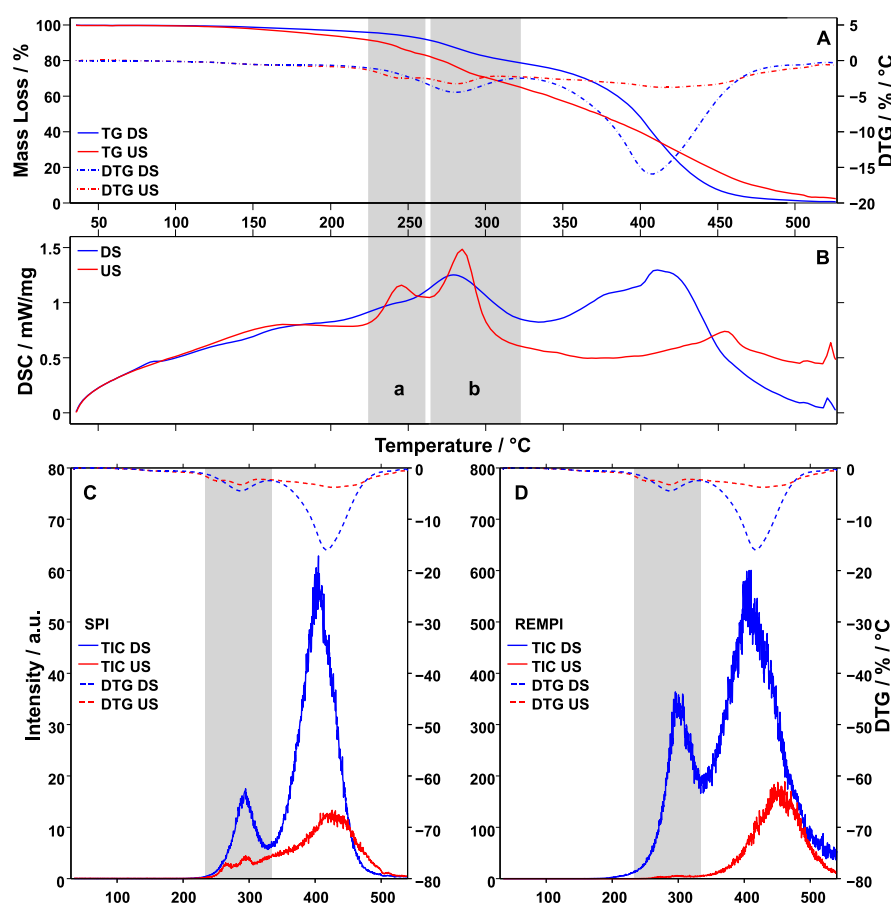
Figure 1. TGA (A) and DSC (B) data of DS and US reveal several different degradation processes with the most pronounced being between 230−330 °C (marked grey) and 330−500 °C (not indicated). Panel (C) shows the evolved total ion current (TIC) obtained by more universal SPI and panel (D) shows the TIC during selective REMPI. The DTG (dashed line) is plotted for comparison and reveals a good correlation to the SPI TIC response.

Table 1. EA and Ash Content of Dried Fouling Samples

| sample	elemental analysis/wt %					H/C/mol/mol	ash content/wt %
	C	H	N	S	Fe		
DS	70.18	6.37	0.39	0.09	3.29	1.09	7.94
US	39.25	4.43	3.05	3.19	31.56	1.35	34.50

the pyrolyzer (model PY-2020iD, double-shot pyrolyzer, Frontier Laboratories) mounted onto a HP 6890 gas chromatograph.[33,34] The sample material undergoes two steps: (1) a thermal desorption process at 330 °C and (2) a pyrolysis step at 500 °C, each held for 1 min. To separate the evolved gas mixture, a 30 m SGE-BPX5 column (250 μm inner diameter, 0.25 μm film, helium at 99.999%, and head pressure at 0.4 bar, split of 1:50) was used with the following temperature program: hold for 20 min at 35 °C, ramp to 330 °C with 5 K/min, and hold for 20 min. The effluent from the column was ionized by a 70 eV electron ionization source and analyzed by a quadrupole mass spectrometer. Mass spectra were recorded in the scan mode from m/z 10 to 500.

RESULTS AND DISCUSSION

Sample Origin and Pretreatment. The fouling samples investigated within this study originate from a steam cracker. They were attained during a turnaround period and originate from downstream the cracking oven (DS) and from upstream the hot zone (US), which is contaminated by heavy molecular weighted byproducts as shown later.

Comparison of TA and mass spectrometric data of measurements from before and after the sample pretreatment (Figure S1) revealed only significant change for small, alkylated benzenes and mid to heavy alkanes evolving at moderate temperatures, presumably unbound constituents. This leads to the assumption that only adsorbed constituents which can be volatilized at rather low temperatures (<130 °C) are removed and, thus, that the macromolecular chemical composition is not affected by the pretreatment.

Simultaneous Thermal Analysis. Before discussing the emitted molecular profiles of the residue samples, the TGA and differential scanning calorimetry (DSC) data can give some insights into general thermal behavior of both samples, summarized in Figure 1. Starting at 130 °C, a slow and steady mass loss of both samples can be registered with a slightly higher rate for US (Figure 1A). However, at 230−330 °C, DS shows one distinct step, while US reveals two less pronounced, consecutive steps in addition to the underlying steady mass loss. From 330 °C onwards, the mass loss rate of DS increases drastically peaking at 420 °C and then decreases until all
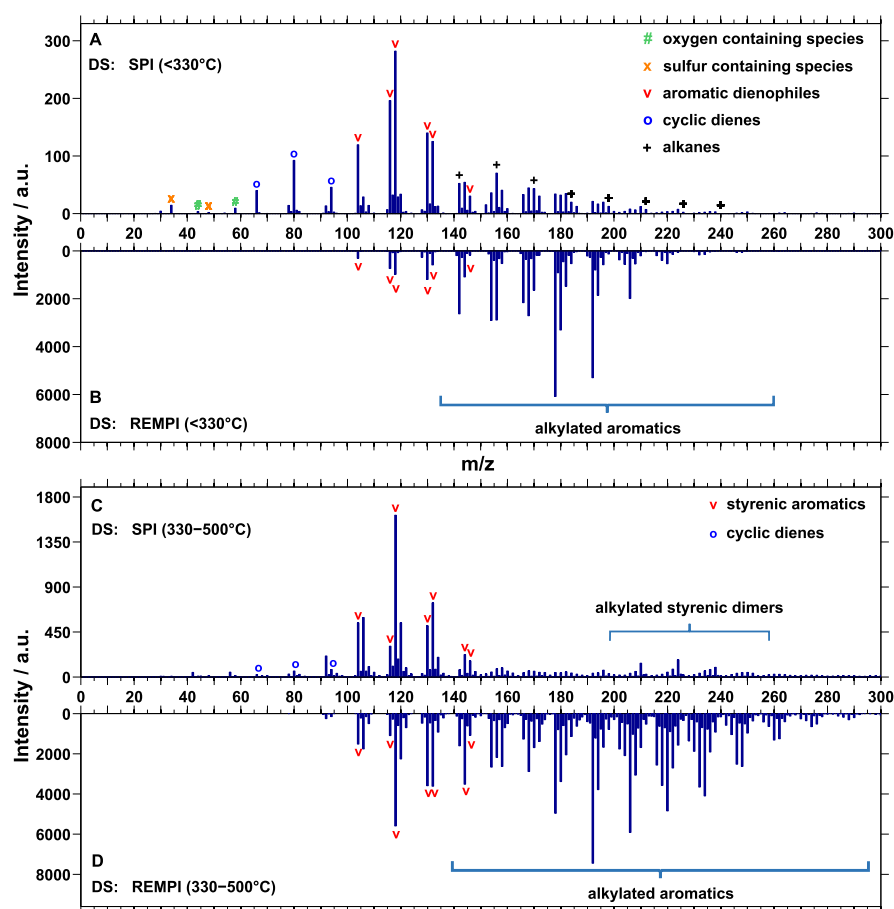
Figure 2. Summed SPI-MS (A) and REMPI-MS (B) spectrum of DS (<330 °C): most pronounced signals belong to alkylated aromatics, styrenic compounds (styrene, indene, propylene benzene etc.), and cyclic dienes. Alkanes contribute very little to the signals, which are shared with alkylated aromatics. During pyrolysis (330−500 °C), the summed SPI-MS (C) and REMPI-MS (D) spectra show a multi modal distribution of alkylated styrenic subunits with its respective maxima at m/z 118 and 236. Little amounts of cyclic dienes evolve as well.

degradable constituents are expended. In contrast, the rate of US is almost constant but also slightly decreases after 420 °C. For better comparison, data and figures have been normalized to the samples' respective total mass loss. The remaining masses are 62 wt % (US) and 29 wt % (DS), which roughly corresponds to the non organic content retrieved from elemental analysis (Table 1).

DSC data reveal enthalpy changes for both samples during the entire analysis (Figure 1B). The mass loss steps observed in TGA between 230 and 330 °C are also detected by DSC and accordingly show two distinct but partially overlapping peaks for US [Figure 1B(a,b)] and one broad endothermic signal for DS. Similar to mass loss, the energy consumption of DS increases from 330 to 420 °C and decreases afterwards, revealing a small shoulder during its increase. In the same temperature range, the energy flux of US measured by DSC decreases at first and then rises until a maximum at 470 °C is reached and decreases again afterwards.

An experiment with several consecutive heating, cooling, and reheating steps was conducted for DS to detect reversible reactions such as intramolecular Diels−Alder reactions (Figure S2). The absence of enthalpy changes during cooling and reheating indicates no or at least undetectable reversible processes. Additionally, measurements with high-resolution TGA and a more sensitive, dedicated DSC system confirmed the minor extent of intramolecular DA reactions (not shown here).

Elemental Analysis. Besides increased coke formation (i.e., carbonation), a substantial proportion of the remaining mass at the end of the temperature program (550 °C) probably consists of metals or other hetero element-containing compounds as indicated by EA (Table 1). The most abundant metal for both samples is iron with 31.56 wt % (US) and 3.29 wt % (DS). Further detected hetero elements in US are sulfur (3.19 wt %), nitrogen (3.05 wt %), nickel (0.38 wt %), chlorine (0.16 wt %), phosphor (0.13%), and many more, whereas DS shows less abundance of hetero elements, for example, nitrogen (0.39 wt %), silicon (0.33 wt %), sodium (0.23 wt %), sulfur (0.09 wt %), and others.

In general, both samples are very diverse in their elemental composition, but their distribution is quite different. US contains higher values for most of the metals as well as for nitrogen and sulfur—only silicon and sodium are more abundant in DS than in US. Thus, DS seems to contain a higher proportion of organic constituents as indicated by C (70.18 wt % vs 39.25 wt %) and H (6.37 wt % vs 4.43 wt %), and the resulting H/C ratios (1.09 vs 1.35) suggest either a higher carbonation or unsaturation/aromaticity.

Photoionization (SPI/REMPI). The advantage of soft photoionization is the almost exclusive generation of molecular ions, leading to simplified, mostly fragment-free mass spectra. Furthermore, due to the fast time-of-flight mass spectrometric detection (10 Hz, averaged over 10 spectra = 1 Hz), highly time-resolved spectra are obtained. Especially complex samples
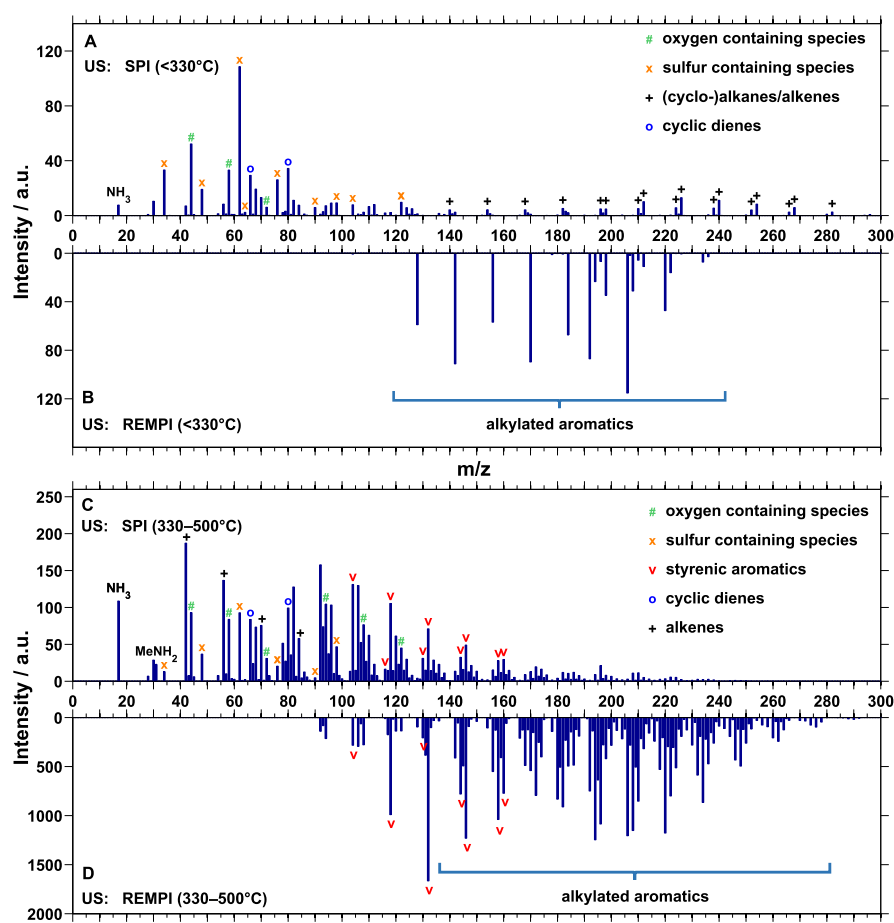
Figure 3. Summed SPI-MS (A) and REMPI-MS (B) spectrum of US (<330 °C); both distinct mass loss steps are depicted together: medium to long (cyclo-)alkanes/alkenes evolve first (220−270 °C) and then a diverse mixture of ammonia, sulfur, and oxygen-containing species as well as small double bond-containing substances are released (270−310 °C). Alkylated naphthalenes and other aromatics show negligible abundances. During pyrolysis (330−500 °C, C,D), the spectrum of sulfur and oxygen-containing species continues to evolve up to 370 °C and then a sudden change toward a complex aromatic pattern, nitrogen-containing species, and alkenes takes place.

can then be interpreted more easily and interesting patterns or masses can be tracked.[11] Simultaneously, bulk gases (e.g., N_2, O_2, H_2O, CO_2) are excluded because of their high ionization energies, preventing the detector from saturation and allowing for an increased dynamic range.

Even though the mass spectrometric data has been normalized to the evaporated mass, the TIC of US for SPI and also for REMPI is much lower compared to DS (factor of 2.85 for SPI and 5.24 for REMPI, respectively) (Figure 1C,D). Because photoionization is dependent on the specific cross section (ionization efficiency) of the evolving analytes, US seems to contain more compounds with lower cross sections. In general, the order of cross sections in SPI for selected CH substance classes is usually $\sigma_{alkanes} < \sigma_{alkenes} < \sigma_{aromatics}$.[35] This finding proves the hypothesis gained by the elemental composition analysis: the organic content of DS is more unsaturated/aromatic than the organic content of US.

Although considerable mass loss occurs beginning at 130 °C, no mass spectrometric signal above the noise level can be detected before reaching 200 °C (SPI) for both samples (Figure 1C). With the more sensitive REMPI (Figure 1D), a rising signal can be recorded for DS starting at 170 °C. The resulting mass loss without detectable MS signal implies evolution of poor or nonionizable species. Several possibilities exist, but reactions such as decarboxylation or dehydration might play a role. The typical release of CO_2 (*m/z* 44, IE: 13.8) or H_2O (*m/z* 18, IE: 12.6 eV) cannot be detected with the given PI-MS setup because the photon energies are too low (SPI: 10.5 eV, REMPI: 9.3 eV).[36] After 200 °C, the SPI TIC of both samples correlates quite well with its respective mass loss rate. For DS, the REMPI signal also correlates with SPI and mass loss, while for US there is almost no REMPI signal during the first phase (200−330 °C) and only moderate intensity during the last phase (350−550 °C).

Molecular pattern information (SPI/REMPI-MS) is obtained by summing the spectra of each phase (<330 and 330−550 °C) (Figure 2 and 3) and comparing it to data received from TD/Py-GC-MS recorded at similar temperatures (Figures S3−S6). Chromatograms obtained by this technique should be comparable to the summed molecular patterns from TGA-PI-MS and give additional chemical information based on the retention times and electron ionization fragment mass spectra. Peaks can be identified by their characteristic fragmentation pattern utilizing the NIST database (NIST MS Search 2.0) or by comparison to standards. This combined approach together with knowledge from literature enables a tentative assignment of the nominal mass values given by the STA-PI-MS setup.[11]

Downstream Fouling. In the first phase (<330 °C), small signals at *m/z* 34 (H_2S), *m/z* 44 (Et = O), *m/z* 48 (SO/
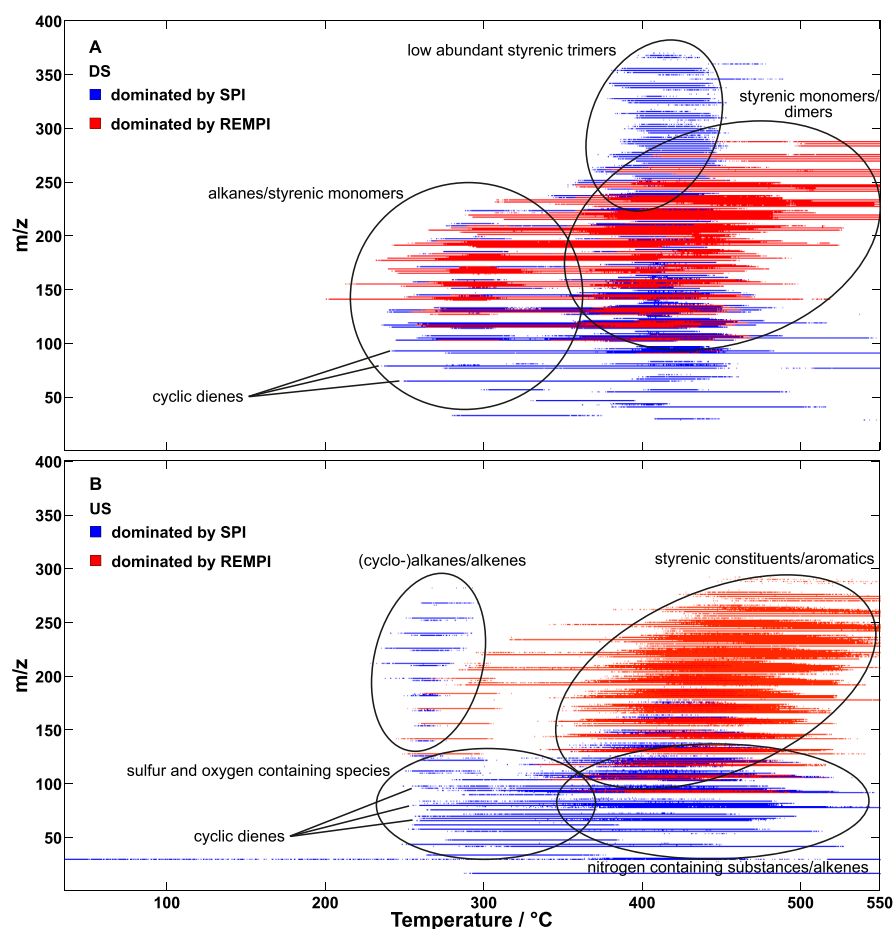
Figure 4. Simplified contour plot of DS (A) and US (B) illustrating the dominance of SPI (blue) and REMPI (red) for the ionization of evolving constituents during TA. Most abundant structural motifs are indicated within the depiction.

MeSH), and m/z 58 (acetone) are observed (Figure 2A). Other low intensity signals (m/z 40, 42, 52, 54, 70) could be assigned to alkynes, alkenes, or dienes (e.g., butadiene).

A highly abundant signal at m/z 66 can be assigned to cyclopentadiene. The identification is supported by comparison with measurements of pyrolyzed DCPD. High agreement was found in their fragment patterns and retention time and the dimer (m/z 132) was also detected in both measurements. Furthermore, the homologue methylcyclopentadiene (m/z 80) can also be readily identified by comparison to a standard measurement. For m/z 94, several peaks can be found in the chromatogram, most likely isomers of dimethyl-/ethylcyclo-pentadienes. Eligible standards were unfortunately not commercially available. In either case, the fragment patterns indicate at least two conjugated double bonds. Only a small part of m/z 92 can be assigned to toluene, while several other peaks of m/z 92 and the one of m/z 78 indicate nonaromatic, conjugated double bond-containing species as well (e.g., fulvenes).

As seen by comparison of the molecular profile to the REMPI data (Figure 2B), the composition changes to an almost purely aromatic pattern starting from m/z 104. Many identified compounds contain at least one nonaromatic double bond, for example styrene (m/z 104), indene (m/z 116), methylstyrene (m/z 118), diethenylbenzene (m/z 130), methylindene (m/z 130), or alkenylbenzenes (m/z 132/ 146). Other prominent peaks are made up by aromatic cores or their alkylated homologues, for example, naphthalene (m/z

128), methylnaphthalene (m/z 142), acenaphthene (m/z 152), acenaphthylene (m/z 154), biphenyl (m/z 154), alkylated naphthalenes (m/z 156), fluorene (m/z 166), anthracene/phenanthrene (m/z 178), or pyrene (m/z 202). A rather small part of DS is composed of saturated, long chain hydrocarbons (C_{10}–C_{17}, <1%/TIC).

When looking at the pyrolysis phase (330–550 °C), intensity, complexity, and mass distribution increase in terms of covered mass range, peak number, and homologous rows (Figure 2C,D). Instead of a mono-modal distribution as found for the first phase, a multi modal distribution becomes evident, reaching up to m/z 380. Multi modes usually imply a more or less regular structure of a chemical motif, such as the highly structured alkylation pattern which can be found for crude oil and petroleum distillates or polymeric pyrolysis pattern (monomer subunit).[28,31] The difference between two modes is about m/z 104, leading to the assumption of an alkylated styrenic structure. Both phases show a similar composition, but the aromatic, oligomeric pattern is much more pronounced during pyrolysis and reaches higher m/z values. Only a few additional low m/z values appear as well as many new signals and higher intensities for higher m/z values (i.e. dimers and trimers). While the monomers and dimers are well detected by REMPI and SPI, trimers can only be seen in SPI (Figure 4A). Usually, REMPI is much more sensitive for aromatics than SPI, but the isolated benzene rings of the trimers and less detector voltage (REMPI: 1.55 kV, SPI: 1.67 kV) might lead to a better sensitivity in SPI in this case. Signals of trimers with prominent

fragments such as m/z 77, 91, 105, 117 etc. can also be found in the Pyr-GC-MS data.

In summary, an alkylated styrenic motif, composed of alkylated styrene, indene, and similar compounds, can be suggested as dominating structure, which decomposes mainly above 330 °C (~80% mass loss, eq 1). A negligible proportion of DS is made up by long alkane chains and carboxylic acids. Nonetheless, their occurrence could not be specified and decarboxylation might lead to a biased (underrepresented) view, while the paraffinic content is overestimated. Although EA shows a certain hetero element content, most of the effluent can be assigned to the CH class and only little signal is related to sulfur-, nitrogen-, or oxygen-containing substances. It is interesting to note the moderate abundance of actually and tentatively assigned cyclic dienes (e.g., cyclopentadienes), particularly present in the first phase.

Scheme 1. Simplified Scheme of the Degradation of the Irregular Polystyrene-like Structure toward Dimers and Monomers (eq 1) and retro-Diels−Alder Reaction of DCPD (eq 2)[a]
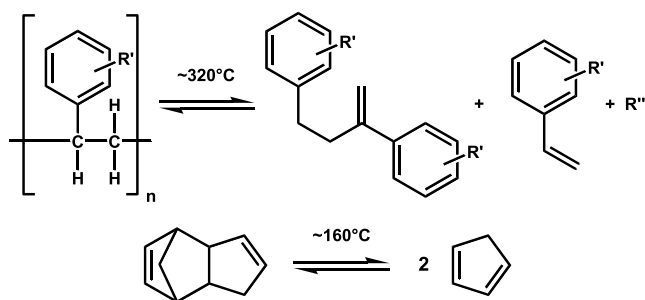
[a]In reality, variations at sidechains (R′), core structure (indene, vinyl naphthalene or similar cores instead of styrene), or shifts/hydrogenation of the double bond lead to a far more complex product mixture. The lower scheme shows the retro-Diels−Alder reaction of DCPD into its monomer cyclopentadiene (eq 2), which was used as a model reaction for the calibration purpose.

Conjugated dienes are typical for (retro-)Diels−Alder reactions and could be good markers to determine the contribution of Diels−Alder fouling in steam cracker residues. One example for a retro-Diels−Alder reaction is the degradation of DCPD (eq 2). Though dienes can react with each other, the unsaturation of the general styrenic structure is also an ideal target for the addition of dienes. One possible explanation for two distinct mass loss steps with similar decomposition patterns is that the same constituents are incorporated in different ways. Because retro-Diels−Alder is hypothesized to play a major role during the first phase, monomers of polystyrene could also be incorporated by this type of reaction. In a converse sense, cyclic dienes might also be incorporated by another type of reaction, which decomposes broadly (330−500 °C) together with the polystyrene structure.

Upstream Fouling. The spectrum in Figure 3A has been summed for <330 °C, including the first two mass loss peaks of US. Though they cannot be completely separated, differences can be distinguished when looking at the time-resolved data (Figure S8). Most of the intensity during the first step (220−270 °C, Figure 1B(a)) results from mid to heavy saturated alkanes (C_{10}–C_{30}, linear and branched), which can be seen quite well on the right hand side of Figure 3A.

Notably, distinct m/z signals occur with −2/−4 splits (−H_2/−$2xH_2$) to the series of saturates. This pattern can be associated to compounds with higher aromaticity or cyclic structures (higher unsaturation/hydrogen-deficiency). Their abundance increases with a decreasing m/z value, until they eventually merge into the underlying and even more pronounced low m/z pattern of the second peak (270−310 °C, Figure 1B(b)).

Many masses in this low m/z range can be related to hetero atom-containing substances. Some of them show low or moderate intensity, for example, m/z 17 (NH_3), m/z 48 (MeSH/SO), m/z 64 (SO_2), m/z 72 (butanone), m/z 90 (butanethiol), m/z 98 (methylthiophene), m/z 104 (pentanethiol), and m/z 122 (diethyldisulfide), while others are highly abundant, for example, m/z 34 (H_2S), m/z 44 (Et = O), m/z 58 (Acetone), m/z 62 (EtSH), and m/z 76 (propenethiol/CS_2). Signals at m/z 66 (cyclopentadiene) and m/z 80 (methylcyclopentadiene) can be assigned confidently. In contrast to DS, signals at m/z 68, 70 and m/z 82, 84 might indicate the abundance of similar C_5/C_6 compounds, but with at least one less double bond equivalent. The REMPI spectrum (Figure 3B) exhibits only minor intensities of (alkylated) naphthalenes and some other unidentified aromatics with low abundance during the first phases (220−330 °C).

Not visible in the summed spectra (Figure 3C,D), but in time-resolved data, is the drastic change in MS patterns during pyrolysis (330−550 °C). At first, the low m/z values described in the first phase remain the same but change suddenly around 370 °C (Figure S9). All signals of sulfur-containing compounds disappear, whereas signals of m/z 17 (NH_3) and m/z 31 ($MeNH_2$) increase/appear. A strong increase can also be noticed for several tentatively assigned alkenes, for example, m/z 42 (propene), m/z 56 (butenes), m/z 70 (pentenes), and m/z 84 (hexenes) and probably dienes, for example, m/z 68 (pentadienes) and m/z 82 (hexadienes). Only a few signals remain almost the same, for example, m/z 58 (acetone), m/z 66 (cyclopentadiene), and m/z 80 (methylcyclopentadiene). Furthermore, a complex mixture of aromatics starts to evolve, resulting in an intense REMPI spectrum (Figure 3D). Moderate signals can be assigned to benzene derivatives (m/z 92, 106, 120) and phenols (m/z 94, 108, 122), while the highest intensities are made up by (alkylated) styrenes (m/z 104−202), indenes (m/z 116−200), biphenyls (m/z 154−264), and naphthalenes (m/z 128−212).

In summary, a small part of US consists of mid to heavy alkanes, which are released during the first distinct mass loss step (220−270 °C). Either the drying procedure was not sufficient for the unbound constituents or they are formed as degradation products. Arguments for degradation are the sharp peak in DSC and the missing, staggered boiling pattern of low to high m/z values. Degradation of a pure polyethylene-like structure is unlikely because common polyethylene degrades above 310 °C.[37] Maybe decarboxylation or the concurrent release of thiols, ketones/aldehydes, and NH_3 is related to this observation. Evolution of a strong sulfur-containing pattern together with a degradation temperature range of 220−370 °C suggests a polythioether-like ([−S−$(CH_2)_n$−]$_m$) or polysulfide-like ([−S−S−$(CH_2)_n$−]$_m$) structure.[38] The appearance of the distinct peak at 270−310 °C (DTG, DSC, SPI), followed by a drastic temporary decline of most of the signals, remains for further studies. Then, after 370 °C, an evolving complex aromatic pattern indicates a polystyrene-like composition for the remaining mass (~60%). Cyclic dienes (m/z 66 and m/z
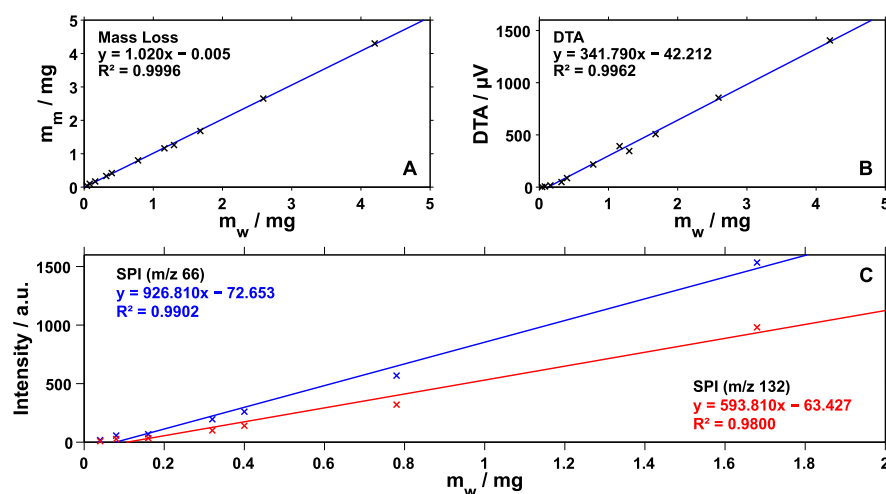
Figure 5. Calibration by TGA (A), DTA (B), and SPI-MS (C) for the retro-Diels-Alder reaction of DCPD into its monomer (eq 2); all data sets follow a linear regression quite well, but only SPI-MS has the required selectivity for quantification.
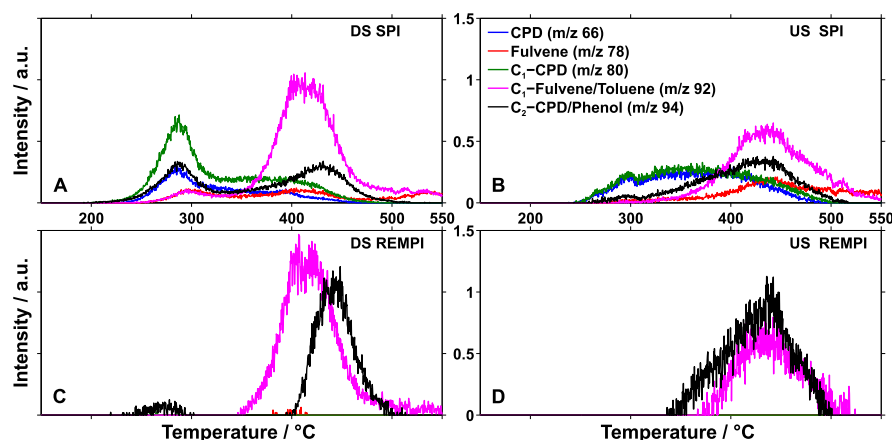
Figure 6. Mass traces of possible Diels−Alder relevant substances, SPI-MS of DS (A) and US (B) as well as REMPI-MS of DS (C) and US (D); DS shows high abundancies of DA monomers during the first phase and a broad release afterwards, while US shows almost only a broad evolution. Mass traces shared by aromatics (m/z 78, 92 and 94) are not suited to estimate the DA content, at least during the second phase.

80) seem to be independent from any change in patterns. Their signals start rising with the appearance of the first peak (220 °C) and also show a temporary increase during the second peak but are mainly broadly released (220−500 °C) until the end of the pyrolysis phase. A general overview of the most abundant patterns in US is given in Figure 4B.

Quantification. A variety of additives can be used to influence side reactions of the cracking process such as fouling. Two typical reagents are radical scavengers for the inhibition of radical fouling and dispersants to minimize Diels−Alder fouling. The optimal dosage of reagents depends on the amount of each reaction during operation, which is not accessible by any means so far. To overcome this problem, quantification of the Diels−Alder content was attempted in this part of the study.

There are different approaches to calibrate the TGA-hyphenated systems for quantification purposes as described in the literature.[39] In this work, STA-PI-MS measurements with DCPD as a model substrate were carried out. DCPD is a Diels−Alder adduct of two cyclopentadiene units and readily degrades into its monomers at about 170 °C (beginning at >150 °C, eq 2).[40] It turned out that all data sets (mass loss, calorimetry, and mass spectrometry) measured with STA-PI-

MS follow a linear regression and might be suited for the aimed approach (Figure 5).

However, the calibration by mass loss (Figure 5A) is the most reliable over the whole range (0.04−4.20 mg). One limitation is the mass accuracy of the thermo-balance (Δm = 0.01 mg), but taking the initial sample weight of ∼7 mg into account, an accuracy of <1% can be achieved. The calibration by differential thermal analysis (DTA) (Figure 5B) works very well for masses >0.16 mg but becomes imprecise below. Its nonlinear behavior directly follows from measurement accuracy again and strongly depends on how well starting and ending points of the process can be determined. As a drawback of the rather accurate TGA/DTA measurements, concurrent processes cannot be discriminated. Even during the simple degradation of only the model substrate, mass loss and DTA result from evaporation of the dimer as well as from degradation and evaporation of the monomer. Because the fouling samples are far more complex and clearly showed simultaneous degradation of at least two different types of structure motives, a more selective calibration method has to be developed.

Selective quantification can be realized by SPI-MS, when specific key substances were assigned to certain processes.
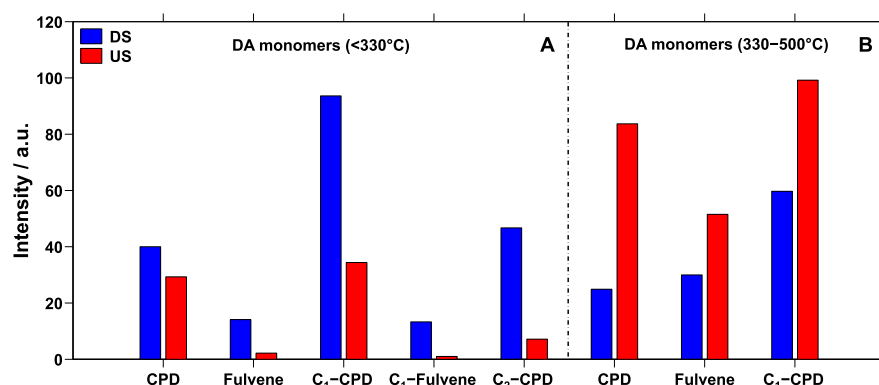
Figure 7. Semi-quantification of Diels−Alder relevant masses by integration of SPI-MS peak areas over the respective phase (<330 °C and 330−500 °C); DS has a higher DA amount than US during the first phase, while US releases more DA monomers during the second phase.

With this approach, the calibration (Figure 5C) is highly sensitive and covers a good mass range (0.04−1.68 mg). SPI-MS has the lowest limit of detection of the three presented calibration methods, so even low values of about 4×10^{-4} mg DCPD are theoretically accessible. Besides, several masses can be tracked, which is important for diverse structures. The major limitation to this method is the PI-MS-setup itself, given by the fluctuation of the laser intensity. Normalization was performed based on standard gas measurements before and after each measurement, but short-term changes could not be corrected and can cause outliers. Nevertheless, calibration by SPI-MS seems the most promising calibration method and is advantageous over the TGA/DTA approach because of its higher sensitivity and specificity.

Semi-Quantification of Diels−Alder-Related Substances. When comparing the overall intensities of several signals of cyclopentadienes (m/z 66, 80, 94) and fulvenes (m/z 78, 92) of US/DS, the values are quite similar (not shown here). However, taking into account that the time-resolved release is quite different for each sample and phase (Figure 6), the picture changes (Figure 7).

DS releases more cyclic dienes than US during the first phase (Figure 7A), whereas US shows higher intensities during the broad evolution (Figure 7B). Either (1) Diels−Alder reactions between dienes and the basic structure took place and the bonding is stronger (e.g., cross linked) than for constituents evolving during the first phase or (2) dienes are incorporated by radical fouling or (3) precursors form dienes as pyrolysis products in situ. For the first two theories, quantification to determine the right dosage of dispersants would be feasible and correct, whereas for the last case, it would lead to false positive results.

When looking at the REMPI data (Figure 6C,D) it becomes clear that m/z 92 and 94 do not exclusively belong to C_1−fulvene and C_2−CPD, respectively. In the first phase (<330 °C), no or only very low REMPI signal is detected for these masses, but during the second phase (330−500 °C), isomeric/isobaric aromatic constituents evolve. Cross checking with data from TD/Py-GC-MS revealed high abundance of toluene and phenol during pyrolysis (330−500 °C) and none or very low abundance of other isomeric/isobaric compounds, leading to the assumption that C_1−fulvene and C_2−CPD only contribute to the retro-Diels−Alder content during the first phase.

In summary, selective (semi-)quantification of Diels−Alder fouling can be achieved with STA-PI-MS, when (1) signals are identified unambiguously, (2) key signals can be assigned to

the specific fouling, and (3) only one feature is tracked per signal (e.g., by selectivity or sufficient resolution/separation). We demonstrated that at least for the first phase, the calibration via SPI-MS fulfills these conditions. Only the broad release up to high temperatures (330−500 °C) rises doubt about the exclusiveness of cyclic dienes toward Diels−Alder reactions in general. The technique is sensitive and specific; masses for cyclic dienes were assigned confidently and unambiguously.

■ CONCLUSIONS

The characterization of two fouling samples was conducted, deploying two different EGA techniques. With STA-PI-MS, thermal processes and evolving organic compounds were observed time resolved (1 Hz) over the entire temperature range. Either SPI (universal soft ionization) or REMPI (selective for aromatics) was used for mass spectrometric detection. The second technique (TD/Py-GC-EI-MS) supports the identification of nominal masses found in PI-MS by providing chemical information (chromatography) and fragmentation patterns (EI-MS).

The composition of both samples (DS/US) is quite diverse, aside from a large proportion of hydrocarbons, several hetero elements, such as iron, sulfur, and nitrogen, are abundant. Carbonization and high contents of metals lead to a nonvaporizable residue during STA-PI-MS measurements. Little amounts of metals might have been present in the used feedstock, but most of it probably comes from embrittlement of the facility.

Focusing on the organic content, it becomes evident, that most of US (∼60 wt %) and DS (∼80 wt %) are made up of a polystyrene structural motif, which mainly decomposes above 330 °C. Diels−Alder adducts and (cyclic) dienes are released with high intensity in a step before, as well as broadly during the decomposition of the basic styrene structure. Whether all or only a part of these dienes are linked to Diels−Alder fouling remains unclear, which complicates the quantification attempts undertaken in this work. For that matter, quantification by SPI-MS is the most promising method, which is advantageous over the less sensitive and selective quantification methods by TGA and DTA.

A very little part of DS (<1%/TIC) and a medium part of US (<5%/TIC) consists of medium to long linear alkanes. In contrast to DS, which only contains small signals for hetero atom-containing compounds, US shows an intense pattern of mainly sulfur and less abundant oxygen-containing substances

(220−370 °C). The higher complexity of US (more elements and dienes) makes it even harder to differentiate the concurrent processes.

Nonetheless, it was proven that STA-PI-MS and TD/Py-GC-EI-MS are useful tools to characterize the main composition of these fouling samples. First attempts to quantify the extent of Diels−Alder product were successfully performed. Future studies will focus on a deeper understanding of the concurrent processes and, in particular, on an unambiguous identification of the evolving constituents. Most likely achieved by improvements of the GC protocol as well as of the resolution of the MS.

■ ASSOCIATED CONTENT

Ⓢ Supporting Information

The Supporting Information is available free of charge on the ACS Publications website at DOI: 10.1021/acs.energy-fuels.9b02886.

Comparison of untreated and treated DS and US fouling samples; consecutive heating (H), cooling (C) and reheating experiment; gas chromatogram of DS; gas chromatogram of US; contour plot of SPI-MS data of DS; contour plot of SPI-MS data of US; and visualization of the sulfur containing pattern change in US (PDF)

■ AUTHOR INFORMATION

Corresponding Author

*E-mail: thorsten.streibel@uni-rostock.de.

ORCID ⊕

Christoph Grimmer: 0000-0002-0034-4677
Christopher P. Rüger: 0000-0001-9634-9239

Notes

The authors declare no competing financial interest.

■ REFERENCES

(1) *Fouling in Refineries*; Speight, J. G., Ed.; Gulf Professional Publishing: Boston, 2015.

(2) Hancock, J. M.; van Zijl, A. W.; Robson, I.; Vachon, J.; Hashmi, A. A chemist's perspective on organic fouling in ethylene operations. *Hydrocarbon Process.* **2014**, *93* (6), 61−66.

(3) Cuoq, F.; Vachon, J.; Jordens, J.; Kwakkenbos, G. Red-oils in ethylene plants: formation mechanisms, structure and emulsifying properties. *Appl. Petrochem. Res.* **2016**, *6*, 397−402.

(4) Cai, H.; Krzywicki, A.; Oballa, M. C. Coke formation in steam crackers for ethylene production. *Chem. Eng. Process.* **2002**, *41*, 199−214.

(5) Vachon, J.; Hancock, J. M.; Robson, I. A chemist's perspective on organic fouling in ethylene operations: update. *Hydrocarbon Process.* **2015**, *94* (10), 49.

(6) Khuong, K. S.; Jones, W. H.; Pryor, W. A.; Houk, K. N. The Mechanism of the Self-Initiated Thermal Polymerization of Styrene. Theoretical Solution of a Classic Problem. *J. Am. Chem. Soc.* **2005**, *127*, 1265−1277.

(7) Nohara, D.; Sakai, T. Kinetic study of model reactions in the gas phase at the early stage of coke formation. *Ind. Eng. Chem. Res.* **1992**, *31*, 14−19.

(8) Diels, O.; Alder, K. Synthesen in der hydroaromatischen Reihe. *Justus Liebigs Ann. Chem.* **1928**, *460*, 98−122.

(9) Saudi Basic Industries Corporation (SABIC), SABIC Technology Center Geleen. *Previous Studies—Personal Communication*.

(10) Streibel, T.; Geißler, R.; Saraji-Bozorgzad, M.; Sklorz, M.; Kaisersberger, E.; Denner, T.; Zimmermann, R. Evolved gas analysis (EGA) in TG and DSC with single photon ionisation mass spectrometry (SPI-MS): molecular organic signatures from pyrolysis of soft and hard wood, coal, crude oil and ABS polymer. *J. Therm. Anal. Calorim.* **2009**, *96*, 795−804.

(11) Rüger, C. P.; Grimmer, C.; Sklorz, M.; Neumann, A.; Streibel, T.; Zimmermann, R. Combination of Different Thermal Analysis Methods Coupled to Mass Spectrometry for the Analysis of Asphaltenes and Their Parent Crude Oils: Comprehensive Characterization of the Molecular Pyrolysis Pattern. *Energy Fuels* **2018**, *32*, 2699−2711.

(12) Meriste, T.; Yörük, C. R.; Trikkel, A.; Kaljuvee, T.; Kuusik, R. TG−FTIR analysis of oxidation kinetics of some solid fuels under oxy-fuel conditions. *J. Therm. Anal. Calorim.* **2013**, *114*, 483−489.

(13) Pitkänen, I.; Huttunen, J.; Halttunen, H.; Vesterinen, R. Evolved Gas Analysis of Some Solid Fuels by TG-FTIR. *J. Therm. Anal. Calorim.* **1999**, *56*, 1253−1259.

(14) Risoluti, R.; Fabiano, M. A.; Gullifa, G.; Vecchio Ciprioti, S.; Materazzi, S. FTIR-evolved gas analysis in recent thermoanalytical investigations. *Appl. Spectrosc. Rev.* **2017**, *52*, 39−72.

(15) Wang, C.; Yang, Y.; Tsai, Y.-T.; Deng, J.; Shu, C.-M. Spontaneous combustion in six types of coal by using the simultaneous thermal analysis-Fourier transform infrared spectroscopy technique. *J. Therm. Anal. Calorim.* **2016**, *126*, 1591−1602.

(16) Wang, Y.; Zhu, Y.; Zhou, Z.; Yang, J.; Pan, Y.; Qi, F. Pyrolysis Study on Solid Fuels: From Conventional Analytical Methods to Synchrotron Vacuum Ultraviolet Photoionization Mass Spectrometry. *Energy Fuels* **2016**, *30*, 1534−1543.

(17) Materazzi, S.; Risoluti, R. Evolved Gas Analysis by Mass Spectrometry. *Appl. Spectrosc. Rev.* **2014**, *49*, 635−665.

(18) Materazzi, S.; Gentili, A.; Curini, R. Applications of evolved gas analysis Part 1: EGA by infrared spectroscopy. *Talanta* **2006**, *68*, 489−496.

(19) Materazzi, S.; Gentili, A.; Curini, R. Applications of evolved gas analysis Part 2: EGA by mass spectrometry. *Talanta* **2006**, *69*, 781−794.

(20) Materazzi, S.; Vecchio, S. Recent Applications of Evolved Gas Analysis by Infrared Spectroscopy (IR-EGA). *Appl. Spectrosc. Rev.* **2013**, *48*, 654−689.

(21) Risoluti, R.; Materazzi, S. Mass spectrometry for evolved gas analysis: An update. *Appl. Spectrosc. Rev.* **2019**, *54*, 87−116.

(22) Streibel, T.; Weh, J.; Mitschke, S.; Zimmermann, R. Thermal Desorption/Pyrolysis Coupled with Photoionization Time-of-Flight Mass Spectrometry for the Analysis of Molecular Organic Compounds and Oligomeric and Polymeric Fractions in Urban Particulate Matter. *Anal. Chem.* **2006**, *78*, 5354−5361.

(23) Zhou, Z.; Chen, X.; Ma, H.; Liu, C.; Zhou, C.; Qi, F. Real-time monitoring biomass pyrolysis via on-line photoionization ultrahigh-resolution mass spectrometry. *Fuel* **2019**, *235*, 962−971.

(24) Fendt, A.; Geissler, R.; Streibel, T.; Sklorz, M.; Zimmermann, R. Hyphenation of two simultaneously employed soft photo ionization mass spectrometers with thermal analysis of biomass and biochar. *Thermochim. Acta* **2013**, *551*, 155−163.

(25) Zimmermann, R.; Saraji-Bozorgzad, M.; Grimmer, C.; Ulbrich, A.; Streibel, T. Erdöl in seine Bestandteile zerlegen und charakterisieren. *Nachr. Chem.* **2016**, *64*, 751−754.

(26) Varga, J.; Wohlfahrt, S.; Fischer, M.; Saraji-Bozorgzad, M. R.; Matuschek, G.; Denner, T.; Reller, A.; Zimmermann, R. An evolved gas analysis method for the characterization of sulfur vapor. *J. Therm. Anal. Calorim.* **2017**, *127*, 955−960.

(27) Geißler, R.; Saraji-Bozorgzad, M.; Streibel, T.; Kaisersberger, E.; Denner, T.; Zimmermann, R. Investigation of different crude oils applying thermal analysis/mass spectrometry with soft photoionisation. *J. Therm. Anal. Calorim.* **2009**, *96*, 813−820.

(28) Saraji-Bozorgzad, M. R.; Streibel, T.; Eschner, M.; Groeger, T. M.; Geissler, R.; Kaisersberger, E.; Denner, T.; Zimmermann, R. Investigation of polymers by a novel analytical approach for evolved gas analysis in thermogravimetry. *J. Therm. Anal. Calorim.* **2011**, *105*, 859−866.

(29) Streibel, T.; Mitschke, S.; Adam, T.; Weh, J.; Zimmermann, R. Thermal desorption/pyrolysis coupled with photo ionisation time-of-

flight mass spectrometry for the analysis and discrimination of pure tobacco samples. *J. Anal. Appl. Pyrolysis* **2007**, *79*, 24−32.

(30) Geissler, R.; Saraji-Bozorgzad, M. R.; Groger, T.; Fendt, A.; Streibel, T.; Sklorz, M.; Krooss, B. M.; Fuhrer, K.; Gonin, M.; Kaisersberger, E.; et al. Single photon ionization orthogonal acceleration time-of-flight mass spectrometry and resonance enhanced multiphoton ionization time-of-flight mass spectrometry for evolved gas analysis in thermogravimetry: Comparative analysis of crude oils. *Anal. Chem.* **2009**, *81*, 6038−6048.

(31) Streibel, T.; Fendt, A.; Geißler, R.; Kaisersberger, E.; Denner, T.; Zimmermann, R. Thermal analysis/mass spectrometry using soft photo-ionisation for the investigation of biomass and mineral oils. *J. Therm. Anal. Calorim.* **2009**, *97*, 615−619.

(32) Mühlberger, F.; Hafner, K.; Kaesdorf, S.; Ferge, T.; Zimmermann, R. Comprehensive on-line characterization of complex gas mixtures by quasi-simultaneous resonance-enhanced multiphoton ionization, vacuum-UV single-photon ionization, and electron impact ionization in a time-of-flight mass spectrometer: Setup and instrument characterization. *Anal. Chem.* **2004**, *76*, 6753−6764.

(33) Otto, S.; Streibel, T.; Erdmann, S.; Sklorz, M.; Schulz-Bull, D.; Zimmermann, R. Application of pyrolysis-mass spectrometry and pyrolysis-gas chromatography-mass spectrometry with electron-ionization or resonance-enhanced-multi-photon ionization for characterization of crude oils. *Anal. Chim. Acta* **2015**, *855*, 60−69.

(34) Otto, S.; Streibel, T.; Erdmann, S.; Klingbeil, S.; Schulz-Bull, D.; Zimmermann, R. Pyrolysis-gas chromatography-mass spectrometry with electron-ionization or resonance-enhanced-multi-photon-ionization for characterization of polycyclic aromatic hydrocarbons in the Baltic Sea. *Mar. Pollut. Bull.* **2015**, *99*, 35−42.

(35) Adam, T.; Zimmermann, R. Determination of single photon ionization cross sections for quantitative analysis of complex organic mixtures. *Anal. Bioanal. Chem.* **2007**, *389*, 1941−1951.

(36) *NIST Chemistry WebBook. NIST Standard Reference Database 69: Ionization Energy Evaluation*; Linstrom, P. J., Mallard, W. G., Eds.; National Institute of Standards and Technology: Gaithersburg MD, 1997; p 20899.

(37) Vasile, C.; Pascu, M. *Practical Guide to Polyethylene*; Rapra Technology Limited: Shawbury, 2005.

(38) Platzer, N.; Mark, H. F.; Bikales, N. M.; Overberger, C. G.; Menges, G.. *Encyclopedia of Polymer Science and Engineering*; Wiley-Interscience: New York, 1985; p 720. *J. Polym. Sci., Part C: Polym. Lett.* **1987**, *25*, 359−360. DOI: 10.1002/pol.1987.140250612

(39) Slager, T. L.; Prozonic, F. M. Simple methods for calibrating IR in TGA/IR analyses. *Thermochim. Acta* **2005**, *426*, 93−99.

(40) Herndon, W. C.; Grayson, C. R.; Manion, J. M. Retro-Diels-Alder reactions. III. Kinetics of the thermal decompositions of exo- and endo-dicyclopentadiene. *J. Org. Chem.* **1967**, *32*, 526−529.

8.3   Publication 3

Characterization of Polyethylene Branching by Thermal Analysis-Photoionization Mass Spectrometry

by

Christoph Grimmer, Lukas Friederici, Thorsten Streibel, Ahmad Naim, Virginie Cirriez, Pierre Giusti, Carlos Afonso, Christopher P. Rüger, Ralf Zimmermann

Characterization of Polyethylene Branching by Thermal Analysis-Photoionization Mass Spectrometry

Christoph Grimmer, Lukas Friederici, Thorsten Streibel, Ahmad Naim, Virginie Cirriez, Pierre Giusti, Carlos Afonso, Christopher P. Rüger,* and Ralf Zimmermann

Read Online

ACCESS | Metrics & More | Article Recommendations | Supporting Information

ABSTRACT: The rising demand for more and more specialized polyethylene represents a challenge for synthesis and analysis. The desired properties are dependent on the structure, but its elucidation is still intricate. For this purpose, we applied thermal analysis hyphenated to single photon ionization mass spectrometry (STA-SPI-MS). The melting and pyrolysis behavior of different types of polyethylene were tracked by DSC and mass loss. Crystallinity and melting point give hints about the branching but are also influenced by the molecular weight distribution. The evolving gas analysis patterns obtained by SPI-MS however, contain specific molecular information about the samples. Shifts in the summed spectra, which can be clearly observed with our technique, result from differently favored degradation reactions due to the respective structure. Pyrolysis gas chromatography mass spectrometry (Py-GC-EI-MS) was used to support the assignment of pyrolysis products. Principal component analysis was successfully applied to reduce the complexity of data and find suitable markers. The obtained grouping is based on the molecular fingerprint of the samples and is strongly influenced by short-chain branching. Short and medium alkenes and dienes have the strongest impact on the first four principal components. Thus, two marker ratios could be defined, which also give a comprehensible and robust grouping. Butene and pentene were the most abundant signals in our set of samples. With STA-PI-MS, a broad range of pyrolysis products can be measured at the same time, possibly extending the range for quantifiable short-chain branches to more than six carbon atoms for PE. Unfortunately, no clear trend between long-chain branching and any grouping was observed. The quite universal and soft single photon ionization enables access to many different compound classes and hence other polymers can be studied.
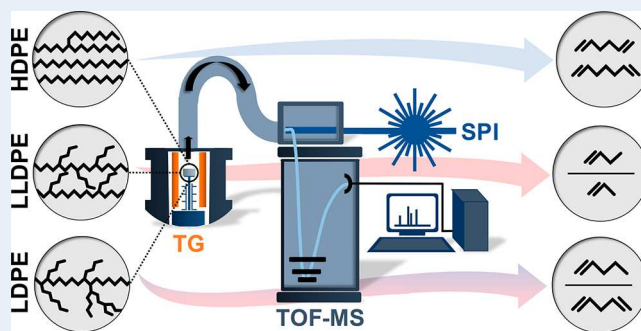
INTRODUCTION

Polyethylene is the world's most-produced synthetic polymer with 116 Mt per year (2015, corresponds to ~29% of total synthetic polymer production).[1] It has excellent properties for a large variety of applications, such as coating, insulation, or wrapping.[2,3] Polyethylene consists of saturated hydrocarbons, and its structure can vary enormously.[4] It is a mixture of many similar but differently long and dissimilarly branched chains. The molecular weight distribution (MWD) and branching are also influenced by the polymerization conditions, particularly the choice of catalyst and whether or not copolymers are used.[5]

The simplest polyethylene structure is linear, which leads to high crystallinity and density (high-density polyethylene, HDPE). Low-density polyethylene (LDPE) exhibits a high degree of long- and short-chain branches and is obtained by radical polymerization. Linear low-density polyethylene (LLDPE) has a large number of relatively short branches as well. It is usually synthesized by usage of copolymers (1-olefins), yielding these short side chains. Besides the types

mentioned above, a variety of other polyethylene materials and even mixtures (or grafting) of these exist.[6]

Branching has a significant impact on the materials' properties and thus its characterization is essential for the understanding of the performance of different PE types.[5,7,8] Chemical analysis, however, is often impeded by the polyethylene's nonpolarity, nonvolatility, inertness, and poor solubility.[8,9] Common mass spectrometric techniques to address polymers, such as matrix-assisted laser desorption (MALDI) or electrospray ionization (ESI) are therefore not applicable or only with difficulties.[10,11] Because structure–property relations work in both directions, one can also measure bulk parameters, for example, differential scanning
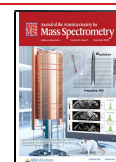
calorimetry (DSC) measurements of the melting process and its enthalpy give insight into crystallinity, which is an indirect indication of branching. Other examples are rheological methods (e.g., zero-shear viscosity, flow activation energy, or linear viscoelastic response), which can be used to estimate long chain branching content.[12] Though useful, these pieces of information alone are too shallow and not unambiguous for one type of branching. Many different parameters have to be measured to yield the whole picture of one sample.

Different methods exist to analyze branching. Infrared spectroscopy (IR) works well to achieve the total methyl group content.[7] Another useful technique is nuclear magnetic resonance (NMR). It can be used to determine short-chain branching (SCB) or long-chain branching (LCB), but it is limited by sensitivity ($\geq$1/1000 branched C atoms) and by its inability to differentiate side chains with more than six carbon atoms.[12,13]

A very sophisticated approach is the use of fractionation methods. Gel permeation chromatography or size exclusion chromatography (GPC or SEC) is well-known in polymer science, which is used for polyethylene as well to determine the molecular weight distribution. For branching, techniques such as temperature rising elution fractionation (TREF) or crystallization analysis fractionation (CRYSTAF) can be used.[5,14] Subsequent IR or NMR measurement of the fractions or coupling to online detectors (IR, light scattering, viscosity, UV/vis, and so forth) is necessary.[4,5,14−16] Combining GPC and analysis of branching is the only possibility to investigate MWD-dependent branching. Probably one of the most comprehensive analysis was achieved by using a triple detector GPC−TREF system.[17]

Pyrolysis gas chromatography (Py-GC) is another common polymer science technique, which is typically used to qualitatively characterize polymers or analyze additives.[15,18] Quantification of branching was also attempted,[13,19] but reliable quantitative determination of branching of poly-ethylene is not accessible yet. Nevertheless, the pyrolysis process offers access to structural information and circumvents nonvolatility by breaking molecules down into smaller and more volatile products. Exhaustive effort has been conducted to understand the pyrolysis of polyethylene, which is handy during analysis and recycling.[13,18−31] In addition, pyrolysis has attracted renewed interest through the concept of waste to fuel in which polyethylene can be used as a feedstock to produce mainly alkanes, 1-olefins, and dienes. The product spectrum can also be shifted to other valuable products when appropriate catalysts are used.[27]

In this study, we aimed to evaluate thermal analysis hyphenated to (soft) single photon ionization mass spectrom-etry (STA-SPI-MS) for the chemical description of branching of different types of polyethylene samples. The objective was to prove STA-SPI-MS as a complementary approach, allowing a more detailed molecular description based on the evolved pyrolysis products at an elevated temperature. SPI-MS (118 nm, 10.5 eV) should be well suited to unravel the differences in the evolving gas analysis patterns of different polyethylene types. It was shown before that STA-SPI-MS can produce clear and almost fragment-free mass spectra of polymers and crude oils.[32−35] After evaluation of the melting and pyrolysis behavior, the average decomposition pattern was examined by means of chemometric tools. Aside from a general proof-of-concept study, the primary motivation is to obtain typical marker compounds or marker compound ratios. For this

purpose, different polyethylene materials (20 samples) were investigated by STA-SPI-MS and DSC and supported by Py-GC-EI-MS investigations.

■ MATERIALS AND METHODS

Materials. The 20 investigated polyethylene materials were received from TOTAL (TRTF, Feluy, Belgium). They consist of different types of polyethylene (LDPE, LLDPE, and HDPE); more details can be found in Supporting Information (Table S1).

STA-SPI-MS. A simultaneous thermal analyzer (STA7200RV, Hitachi) was coupled to a custom photo-ionization time-of-flight mass spectrometer (PI-MS), which utilizes single photon ionization (SPI). A few milligrams (3−4 mg) of the sample material were placed in an aluminum crucible. Thermal analysis was carried out with a heating rate of 20 K/min under nitrogen atmosphere (200 mL/min) from 45 to 550 °C. Evolving constituents of the effluent from the thermal analyzer were sampled via a heated interface and transfer line (3.50 m length and 200 μm inner diameter at 280 °C).[36−39] Evolved gas was sampled as a result of the pressure difference between the balance at atmospheric pressure and the ion source at reduced pressure (roughly 2 × 10^{-5} mbar). Subsequent SPI TOF-MS analysis is described in detail elsewhere.[34,35,40] In brief, 355 nm laser pulses (25 mJ pulse energy, 10 Hz repetition rate, and 5 ns pulse width), generated from a Nd:YAG laser (Surelite III, Continuum, Inc., Santa Clara, CA, U.S.A.), were sent through a xenon-filled gas cell (Xe 4.0, 12 mbar), yielding vacuum ultraviolet photons by nonlinear frequency tripling (118 nm = 10.5 eV). The molecular ions formed by SPI are recorded with an acquisition frequency of 10 Hz from 5−500 m/z with a reflectron TOF-MS (Stefan Kaesdorf, Munich, Germany) using a multichannel plate detector. Data processing and analysis were carried out with instrument-specific LabView (2014) graphical user interface and self-written MATLAB (R 2018b) scripts.

DSC. The determination of melting enthalpies was performed with a simultaneous thermal analyzer (STA 449 F3 Jupiter, Netzsch), which utilizes differential scanning calorimetry. The temperature program was as follows: heating from 35 to 180 °C (10 K/min, 40 mL/min N$_2$), natural cooling to 70 °C (∼1 K/min, 500 mL/min N$_2$) and reheating to 180 °C (10 K/min, 40 mL/min N$_2$). Preheating and cooling is necessary to erase the thermal memory of the samples.

Py-GC-EI-MS. For pyrolysis gas chromatographic analysis, 0.3−0.7 mg of the prepared sample was injected into the pyrolyzer (model PY-2020iD, double-shot pyrolyzer, Frontier Laboratories) mounted onto a HP 6890 gas chromato-graph.[41,42] The sample material undergoes a pyrolysis step at 500 °C, held for 1 min. To separate the evolved gas mixture, a 30 m SGE-BPX5 column (250 μm inner diameter, 0.25 μm film, helium at 99.999%, and head pressure at 0.4 bar, split of 1:50) was used with the following temperature program: hold for 20 min at 40 °C, ramp to 330 °C with 10 K/min, and hold for 15 min. The effluent from the column was ionized by a 70 eV electron ionization source and analyzed by a quadrupole mass spectrometer with a secondary electron multiplier detector. Mass spectra were recorded in scan mode from 40−500 m/z.

Data Analysis. All samples were measured 5−7 times by STA-SPI-MS, and each replicate was first blank corrected (subtraction of the blank signal intensity) and then normalized by its total ion current (TIC). A summed SPI-MS spectrum of

every replicate was calculated. Different tests were used on each m/z value of a sample to eliminate outliers (Grubbs test: removes one outlier per iteration based on hypothesis testing), test normal distribution, and variance homogeneity (MATLAB function "vartestn" using "LeveneAbsolute" as input; computed by performing ANOVA on the absolute deviations of the data values from their group means). Grubbs test was performed with the "isoutlier" function of MATLAB. Then, based on the variance homogeneity, either ANOVA ($p > 0.5$) or Welch-ANOVA ($p \leq 0.5$) was applied to keep only significant different variables. From the resulting data matrix (measurements varying in sample versus mass spectrometric signals) values with m/z below 31 or above 350 were removed. The refined data matrix was used as input for a principal component analysis (PCA) run on correlation (MATLAB function "pca") to further reduce the number of observables to a lower number of variables. PCA was performed on centered (subtracting column means) data using the singular value decomposition algorithm (SVD).

■ RESULTS AND DISCUSSION

Thermal Analysis and Crystallinity. The melting enthalpy of polyethylene (PE) contains valuable information about branching but is also influenced by the molecular weight distribution (MWD) and the former solidification conditions. It can be directly translated into crystallinity, when dividing the measured enthalpy of a sample by the value of a theoretically completely crystalline PE (293 J/g).[43] Very low, but also high, molecular weights are expected to interfere with the crystallization process as does fast cooling.[44] Short chains increase the amount of ends relative to the mass/length, and these ends obstruct the regular arrangement of the chains needed to form crystallites. Longer chains have a more favorable end-to-mass ratio but are kinetically hindered to arrange. The effect is more severe the longer the main-/side-chains and the faster the cooling conditions are. Heating, slow cooling, and then reheating is usually applied to erase the thermal memory and achieve a better recrystallization before the actual measurement. In our experiments, the cooling rate was ~1 K/min (natural cooling) and the heating rate was 10 K/min, which is in the typical range of these experiments.[2,45] Lowering the rates can improve measurement accuracy,[44] but these were chosen to find a compromise between acceptable measurement accuracy, time consumption, and feasibility toward our mass spectrometric coupling.[32,33] The TA results are well suited to compare the samples among each other and guide our mass spectrometric interpretation.

Crystallinity was found to be in the range of 24–70%, while the melting points are between 111–129 °C (Figure 1). The samples were named after their synthesis routes (mPE, metallocene catalyst; LDPE, radical polymerization; ZPE, Ziegler–Natta catalyst; CPE, Phillips catalyst), sorted by ascending crystallinity, and numbered in the same manner. Many mPE samples have densities that are usually associated with LDPE (0.915–0.935 g/cm³) or LLDPE (0.87–0.94 g/cm³), whereas the others are in the range of HDPE (0.94–0.97 g/cm³) (Table S1). Because of their synthesis route, the low density mPE are most likely LLDPE. In general, the received mPE samples are quite diverse; they do not only differ in density but also in crystallinity and other parameters.

It is known from literature that crystallinity and MWD influence the melting point. However, the behavior is not always linear; the higher the crystallinity and/or the molecular
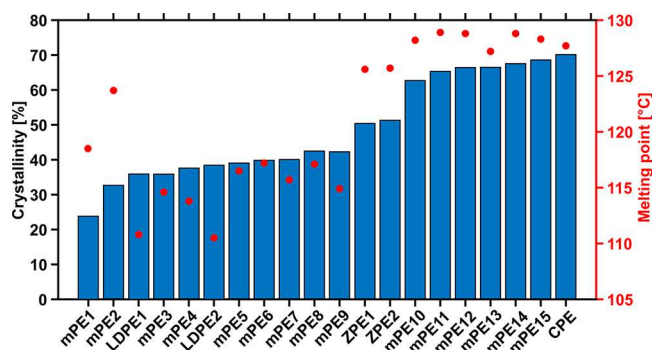
Figure 1. Crystallinity and melting point information obtained by DSC. Crystallinity can be calculated by dividing the measured value of a sample by the literature value for a completely crystalline PE.[43]

weight is, the higher the melting point is.[44] A trend between crystallinity and the corresponding melting point can be recognized (Figure 1), whereas the influence of the MWD is harder to predict because of its multiple dependencies. When plotting crystallinity against melting point, a rough grouping of the samples types is obtained (Figure S1). But because of the interwoven relation of crystallinity, melting point, and their shared dependencies, its significance might be limited or at least hard to read.

Pyrolysis begins slowly at ~420 °C, increases with rising temperature and is completed at 520 °C (Figure 2). Most of
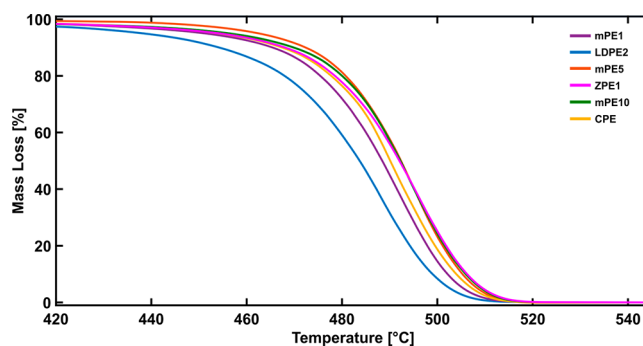
Figure 2. Mass loss curves of selected representative PE (based on crystallinity and PE type). The degradation process starts slowly at about 420 °C, has its maximum at 492−499 °C, and is completed at 520 °C. Most of the samples behave almost identical, and only LDPE1 and LDPE2 are shifted to lower temperatures.

the samples behave almost identically, and only the maxima of LDPE1−2 are shifted toward lower temperatures, resulting in a lower and broader derivative thermogravimetric peak (DTG, Figure S3). It seems that the degradation is also dependent on MWD and branching (LDPE vs rest), and the minor differences between similar samples (mPE, ZPE, and CPE) cannot be resolved. Degradation is based on different cleavage reactions, which lead to smaller, more volatile fragments and eventually to mass loss. At the end of this process, the entire sample is volatilized with no detectable residue in the pan.[28] The fragments are continuously transferred into the ionization chamber of the time-of-flight mass spectrometer, resulting in temperature-resolved mass spectra of the pyrolysis process. Although crystallinity, melting point, and probably the mass loss curve contain valuable information about branching, their interpretability is limited and more distinct information on a molecular level is needed.

Mass Spectrometric Characterization of Pyrolysis Products. The TIC of a PE sample is qualitatively the same as its DTG curve (Figure 3). Single photon ionization (SPI) is
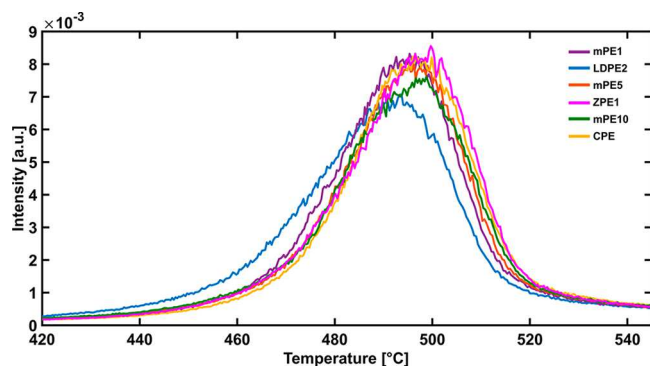
Figure 3. TIC of selected representative PE, obtained by STA-SPI-MS. The TIC is qualitatively the same as the DTG (Figure S3).

a soft and relatively universal technique, which tracks the evolving pattern. Thus, the TIC correlates quite well with the mass loss, and the already discussed behavior can be recognized.

Mass loss and TIC are not significantly different enough, but the summed mass spectra reveal interesting molecular information. The softness of SPI enables access to almost fragment-free spectra of molecular ions, which are in the range of 42−390 m/z for PE (Figure 4). Identification of the signals is easily conducted, based on molecular weight, literature knowledge, and by interpretation of the supporting Py-GC-EI-MS data. Small alkenes and dienes dominate the low m/z region (42−98 m/z) and level off in the medium-high region
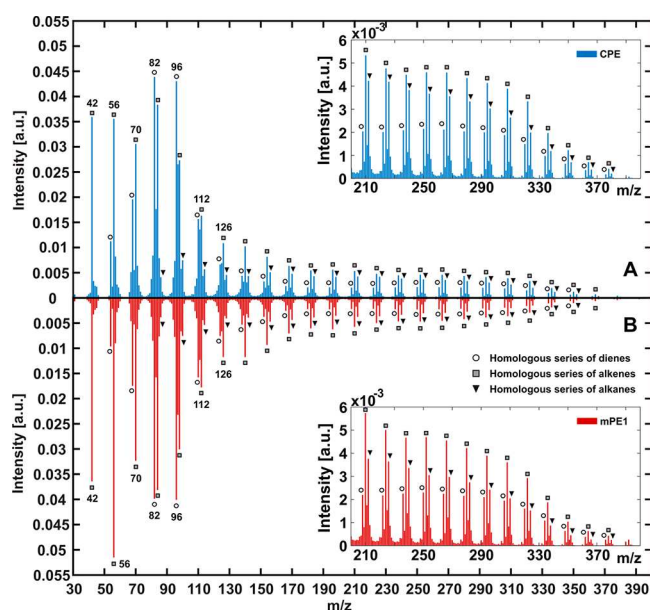

Figure 4. Summed spectrum over the entire temperature range of STA-SPI-MS of CPE (A) as an example of a highly crystalline PE (crystallinity of ~70%) and of mPE1 (B) as an example of a lowly crystalline PE (crystallinity of ~24%). The smallest detectable signal is 42 m/z (propene); at higher masses, triplets containing a diene, alkene, and alkane with the same carbon number occur up to ~390 m/z. Differences between CPE and mPE1 can be mainly seen in the low m/z region.

(98−180 m/z), while alkanes are lowly abundant between 86−380 m/z. Odd m/z values are due to the ^{13}C isotopic signal as well as due to a minor degree of fragmentation of alkenes and dienes forming heavier members of the classical electron impact homologue fragmentation rows. Unfortunately, STA-SPI-MS cannot differentiate between isomers, but the Py-GC-EI-MS device is able to separate linear and branched constituents of the same molecular weight (Figures S4 and S5). In the case of a completely linear PE, all signals are derived only from linear constituents, whereas branched PE yields mainly linear and some branched species in which the ratio is dependent on the degree of branching. Even the highly crystalline CPE reveals branched compounds (Figure S5) and thus comprises at least some branching. In either case, the alkenes and dienes are always terminal (1-alkenes or α,ω-dienes). Data from Py-GC-EI-MS are very interesting, but the pyrolysis conditions are not the same as in the thermal analyzer (TA) and its resolution and sensitivity are limited when focusing on the complex fingerprint of a branched sample. In addition, it is very elaborate to resolve small compounds, which comprise a lot of information on the short-chain branching, and larger constituents at the same time.

Valuable mechanistic thoughts were published by Ueno et al.[28] Usually, the degradation cascade is initiated by a random C—C bond scission, because C—C bonds are weaker than C—H bonds (Reaction Scheme 1). Besides, a variety of secondary reactions takes place. Primary or secondary formed radicals can abstract a H atom. This happens either by

**Scheme 1. Initiation Is Caused by Random C—C Bond Scission[a]**
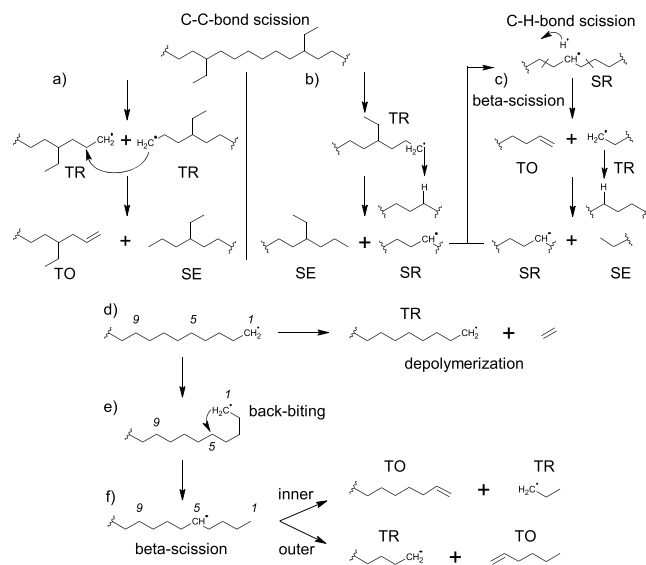
[a]Different secondary reactions are possible: termination of two terminal radicals (TR) by recombination (not shown), (a) termination by radical disproportionation yielding a terminal olefin (TO) and a saturated end (SE), (b) propagation of a TR by H-abstraction yielding SE and a secondary radical (SR), (c) SR obtained by radical attack or by C—H bond scission breaking in beta-position yielding TR and TO. Beta-scission can happen on either side of the SR. (d) Beta-scission of a TR is called depolymerization, (e) backbiting results in a shift of the radical to more or less defined positions, (f) it is discriminated between inner and outer scission relative to the shorter fragment.[28]

intermolecular interaction (Reaction Scheme 1b) or more directed by intramolecular backbiting. While intramolecular backbiting is directed for H atoms close to the radical, it should become more and more undirected with growing distance. Favorable arrangements for close backbiting are usually of cyclic nature with low ring strain, resulting often in 1−5 or 1−6 transfer of the radical (Reaction Scheme 1e). Repetitive backbiting can lead to 1−5−9(10) or 1−6−10(11) transfers. Termination occurs when two radicals recombine or are disproportionate (Reaction Scheme 1 a).

As stated before, C−H bond scission is unlikely but still possible. The outcome of most H-abstraction reactions is almost always a secondary radical, which reacts similarly to a primary radical but yields different long products after beta-scission.[28] Beta-scission of a primary radical is called depolymerization, because of the produced ethylene. Secondary radicals can either cleave in the inner- or outerposition (reaction Scheme 1f). Following this logic, terminal dienes are obtained when an inner beta-scission (or radical disproportionation) happens on the other end of a before-formed alkene. Though unlikely, even terminal trienes should be possible when a double bond is formed on the branches of a diene. Other reactions are theoretically possible as well but are either unlikely or were not observed. For example, a radical attack on a C atom or recombination with at least one secondary radical, resulting in additional branching, was not detected in Py-GC spectra of linear PE samples.[18,25] It is known from literature that hydrogen is formed during pyrolysis, especially when higher temperatures are applied.[26,28] However, we cannot detect compounds with ionization energies higher than 10.5 eV such as hydrogen, ethylene, or propane with SPI-MS, and these species do not contain much structural information.

It is known that the degradation is mainly driven by the propagation cascade.[28] Many cleavage reactions take place at or close to just formed chain-ends. This also explains, why the mass spectra are dominated by high intensities of low m/z values. Either random C—C bond scission at a branch, or H-abstraction at a branch or at a C atom on the main chain close to a branch and subsequent beta-scission, are needed to get branching fragments. Any PE variation yields the same masses, but differences in branching and the MWD lead to shifts in the detected SPI-MS patterns.

When comparing summed SPI-MS data of two very differently branched PE in more detail (Figure 5), it becomes apparent that the same signals are abundant with different intensities. Sample mPE1 (highly short-chain branched [9 wt % C6-], no long chain branching) exhibits a very high intensity of butene (56 m/z) and higher intensities for a lot of small, medium, and long alkenes. In contrast, sample CPE (no short-chain branching but long chain branched) shows high intensities of short dienes (54, 68, 82, 96 m/z) and long alkanes. The elevated butene signal of mPE1 is derived from a high amount of butyl-side chains, which was incorporated by usage of 1-hexene as a copolymer during synthesis. LDPE has high intensities for butene and pentene, which were incorporated by the typical backbiting mechanism during synthesis (1−5 transfer and 1−6 tranfer, respectively). Alkenes are products, which can be formed from a single cleavage, whereas dienes need at least two reactions. The chance to obtain a volatile fragment with less degradation reactions is higher for short-chain branched samples, than for long-chain branched or linear PE. Mechanistic studies to explain these processes more in-depth are advised.
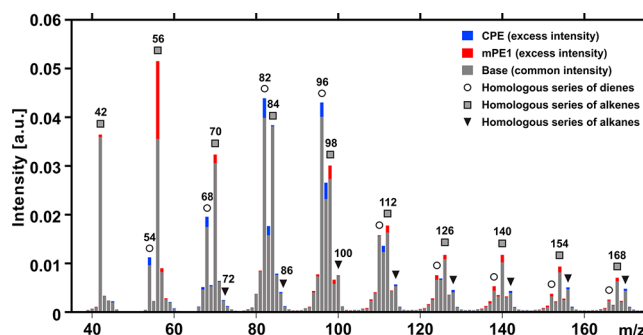

Figure 5. Difference plot of the summed spectrum over the entire temperature range of STA-SPI-MS of highly crystalline CPE (blue) and lowly crystalline mPE1 (red). Differences between CPE and mPE1 can be seen mainly in the intensity of low m/z signals. In particular, butene (56 m/z), medium, and long alkenes are pronounced for mPE1, whereas several dienes (54, 68, 82, 96 m/z) are pronounced for CPE.

We are able to clearly and reliably detect differences between our samples on a molecular level, even though the differences can be rather small. Because of the complexity of the diverse sample set and many observables, we applied chemometric tools for simplification.

Exploratory Data Analysis: Principal Component Analysis. PCA is an unsupervised method and was used because only limited quantitative information was available.

A distribution of the samples is revealed, when the first two principal components (PC) are plotted (Figure 6). An
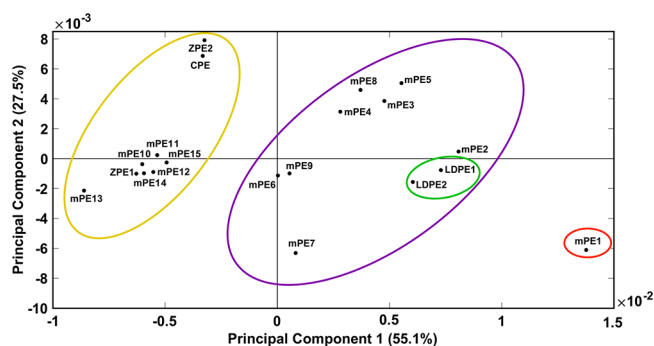

Figure 6. Scatter plot of the first two principal components PC of the PCA. Groups are encircled based on sample information; mPE1 (red circle, 9 wt % C6-) is the most short-chain branched PE. While the purple circle contains medium short-chain branched samples (2−7 wt % C6-) and LDPE1−2 (green circle), the yellow circle contains no or little short-chain branched samples (0−1 wt % C6-). The summed mass spectrometric data over the entire temperature range of the STA-SPI-MS were used as data input.

additional spreading between LDPE1−2 and the rest is seen when looking at PC3 (10.0% explained variance, Figure S6). Four well-separated groups can be defined: highly short-chain branched (red), medium short-chain branched (purple), no or little short-chain branched (yellow), and radical polymerized (green) PE. An explanation for the spreading within one group might be the dependency of SPI-MS signals of more variables (MWD, medium and long-chain branching) than just very short-chain branching. On the other hand, an explanation for the clustering of quite different samples such as ZPE2 (1 wt % C6-, no long-chain branching, 51% crystallinity) and CPE (0

wt % C6-, a lot of long-chain branching, 70% crystallinity) was not found yet.

General problems associated with unsupervised methods are that extreme samples distort the overall outcome and the found principal components do not necessarily represent real underlying causes. Many variables are combined, leading to less influence of single signals. However, we can learn from PCA and its loadings (Figure 7) that certain small alkenes and
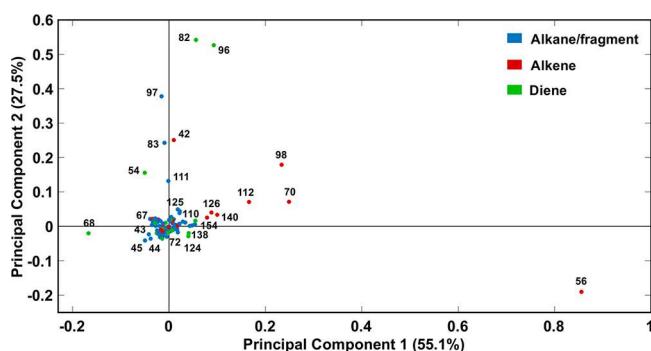

Figure 7. Loadings of the first two principal components; the explained variance is written within brackets. PC1 is mainly influenced by short and medium alkenes (56, 70, 98, 112 m/z) in the positive and pentadiene (68 m/z) in the negative direction. PC2 is strongly influenced by hexadiene (82 m/z) and heptadiene (96 m/z). Short and medium alkenes (42, 98, 70, 112 m/z) have a positive effect here as well, but butene (56 m/z) correlates negatively. The summed mass spectrometric data over the entire temperature range of the STA-SPI-MS were used for PCA. Odd m/z values, such as 83, 97, 111 and 125, are most likely a result of a minor degree of fragmentation for the respective alkenes.

dienes have a huge impact on the clustering. PC1 mainly separates according to short and medium alkenes, above all butene (56 m/z) and pentene (70 m/z). These two are especially important, because of the radical backbiting process and when respective copolymers are used. Pentadiene (68 m/z) is located on the same axis but correlates negatively. Some small and medium alkenes also contribute to PC2. Butene correlates negatively here, while propene (42 m/z), heptene (98 m/z), and others show positive values. Hexadiene (82 m/z) and heptadiene (96 m/z) have the biggest influence.

The variables from PCA can now be used as typical markers in an attempt to semiquantify the amount of specific short-chain branches such as butyl and pentyl side-chains. A nice distribution is obtained (Figure 8), when plotting the signal ratios of 70/68 versus 56/42. This concept is easily accessible, comprehensible, and robust toward some measurement errors. It can be extended or adapted when other branches come in question. A trend concerning differences in long-chain branching cannot be recognized in PCA (Figure 6) nor the marker ratio plot (Figure 8), assuming our estimates are correct in the first place. The effect of MWD and longer side-chains need to be studied in-depth. Nevertheless, STA-PI-MS might enhance the range of quantifiable chains from state of the art ^{13}C NMR ($\leq$C6 chains) to higher numbers, because longer chains can be discriminated.

◼ CONCLUSION

We applied STA-SPI-MS as a complementary technique to elucidate the branching of different types of PE. The melting and pyrolysis behavior of 20 samples was measured by DSC
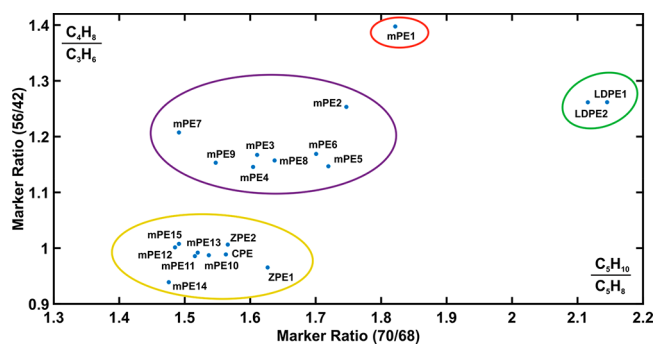
Figure 8. Marker ratio plot based on characteristic m/z-values found in PCA based on the mass spectrometric response of the STA-SPI-MS. The markers were chosen, because of their strong influence in the first four principal components. Clustering depends strongly on the measured short chain branching by ^{13}C NMR (wt % C6−).

and mass loss, and the melting enthalpy was translated into crystallinity. Bulk data (crystallinity vs melting point) can be used to obtain a good grouping of the samples, but it is only read with difficulties. The summed SPI-MS patterns, however, contain rich molecular information about the samples. Differences between the patterns were clearly observed with our technique and are supported by Py-GC-EI-MS data. Because of a multitude of observables and only small differences, multivariate statistic was successfully applied to reduce the complexity of data and find suitable markers. The grouping obtained by PCA is based on the molecular fingerprint of the samples and is strongly influenced by short-chain branching determined by ^{13}C NMR. Alkenes, above all butene (56 m/z), pentene (70 m/z), and propene (42 m/z), and dienes, such as pentadiene (68 m/z), hexadiene (82 m/z) and heptadiene (96 m/z), have the strongest influence on the first four principal components. Thus, two marker ratios (70/68 vs 56/42) could be defined, which also give a comprehensible and robust grouping. Butyl and pentyl side-chains were the most abundant branches in our set of samples, but other chain lengths are important for industry and academia as well. Therefore, the proposed marker ratios can be easily adjusted. With STA-PI-MS, a broad range of pyrolysis products can be measured at the same time, possibly extending the range for quantifiable short-chain branches to more than six carbon atoms for PE. Unfortunately, no clear trend between long-chain branching and any grouping was observed, calling for more experiments in that direction. The quite universal and soft single photon ionization enables access to many different compound classes, and hence other polymers can to be studied. Further studies should focus on the influence of longer side-chain branching and the MWD on the pyrolysis pattern.

◼ ASSOCIATED CONTENT

Ⓢ Supporting Information

The Supporting Information is available free of charge at https://pubs.acs.org/doi/10.1021/jasms.0c00291.

> Information about the polyethylene materials; scatter-plot of melting point and crystallinity; mass loss curves of representative samples; derivative of the mass loss curves (DTG) of representative samples; Py-GC-EI-MS of mPE1 and CPE; zoomed plot of Py-GC-EI-MS data of mPE1 and CPE; 3D plot of the first three principal components (PDF)

■ AUTHOR INFORMATION

Corresponding Author

   Christopher P. Rüger − *Joint Mass Spectrometry Centre/Chair of Analytical Chemistry, University of Rostock, 18059 Rostock, Germany; International Joint Laboratory - iC2MC: Complex Matrices Molecular Characterization, TRTG, 76700 Harfleur, France;* ● orcid.org/0000-0001-9634-9239; Email: christopher.rueger@uni-rostock.de

Authors

   Christoph Grimmer − *Joint Mass Spectrometry Centre/Chair of Analytical Chemistry, University of Rostock, 18059 Rostock, Germany;* ● orcid.org/0000-0002-0034-4677

   Lukas Friederici − *Joint Mass Spectrometry Centre/Chair of Analytical Chemistry, University of Rostock, 18059 Rostock, Germany*

   Thorsten Streibel − *Joint Mass Spectrometry Centre/Chair of Analytical Chemistry, University of Rostock, 18059 Rostock, Germany; Joint Mass Spectrometry Centre/Cooperation Group Comprehensive Molecular Analytics, Helmholtz Zentrum München, 85764 Neuherberg, Germany*

   Ahmad Naim − *TOTAL Refining and Chemicals, Total Research and Technologies Gonfreville, 76700 Harfleur, France; CNRS/Université de Rouen, UMR 6014 COBRA, 76821 Mont Saint Aignan Cedex, France; International Joint Laboratory - iC2MC: Complex Matrices Molecular Characterization, TRTG, 76700 Harfleur, France;* ● orcid.org/0000-0002-0746-6335

   Virginie Cirriez − *TOTAL Research and Technology Feluy, Zone Industrielle C, Feluy B-7181, Belgium*

   Pierre Giusti − *TOTAL Refining and Chemicals, Total Research and Technologies Gonfreville, 76700 Harfleur, France; International Joint Laboratory - iC2MC: Complex Matrices Molecular Characterization, TRTG, 76700 Harfleur, France;* ● orcid.org/0000-0002-9569-3158

   Carlos Afonso − *CNRS/Université de Rouen, UMR 6014 COBRA, 76821 Mont Saint Aignan Cedex, France; International Joint Laboratory - iC2MC: Complex Matrices Molecular Characterization, TRTG, 76700 Harfleur, France;* ● orcid.org/0000-0002-2406-5664

   Ralf Zimmermann − *Joint Mass Spectrometry Centre/Chair of Analytical Chemistry, University of Rostock, 18059 Rostock, Germany; Joint Mass Spectrometry Centre/Cooperation Group Comprehensive Molecular Analytics, Helmholtz Zentrum München, 85764 Neuherberg, Germany*

Complete contact information is available at:
https://pubs.acs.org/10.1021/jasms.0c00291

Notes

The authors declare no competing financial interest.

■ REFERENCES

(1) Geyer, R.; Jambeck, J. R.; Law, K. L. Production, use, and fate of all plastics ever made. *Science advances* **2017**, *3* (7), e1700782.

(2) Li, D.; Zhou, L.; Wang, X.; He, L.; Yang, X. Effect of Crystallinity of Polyethylene with Different Densities on Breakdown Strength and Conductance Property. *Materials* **2019**, *12* (11), 1746−1758.

(3) Li, P.; Xue, Y.; Wu, X.; Sun, G.; Ji, X.; Bo, S. Microstructure characterization of one high-speed extrusion coating polyethylene resin fractionated by solvent gradient fractionation. *J. Polym. Res.* **2018**, *25* (5), 1−10.

(4) Monrabal, B. Polyolefin Characterization: Recent Advances in Separation Techniques. In *Polyolefins: 50 years after Ziegler and Natta I*; Kaminsky, W., Ed.; Advances in Polymer Science Springer: Berlin, Heidelberg, 2013; Vol. 257, pp 203−251.

(5) Monrabal, B.; Blanco, J.; Nieto, J.; Soares, J. B. P. Characterization of homogeneous ethylene/1-octene copolymers made with a single-site catalyst. CRYSTAF analysis and calibration. *J. Polym. Sci., Part A: Polym. Chem.* **1999**, *37*, 89−93.

(6) Eselem Bungu, P. S.; Pflug, K.; Busch, M.; Pasch, H. Comprehensive analysis of novel grafted polyethylenes using multidimensional fractionation methods. *Polym. Chem.* **2018**, *9*, 5051−5065.

(7) Cudby, M. E. A.; Bunn, A. Determination of chain branching in low density polyethylene by 13C nuclear magnetic resonance and infra-red spectroscopy. *Polymer* **1976**, *17*, 345−347.

(8) Macko, T.; Brüll, R.; Zhu, Y.; Wang, Y. A review on the development of liquid chromatography systems for polyolefins. *J. Sep. Sci.* **2010**, *33*, 3446−3454.

(9) Malik, M. I.; Pasch, H. Field-flow fractionation: New and exciting perspectives in polymer analysis. *Prog. Polym. Sci.* **2016**, *63*, 42−85.

(10) Drzeżdżon, J.; Jacewicz, D.; Sielicka, A.; Chmurzyński, L. MALDI-MS for polymer characterization − Recent developments and future prospects. *TrAC, Trends Anal. Chem.* **2019**, *115*, 121−128.

(11) Moscato, B.; Landis, C. Are carbodiimide-quenched polyethylene distributions representative of bulk polymer samples? Analysis of metallocene-catalyzed ethylene polymerization by ESI-MS, MALDI, GPC and NMR. *Chem. Commun.* **2008**, 5785−5787.

(12) van Ruymbeke, E.; Stéphenne, V.; Daoust, D.; Godard, P.; Keunings, R.; Bailly, C. A sensitive method to detect very low levels of long chain branching from the molar mass distribution and linear viscoelastic response. *J. Rheol.* **2005**, *49*, 1503−1520.

(13) Eckerle, P.; Pursch, M.; Cortes, H. J.; Sun, K.; Winniford, B.; Luong, J. Determination of short-chain branching content in polyethylene by pyrolysis comprehensive multidimensional gas chromatography using low thermal mass column technology. *J. Sep. Sci.* **2008**, *31*, 3416−3422.

(14) Wild, L.; Ryle, T. R.; Knobeloch, D. C.; Peat, I. R. Determination of branching distributions in polyethylene and ethylene copolymers. *J. Polym. Sci., Polym. Phys. Ed.* **1982**, *20*, 441−455.

(15) Pasch, H. Recent developments in polyolefin characterization. *Macromol. Symp.* **2001**, *165*, 91−98.

(16) DesLauriers, P. J.; Rohlfing, D. C.; Hsieh, E. T. Quantifying short chain branching microstructures in ethylene 1-olefin copolymers using size exclusion chromatography and Fourier transform infrared spectroscopy (SEC−FTIR). *Polymer* **2002**, *43*, 159−170.

(17) Yau, W. W.; Gillespie, D. New approaches using MW-sensitive detectors in GPC−TREF for polyolefin characterization. *Polymer* **2001**, *42*, 8947−8958.

(18) Tsuge, S.; Ohtani, H. Structural characterization of polymeric materials by Pyrolysis—GC/MS. *Polym. Degrad. Stab.* **1997**, *58*, 109−130.

(19) Ohtani, H.; Tsuge, S.; Usami, T. Determination of short-chain branching up to C6 in low-density polyethylenes by high-resolution pyrolysis-hydrogenation gas chromatography. *Macromolecules* **1984**, *17*, 2557−2561.

(20) Cody, R. B.; Fouquet, T. N. J.; Takei, C. Thermal desorption and pyrolysis direct analysis in real time mass spectrometry for qualitative characterization of polymers and polymer additives. *Rapid Commun. Mass Spectrom.* **2020**, *34*, e8687.

(21) Farenc, M.; Witt, M.; Craven, K.; Barrère-Mangote, C.; Afonso, C.; Giusti, P. Characterization of Polyolefin Pyrolysis Species Produced Under Ambient Conditions by Fourier Transform Ion Cyclotron Resonance Mass Spectrometry and Ion Mobility-Mass Spectrometry. *J. Am. Soc. Mass Spectrom.* **2017**, *28*, 507−514.

(22) Kiran, E.; Gillham, J. K. Pyrolysis-molecular weight chromatography: A new on-line system for analysis of polymers. II. Thermal decomposition of polyolefins: Polyethylene, polypropylene, polyisobutylene. *J. Appl. Polym. Sci.* **1976**, *20*, 2045−2068.

(23) Poutsma, M. L. Reexamination of the Pyrolysis of Polyethylene: Data Needs, Free-Radical Mechanistic Considerations, and Thermochemical Kinetic Simulation of Initial Product-Forming Pathways. *Macromolecules* **2003**, *36*, 8931−8957.

(24) Ratkiewicz, A. Kinetics of the C−C bond beta scission reactions in alkyl radicals. *Phys. Chem. Chem. Phys.* **2011**, *13*, 15037−15046.

(25) Bockhorn, H.; Hornung, A.; Hornung, U.; Schawaller, D. Kinetic study on the thermal degradation of polypropylene and polyethylene. *J. Anal. Appl. Pyrolysis* **1999**, *48*, 93−109.

(26) Murata, K.; Sato, K.; Sakata, Y. Effect of pressure on thermal degradation of polyethylene. *J. Anal. Appl. Pyrolysis* **2004**, *71*, 569−589.

(27) Serrano, D. P.; Aguado, J.; Escola, J. M.; Rodríguez, J. M.; San Miguel, G. An investigation into the catalytic cracking of LDPE using Py−GC/MS. *J. Anal. Appl. Pyrolysis* **2005**, *74*, 370−378.

(28) Ueno, T.; Nakashima, E.; Takeda, K. Quantitative analysis of random scission and chain-end scission in the thermal degradation of polyethylene. *Polym. Degrad. Stab.* **2010**, *95*, 1862−1869.

(29) Tsuchiya, Y.; Sumi, K. Thermal decomposition products of polyethylene. *J. Polym. Sci., Part A-1: Polym. Chem.* **1968**, *6*, 415−424.

(30) Madorsky, S. L. Rates of thermal degradation of polystyrene and polyethylene in a vacuum. *J. Polym. Sci.* **1952**, *9*, 133−156.

(31) Kuroki, T.; Sawaguchi, T.; Niikuni, S.; Ikemura, T. Mechanism for long-chain branching in the thermal degradation of linear high-density polyethylene. *Macromolecules* **1982**, *15*, 1460−1464.

(32) Saraji-Bozorgzad, M.; Geissler, R.; Streibel, T.; Mühlberger, F.; Sklorz, M.; Kaisersberger, E.; Denner, T.; Zimmermann, R. Thermogravimetry coupled to single photon ionization quadrupole mass spectrometry: a tool to investigate the chemical signature of thermal decomposition of polymeric materials. *Anal. Chem.* **2008**, *80*, 3393−3403.

(33) Saraji-Bozorgzad, M.; Geißler, R.; Streibel, T.; Sklorz, M.; Kaisersberger, E.; Denner, T.; Zimmermann, R. Hyphenation of a thermobalance to soft single photon ionisation mass spectrometry for evolved gas analysis in thermogravimetry (TG-EGA). *J. Therm. Anal. Calorim.* **2009**, *97*, 689−694.

(34) Streibel, T.; Fendt, A.; Geißler, R.; Kaisersberger, E.; Denner, T.; Zimmermann, R. Thermal analysis/mass spectrometry using soft photo-ionisation for the investigation of biomass and mineral oils. *J. Therm. Anal. Calorim.* **2009**, *97*, 615−619.

(35) Geissler, R.; Saraji-Bozorgzad, M. R.; Gröger, T.; Fendt, A.; Streibel, T.; Sklorz, M.; Krooss, B. M.; Fuhrer, K.; Gonin, M.; Kaisersberger, E.; Denner, T.; Zimmermann, R. Single Photon Ionization Orthogonal Acceleration Time-of-Flight Mass Spectrometry and Resonance Enhanced Multiphoton Ionization Time-of-Flight Mass Spectrometry for Evolved Gas Analysis in Thermogravimetry: Comparative Analysis of Crude Oils. *Anal. Chem.* **2009**, *81*, 6038−6048.

(36) Grimmer, C.; Rüger, C. P.; Streibel, T.; Cuoq, F.; Kwakkenbos, G.; Cordova, M.; Peñalver, R.; Zimmermann, R. Description of Steam Cracker Fouling and Coking Residues by Thermal Analysis-Photoionization Mass Spectrometry. *Energy Fuels* **2019**, *33*, 11592−11602.

(37) Zimmermann, R.; Saraji-Bozorgzad, M.; Grimmer, C.; Ulbrich, A.; Streibel, T. Erdöl in seine Bestandteile zerlegen und charakterisieren. *Nachr. Chem.* **2016**, *64*, 751−754.

(38) Rüger, C. P.; Grimmer, C.; Sklorz, M.; Neumann, A.; Streibel, T.; Zimmermann, R. Combination of Different Thermal Analysis Methods Coupled to Mass Spectrometry for the Analysis of Asphaltenes and Their Parent Crude Oils: Comprehensive Characterization of the Molecular Pyrolysis Pattern. *Energy Fuels* **2018**, *32*, 2699−2711.

(39) Streibel, T.; Mitschke, S.; Adam, T.; Weh, J.; Zimmermann, R. Thermal desorption/pyrolysis coupled with photo ionisation time-of-flight mass spectrometry for the analysis and discrimination of pure tobacco samples. *J. Anal. Appl. Pyrolysis* **2007**, *79*, 24−32.

(40) Mühlberger, F.; Hafner, K.; Kaesdorf, S.; Ferge, T.; Zimmermann, R. Comprehensive on-line characterization of complex gas mixtures by quasi-simultaneous resonance-enhanced multiphoton ionization, vacuum-UV single-photon ionization, and electron impact ionization in a time-of-flight mass spectrometer: setup and instrument characterization. *Anal. Chem.* **2004**, *76*, 6753−6764.

(41) Otto, S.; Streibel, T.; Erdmann, S.; Sklorz, M.; Schulz-Bull, D.; Zimmermann, R. Application of pyrolysis-mass spectrometry and pyrolysis-gas chromatography-mass spectrometry with electron-ionization or resonance-enhanced-multi-photon ionization for characterization of crude oils. *Anal. Chim. Acta* **2015**, *855*, 60−69.

(42) Otto, S.; Streibel, T.; Erdmann, S.; Klingbeil, S.; Schulz-Bull, D.; Zimmermann, R. Pyrolysis-gas chromatography-mass spectrometry with electron-ionization or resonance-enhanced-multi-photon-ionization for characterization of polycyclic aromatic hydrocarbons in the Baltic Sea. *Mar. Pollut. Bull.* **2015**, *99*, 35−42.

(43) Wunderlich, B.; Czornyj, G. A Study of Equilibrium Melting of Polyethylene. *Macromolecules* **1977**, *10*, 906−913.

(44) Gopalan, M. R.; Mandelkern, L. Effect of crystallization temperature and molecular weight on the melting temperature of linear polyethylene. *J. Phys. Chem.* **1967**, *71*, 3833−3841.

(45) Liang, X.-k.; Luo, Z.; Yang, L.; Wei, J.-t.; Yuan, X.; Zheng, Q. Rheological properties and crystallization behaviors of long chain branched polyethylene prepared by melt branching reaction. *J. Polym. Eng.* **2018**, *38*, 7−17.

8.4   Publication 4

Real time monitoring of slow pyrolysis of polyethylene terephthalate (PET) by different mass spectrometric techniques

by

Asma Dhahak, Christoph Grimmer, Anika Neumann, Christopher P. Rüger, Martin Sklorz, Thorsten Streibel, Ralf Zimmermann, Guillain Mauviel, Valérie Burkle-Vitzthum

Real time monitoring of slow pyrolysis of polyethylene terephthalate (PET) by different mass spectrometric techniques

Asma Dhahak [a], Christoph Grimmer [b], Anika Neumann [b], Christopher Rüger [b], Martin Sklorz [b,c], Thorsten Streibel [b,c], Ralf Zimmermann [b,c], Guillain Mauviel [a], Valérie Burkle-Vitzthum [a,*]

[a] Laboratory of Reactions and Process Engineering (LRGP), National Centre for Scientific Research (CNRS), University of Lorraine, National School of Chemical Industries (ENSIC), 1 Rue Grandville, 54000 Nancy, France
[b] Joint Mass Spectrometry Centre, Chair of Analytical Chemistry, Institute of Chemistry, University of Rostock, 18059 Rostock, Germany
[c] Joint Mass Spectrometry Centre, Cooperation Group Comprehensive Molecular Analytics, Helmholtz Zentrum München-German Research Center of Environmental Health (GmbH), Ingolstädter Landstrasse 1, 85764 Neuherberg, Germany

ABSTRACT

In the context of waste upgrading of polyethylene terephthalate (PET) by pyrolysis, this study presents three on-line mass spectrometric techniques with soft ionization for monitoring the emitted decomposition products and their thermal dependent evolution profiles. Pyrolysis experiments were performed using a thermogravimetric analyzer (TGA) under nitrogen atmosphere with a heating rate of 5 °C/min from 30 °C to 600 °C. Single-photon ionization (SPI at 118 nm/10.5 eV) and resonance enhanced multiple photon ionization (REMPI at 266 nm) were used with time-of-flight mass spectrometry (TOF-MS) for evolved gas analysis (TGA-SPI/REMPI-TOFMS). Additionally, the chemical signature of the pyrolysis products was investigated by atmospheric pressure chemical ionization (APCI) ultra high resolution Fourier Transform ion cyclotron resonance mass spectrometry (FT-ICR MS) which enables assignment of molecular sum formulas (TGA-APCI FT-ICR MS). Despite the soft ionization by SPI, the fragmentation of some compounds with the loss of the [O-CH = CH2] fragment is observed. The major compounds were acetaldehyde (*m/z* 44), benzoic acid (*m/z* 122) and a fragment of *m/z* 149. Using REMPI, aromatic species were selectively detected. Several series of pyrolysis products were observed in different temperature intervals, showing the presence of polycyclic aromatic hydrocarbons (PAHs), especially at high temperatures. FT-ICR MS data showed, that the CHO_4 class was the most abundant compound class with a relative abundance of 45.5%. The major compounds detected with this technique corresponded to *m/z* 193.0495 ($C_{10}H_9O_4^+$) and 149.0233 ($C_8H_5O_3^+$). Based on detailed chemical information, bulk reaction pathways are proposed, showing the formation of both cyclic monomer/dimer and linear structures.

© 2020 Elsevier Ltd. All rights reserved.

1. Introduction

Pyrolysis is a versatile thermochemical technique that converts a solid material into useful gaseous, liquid, and solid products in absence of oxygen. This technique can be used to valorize various products, such as polymers, biomass, and tires. The material chosen in this study is polyethylene terephthalate (PET). PET is the third frequently consumed polymer in Europe after polypropylene and low density polyethylene (Kawecki et al., 2018). It is frequently used to make a variety of consumer goods, such as synthetic polyester fibers, bottles and films (Kawecki et al., 2018; Zander et al., 2018).

The pyrolysis of PET yields a complex mixture of products which consists of aldehydes (e.g., acetaldehyde, benzaldehyde), carbon oxides (CO_2 and CO), aliphatic hydrocarbons C_1-C_4 (e.g., CH_4, C_2H_4), aromatic species (e.g., benzene, toluene, styrene), carboxylic acids such as benzoic acid and its derivatives (e.g., acetylbenzoic acid, methylbenzoic acid, ethylbenzoic acid), terephthalic acid and vinyl terephthalate as well as esters (e.g., di-vinyl terephthalate, vinyl benzoate), ketones (e.g., acetophenone, benzophenone, fluorenone) and other compounds (Artetxe et al., 2010; Dzięcioł and Trzeszczyński, 2001; Dzięcioł and Trzeszczyński, 2000; Kumagai et al., 2017; Sophonrat et al., 2017; Yoshioka et al., 2004).

Different conventional methods were used in literature to characterize the pyrolysis products by online or offline analysis. Concerning offline analysis (i.e. after condensation), the most used

analytical methods are Gas Chromatography coupled to Mass Spectrometry (GC-MS) and High Performance Liquid Chromatography (HPLC) (Çit et al., 2010; Dhahak et al., 2019). However, offline analysis does not allow the characterization of heavy species, which might be produced during the pyrolysis. For online analysis, PET pyrolysis experiments were mainly coupled to Fourier Transform Infrared Spectroscopy (FTIR), High Resolution Pyrolysis Gas-Chromatography and micro- GC (Badia et al., 2013; Czégény et al., 2012; Dhahak et al., 2019; Ohtani et al., 1986). These techniques are not able to analyze high mass compounds. Online analyses have the advantage of avoiding spurious reactions that can occur during the product condensation, and thus help predicting the genuine pyrolysis reaction pathways.

In the last decades, time of flight mass spectrometry (TOF-MS) has been widely applied (Lee et al., 2017; Shi et al., 2018; Wu et al., 2011). It provides high sensitivity and high acquisition speed (Green and Martin, 2006; Qian and Dechert, 2002). The identification of complex mixtures however often requires high resolution mass spectrometry which allows resolving multiple peaks with the same nominal m/z (Barrow et al., 2014). Fourier transform ion cyclotron resonance mass spectrometry (FT-ICR MS) has proven high potential for detecting and identifying compounds without pre-separation by chromatography (Bae et al., 2010; Kekäläinen et al., 2014). Molecular formula can be assigned to the resolved signals, typically within ppm mass accuracy (Huba et al., 2016).

Different ionization methods are available for mass spectrometry, all exhibiting different advantages and drawbacks. In fact, electron ionization (EI) in vacuum is the method commonly used for the evolved gas analysis of pyrolysis gases. It is a "hard" and universal ionization mode (Jia et al., 2016; Yuzawa et al., 2013). It leads to strong fragmentation of the molecule because of the high ionization energy generally deployed (70 eV) (Hsu and Ni, 2018). Consequently, the EI mass spectrum is complicated to interpret because of the absence of the molecular ions and strong overlapping signals of complex mixtures impeding data interpretation. In contrast, soft ionization techniques such as chemical ionization (CI), atmospheric pressure chemical ionization (APCI), electrospray ionization (ESI) or vaccum photo ionization (PI), a molecular ion (radical cation and/or protonated ion species) can be preserved and fragmentation is greatly diminished (Wang et al., 2015), although all to the latter methods are less universal than EI.

Photo ionization (PI) coupled to mass spectrometry has been widely used for the characterization of complex mixtures. PI can be divided in single-photon ionization (SPI) and resonance-enhanced multiphoton ionization (REMPI). SPI commonly involves a single-photon in the vacuum ultraviolet range (VUV) to ionize the molecule in one step, inducing little or no fragmentation (Giri et al., 2017; Hsu and Ni, 2018). The photon energy commonly used is between 7.5 and 11.8 eV, corresponding to a wavelength of 165–105 nm (Giri et al., 2017). In other words, only organic molecules with ionization energy lower than the photon energy can be ionized. Many types of lasers can be used to generate VUV light with different wavelengths such as Nd:YAG (118 nm; 10.48 eV (Rüger et al., 2018)), F_2 (157 nm; 7.9 eV (Trukhin and Golant, 2009)), H_2 (160 nm; 7.75 eV (Fukuzawa and Tanimizu, 1978)). Fig. 1 represents the ionization energies (IE) of compounds identified during PET pyrolysis (Sovová et al., 2008). IE are available from the
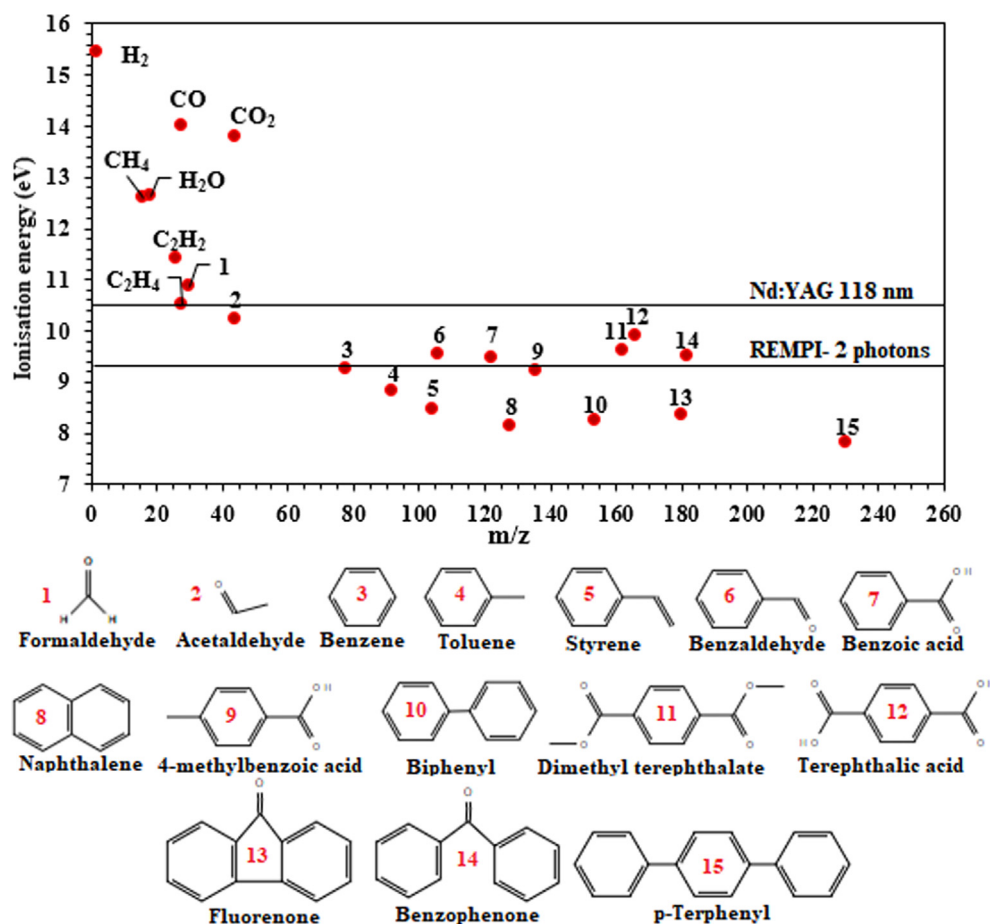

Fig. 1. Ionization energies of selected molecules identified in PET pyrolysis (adapted from refs (Hanley and Zimmermann, 2009; Jia et al., 2016)).

National Institute of Standards and Technology (NIST) ("NIST Chemistry webbook [Gas phase ion energetics data] Available online : https://webbook.nist.gov/chemistry/). IE of most compounds are below the photon energy, except certain small molecules, such as CO, CO_2, H_2O, H_2, and CH_4. Carbon oxides might represent a major proportion of PET pyrolysis gases, but cannot be ionized with common setups.

Unlike SPI, REMPI uses ultraviolet (UV) light, requiring at minimum two photons in which a single-photon or multiple photons absorbed excites an intermediate state and a second photon ionizes the atom or molecule (Jia et al., 2016). The soft ionization pathway, due to the low photon energies, leads to few fragmentation which facilitates the interpretation of the mass spectra. In addition, REMPI allows the selective detection of vibronic structure species such as mono- or polycyclic aromatic compounds and their derivatives (Dorfner et al., 2004; Zimmermann et al., 1999).

Another soft ionization technique commonly used, especially for FT-ICR MS, is atmospheric pressure chemical ionization (APCI) (Crepier et al., 2018). Corona discharge induced ion- molecule reactions in gas phase, generating radical cations or protonated molecule ions with little fragmentation (Li et al., 2015; Tose et al., 2015). This technique allows the detection of polar and medium polar compounds, preferably oxygenated species (Parr et al., 2018; Rüger et al., 2018). Due to instrumental limits of the FT–ICR MS, the mass range is between 100 and 1000. More details on the APCI process are given elsewhere (Li et al., 2015).

Numerous studies on pyrolysis have been performed by coupling thermogravimetry or pyrolysis experiments with the analytical techniques described above (Huang et al., 2017; Shi et al., 2018; Wu et al., 2011; Xu et al., 2017). These techniques provide not only the chemical formula of the analytes but also their evolution profile in real time. Consequently, temperature dependent pyrolysis products can be analyzed. So far, numerous studies focused on polymers such as polyethylene, polypropylene, polystyrene and polyvinyl chloride (Huang et al., 2017; Kai et al., 2019; Saraji-Bozorgzad et al., 2008; Wang et al., 2015; Wu et al., 2011; Zhou et al., 2019). However, limited studies have been conducted on oxygenated macromolecules such as polyethylene terephthalate (PET). Some PET pyrolysis experiments have been conducted on-line by using conventional analytical tools such as thermogravimetry (TGA) coupled to mass spectrometry (Gupta et al., 2004), TGA coupled to Fourier transform infrared spectroscopy (FTIR) (Badia et al., 2013; Czégény et al., 2012; Kinoshita et al., 1993; Pan et al., 2016), and Pyrolysis-gas chromatography (PyGC) (Ohtani et al., 1986).

In this study, three different analytical techniques were coupled to thermogravimetry for on-line monitoring of volatile compounds emitted by the slow pyrolysis of PET. Single-photon ionization (SPI) at 118 nm (10.5 eV) and resonance enhanced multi photon ionization (REMPI) at 266 nm were coupled to a time of flight mass spectrometer (TOF-MS). SPI is aiming at detection of organic species whose ionization energy are lower than 10.5 eV, whereas REMPI is suitable for the sensitive detection of aromatic and polyaromatic constituents. Another thermogravimetry analyzer was coupled to a Fourier transform ion cyclotron resonance mass spectrometer (FT-ICR MS) using atmospheric pressure chemical ionization (APCI). APCI FT-ICR MS is suitable to ionize medium-polar and polar species with a mass range [100–1000]. Using the FT-ICR MS exact mass data, detailed chemical information was gained and combined with the results obtained with SPI and REMPI. This procedure allowed for the detailed description of the pyrolysis process.

2. Materials and methods

2.1. Materials

PET was purchased from Goodfellow SARL (Lille, France) in a powder form (particle size of 300 μm). This polymer is amorphous with a crystallinity of 16%. The elemental analysis of carbon, hydrogen and oxygen content in PET was determined using a Flash Smart CHNS/O Analyser by Thermo Fisher Instrument. The oxygen content was calculated by difference. The results showed that PET contains about 45.5% carbon by mass, 36.4% hydrogen and 18.2% oxygen.

2.2. Instrumentation

2.2.1. Thermogravimetry coupled to SPI/REMPI-TOF-MS

A schematic overview of TG-REMPI/SPI-TOF-MS is presented in Fig. 2a) (Rüger et al., 2018). The thermobalance (STA 409, Netzsch Geratebau, Selb, Germany) was on-line coupled to the ionization source of the mass spectrometer using a heated transfer line (280 °C, ID 280 μm × 2.25 m length). 8–10 mg of PET was filled in an aluminum oxide crucible and heated up to 550 °C with a constant heating rate of 5 °C/min. The nitrogen flow rate around the sample was fixed to 50 mL/min for reactive gas and 50 mL/min for protective gas.

The ionization source was operated under vacuum conditions (around 10^{-4} mbar) which allows transferring an aliquot fraction of evolved gas out of the thermobalance inside the mass spectrometer based on the pressure gradient. A Nd:YAG laser (Surelite III, Continuum, Inc., Santa Clara, CA, U.S.A; wavelength: 1064 nm (Czech et al., 2016)) was used in this experiment. A beam at 355 nm was produced by frequency tripling conversion. It operated with pulse energies of 25 mJ, pulse width of 5 ns, and repetition
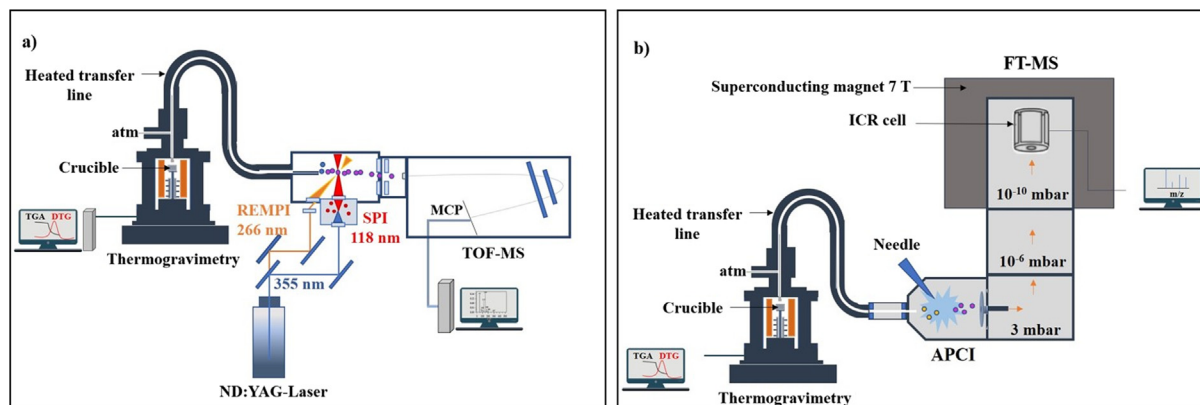

Fig. 2. Schematic of the instrumental setup of: (a) TGA-REMPI/SPI-TOF-MS; (b) TGA-APCI FT-ICR MS (adapted from refs (Rüger et al., 2018; Rüger et al., 2015).

rate of 10 Hz. For SPI, the wavelength was again tripled, generating a vacuum ultraviolet light (118 nm, 10.5 eV), by using a xenon-filled gas cell (Xe 4.0, 12 mbar). For REMPI, a wavelength of 266 nm (4.66 eV) was obtained by frequency-quadrupling of the Nd:YAG laser 1064 nm. Consequently, the energy ionization with REMPI using two photons is 9.32 eV. Further details are available elsewhere (Czech et al., 2016; Fendt et al., 2013).

Once the ions are generated, they are m/z-separated using a reflectron TOF analyzer (Kaesdorf Instrumente für Forschung and Industrie, Munich, Germany) and detected by a microchannel plate (MCP, Chevron Plate, Burle Electro-Optics Inc.) (Czech et al., 2016; Rüger et al., 2018). The ions were recorded up to m/z 500. A custom LabView-software was used for data processing (Czech et al., 2016).

2.2.2. Thermogravimetry coupled to APCI/FT-ICR-MS

A thermobalance (STA 209, Netzsch Gerätebau GmbH, Germany) was used for pyrolysis experiments (Fig. 2b). A mass of 1–1.5 mg sample was loaded in an aluminum crucible and heated under a constant nitrogen flow of 200 mL/min from 20 °C to 600 °C with a heating rate of 5 °C/min. Approximately 2 mL/min of the evolved gas mixture was transferred to the ionization chamber via a slight overpressure of 5 mbar by a heated transfer line (deactivated fused silica capillary, 2 m, 0.53 mm ID, 300 °C). The chemical ionization was carried out by a modified Bruker GC-APCI II source, operating at atmospheric pressure in positive ion mode. For ionization, a stainless-steel needle was used, generating a corona discharge with a current of 2.5 μA. More details have been given elsewhere (Rüger et al., 2015). The ions produced were detected by a Bruker Apex II ultra FT–MS equipped with a 7T magnet (InfinityCell, Bruker Daltonics, Bremen, Germany). A mass range of 100–1000 was recorded with five microscans per spectrum. A 4 Megaword transient of approximately 2 s length was applied, offering an ultrahigh resolution of 260,000 at m/z 400 was obtained.

Data processing was carried out using Bruker DataAnalysis for m/z-calibration of the spectra and a self-written tool CERES based on Matlab scripting for further processing and sum formula calculation. Every measurement was internal linearly calibrated in DataAnalysis and again every single spectrum during processing in CERES. For sum formula assignment, the following restrictions were applied: $C_{4-100}H_{4-200}N_0O_{15}S_0$, H/C ratio of 0–3 and Double Bond Equivalent (DBE) of 0–40.

3. Results and discussion

3.1. Evolved gas analysis by Single-photon ionization (SPI) mass spectrometry

Fig. 3a) shows the residual mass (TGA), the derivative of the mass loss signal (DTG) and the total ion current (TIC) as a function of temperature. Over the whole pyrolysis time, the TIC is obtained by adding all ions of the spectra obtained at a defined time. Visibly, the evolution of TIC coincides with the DTG curve. This indicates that SPI detected some of the major volatile degradation products of the PET pyrolysis, excluding CO_2 and CO. The decomposition starts at roughly 350 °C and lasts approximately up to 500 °C. The maximum of TIC and DTG corresponds to 435 ± 1 °C.

Fig. 3b) displays the average mass spectra for selected temperature ranges of the emitted compounds. The structure of the molecules was determined based on literature (Guo et al., 2015) (Sovová et al., 2008). It should be noted that the temperature indicates the evaporation of molecules and they can be generated before in the condensed phase. Signal intensities increase steadily up to a temperature of 450 °C. In the 350–400 °C temperature range, major

degradation products appear, and their intensities increase as the pyrolysis temperature increases. Signals at m/z 44, 122, and 166 most likely correspond to acetaldehyde, benzoic acid, and terephthalic acid, respectively. Based on the literature, the peak corresponding to m/z 149 is a characteristic fragment of vinyl terephthalate (M_w = 192 g/mol) which is reported to be one of the primary compounds of PET degradation (Garozzo et al., 1987; Plage and Schulten, 1990). Thus, a mass loss of m/z 43 occurs, which can be attributed to a [O-CH=CH$_2$] fragment (Garozzo et al., 1987; Plage and Schulten, 1990). Despite soft ionization, the carbon - carbon double bond (C=C) is destabilized followed by the oxygen ester, undergoing photo-fragmentation under these conditions (Van Dam and Oskam, 1978). An example in the literature of photoionization of vinyl butyrate which has the same fragment in its structure proved that the fragmentation occurs from 9.5 eV by losing m/z 43 (Czekner et al., 2018). Losing the same group, the peaks at m/z 105 and 175 may also be the results of fragmentation of vinyl benzoate (M_w = 148 g/mol) and di-vinyl terephthalate (M_w = 218 g/mol), respectively. On the other hand, the intensities of major products reach a maximum between 400 °C and 450 °C and decrease there after which shows either the end of the pyrolysis or the presence of secondary reactions causing their intensities diminution. The intensity of terephthalic acid (m/z 166) decreases slightly between 450 and 500 °C, even so it becomes the compound with the highest intensity at high temperatures, as shown in Fig. 3b).

Possible peak assignments of major compounds are summarized in Table S1. The mixture mostly contains acids and vinyl end groups. The same observation was made by (Garozzo et al., 1987) using electron ionization at low electron energy (18 eV) for copolyesters containing ethylene terephthalate and p-oxybenzoate units. They studied the on-line pyrolysis coupled to mass spectrometry with a heating rate of 10 °C/min. (Garozzo et al., 1987) observed the loss of 43 [O—CH=CH$_2$] and 17 [OH] mass units, confirming the metastable transitions of fragments and indicating the presence of open chain structures with carboxyl and vinyl end groups. Each compound corresponding to a specific m/z can be easily real-time-monitored. The thermal evolution profiles of major m/z are plotted in Fig. 3c). Acetaldehyde (m/z 44) is the first compound detected by TOF-MS, at about 315 °C, followed by benzoic acid (m/z 122) at 350 °C. The terephthalic acid (m/z 166) is detected at 371 °C, 21 °C after the detection of benzoic acid and 7 °C after benzene (m/z 78). The maximum productions of major compounds are observed at 431 °C, except for terephthalic acid (m/z 166) which is observed at 440 °C. Interestingly, the benzene curve shows a bimodal emission behaviour in which the maximum of the first peak is detected at 427 °C and the second maximum at 470 °C. Benzene goes through a minimum at 447 °C. The same trend was observed in (Dhahak et al., 2019) using a horizontal reactor. In this study, online monitoring of gases (carbon oxides, ethylene and benzene) during slow pyrolysis (5 °C / min) was performed. Benzene profile also showed two peaks at 431 °C and 469 °C. The first and the second peaks may be due to the decarboxylation of benzoic acid and terephthalic acid, respectively. The production of benzene is accelerated at higher temperature, as shown in Fig. 3c).

3.2. Evolved gas analysis by Resonance-enhanced multiphoton ionization (REMPI) mass spectrometry

Using REMPI, only aromatic species can be detected. However, aromatic carboxylic acids such as terephthalic acid and benzoic acid cannot be ionized because of their high ionization energy (Fig. 1). Benzene, which has a ionization energy of 9.24 eV, also requires a little more energy to be ionized (≥9.5 eV) (Boesl et al., 1978). Fig. 4a) shows the TIC and DTG curves. Contrary to the SPI-TIC, REMPI-TIC exhibits a bi-modal behavior as the tempera-
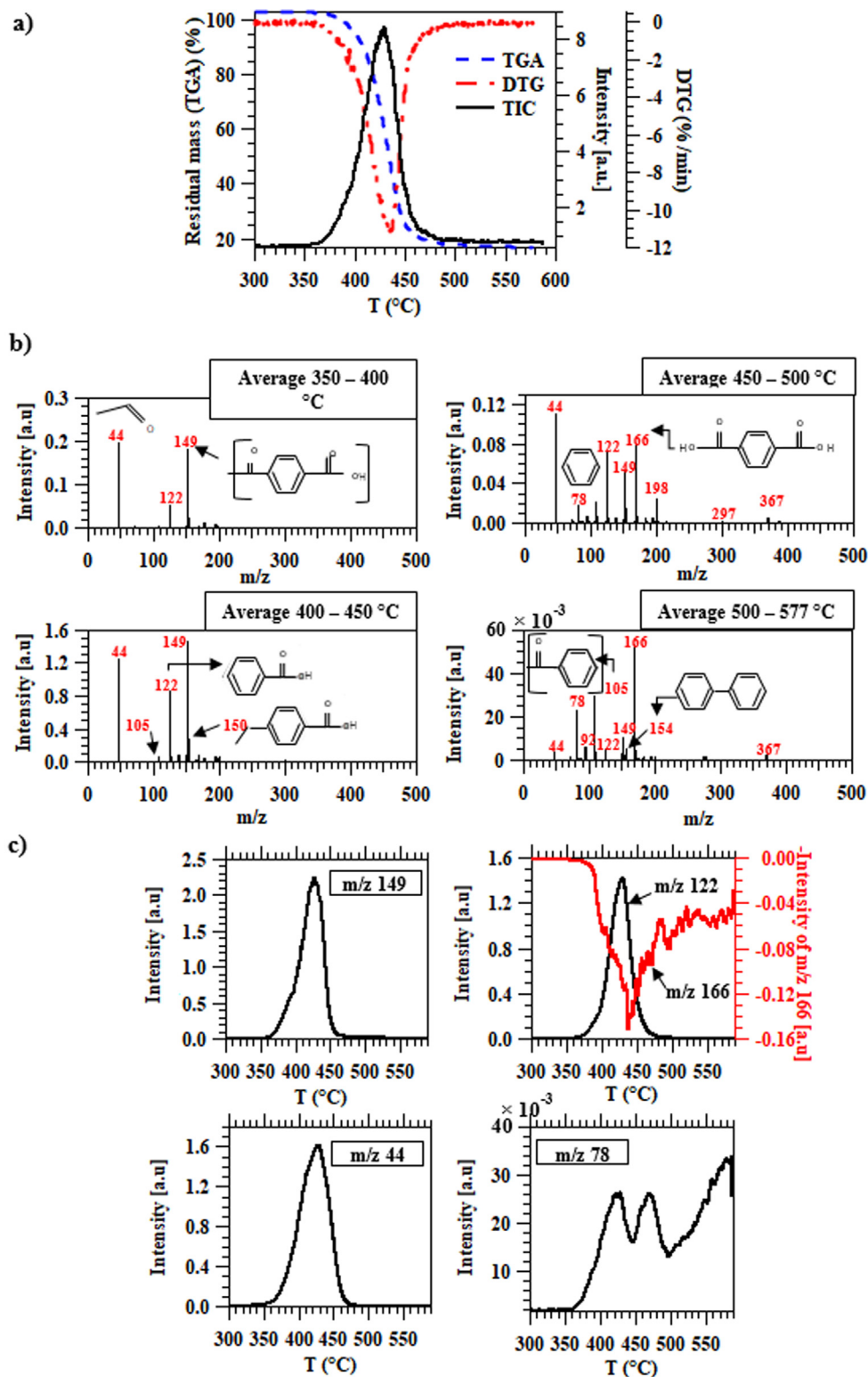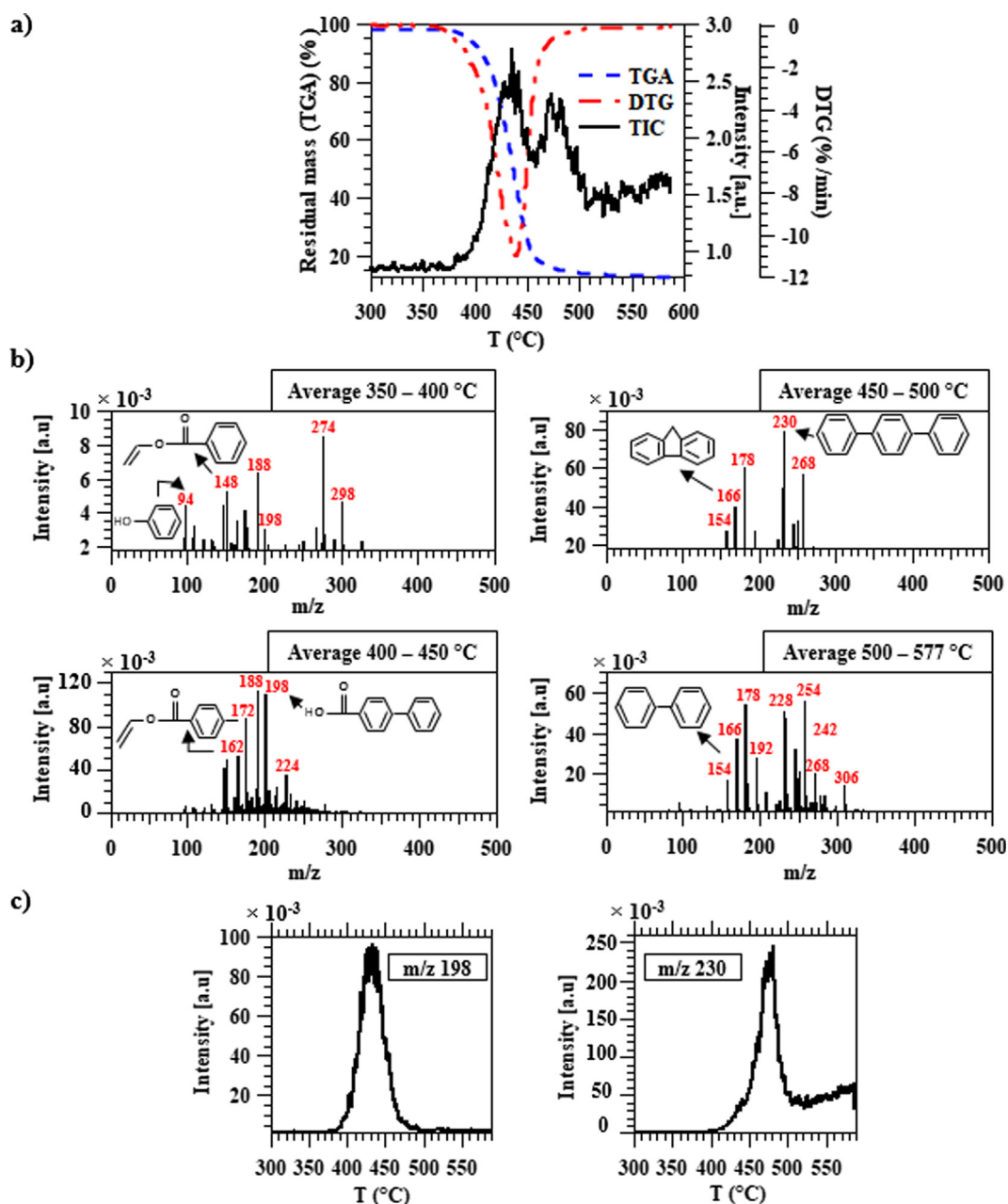
Fig. 3. TGA-SPI TOF-MS results: (a) TGA, DTG, TIC curves, (b) Average mass spectra of the products at various temperatures, (c) thermal evolution profiles of major *m/z*.

ture increases. The first peak coincides with the DTG curve, whereas the second peak appears in a region where the mass loss is almost finished, indicating the presence of secondary reactions with a small mass loss. The maximum peaks correspond to 435 °C and 473 °C, respectively. These two peaks highlight the presence of two different mechanisms responsible for the formation of aromatic species such as polycyclic aromatic hydrocarbons

(PAHs). REMPI mass spectra are shown in Fig. S1. For both peaks observed in the REMPI-TIC curve, an average mass spectrum is presented in Fig. S2. The mass spectrometric pattern is significantly different when comparing the two stages, and they depend mainly on temperature. The effect of temperature on the pyrolysis product intensities is depicted in Fig. 4b). As can be seen, a higher variety of compounds is detected in REMPI than in SPI. Different series of

Fig. 4. TGA-REMPI TOF-MS results: (a) TGA, DTG, TIC curves, (b) Average mass spectra of the products at various temperatures, (c) thermal evolution profiles of major m/z.

pyrolysis products are observed at different temperature intervals. This evolved gas complexity confirms the presence of different and various reactions involved in the pyrolysis of PET. In fact, between 300 °C and 350 °C, m/z of 274, 298, 264, and 288 are detected with low average intensities. With the increase of temperature, the mass spectrum shows other peaks such as m/z of 192, 188, 148, 144, 94, and 162. The m/z of 148, 94, and 162 presumably correspond to vinyl terephthalate, vinyl benzoate, phenol, and vinyl 4-methylbenzoate, respectively. Using REMPI, compounds with [O—CH=CH$_2$] do not undergo a photo-fragmentation, because of the low energy. However, their sensitivity of detection by REMPI is much lower than by SPI.

The signal intensities of aromatic products increase at higher temperatures. The highest intensities are observed between 400 °C and 450 °C, which corresponds to the maximum decomposition rate of PET. In this phase, the major compounds correspond to m/z of 188, 198, 172, and 162. At higher temperature (450–577 °C), other compounds appear such as m/z 254, 228, 178, 230, 166, and 154. Based on literature (Hujuri et al., 2013; Sovová et al., 2008), those peaks may be attributed to 1,2′-binaphthalene, benzo[a]anthracene, anthracene or/and phenanthrene, terphenyl, 9H-fluorene and biphenyl or/and acenaphthene, respectively (Table S1). The presence of PAHs is mainly detected between 450 and 500 °C, confirming the presence of secondary reactions and most likely causing the second peak in REMPI-TIC.

The evolution profile of major peaks is shown in Fig. 4c). The maximum productions of the different aromatics do not occur at the same time. Terphenyl, which corresponds to m/z 230, approximately appears at 415 °C and reaches a maximum at 477 °C. The peak at m/z 198, which may probably correspond to biphenyl-4-carboxylic acid (C$_{13}$H$_{10}$O$_2$) (Deng et al., 2006; Guo et al., 2015; Sovová et al., 2008), evolves starting from 389 °C to 492 °C. Its maximum production occurs at 439 °C. The evolution profile of m/z 198 detected by REMPI resembles to the SPI signals (Fig. S3).

3.3. Evolved gas analysis by TGA-APCI FT-ICR MS

The DTG, TIC, and temperature curves revealed by thermogravimetric coupling to APCI FT-ICR MS are shown in Fig. S4. The temporal evolution of the decomposition rate (DTG) is consistent with the TIC curve, showing a single peak. A similar trend was observed by SPI-TOF-MS (Section 3.1). The maximum decomposition rate is found at about 417 °C. Typical diagrams are constructed to facilitate the visualization and interpretation of high-resolution mass spectrometric data, such as double bond equivalence (DBE) against carbon number and Van-Kreleven plot. DBE is a measure of unsaturation (double bonds and rings) in a molecule and contributes to the prediction of the chemical structure from a given elemental formula. Besides, Van-Krevelen diagram is a graphical distribution of H/C ratio versus O/C, providing an overall view on compound categories (Miettinen et al., 2017; Oni et al., 2015). The evolution of double bond equivalence (DBE) versus carbon number is shown in Fig. 5.a). It indicates that there are compounds with DBE values ranging from 2 to 15 and carbon numbers ranging from C_6 to C_{20}. The high DBE values confirm the presence of polycyclic aromatic hydrocarbons. Most of the detected compounds have a relatively low abundance (in blue color). The highest abundances (red color) correspond to species with a carbon number C_8-C_{10} and a DBE of 6–7. The core structure of these compounds is probably based on one benzene ring (DBE of 4) or two aromatic rings (DBE of 7). Fig. 5.b) represents the Van-Krevelen plot, highlighting different compound classes. For instance, a complex mixture of aromatic compounds with expanded oxygen content is mainly distributed within a H/C range of 0.7–1 and O/C values in the range of 0.1–0.5, as well as highly unsaturated compounds (H/C $\leq$1.5) and little aliphatic compounds (1.5 $\leq$ H/C $\leq$ 2) (Li et al., 2018). Furthermore, polycyclic and aromatic compounds without oxygen are also present with H/C $\approx$ 0.5–1 and account for roughly 6.4% of the overall signal. The class distribution of detected species is shown in Fig. 5c). Seven classes are observed
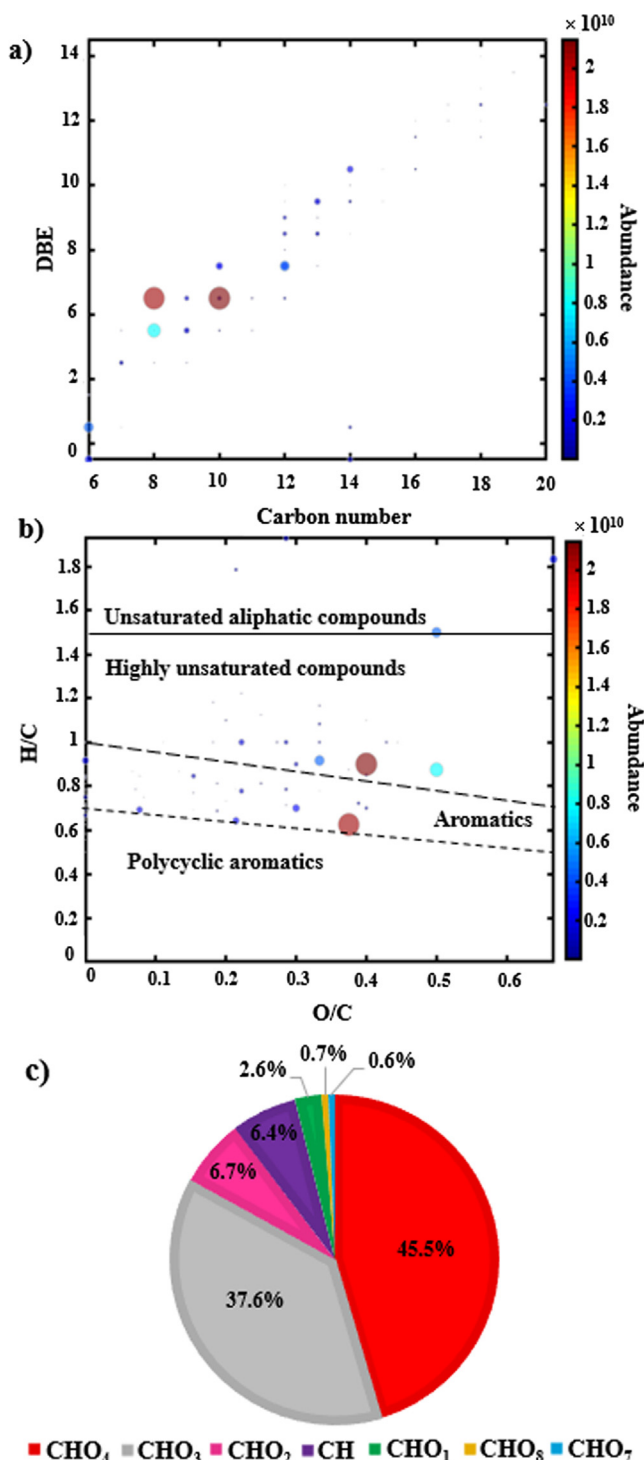

Fig. 5. TGA-APCI FT-ICR MS results: (a) Double bond equivalent (DBE) vs carbon number plot, b) Van Krevelen plot (H/C vs O/C), (c) Pie chart representing the compound class distribution. In (a) and (b), the size of the dots is proportional to the abundance.
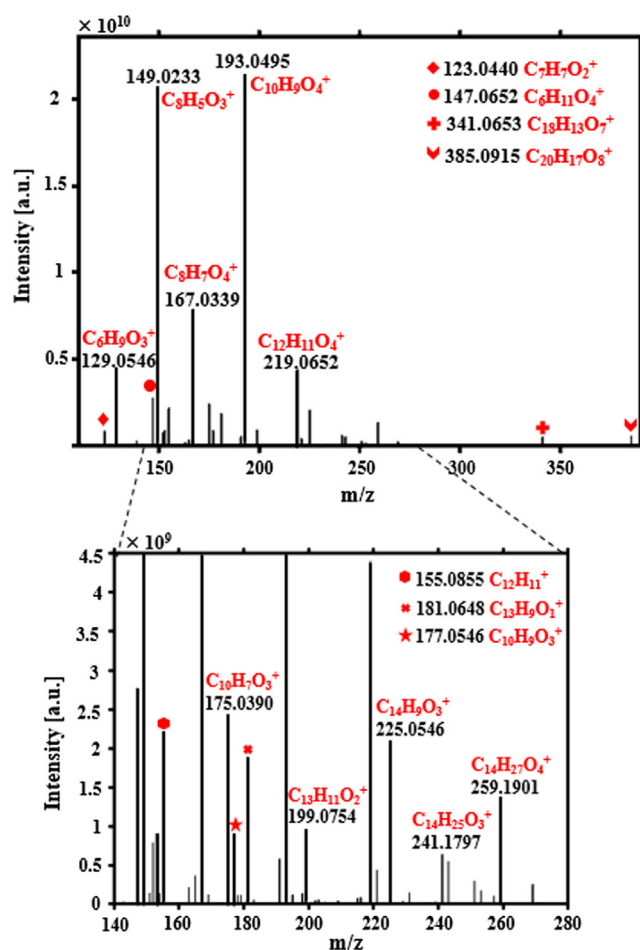

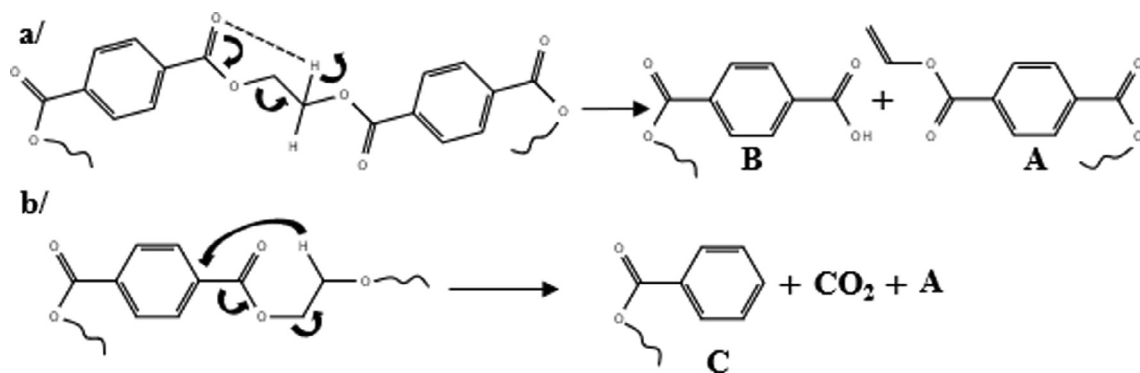**Fig. 6.** Average APCI FT-ICR MS spectrum of pyrolysis products of PET.

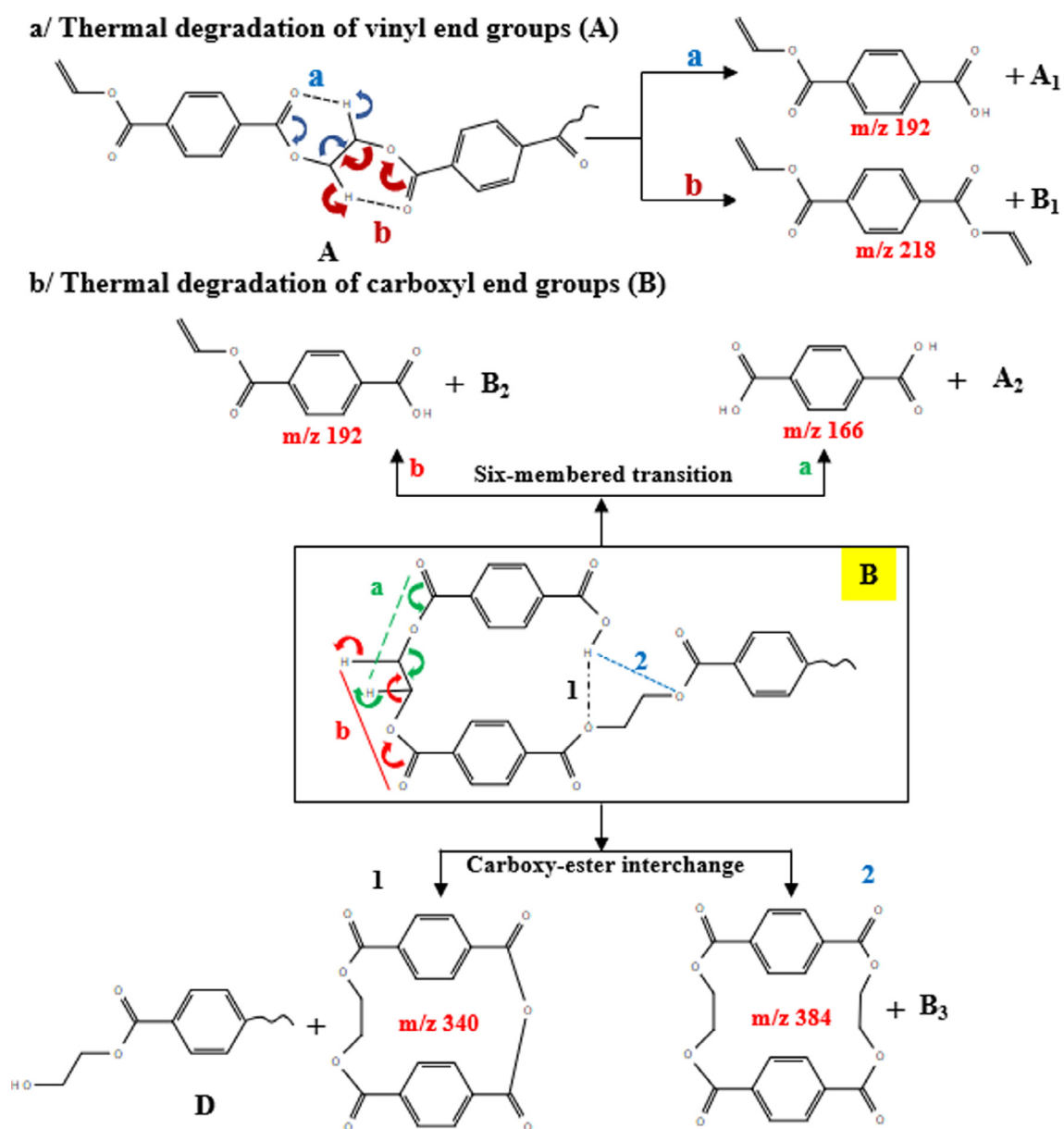Fig. 7. Intramolecular possibilities in PET degradation.

Fig. 8. Proposed reaction pathways for the degradation of: a/ vinyl end groups, b/ carboxyl end groups.

in APCI FT-ICR MS in which the oxygenated category CHO_x is the prevailing class. The most abundant CHO_x compounds are those containing 4 and 3 oxygen atoms with a percentage of 45.5% and 37.6% respectively. Very low abundances of highly oxygenated compounds (7 and 8) (<1%) are also detected.

An APCI FT-ICR mass spectrum is shown in Fig. 6. A unique molecular formula is attributed to each peak detected using the accurate mass measurement.

The species are detected mainly as protonated molecule $[M+H]^+$ and to a part as molecular cation $[M]^+$, where M refers to the molecule. Seventy-seven peaks are assigned unambiguously in the 100–400 m/z range. Possible peak assignments of major compounds are summarized in Table S1. The highest intensities are observed at m/z 193.0495 and 149.0233, corresponding to $C_{10}H_9O_4^+$ and $C_8H_5O_3^+$ respectively. The peak at m/z 385.0915 ($C_{20}H_{17}O_8^+$) is the highest mass obtained by FT-ICR-MS and may

be attributed to cyclic or/and linear dimer (Nasser et al., 2005). (Ubeda et al., 2018) reported similar results. In their study, they analyzed the oligomer of PET by using ultra-high-performance liquid chromatography-quadrupole time-of-flight mass spectrometry (UPLC-MS-QTOF). They found that the cyclic monomer and dimer are characterized by an exact m/z of 193.0498 and 385.0915, respectively. Signals corresponding to m/z 219.0652 ($C_{12}H_{11}O_4^+$) and m/z 167.0339 ($C_8H_7O_4^+$) can be attributed to divinyl terephthalate and terephthalic acid, respectively. The temporal evolution profiles of the compounds with the highest intensities are shown in Fig. S5. Peaks at m/z 193.0495 ($C_{10}H_9O_4^+$) and 149.0233 ($C_8H_5O_3^+$) are detected by FT-ICR MS at the same temperature, about 346 °C. Terephthalic acid (m/z 167.0339 ($C_8H_7O_4^+$)) is detected at 361 °C. A cyclic dimer (m/z 385.0915 ($C_{20}H_{17}O_8^+$)) and an anhydride compound at m/z 341.0653 ($C_{18}H_{13}O_7^+$) appear later at 381 °C (Fig. S6). These compounds are among the primary
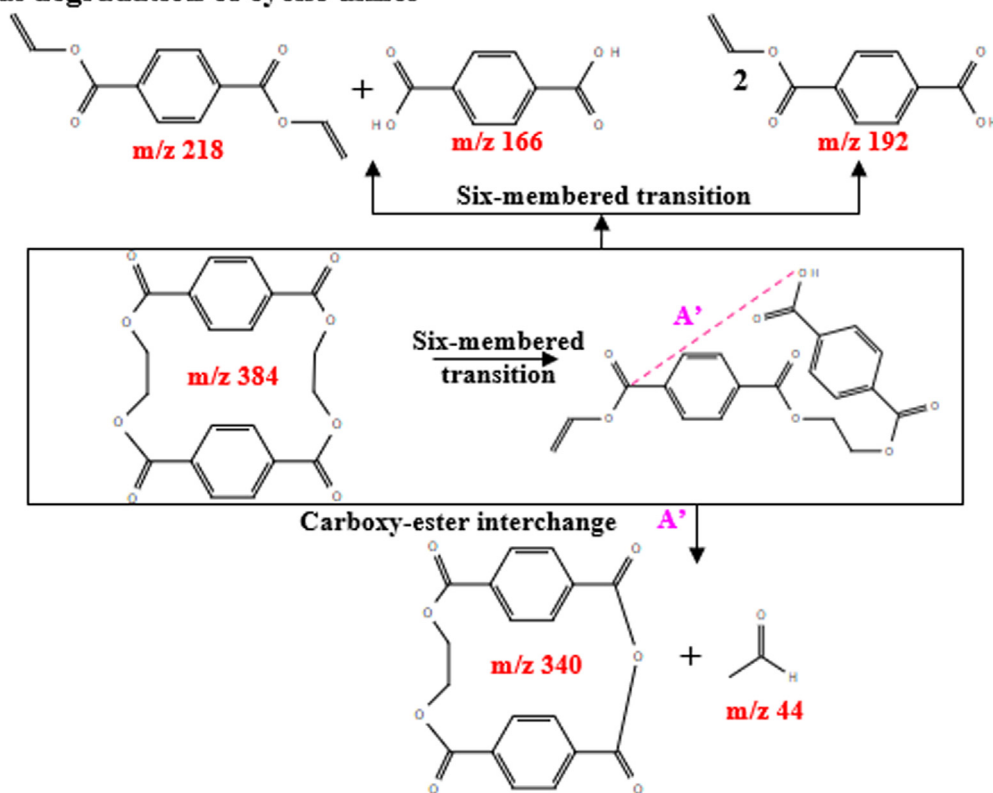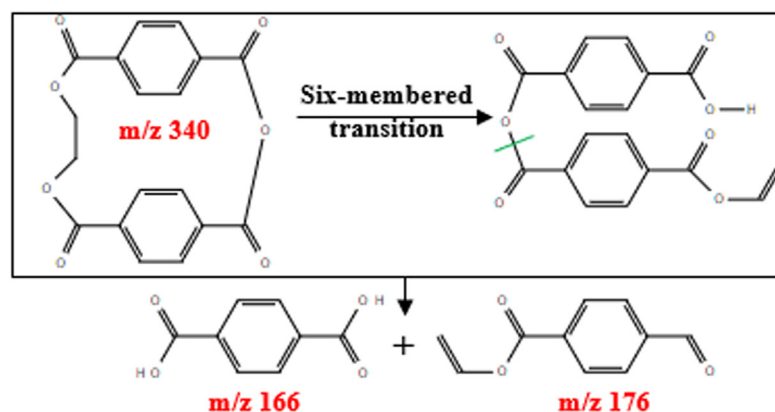

Fig. 9. Proposed reaction pathways for the degradation of: a/cyclic dimer, b/ cyclic anhydride.

products of the degradation of PET, and their delayed detection may indicate that they are generated in condensed phase (solid or liquid) and transferred into the gas phase at higher temperatures.

In the literature, (Dhahak et al., 2020) characterized molecules formed during PET pyrolysis and analyzed offline by Fourier Transform Ion Cyclotron Resonance Mass Spectrometry (FT ICR–MS) coupled to electrospray (ESI). Some molecules such as m/z 358 and m/z 550 that had been detected by ESI-FT-ICRMS are not observed in the present study and this seems to indicate that these molecules may be formed by repolymerization in the condensers or in the cold zone. This highlights the strength of online analysis versus offline analysis.

3.4. Possible reaction pathways for PET degradation

Different reaction pathways for PET degradation can be proposed, involving most likely two back-biting possibilities through a concerted mechanism (Fig. 7). Reaction in Fig. 7a) is more energetically favorable than the reaction in Fig. 7b), involving the six-membered cyclic transition state, as reported in previous studies (Hujuri et al., 2013; Montaudo et al., 1993; Plage and Schulten, 1990). The transition state energy of dissociation is about 50 kcal/mol (Dayma et al., 2019). It leads to the formation of carboxyl and vinyl end groups. In the second possibility, PET may undergo a decarboxylation reaction, producing benzene and vinyl
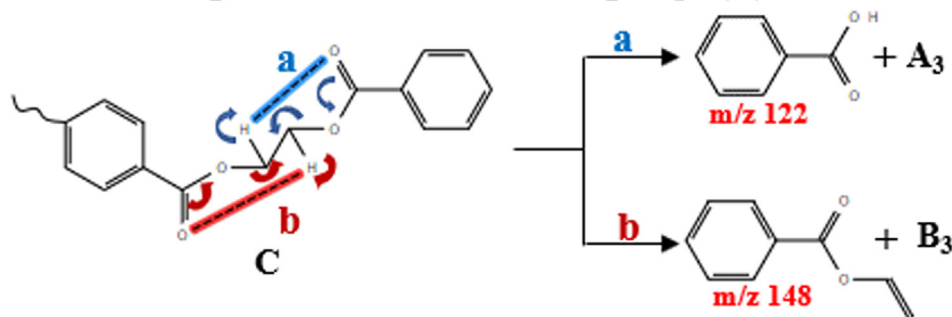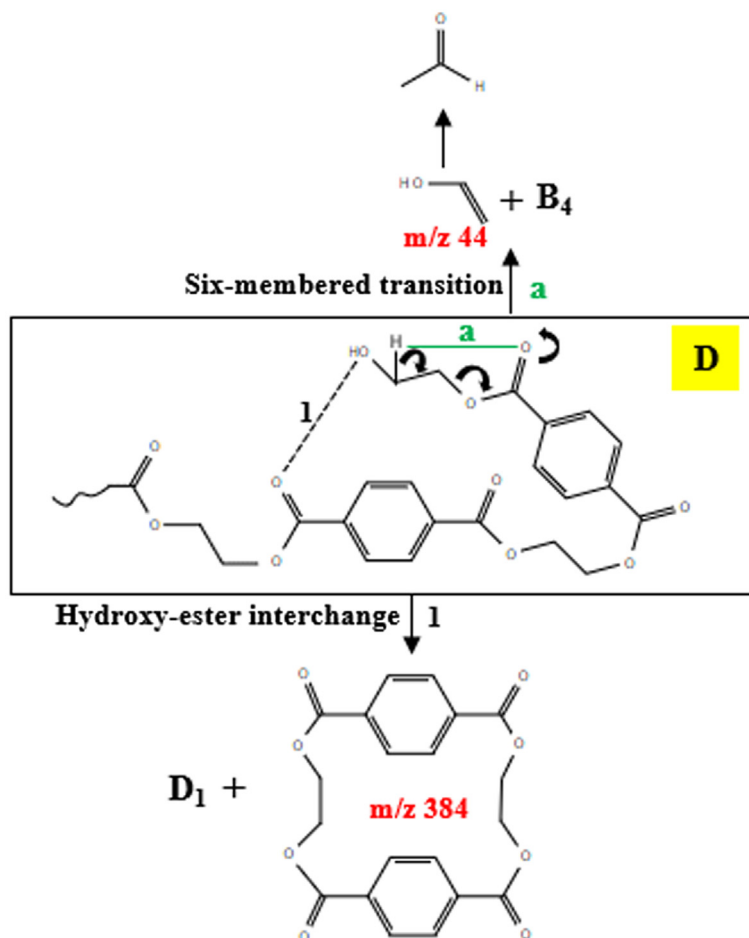

Fig. 10. Proposed reaction pathways for the degradation of: a/benzene end groups, b/ hydroxyl end groups.

end groups. Vinyl decompose via six-membered cyclic transition state, as shown in Fig. 8a), producing di-vinyl terephthalate (*m/z* 218), vinyl terephthalate (*m/z* 192), as expected (Hujuri et al., 2013), and other carboxyl and vinyl end groups, having lower molecular weights. Carboxyl end groups may undergo two different reactions Fig. 8b). In fact, a six-membered cyclic transition state which generates terephthalic acid (*m/z* 166), vinyl terephthalate (*m/z* 192), and carboxyl and vinyl end groups, according to two different branches in the same molecule.

Additionally, an intramolecular carboxy-ester interchange may take place, leading to the formation of cyclic products, such as cyclic dimer (*m/z* 384), hydroxy and carboxy end groups. (Montaudo et al., 1993) investigated the direct pyrolysis of PET using negative chemical ionization. They found that cyclic oligomers are the primary products at about 300 °C that decompose further by β-H transfer reactions at 400 °C generating open-chain oligomers with olefin and carboxylic end groups.

(Samperi et al., 2004) also studied the isothermal degradation of PET in the temperature range of 270–370 °C using matrix-assisted laser desorption ionization–time of flight (MALDI-TOF) mass spectrometry and NMR analysis. They indicated the formation of cyclic oligomers, and proposed their structural characterization. Anhydrides containing oligomer may also be generated at *m/z* 340, which is in agreement with literature (Samperi et al., 2004).

Possible reaction pathways for the degradation of cyclic dimer and anhydrides are shown in Fig. 9. Six-membered transition state occurs to generate linear dimer and anhydride. These linear dimers may undergo carboxy-ester interchange producing cyclic anhydrides and acetaldehyde. Fig. 10.a) shows that benzoic acid (*m/z* 122), vinyl benzoate (*m/z* 148) and carboxyl and vinyl end groups can be generated via the six-membered transition in benzene end groups (C).

In the case of hydroxy end groups, an intramolecular hydroxy-ester interchange, as shown in Fig. 10b), may occur and produces cyclic dimer (Murillo et al., 2010). In literature, the presence of hydroxy end in the structure accelerates the interchange reaction and favored the formation of cyclic products (Chikh et al., 2003; Kamoun et al., 2006). Vinyl alcohol (*m/z* 44) is also generated via six-membered transition, however, it transforms to acetaldehyde, which is one of primary volatile products in PET degradation (Fig. 10b). Among the volatile PET degradation species are ethylene (C_2H_4), which is formed with a smaller extent. An intermolecular reaction through an eight-membered transition between PET and vinyl end groups is proposed for its formation (Fig. 11) (Levchik and Weil, 2004).

In addition, tentative degradation pathways of major products are illustrated in Fig. 12. The routes proposed here are consistent with the main products identified by the three techniques. The starting point is the di-vinyl terephthalate (*m/z* 218). In literature, Taylor reported various reactions occurred in vinyl acetate decomposition between 363 and 448 °C (Taylor, 1983). By analogy, every compounds with a $[(C{=}O)O(CH{=}CH_2)]$ segment undergoes the same routes.

Traces of acetylene (C_2H_2) also exists in PET degradation (Sovová et al., 2008; Turnbull et al., 2013). Unfortunately, it cannot be detected with the three techniques because of its high ionization energy and lower molecular weight. The formation of acetylene may be the by-product of vinyl end groups degradation.
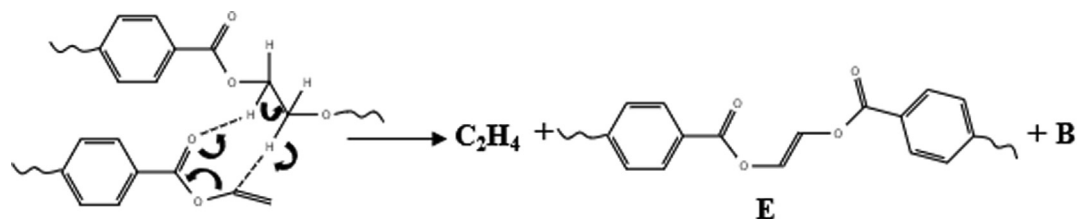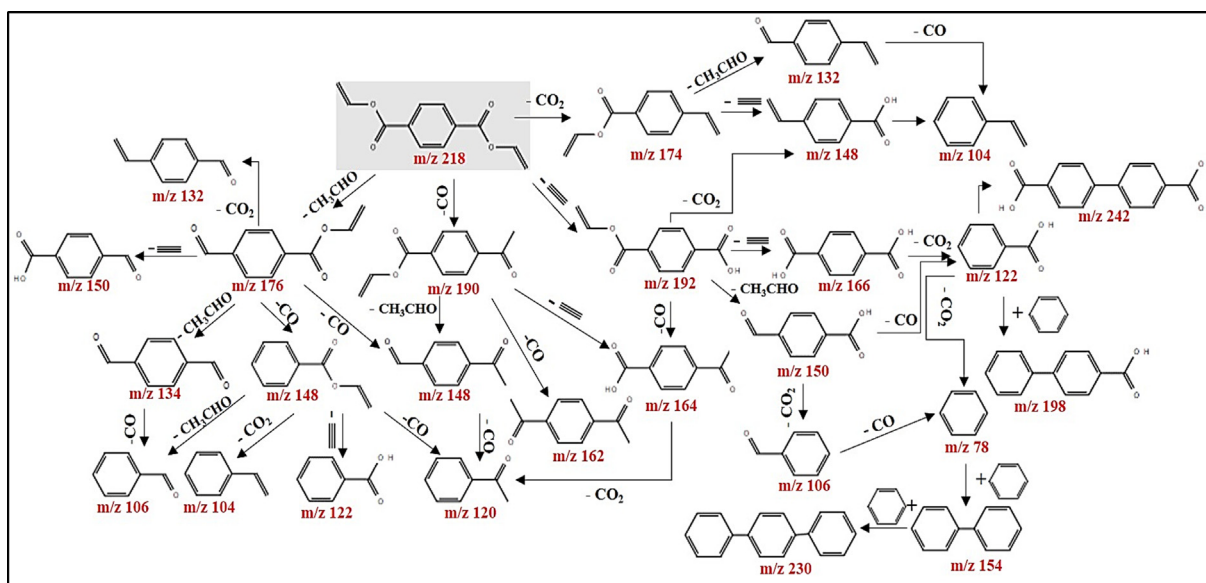

Fig. 11. Formation of ethylene.

Fig. 12. Proposed reaction pathways for the degradation of major products.

Polycyclic aromatic hydrocarbons (PAHs), such as biphenyl (m/z 154) and terphenyl (m/z 230), are also presented. They are most likely produced via benzene.

4. Conclusion

In this study, three different soft ionization mass spectrometric approaches have been applied, allowing a comprehensive overview and understanding of the slow pyrolysis of PET in real time. The originality of this paper firstly lies in on-line monitoring of the emitted decomposition products and their thermal dependent evolution profiles. Secondly, the combination of these techniques allows the almost complete identification of volatile species and therefore, the typical reactions that can occur. TG-SPI-TOF-MS was used for the description of organic species with ionization energies below 10.5 eV. This technique showed that the main major peaks were acetaldehyde (m/z 44), benzoic acid (m/z 122) and a peak at m/z 149 which is a fragment of the monomer of PET (m/z 192). Despite the use of soft ionization, some compounds fragmented with the loss of a [O—CH=CH$_2$] fragment. Aromatic compounds, such as benzene and toluene, exhibited a bi-modal behavior in their profiles showing the existence of two different reactions involved in their formation. The second soft ionization technique used was REMPI-TOF-MS, selective for aromatic species. REMPI-TIC has the same trend as the benzene profile. Different series of pyrolysis products are observed in different temperature intervals. The main products correspond to m/z 230, 178, and 254. Possible structures were proposed in SPI and REMPI techniques. Additionally, FT-ICR MS was applied, detecting medium-polar and polar species in a mass range of [100–40]. Compounds with DBE values ranging from 2 to 15 and carbon numbers ranging from C_6 to C_{20} were detected. Seven classes were observed in which the most abundant was CHO$_4$, with a percentage of 45.5%. Detailed chemical information was gained using FT-ICR exact mass data. The signals with the highest intensities found in mass spectrum are m/z 193.0495 and 149.0233, corresponding to $C_{10}H_9O_4^+$ and $C_8H_5O_3^+$ respectively. Possible structures for some peaks were suggested, helping the construction of reaction pathways that showed the formation of both cyclic monomer and dimer and linear compounds. Typical reactions (intramolecular exchange, via hydroxy-ester and carboxy-ester interchange and six-membered transition state, and intermolecular exchange) have been proposed which may explain the majority of products emitted.

Declaration of Competing Interest

The authors declare that they have no known competing financial interests or personal relationships that could have appeared to influence the work reported in this paper.

Acknowledgements

Appendix A. Supplementary material

Supplementary data to this article can be found online at https://doi.org/10.1016/j.wasman.2020.03.028.

References

Artetxe, M., Lopez, G., Amutio, M., Elordi, G., Olazar, M., Bilbao, J., 2010. Operating conditions for the pyrolysis of poly-(ethylene terephthalate) in a conical spouted-bed reactor. Ind. Eng. Chem. Res. 49, 2064–2069. https://doi.org/10.1021/ie900557c.

Badia, J.D., Martinez-Felipe, A., Santonja-Blasco, L., Ribes-Greus, A., 2013. Thermal and thermo-oxidative stability of reprocessed poly(ethylene terephthalate). J. Anal. Appl. Pyrol. 99, 191–202. https://doi.org/10.1016/j.jaap.2012.09.003.

Bae, E., Na, J.G., Chung, S.H., Kim, H.S., Kim, S., 2010. Identification of about 30 000 chemical components in shale oils by electrospray ionization (ESI) and atmospheric pressure photoionization (APPI) coupled with 15 T fourier transform ion cyclotron resonance mass spectrometry (FT-ICR MS) and a comparison to. Energy Fuels 24, 2563–2569. https://doi.org/10.1021/ef100060b.

Barrow, M.P., Peru, K.M., Headley, J.V., 2014. An added dimension: GC atmospheric pressure chemical ionization FTICR MS and the athabasca oil sands. Anal. Chem. 86, 8281–8288. https://doi.org/10.1021/ac501710y.

Boesl, U., Neusser, H.J., Schlag, E.W., 1978. Two-photon ionization of polyatomic molecules in a mass spectrometer. Zeitschrift für Naturforsch. A 33, 1546–1548. https://doi.org/10.1002/chin.197913069.

Chikh, L., Arnaud, X., Guillermain, C., Tessier, M., Fradet, A., 2003. Cyclizations in hyperbranched aliphatic polyesters and polyamides. Macromol. Symp. 199, 209–221. https://doi.org/10.1002/masy.200350918.

Çit, I., Sinaǧ, A., Yumak, T., Uçar, S., Misirlioǧlu, Z., Canel, M., 2010. Comparative pyrolysis of polyolefins (PP and LDPE) and PET. Polym. Bull. 64, 817–834. https://doi.org/10.1007/s00289-009-0225-x.

Crepier, J., Le Masle, A., Charon, N., Albrieux, F., Duchene, P., Heinisch, S., 2018. Ultra-high performance supercritical fluid chromatography hyphenated to atmospheric pressure chemical ionization high resolution mass spectrometry for the characterization of fast pyrolysis bio-oils. J. Chromatogr. B 1086, 38–46. https://doi.org/10.1016/j.jchromb.2018.04.005.

Czech, H., Schepler, C., Klingbeil, S., Ehlert, S., Howell, J., Zimmermann, R., 2016. Resolving coffee roasting-degree phases based on the analysis of volatile compounds in the roasting off-gas by Photoionization Time-of-Flight Mass Spectrometry (PI-TOFMS) and statistical data analysis: Toward a PI-TOFMS roasting model. Agric. food Chem. 64, 5223–5231. https://doi.org/10.1021/acs.jafc.6b01683.

Czégény, Z., Jakab, E., Blazsó, M., Bhaskar, T., Sakata, Y., 2012. Thermal decomposition of polymer mixtures of PVC, PET and ABS containing brominated flame retardant: formation of chlorinated and brominated organic compounds. J. Anal. Appl. Pyrol. 96, 69–77. https://doi.org/10.1016/j.jaap.2012.03.006.

Czekner, J., Taatjes, C.A., Osbornb, D.L., Meloni, G., 2018. Study of low temperature chlorine atom initiated oxidation of methyl and ethyl butyrate using synchrotron photoionization TOF-mass spectrometry. Phys. Chem. Chem. Phys. 20, 5785–5794. https://doi.org/10.1039/c7cp08221e.

Dayma, G., Thion, S., Lailliau, M., Serinyel, Z., Dagaut, P., Sirjean, B., Fournet, R., 2019. Kinetics of propyl acetate oxidation: Experiments in a jet-stirred reactor, ab initio calculations, and rate constant determination. Proc. Combust. Inst. 37, 429–436. https://doi.org/10.1016/j.proci.2018.05.178.

Deng, Y., Wang, Y.Z., Ban, D.M., Liu, X.H., Zhou, Q., 2006. Burning behavior and pyrolysis products of flame-retardant PET containing sulfur-containing aryl polyphosphonate. J. Anal. Appl. Pyrol. 76, 198–202. https://doi.org/10.1016/j.jaap.2005.11.002.

Dhahak, A., Carré, V., Aubriet, F., Mauviel, G., Burklé-Vitzthum, V., 2020. Analysis of products obtained from slow pyrolysis of Polyethylene Terephthalate by Fourier Transform Ion Cyclotron Resonance Mass Spectrometry coupled to Electrospray Ionization (ESI) and Laser Desorption Ionization (LDI). Ind. Eng. Chem. Res. 59, 1495–1504. https://doi.org/10.1021/acs.iecr.9b05879.

Dhahak, A., Hild, G., Rouaud, M., Mauviel, G., Burkle-Vitzthum, V., 2019. Slow pyrolysis of polyethylene terephthalate: online monitoring of gas production and quantitative analysis of waxy products. J. Anal. Appl. Pyrolysis 142,. https://doi.org/10.1016/j.jaap.2019.104664 104664.

Dorfner, R., Ferge, T., Yeretzian, C., Kettrup, A., Zimmermann, R., 2004. Laser mass spectrometry as on-line sensor for industrial process analysis: process control of coffee roasting. Anal. Chem. 76, 1386–1402. https://doi.org/10.1063/1.1405610.

Dzięcioł, M., Trzeszczyński, J., 2001. Temperature and atmosphere influences on smoke composition during thermal degradation of poly(ethylene terephthalate). J. Appl. Polym. Sci. 81, 3064–3068. https://doi.org/10.1002/app.1757.

Dzięcioł, M., Trzeszczyński, J., 2000. Volatile products of poly(ethylene terephthalate) thermal degradation in nitrogen atmosphere. Appl. Polym. Sci. 77, 1894–1901.

Fendt, A., Geissler, R., Streibel, T., Sklorz, M., Zimmermann, R., 2013. Hyphenation of two simultaneously employed soft photo ionization mass spectrometers with thermal analysis of biomass and biochar. Thermochim. Acta 551, 155–163. https://doi.org/10.1016/j.tca.2012.10.002.

Garozzo, D., Giuffrida, M., Montaudo, G., Lenz, R.W., 1987. Mass spectrometric characterization of poly(ethylene Terephthalate-co-p-Oxybenzoate). J. Polym. Sci. Part A Polym. Chem. 25, 271–284.

Giri, A., Coutriade, M., Racaud, A., Okuda, K., Dane, J., Cody, R.B., Focant, J.F., 2017. Molecular characterization of volatiles and petrochemical base oils by photoionization GC×GC-TOF-MS. Anal. Chem. 89, 5395–5403. https://doi.org/10.1021/acs.analchem.7b00124.

Green, C.S., Martin, H., 2006. Fragment-free accurate mass measurement of complex mixture components by gas chromatography/field ionization-orthogonal acceleration time-of-flight mass spectrometry: an unprecedented capability for mixture analysis. Rapid Commun. Mass Spectrom. 15, 236–239. https://doi.org/10.1002/1097-0231(20010215)15:3<236::AID-RCM197>3.0.CO;2-B.

Guo, D.M., Fu, T., Ruan, C., Wang, X.L., Chen, L., Wang, Y.Z., 2015. A new approach to improving flame retardancy, smoke suppression and anti-dripping of PET: Via arylene-ether units rearrangement reactions at high temperature. Polymer (Guildf). 77, 21–31. https://doi.org/10.1016/j.polymer.2015.09.016.

Gupta, Y.N., Chakraborty, A., Pandey, G.D., Setua, D.K., 2004. Thermal and thermooxidative degradation of engineering thermoplastics and life estimation. Appl. Polym. Sci. 92, 1737–1748. https://doi.org/10.1002/app.20134.

Hanley, L., Zimmermann, R., 2009. Light and molecular ions: the emergence of vacuum UV single-photon ionization in MS. Anal. Chem. 81, 4174–4182. https://doi.org/10.1021/ac8013675.

Hsu, H., Ni, C.-K., 2018. Vacuum ultraviolet single-photon postionization of amino acids. Appl. Sci. 8, 1–14. https://doi.org/10.3390/app8050699.

Huang, Q., Liu, C., Wei, R., Wang, J., 2017. Experimental study of polyethylene pyrolysis and combustion over HZSM-5, HUSY, and MCM-41. J. Hazard. Mater. 333, 10–22. https://doi.org/10.1016/j.jhazmat.2017.03.029.

Huba, A.K., Huba, K., Gardinali, P.R., 2016. Understanding the atmospheric pressure ionization of petroleum components: The effects of size, structure, and presence of heteroatoms. Sci. Total Environ. 568, 1018–1025. https://doi.org/10.1016/j.scitotenv.2016.06.044.

Hujuri, U., Ghoshal, A.K., Gumma, S., 2013. Temperature-dependent pyrolytic product evolution profile for polyethylene terephthalate. J. Appl. Polym. Sci. 130, 3993–4000. https://doi.org/10.1002/app.39681.

Jia, L., Le, Y., Brech, Mauviel, G., Qi, F., Fr zowein, M.B., Ehlert, S., Zimmermann, R., Dufour, A., 2016. Online analysis of biomass pyrolysis tar by photoionization mass spectrometry. Energy Fuels 30, 1555–1563. https://doi.org/10.1021/acs.energyfuels.5b02274.

Kai, X., Yang, T., Shen, S., Li, R., 2019. TG-FTIR-MS study of synergistic effects during co-pyrolysis of corn stalk and high-density polyethylene (HDPE). Energy Convers. Manag. 181, 202–213. https://doi.org/10.1016/j.enconman.2018.11.065.

Kamoun, W., Salhi, S., Rousseau, B., El Gharbi, R., Fradet, A., 2006. Furanic-aromatic copolyesters by interchange reactions between poly(ethylene terephthalate) and poly[ethylene 5,5′-isopropylidene-bis(2- furoate)]. Macromol. Chem. Phys. 207, 2042–2049. https://doi.org/10.1002/macp.200600390.

Kawecki, D., Scheeder, P.R.W., Nowack, B., 2018. Probabilistic material flow analysis of seven commodity plastics in Europe. Environ. Sci. Technol. 52, 9874–9888. https://doi.org/10.1021/acs.est.8b01513.

Kekäläinen, T., Venäläinen, T., Jänis, J., 2014. Characterization of birch wood pyrolysis oils by ultrahigh-resolution fourier transform ion cyclotron resonance mass spectrometry: Insights into thermochemical conversion. Energy Fuels 28, 4596–4602. https://doi.org/10.1021/ef500849z.

Kinoshita, R., Teramoto, Y., Yoshida, H., 1993. TG-DTA/FT-IR method for analyzing thermal decomposition mechanism of polyesters. J. Therm. Anal. 40, 605–611. https://doi.org/10.1007/BF02546630.

Kumagai, S., Yamasaki, R., Kameda, T., Saito, Y., Watanabe, A., Watanabe, C., Teramae, N., Yoshioka, T., 2017. Tandem μ-reactor-GC/MS for online monitoring of aromatic hydrocarbon production via CaO- catalysed PET pyrolysis. React. Chem. Eng. 2, 776–784. https://doi.org/10.1039/C7RE00097A.

Lee, J., Lee, T., Tsang, Y.F., Oh, J.I., Kwon, E.E., 2017. Enhanced energy recovery from polyethylene terephthalate via pyrolysis in CO2 atmosphere while suppressing acidic chemical species. Energy Convers. Manag. 148, 456–460. https://doi.org/10.1016/j.enconman.2017.06.026.

Levchik, S.V., Weil, E.D., 2004. A review on thermal decomposition and combustion of thermoplastic polyesters. Polym. Adv. Technol. 15, 691–700. https://doi.org/10.1002/pat.526.

Li, D.X., Gan, L., Bronja, A., Schmitz, O.J., 2015. Gas chromatography coupled to atmospheric pressure ionization mass spectrometry (GC-API-MS): review. Anal. Chim. Acta 891, 43–61. https://doi.org/10.1016/j.aca.2015.08.002.

Li, X., Sun, G., Chen, S., Fang, Z., Yuan, H., Shi, Q., Zhu, Y., 2018. Molecular chemodiversity of dissolved organic matter in paddy soils. Environ. Sci. Technol. 52, 963–971. https://doi.org/10.1021/acs.est.7b00377.

Miettinen, I., Kuittinen, S., Paasikallio, V., Mäkinen, M., Pappinen, A., Jänis, J., 2017. Characterization of fast pyrolysis oil from short-rotation willow by high-resolution Fourier transform ion cyclotron resonance mass spectrometry. Fuel 207, 189–197. https://doi.org/10.1016/j.fuel.2017.06.053.

Montaudo, G., Puglisi, C., Samperi, F., 1993. Primary thermal degradation mechanisms of PET and PBT. Polym. Degrad. Stab. 42, 13–28. https://doi.org/10.1016/0141-3910(93)90021-A.

Murillo, E.A., Vallejo, P.P., López, B.L., 2010. Characterization of hydroxylated hyperbranched polyesters of fourth and fifth generation. E-Polymers 10, 1347–1358. https://doi.org/10.1515/epoly.2010.10.1.1347.

Nasser, A.L.M., Lopes, L.M.X., Eberlin, M.N., Monteiro, M., 2005. Identification of oligomers in polyethyleneterephthalate bottles for mineral water and fruit juice development and validation of a high-performance liquid chromatographic method for the determination of first series cyclic trimer. J. Chromatogr. A 1097, 130–137. https://doi.org/10.1016/j.chroma.2005.08.023.

NIST Chemistry webbook [Gas phase ion energetics data] Available online : (last accessed Mai 2019) [WWW Document], n.d. (https://webbook.nist.gov/chemistry/)

Ohtani, H., Kimura, T., Tsuge, S., 1986. Analysis of thermal by high-resolution degradation of terephthalate chromatography. Anal. Sci. 2, 179–182.

Oni, O., Schmidt, F., Miyatake, T., Kasten, S., Friedrich, M.W., 2015. Microbial communities and organic matter composition in surface and subsurface sediments of the helgoland mud area. North Sea. Front. Microbiol. 6, 1290. https://doi.org/10.3389/fmicb.2015.01290.

Pan, Y., Wang, W., Pan, H., Zhan, J., Hu, Y., 2016. Fabrication of montmorillonite and titanate nanotube based coatings: Via layer-by-layer self-assembly method to enhance the thermal stability, flame retardancy and ultraviolet protection of polyethylene terephthalate (PET) fabric. RSC Adv. 6, 53625–53634. https://doi.org/10.1039/c6ra05213d.

Parr, M.K., Wüst, B., Teubel, J., Joseph, J.F., 2018. Splitless hyphenation of SFC with MS by APCI, APPI, and ESI exemplified by steroids as model compounds. J. Chromatogr. B 1091, 67–78. https://doi.org/10.1016/j.jchromb.2018.05.017.

Plage, B., Schulten, H.R., 1990. Thermal degradation and mass spectrometric fragmentation processes of polyesters studied by time-/temperature-resolved pyrolysis-field ionization mass spectrometry. Macromolecules 23, 2642–2648. https://doi.org/10.1021/ma00212a008.

Qian, K., Dechert, G.J., 2002. Recent advances in petroleum characterization by GC field ionization time-of-flight high-resolution mass spectrometry. Anal. Chem. 74, 3977–3983. https://doi.org/10.1021/ac020166d.

Rüger, C.P., Grimmer, C., Sklorz, M., Neumann, A., Streibel, T., Zimmermann, R., 2018. Combination of different thermal analysis methods coupled to mass spectrometry for the analysis of asphaltenes and their parent crude oils: comprehensive characterization of the molecular pyrolysis pattern. Energy Fuels 32, 2699–2711. https://doi.org/10.1021/acs.energyfuels.7b02762.

Rüger, C.P., Miersch, T., Schwemer, T., Sklorz, M., Zimmermann, R., 2015. Hyphenation of thermal analysis to ultrahigh-resolution mass spectrometry (fourier transform ion cyclotron resonance mass spectrometry) using atmospheric pressure chemical ionization for studying composition and thermal degradation of complex materials. Anal. Chem. 87, 6493–6499. https://doi.org/10.1021/acs.analchem.5b00785.

Samperi, F., Puglisi, C., Alicata, R., Montaudo, G., 2004. Thermal degradation of poly (ethylene terephthalate) at the processing temperature. Polym. Degrad. Stab. 83, 3–10. https://doi.org/10.1016/S0141-3910(03)00166-6.

Saraji-Bozorgzad, M., Geissler, R., Streibel, T., Mühlberger, F., Sklorz, M., Kaisersberger, E., Denner, T., Zimmermann, R., 2008. Thermogravimetry coupled to single photon ionization quadrupole mass spectrometry: A tool to investigate the chemical signature of thermal decomposition of polymeric materials. Anal. Chem. 80, 3393–3403. https://doi.org/10.1021/ac702599v.

Shi, Z., Jin, L., Zhou, Y., Li, H., Li, Y., Hu, H., 2018. In-situ analysis of catalytic pyrolysis of Baiyinhua coal with pyrolysis time-of-flight mass spectrometry. Fuel 227, 386–393. https://doi.org/10.1016/j.fuel.2018.04.109.

Sophonrat, N., Sandström, L., Johansson, A.C., Yang, W., 2017. Co-pyrolysis of mixed plastics and cellulose: an interaction study by Py-GC×GC/MS. Energy Fuels 31, 11078–11090. https://doi.org/10.1021/acs.energyfuels.7b01887.

Sovová, K., Ferus, M., Matulková, I., Španěl, P., Dryahina, K., Dvořák, O., Civiš, S., 2008. A study of thermal decomposition and combustion products of disposable polyethylene terephthalate (PET) plastic using high resolution fourier transform infrared spectroscopy, selected ion flow tube mass spectrometry and gas chromatography mass spectrometr. Mol. Phys. 106, 1205–1214. https://doi.org/10.1080/00268970802077876.

Fukuzawa, T., Tanimizu, S., 1978. Flourescence decay characteristics of Tb3+-activated phosphates under H2-VUV laser excitation. J. Lumin. 16, 447–456.

Taylor, R., 1983. The mechanism of thermal elimination. Part 17. rate data for pyrolysis of vinyl acetate and 1,2-diacetoxyethane. J. Chem. Soc. Perkin Trans. 2 0, 1157–1160.

Tose, L.V., Cardoso, F.M.R., Fleming, F.P., Vicente, M.A., Silva, S.R.C., Aquije, G.M.F.V., Vaz, B.G., Romão, W., 2015. Analyzes of hydrocarbons by atmosphere pressure chemical ionization FT-ICR mass spectrometry using isooctane as ionizing reagent. Fuel 153, 346–354. https://doi.org/10.1016/j.fuel.2015.03.004.

Trukhin, A.N., Golant, K.M., 2009. Peculiarities of photoluminescence excited by 157 nm wavelength F2 excimer laser in fused and unfused silicon dioxide. J. Non-Cryst. Solids 355, 1719–1725. https://doi.org/10.1016/j.jnoncrysol.2009.06.020.

Turnbull, L., Liggat, J.J., Macdonald, W.A., 2013. Thermal degradation chemistry of poly(ethylene naphthalate) - a study by thermal volatilisation analysis. Polym. Degrad. Stab. 98, 2244–2258. https://doi.org/10.1016/j.polymdegradstab.2013.08.018.

Ubeda, S., Aznar, M., Nerín, C., 2018. Determination of oligomers in virgin and recycled polyethylene terephthalate (PET) samples by UPLC-MS-QTOF. Anal. Bioanal. Chem. 410, 2377–2384. https://doi.org/10.1007/s00216-018-0902-4.

Van Dam, H., Oskam, A., 1978. He(I) and He(II) photoelectron spectra of some substituted ethylenes. J. Electron Spectros. Relat. Phenomena 13, 273–290.

Wang, Y., Huang, Q., Zhou, Z., Yang, J., Qi, F., Pan, Y., 2015. Online study on the pyrolysis of polypropylene over the HZSM-5 zeolite with photoionization time-of-flight mass spectrometry. Energy Fuels 29, 1090–1098.

Wu, Q., Hua, L., Hou, K., Cui, H., Chen, W., Chen, P., Wang, W., Li, J., Li, H., 2011. Vacuum ultraviolet lamp based magnetic field enhanced photoelectron ionization and single photon ionization source for online time-of-flight mass spectrometry. Anal. Chem. 83, 8992–8998. https://doi.org/10.1021/ac201791n.

Xu, J., Zhuo, J., Zhu, Y., Pan, Y., Yao, Q., 2017. Analysis of volatile organic pyrolysis products of bituminous and anthracite coals with single-photon ionization time-of-flight mass spectrometry and gas chromatography/mass spectrometry. Energy Fuels 31, 730–737. https://doi.org/10.1021/acs.energyfuels.6b02335.

Yoshioka, T., Grause, G., Eger, C., Kaminsky, W., Okuwaki, A., 2004. Pyrolysis of poly (ethylene terephthalate) in a fluidised bed plant. Polym. Degrad. Stab. 86, 499–504. https://doi.org/10.1016/j.polymdegradstab.2004.06.001.

Yuzawa, T., Watanabe, C., Nemoto, N., Ohtani, H., 2013. Rapid evaluation of photo, thermal and oxidative degradation of high impact polystyrene by a xenon lamp-based online ultraviolet irradiation-pyrolysis-GC/MS system. Polym. Degrad. Stab. 98, 671–676. https://doi.org/10.1016/j.polymdegradstab.2012.11.005.

Zander, N.E., Gillan, M., Lambeth, R.H., 2018. Recycled polyethylene terephthalate as a new FFF feedstock material. Addit. Manuf. 21, 174–182. https://doi.org/10.1016/j.addma.2018.03.007.

Zhou, Z., Chen, X., Wang, Y., Liu, C., Ma, H., Zhou, C., 2019. Bioresource technology online photoionization mass spectrometric evaluation of catalytic co-pyrolysis of cellulose and polyethylene over HZSM-5. Bioresour. Technol. 275, 130–137. https://doi.org/10.1016/j.biortech.2018.12.045.

Zimmermann, R., Heger, H.J., Kettrup, A., 1999. On-line monitoring of traces of aromatic-, phenolic- and chlorinated components in flue gases of industrial scale incinerators and cigarette smoke by direct-inlet laser ionization-mass spectrometry (REMPI-TOFMS). Fresenius. J. Anal. Chem. 363, 720–730. https://doi.org/10.1007/s002160051281.

9   Curriculum Vitae

CHRISTOPH GRIMMER

Personal data	**Contact details**

Date of birth: 02.05.1991   Address: Margaretenstr. 53, 18057 Rostock

Place of birth: Ludwigslust   Email: grimmer.christoph@web.de

Nationality: German

Education

01/2016–01/2021   PhD student, Chair for Analytical Chemistry, University of Rostock

10/2013–09/2015   Master of Science, Chemistry, University of Rostock, Final Grade: 1.3

10/2010–09/2013   Bachelor of Science, Chemistry, University of Rostock, Final Grade: 2.5

07/2009   Abitur, Goethe Gymnasium Ludwigslust, Final Grade: 1.8

Working Experience

01/2016–09/2020   Scientist, Chair of Analytical Chemistry, University of Rostock

10/2015–12/2015   Scientist, Leibniz Institute for Catalysis, "Cycloaddition of CO_2 and epoxides"

08/2008–08/2009   Voluntary ecological year at the Water and Ground Association of Ludwigslust

Rostock, _____   _____

Christoph Grimmer